

**Evaluation of the human cognitive detection of
road surfaces based on the feedback vibrations
provided by the automobile steering wheel**

Tania Paloma Berber-Solano

A thesis submitted for the Degree of Doctor of Philosophy

Department of Mechanical Engineering

The University of Sheffield

December 2008

I dedicate this thesis to my loved parents,

María Concepción Solano González and

José Manuel Berber Rosas

*what I have done today is only because of you,
your efforts and love to me has made this work possible*

Acknowledgments

I would like to acknowledge a considerable debt to the many people, without whose contributions and assistance, the completion of this thesis could not have been realised.

I would like to thank CONACyT for their sponsorship and support which allowed me to initiate this research, and would like also to thank MIRA and Michelin for providing the several steering data for the research.

I would like to express my sincere gratitude to Professor Joseph A. Giacomin who supervised this research and has given me the gift of excellent advice and unwavering support. I am deeply indebted to him, without his help this work would not be possible. I would like also to thank my supervisor Professor Wieslaw J. Staszewski for his valuable contributions and support during this research work.

I would like to acknowledge my colleagues of the Perception Enhancement System Group (PES Group) for their support, friendship, feedback and contribution to my work. Dr. Marco Ajovalasit deserves special mention as an outstanding friend and colleague throughout my time at the University of Sheffield.

I would like to thank to Dr. Guillermo Urriolagoitia and Dr Luis H. Hernández (I.P.N. ESIME Zacatenco) for trusting in me since the first time we met and for your invaluable support. I will never forget the opportunity that you both gave to me.

I would like also to express my gratitude to the Friends of Acapulco Charity Organization for their economical support during my high school and bachelor studies.

I would like to express my deepest thanks to my family and my boyfriend, who collectively nurtured me with tireless love and support before, during, and since I started this research work. My parents, María Concepción and José Manuel; my sister, Mara; my brother, José Manuel; my first nephew 'Chobi' and my loved boyfriend, Martín, who shared with me this great experience, supported and encouraged me when needed.

Some debts are hard to put into words, but all know why their names are here: *Brozo, Williberto, Chaparro, Prieto, Broza and Coma.*

SUMMARY

This thesis describes the study of the human cognitive detection of road surfaces based on the feedback vibrations provided by the automobile steering wheel. It introduces the possibility of measuring the effects of various forms of steering wheel vibration signal on the human detection of road surface type. The identification of the key parameters which are controlling the human detection of road type might serve as the basis for the development of a steering perception enhancement system, which would act as interface between the driver and the mechanical and electromechanical elements of the steering system.

The steering wheel is commonly considered the most important source of haptic feedback information for the automobile driver. This is due to the great sensitivity of the skin tactile receptors of the hand, as well as the lack of intermediate structures such as shoes and clothing which can act to attenuate the transmission of vibrational stimuli to the driver. However, the achievement of higher levels of comfort in modern automobiles has sometimes come at the expense of a lack of driver involvement since new mechanisms are not carrying meaningful stimuli to the driver, and this in terms of safety is not good. The issue of driver involvement can become critical in the case of by-wire systems since these systems do not necessarily have a predetermined path, or transfer mechanism, for carrying stimuli to the driver. The question of what stimuli should reach the driver and the search of understanding how drivers perceive the information received by means of the steering wheel vibrational stimuli has therefore assumed great importance. Towards this goal the research performed a series of tests in which human subjects were exposed to rotational stimuli in a laboratory test rig (steering wheel) in order to identify which are the

parameters used by the drivers to detect the road surface type. Eight different tests were conducted in which a group of fifteen different test subjects took part for the overall thesis work.

Chapter 1 gives an overview of the automotive steering vibration as a research problem and the need of evaluating the human ability to cognitively detect road surfaces. This chapter, additionally, presents the different architectures of conventional steering systems which are currently in mass production. This part of the chapter explains the mechanical structure of the steering systems in common use, the types of power assist steering and a brief description of the nearest future of the steering system. The aspects affecting the human perception of steering vibrations are described in this chapter: discomfort caused by automotive steering vibration, the existing methods for the description and the evaluation of the steering vibrations and the description of a perception enhancement for automotive steering system. This chapter also introduces the objectives of the research and their possible contribution to the industry.

Chapter 2 provides the definitions, techniques and algorithms from the field of digital signal processing fundamental towards the understanding of the experiments performed during the research. Chapter 3, instead, provides the definitions from the field of human cognition.

Chapter 4 describes the steering wheel acceleration data used in the research presented in this thesis. Three measurement tests are described from which were obtained the steering vehicle vibration. Each of the three measurement test describes: the steering acceleration measurement, the characteristics and specifications of the automobile used during the test, the type of road surfaces measured and the signal processing analysis of each steering data.

In chapter 5 is investigated the effect of the steering wheel acceleration magnitude on the human ability to detect road surface type. Four different road surfaces were employed as test stimuli. They were a cobblestone surface, a concrete surface, a low bump surface and a tarmac surface, each of which was rescaled to six acceleration magnitudes (0.8, 0.9, 1.0, 2.0, 3.0 and 4.0).

The results from the acceleration magnitude experiment establish that a single, optimal, vibration magnitude does not exist which is valid for all road surfaces. The optimal vibration magnitude for detection appears to be related to the characteristics of the cognitive model which the test subjects associate with the surface in question. The results also suggest that detection is not strictly optimal at the natural vibration magnitude encountered in automobiles.

In Chapter 6 is investigated the effect of steering wheel acceleration frequency distribution on human detection of road type in order to identify which energy band is most used by drivers to detect road surface type. Two different experiments are described in this chapter. The first experiment investigates the effect of frequency bandwidth. Two different road surfaces were employed, a cobblestone surface and a tarmac surface. For each road type, five frequency bandwidths of 0-20 Hz, 0-40 Hz, 0-60 Hz, 0-80 Hz and 0-100 Hz were achieved by means of frequency domain filtering. The original stimuli were filtered such that the effect of the frequency bandwidth of the stimuli on the human cognitive response could be studied. The second experimental test described in Chapter 6 investigates the effect of vibrational energy distribution of road surface stimuli on the human ability to detect road surface type. Three different road surfaces were employed, a motorway surface, a broken concrete surface and a broken lane surface. Each road stimuli was manipulated by means of digital Butterworth filters in order to eliminate five frequency ranges from the steering wheel acceleration spectrum which were considered important subdivisions of the vehicle's vibrational energy. Selected frequency ranges were from 0-6, 6-13, 13-27, 27-60 and 60-150 Hz for the motorway stimuli, 0-6, 6-12, 12-27, 27-53 and 53-150 Hz for the broken concrete stimuli and 0-6, 6-9, 9-22, 22-58 and 58-150 Hz for the broken lane stimuli.

From both experiments, the results suggest that the perceptual and cognitive mechanisms used by the test subjects require vibrational information which contains the higher energy level approximately from 20 Hz to 80 Hz. These results provide a clear indication of the frequency band used by humans to judge road surface type when driving current production automobiles.

In chapter 7 is investigated the effect of steering wheel acceleration compression and expansion on human detection of road type in order to determine if some effects used in

the music field could improve the steering stimuli for the detection task. Three different road surfaces were employed as test stimuli. They were a cobblestone surface, a concrete surface, and a tarmac surface, each of which was compressed and expanded by means of scale values of 0.40, 0.60, 0.80 and 0.90 which were selected as compressor factors; and of 1.10, 1.50, 2.00 and 2.50 which were selected as expander factors. The selected compressor and expander factors include the common values used for music enhancement which are approximately 0.40 when compressing and 1.10 when expanding.

The results suggest that a single, optimal and fixed compression factor of 0.90 exists which is valid for all three road surfaces. The results suggest that the highest peaks which occur in a steering wheel time history several times act as masking for parts of the steering wheel stimuli which are vital clues for an automobile driver.

In Chapter 8 is investigated the effect of the transient events, in terms of number and size, which are contained in the steering wheel acceleration stimuli. Three different road surfaces were employed as test stimuli which were a cobblestone surface, a concrete surface and a tarmac surface, each of which was manipulated by means of the Mildly Non-stationary Mission Synthesis (MNMS) algorithm in order to produce test stimuli which were selectively modified in terms of the number, and size, of the transient vibration events they contained. Test stimuli contained transient events which were chosen using trigger values in the range from 2.4 to 3.4 standard deviations. Test stimuli were also produced from each of the three experimentally acquired signals using four time compression ratios of 1.0, 2.0, 3.0 and 4.0 and five transient event scale factors of 0.8, 1.0, 2.0, 3.0 and 4.0.

The results suggest that the average driver require vibrational information which content transient events with a standard deviation spanning from 2.6 to 3.2. The results suggest that no single time compression ratio and no single bump scale factor exists which is valid for all driving conditions. The results suggest, however, that controlling the number and the scale of the transient events large detection improvements could be achieved.

In the Chapter 9 is investigated if the implementation of the most promising feedback settings which were found in the various individuals tests performed in this research could optimise the automotive steering vibration feedback for the purposes of road surface

detection. A group of ten different road surfaces were employed as test stimuli which were a broken surface, a broken concrete surface, a broken lane surface, a cobblestone surface, a cobblestone city, a concrete surface, a country lane, motorway surface, a noise surface and a tarmac surface. Each road surface was manipulated by means of the MNMS algorithm using the settings found to achieve general improvements in the rate of road surface detection. These settings include: 1) Test stimuli should contain transient events which are extracted from the key frequency band in the range from approximately 20 Hz to 60; 2) The steering vibration should contain transient events which are chosen using a trigger value of 2.6; 3) Test stimuli from each of the ten experimentally acquired signals should be produced by implementing a time compression ratio of 2.0 and also a bump scale factor of 2.0.

The results present improvements in detection of eight of the ten stimuli investigated, however, degradation in detection was found for the remaining two surfaces in the study. This result makes this first approach of steering vibration feedback guidelines no optimal to define the system specifications for a Perception Enhancement System (PES) for an automobile steering system.

The conclusions of the research are presented in Chapter 10 in which are also included the suggestions for further research activities.

The following findings can be drawn from the research:

- the human road detection is not strictly optimal at the natural vibration magnitude encountered in automobiles.
- a single, fixed, feedback gain from the vehicle to the steering wheel will result optimal in only a small number of driving conditions.
- the long term memory model used by drivers to judge road surface type contains information about oscillatory frequencies in excess of 60 – 80 Hz in order to guarantee efficient detection of the road surface by the driver.
- the 20 to 80 Hz frequency interval was found to provide vital clues to automobile drivers regarding the roads over which they drive and the dynamic response of the vehicle.

- music effects such as compressors and expanders widely used in the music field to enhance the human perception of the music recording can also enhance the human perception in the case of steering vibrational signals.
- a single, optimal and fixed compression factor of 0.90 exists which is valid for all driving condition tested.
- individual transient vibration events play a key role in the human detection of road surface type in driving situations achieving large improvements in the rate of correct detection by means of selective manipulation of the steering vibration stimuli.
- the first set of guidelines for automotive steering vibration feedback proposed by the research was found to clearly improve the human road detection in many driving scenarios, however, degradation in detection in a few cases make it not possible to be implemented as a PES for an automobile steering system.

CONTENTS

Acknowledgments	II
SUMMARY	III
CONTENTS	IX
INDEX OF FIGURES	XII
INDEX OF TABLES	XVIII
NOMENCLATURE	XIX
1. Automotive Steering Vibration as a Research Problem	1
1.1 Automotive Steering System Architectures.....	3
1.2 Discomfort Caused by Automotive Steering Vibration.....	6
1.3 Feel and Information Arising from Automotive Steering Vibration.....	10
1.4 Perception Enhancement for Automotive Steering Systems.....	11
1.5 The Objectives of the Research.....	12
2. Signal Processing Methods	15
2.1 Classification of signals.....	15
2.1.1 The Random Process.....	16
2.1.1.1 The Gaussian Distribution.....	16
2.1.1.2 Stationarity and Ergodicity.....	17
2.2 Global Signal Statistical Parameters.....	18
2.2.1 Mean Value and Standard Deviation Value.....	19
2.2.2 Root Mean Square Value.....	19
2.2.3 Skewness Value.....	19
2.2.4 Kurtosis Value.....	20
2.2.5 Crest Factor Value.....	20
2.2.6 Vibration Dose Value.....	21
2.3 Frequency Domain Analysis.....	21
2.3.1 The Fourier Transform.....	21
2.3.2 The Discrete Fourier Transform (DFT).....	22
2.3.3 The Fast Fourier Transform (FFT).....	23
2.4 Time-Frequency Domain Analysis: The Wavelet Transform.....	24
2.4.1 The Continuous Wavelet Transform.....	26
2.4.2 The Orthogonal Wavelet Transform.....	27
2.5 Signal Processing Techniques used in Audio Mastering.....	28
2.5.1 Gain Changers.....	28
2.5.2 Compressors.....	29
2.5.3 Expander.....	30
2.6 Signal Processing Techniques used in Vibro-acoustic Mission Synthesis.....	32
2.6.1 The Mildly Non stationary Mission Synthesis Algorithm.....	32
2.6.2 The First Stage: Synthetic Fourier Base Signal.....	34
2.6.3 The Second Stage: Wavelet Decomposition and Wavelet Level Grouping.....	34
2.6.4 The third stage: bump event selection and processing.....	35
2.6.5 The Fourth Stage: Bump Reinsertion.....	36
2.6.5.1 Proportional Reinsertion.....	36
2.6.5.2 Maximum Reinsertion.....	37
2.6.5.3 Reinsertion correlation procedure.....	37
2.6.6 Synchronisation Procedures.....	37
2.6.6.1 Non-synchronised procedure.....	38

2.6.6.2	Synchronisation procedure 1: wavelet group synchronisation	38
2.6.6.3	Synchronisation procedure 2	40
2.6.7	Mission Synthesis Results	41
3.	Considerations from Human Cognition.....	42
3.1	Human Perception	42
3.2	Human Memory.....	43
3.3	Parameters Affecting Decision Making.....	45
3.4	Theory of Signal Detection.....	46
3.4.1	Ideal Observers	47
3.4.2	Detectability Measure, d'	49
3.4.3	The ROC curve	51
4.	Steering Vibration Measured from Road Testing	54
4.1	Experimental Vibration Tests	55
4.2	MIRA Tests	56
4.2.1	Acceleration Measurement	56
4.2.2	Automobile Specifications.....	56
4.2.3	Description of Road Surfaces	57
4.2.4	Signal Processing Analysis.....	58
4.3	Michelin Tests	61
4.3.1	Acceleration Measurement	61
4.3.2	Automobile Specifications.....	62
4.3.3	Description of Road Surfaces	62
4.3.4	Signal Processing Analysis.....	63
4.4	Uxbridge Tests	64
4.4.1	Acceleration Measurement	65
4.4.2	Automobile Specifications.....	66
4.4.3	Description of Road Surfaces	66
4.4.4	Signal Processing Analysis.....	69
4.5	The Selected Steering Wheel Vibration Stimuli.....	72
5.	Test to evaluate the Effect of Steering Wheel Acceleration Magnitude on the Human Detection.....	74
5.1	Experimental Apparatus	75
5.1.1	Test Facility Specifications.....	75
5.1.2	Accuracy of the Steering Wheel Test Rig.....	76
5.2	Experiment to Measure the Effect of Acceleration Magnitude	78
5.2.1	Test Subjects.....	79
5.2.2	Test Stimuli.....	80
5.2.3	Test Protocol.....	80
5.2.4	Results from the Experiment to Measure the Effect of Steering Wheel Acceleration Magnitude.....	81
5.2.5	Observations and Discussion	86
6.	Test to determine the Effect of Steering Wheel Acceleration Frequency Distribution on the Human Detection.....	88
6.1	Two experiments in the Detection of Road Surface Type.....	89
6.1.1	Test subjects	89
6.2	Experiment to Measure the Effect of Frequency Bandwidth.....	90
6.2.1	Test Stimuli.....	91
6.2.2	Test Protocol.....	91
6.2.3	Results from the Experiment to Measure the Effect of Frequency Bandwidth.....	92
6.2.4	Observations and Discussion	94
6.3	Experiment to Measure the Effect of the Vibrational Energy Distribution	95
6.3.1	Test Stimuli.....	96
6.3.2	Test Protocol.....	98
6.3.3	Results from the Experiment to Measure the Effect of the Vibrational Energy Distribution.....	99
6.3.4	Observation and Discussion from the Experiment to Measure the Effect of Vibrational Energy Distribution	103
7.	Test to determine the Effect of Compression and Expansion of the Steering Wheel Acceleration Signal.....	105

7.1	Experiment to Measure the Effect of Compression and Expansion of Steering Wheel Acceleration Signals	106
7.1.1	Test subjects	106
7.1.2	Test Stimuli.....	107
7.1.3	Test Protocol.....	111
7.1.4	Results from the Experiment to Measure the Effect of Compression and Expansion of Steering Wheel Acceleration Signals	112
7.1.5	Observations and Discussion	115
8.	Test to determine the Effect of Steering Wheel Acceleration Transient Events on the Human Detection	117
8.1	Three experiments in the Detection of Road Surface Type	118
8.1.1	Test subjects	119
8.2	Experiment to Evaluate the Effect of Threshold Level on the Human Detection of Road Surface Type	120
8.2.1	Test Stimuli.....	120
8.2.2	Test Protocol.....	122
8.2.3	Results from the Experiment to Evaluate the Effect of Threshold Trigger Level on the Human Detection of Road Surface Type	123
8.3	Experiments to Measure the Effect of the Number of Transient Events and the Scale of Transient Events	126
8.3.1	Test Stimuli.....	126
8.3.2	Test Protocol.....	128
8.3.3	Results from the Experiment to Measure the Effect of the Number and Scaling of Transient Events	129
8.3.4	Observations and Discussion	133
9.	Experiment to determine the effectiveness of a first set of guidelines for automotive steering vibration feedback.....	135
9.1	Experiment to Measure the effect of the first set of guidelines for automotive steering vibration feedback	137
9.1.1	Test Subjects.....	137
9.1.2	Test Stimuli.....	138
9.1.3	Test Protocol.....	140
9.1.4	Results from the Experiment to Measure the Effect of the first set of guidelines for an automotive steering vibration feedback	141
9.1.5	Observations and Discussions	143
10.	Conclusions and Recommendations for Future Research	144
10.1	Summary of the Research Findings.....	144
10.2	Research Limitations and Sources of Error	147
10.3	Suggested Future Research.....	149
	References	151
	APPENDIX A.....	162
A.1	Technical Specifications of the equipment used to measure the steering wheel vibration for the Uxbridge test.....	162
	APPENDIX B.....	167
B.1	Drawings of the geometrical dimensions of the steering wheel clamp used for vibration measurements	167
	APPENDIX C.....	171
C.1	Description and Technical Specifications of the equipment used in the experimental laboratory test	171
	APPENDIX D.....	176
D.1	ROC points for the laboratory experiment to measure the effect of steering wheel acceleration compression or expansion on the human detection of road surface type.....	176
D.2	ROC points for the laboratory experiment to measure the effect of steering wheel acceleration Threshold Trigger Level on the human detection of road surface type	186
D.3	ROC points for the laboratory experiment to measure the effect of the number of the transient events on the human detection of road surface type	188
D.4	ROC points for the laboratory experiment to measure the effect of the scale of the transient events on the human detection of road surface type	190
D.5	ROC points for the laboratory experiment to measure the effect of the first set of guidelines for an automotive steering feedback	192

INDEX OF FIGURES

Figure 1.1 Mechanical Steering System (Adapted from Wolfgang, 2000).....	4
Figure 1.2 Hydraulic Power Steering System (Adapted from Wolfgang, 2000).....	4
Figure 1.3 Current Steering Systems (Wolfgang, 2000): (a) Electro Hydraulic Power Steering System and (b) Electric Power Steering System.	5
Figure 1.4 A steer by-wire system in an automobile.....	6
Figure 1.5 Coordinate system for the hand. Anatomical Coordinate System and Basic-centric Coordinate System (Adapted from ISO 5349, 2001 and BS 6842, 2001).	8
Figure 1.6 Comparison between the proposed frequency weighting W_s for rotational steering wheel vibration and frequency weighting W_b (Adapted from Giacomini et. al, 2004).....	9
Figure 1.7 An approach of a perception enhancement system for a ‘by-wire’ steering (Giacomini and Woo, 2004).....	12
Figure 2.1 The classification of random signals.	16
Figure 2.2 The Gaussian distribution	17
Figure 2.3 Examples of a stationary and non-stationary time histories: (a) stationary Gaussian signal (Highway Surface), (b) Mildly Non-stationary signal (Speed Circuit Surface) and (c) Heavily Non-stationary signal (Bump).	18
Figure 2.4 Comparisons of Skewness (Adapted from Harris and Ledwith, 1974).	20
Figure 2.5 Comparisons of Kurtosis (Adapted from Harris and Ledwith, 1974).....	20
Figure 2.6 Sampling a continuous function of time at regular intervals (Newland, 1993).	22
Figure 2.7 Partitioning the sequences x_r into two half sequences y_r and z_r (Newland, 1993).	23
Figure 2.8 Comparison between waveforms before and after Mastering.....	29
Figure 2.9 The output of a compressor is linear below the threshold and follows an input/output gain reduction ratio above this point (Adapter from Huber and Runstein, 2005).....	30
Figure 2.10 The output of a limiter is linear below the threshold and follows a high input/output gain reduction ratio (10:1, 20:1, or more) above this point (Adapter from Huber and Runstein, 2005).....	30
Figure 2.11 Typical expansion curves for expanders: output level versus Input level.	31
Figure 2.12 The output of a gate is linear above the threshold and follows an infinite expansion slope below this point gate (Huber and Runstein, 2005).	32
Figure 2.13 Schematic representations of the wavelet decomposition and grouping procedure (Adapted from Giacomini et al., 1999).....	35
Figure 2.14 (a) Schematic diagram of bump identification using trigger levels and (b) Schematic diagrams of the determination of a temporal bump time extent (Adapted from Abdulla et al, 2004).....	36
Figure 2.15 Non-synchronised bump reinsertion procedure (Adapted from Giacomini et al., 1999).....	38
Figure 2.16 Synchronised bump reinsertion procedure 1 (Adapted from Giacomini et al., 1999).....	39

Figure 2.17 Synchronised bump reinsertion procedure 2 (Adapted from Giacomini et al., 1999).....	40
Figure 2.18 MNMS algorithm flowchart (Adapted from Giacomini et al, 1999).	41
Figure 3.1 The flow of information through the memory system as proposed by Atkinson and Shiffrin (1968).....	43
Figure 3.2 Theoretical probability distributions of a “noise” and of a “signal – plus – noise” for two different values of signal strength (Adapted from Baird and Noma, 1978).	47
Figure 3.3 The signal detection diagram (Adapter from Heeger, 2003).	50
Figure 3.4 Distributions of a “noise” and a “signal plus noise” expressed in Z score values (Gescheider, 1997).	51
Figure 3.5 ROC curves for different detection criteria.	51
Figure 3.6 ROC curve for the signal plus noise and the noise distribution shown ($d' = 1$) obtained over different observer’s criterion.....	52
Figure 3.7 A basic ROC points graph showing four observers’ pair responses.....	53
Figure 4.1 Road surfaces used by MIRA for their steering wheel vibration tests.	57
Figure 4.2 10 second segments of the tangential acceleration time history measured at the steering wheel for each of the four road surfaces (The MIRA test).	59
Figure 4.3 Power Spectral Densities (PSD) calculated from the four tangential acceleration time histories of the 2 minute duration which were measured at the steering wheel (The MIRA test).....	61
Figure 4.4 Road surfaces used by Michelin for their steering wheel vibration tests.	62
Figure 4.5 10 second segments of the tangential acceleration time history measured at the steering wheel for each of the two road surfaces (The Michelin test).	63
Figure 4.6 Power Spectral Densities (PSD) calculated from the two tangential acceleration time histories of the 2 minute duration which were measured at the steering wheel (The Michelin test).....	64
Figure 4.7 Test measurements point for the accelerometer position at the steering wheel.....	65
Figure 4.8 Road surfaces used by the author for the Uxbridge steering wheel test.....	67
Figure 4.8 Road surfaces used by the author for the Uxbridge steering wheel test (continuation).	68
Figure 4.9 10 second segments of the tangential acceleration time history measured at the steering wheel for each of the eight road surfaces (The Uxbridge test).	70
Figure 4.10 Power Spectral Densities (PSD) calculated from the four tangential acceleration time histories of the 1 minute duration which were measured at the steering wheel (The Uxbridge test).....	72
Figure 4.11 Distribution of the statistical values of the fourteen road surfaces: <i>r.m.s.</i> acceleration level against VDV value.	73
Figure 5.1 Steering wheel rotational vibration test facility.....	75
Figure 5.2 Use of compensator digital filter: a) Comparison between target and test rig acceleration PSDs before filtering b) Comparison between target and test rig acceleration PSDs after filtering.	77
Figure 5.3 Results of the experiment to measure the effect of steering wheel acceleration magnitude on the human detection of road surface type in terms of percent correct detection (n=15).....	82
Figure 5.4 Results of the experiment to measure the effect of steering wheel acceleration magnitude on the human detection of road surface type in detectability index d' value (n=15).....	84
Figure 5.5 ROC points of tarmac surface for the laboratory experiment to measure the effect of steering wheel acceleration magnitude on the human detection of road surface type (n=15).....	85
Figure 5.6 ROC points of concrete surface for the laboratory experiment to measure the effect of steering wheel acceleration magnitude on the human detection of road surface type (n=15).	85
Figure 5.7 ROC points of cobblestone surface for the laboratory experiment to measure the effect of steering wheel acceleration magnitude on the human detection of road surface type (n=15).	86
Figure 5.8 ROC points of low bump surface for the laboratory experiment to measure the effect of steering wheel acceleration magnitude on the human detection of road surface type (n=15).	86

Figure 6.1 Results of the experiment to measure the effect of steering wheel acceleration frequency bandwidth on the human detection of road surface type (n=15), in terms of: (a) Percent correct detection rate and (b) detectability d' value detection.	93
Figure 6.2 ROC points of cobblestone surface for the laboratory experiment to measure the effect of steering wheel acceleration frequency bandwidth on the human detection of road surface type (n=15).	94
Figure 6.3 ROC points of tarmac surface for the laboratory experiment to measure the effect of steering wheel acceleration frequency bandwidth on the human detection of road surface type (n=15).	94
Figure 6.4 Power spectral densities of the experimentally acquired steering wheel acceleration signals, along with the frequency intervals selected for consideration for each type of road.....	97
Figure 6.5 Laboratory test stimuli for the Motorway road surface that were produced by means of digital Butterworth high-pass and band-pass eliminating filters.	98
Figure 6.6 Results of the laboratory experiments regarding the effect of the vibrational energy distribution of the steering wheel acceleration signal on the human detection of road surface type (n= 15).	100
Figure 6.7 Results of the laboratory experiments regarding the effect of the vibrational energy distribution of the steering wheel acceleration signal on the human detection of road surface type (n= 15).	101
Figure 6.8 ROC points for the Motorway surface stimuli regarding the effect of the vibrational energy distribution of the steering wheel acceleration signal (n= 15).....	102
Figure 6.9 ROC points for the Broken Concrete surface stimuli regarding the effect of the vibrational energy distribution of the steering wheel acceleration signal (n= 15).....	102
Figure 6.10 ROC points for the Broken Lane surface stimuli regarding the effect of the vibrational energy distribution of the steering wheel acceleration signal (n= 15).....	103
Figure 7.1 Standard deviation values used as critical threshold levels above which gain reduction or amplification was performed.	108
Figure 7.2 The effect of various compressor and expander factors used at the tarmac stimuli when the critical threshold levels are taken to be the three standard deviation values.....	109
Figure 7.3 Results of the experiment to measure the effect of compression and expansion of the steering wheel acceleration signals on the human detection of road type in percent correct detection (n=15) where: (a, b) Results at threshold level of ± 3 STD (c, d) Results at threshold level of ± 2 STD (e, f) Results at threshold level of ± 1 STD	113
Figure 7.4 Results of the experiment to measure the effect of compression and expansion of the steering wheel acceleration signals on the human detection of road type in detectability index d' value (n=15) where: (a, b) Results at threshold level of ± 3 STD (c, d) Results at threshold level of ± 2 STD (e, f) Results at threshold level of ± 1 STD	115
Figure 8.1 Power Spectral Densities (PSD) of the experimentally acquired steering wheel acceleration signals, showing the wavelet groups chosen for use in the current study.....	121
Figure 8.2 Results of the laboratory experiments regarding the effect of threshold level of the steering wheel acceleration signal on the human detection of road surface type in percent correct detection (n= 15).....	124
Figure 8.3 Results of the laboratory experiments regarding the effect of threshold level steering wheel acceleration signal on the human detection of road surface type in detectability index d' value (n= 15).	125
Figure 8.4 Power Spectral Densities (PSD) of the experimentally acquired steering wheel acceleration signals, showing the wavelet groups chosen for use in the study.....	127
Figure 8.5 Power Spectral Density of the original concrete road base stimuli and of the test stimuli obtained using compression ratios of 1.0, 2.0, 3.0 and 4.0.	128
Figure 8.6 Results of the laboratory experiments regarding the effect of the number of transient events of the steering wheel acceleration signal on the human detection of road surface type plotted in terms of percent correct detection (n= 15).	130
Figure 8.7 Results of the laboratory experiments regarding the effect of the number of transient events of the steering wheel acceleration signal on the human detection of road surface type plotted in terms of detectability index d' value (n= 15).	131
Figure 8.8 Results of the laboratory experiments regarding the effect of the transient events scaling of the steering wheel acceleration signal on the human detection of road surface type plotted in terms of percent correct detection (n= 15).	132

Figure 8.9 Results of the laboratory experiments regarding the effect of the transient events scaling of the steering wheel acceleration signal on the human detection of road surface type plotted in terms of detectability index d' value (n= 15).....	133
Figure 9.1 Power Spectral Densities (PSD) of the experimentally acquired steering wheel acceleration signals, showing the wavelet groups chosen for use in the experiment.....	139
Figure 9.2 Results of the laboratory experiments regarding the effect of the first set of guidelines for automotive steering vibration feedback on the human detection of road surface type in terms of percent detection rate (n= 15).....	142
Figure A.1 SVAN 947 Sound and Vibration Level Meter and Analyser manufactured by SVANTEK Ltd. used for the experimental steering vibration measurements. Part I.....	163
Figure A.2 SVAN 947 Sound and Vibration Level Meter and Analyser manufactured by SVANTEK Ltd. used for the experimental steering vibration measurements. Part II.	164
Figure A.3 Technical specifications for the LIVT™ accelerometer Series 3055B1 used for the experimental steering vibration measurements. Part I.....	165
Figure A.4 Technical specifications for the LIVT™ accelerometer Series 3055B1 used for the experimental steering vibration measurements. Part II.....	166
Figure B.1 Ensemble drawing of the steering wheel clamp used to measure the steering wheel vibration for the Uxbridge test.....	168
Figure B.2 Geometrical dimensions of the upper part of the steering wheel clamp used to measure the steering wheel vibration for the Uxbridge test.	169
Figure B.3 Geometrical dimensions of the lower part of the steering wheel clamp used to measure the steering wheel vibration for the Uxbridge test.	170
Figure C.1 Accelerometer position at the rotational steering wheel test rig, located on the top left side of the wheel.....	171
Figure C.2 Technical specifications for the monoaxial EGAS accelerometer used for the experimental laboratory tests.	172
Figure C.3 ENTRAN Certificate of calibration and specifications for the monoaxial EGAS accelerometer used to measure the steering wheel vibration test rig along the z-axis.....	173
Figure C.4 Technical specification for the multi-channel signal conditioning MSC6.	174
Figure C.5 Technical specification for the power amplifier PA100E and the shaker V20 used during the experimental laboratory tests.	175
Figure D.1 ROC points of concrete surface for the laboratory experiment to measure the effect of steering wheel acceleration compression on the human detection of road surface type ($\pm 3STD$, n=15).	177
Figure D.2 ROC points of concrete surface for the laboratory experiment to measure the effect of steering wheel acceleration expansion on the human detection of road surface type ($\pm 3STD$, n=15).	177
Figure D.3 ROC points of cobblestone surface for the laboratory experiment to measure the effect of steering wheel acceleration compression on the human detection of road surface type ($\pm 3STD$, n=15).	178
Figure D.4 ROC points of cobblestone surface for the laboratory experiment to measure the effect of steering wheel acceleration expansion on the human detection of road surface type ($\pm 3STD$, n=15).	178
Figure D.5 ROC points of tarmac surface for the laboratory experiment to measure the effect of steering wheel acceleration compression on the human detection of road surface type ($\pm 3STD$, n=15).....	179
Figure D.6 ROC points of tarmac surface for the laboratory experiment to measure the effect of steering wheel acceleration expansion on the human detection of road surface type ($\pm 3STD$, n=15).	179
Figure D.7 ROC points of concrete surface for the laboratory experiment to measure the effect of steering wheel acceleration compression on the human detection of road surface type ($\pm 2STD$, n=15).	180
Figure D.8 ROC points of concrete surface for the laboratory experiment to measure the effect of steering wheel acceleration expansion on the human detection of road surface type ($\pm 2STD$, n=15).	180
Figure D.9 ROC points of cobblestone surface for the laboratory experiment to measure the effect of steering wheel acceleration compression on the human detection of road surface type ($\pm 2STD$, n=15).	181

Figure D.10 ROC points of cobblestone surface for the laboratory experiment to measure the effect of steering wheel acceleration expansion on the human detection of road surface type ($\pm 2\text{STD}$, $n=15$).	181
Figure D.11 ROC points of tarmac surface for the laboratory experiment to measure the effect of steering wheel acceleration compression on the human detection of road surface type ($\pm 2\text{STD}$, $n=15$).	182
Figure D.12 ROC points of tarmac surface for the laboratory experiment to measure the effect of steering wheel acceleration expansion on the human detection of road surface type ($\pm 2\text{STD}$, $n=15$).	182
Figure D.13 ROC points of concrete surface for the laboratory experiment to measure the effect of steering wheel acceleration compression on the human detection of road surface type ($\pm 1\text{STD}$, $n=15$).	183
Figure D.14 ROC points of concrete surface for the laboratory experiment to measure the effect of steering wheel acceleration expansion on the human detection of road surface type ($\pm 1\text{STD}$, $n=15$).	183
Figure D.15 ROC points of cobblestone surface for the laboratory experiment to measure the effect of steering wheel acceleration compression on the human detection of road surface type ($\pm 1\text{STD}$, $n=15$).	184
Figure D.16 ROC points of cobblestone surface for the laboratory experiment to measure the effect of steering wheel acceleration expansion on the human detection of road surface type ($\pm 1\text{STD}$, $n=15$).	184
Figure D.17 ROC points of tarmac surface for the laboratory experiment to measure the effect of steering wheel acceleration compression on the human detection of road surface type ($\pm 1\text{STD}$, $n=15$).	185
Figure D.18 ROC points of tarmac surface for the laboratory experiment to measure the effect of steering wheel acceleration expansion on the human detection of road surface type ($\pm 1\text{STD}$, $n=15$).	185
Figure D.19 ROC points for the Broken Concrete surface stimuli regarding the effect of the threshold trigger level (TTL) of the steering wheel acceleration signal ($n= 15$).	186
Figure D.20 ROC points for the broken lane surface stimuli regarding the effect of the threshold trigger level (TTL) of the steering wheel acceleration signal ($n= 15$).	187
Figure D.21 ROC points for the Cobblestone surface stimuli regarding the effect of the threshold trigger level (TTL) of the steering wheel acceleration signal ($n= 15$).	187
Figure D.22 ROC points for the cobblestone surface stimuli regarding the effect of the number of the transient events of the steering wheel acceleration signal ($n= 15$).	188
Figure D.23 ROC points for the concrete surface stimuli regarding the effect of the number of the transient events of the steering wheel acceleration signal ($n= 15$).	188
Figure D.24 ROC points for the tarmac surface stimuli regarding the effect of the number of the transient events of the steering wheel acceleration signal ($n= 15$).	189
Figure D.25 ROC points for the cobblestone surface stimuli regarding the effect of the scale of the transient events of the steering wheel acceleration signal ($n= 15$).	190
Figure D.26 ROC points for the concrete surface stimuli regarding the effect of the scale of the transient events of the steering wheel acceleration signal ($n= 15$).	190
Figure D.27 ROC points for the tarmac surface stimuli regarding the effect of the scale of the transient events of the steering wheel acceleration signal ($n= 15$).	191
Figure D.28 ROC points for the original and the manipulated broken surface stimuli regarding the effect of first set of guidelines for an automotive steering feedback ($n= 15$).	192
Figure D.29 ROC points for the original and the manipulated broken concrete surface stimuli regarding the effect of first set of guidelines for an automotive steering feedback ($n= 15$).	192
Figure D.30 ROC points for the original and the manipulated broken lane surface stimuli regarding the effect of first set of guidelines for an automotive steering feedback ($n= 15$).	192
Figure D.31 ROC points for the original and the manipulated cobblestone surface stimuli regarding the effect of first set of guidelines for an automotive steering feedback ($n= 15$).	193
Figure D.32 ROC points for the original and the manipulated cobblestone city surface stimuli regarding the effect of first set of guidelines for an automotive steering feedback ($n= 15$).	193

Figure D.33 ROC points for the original and the manipulated concrete surface stimuli regarding the effect of first set of guidelines for an automotive steering feedback (n= 15).....	193
Figure D.34 ROC points for the original and the manipulated country lane surface stimuli regarding the effect of first set of guidelines for an automotive steering feedback (n= 15).....	194
Figure D.35 ROC points for the original and the manipulated motorway surface stimuli regarding the effect of first set of guidelines for an automotive steering feedback (n= 15).....	194
Figure D.36 ROC points for the original and the manipulated noise surface stimuli regarding the effect of first set of guidelines for an automotive steering feedback (n= 15).....	194
Figure D.37 ROC points for the original and the manipulated tarmac surface stimuli regarding the effect of first set of guidelines for an automotive steering feedback (n= 15).....	195

INDEX OF TABLES

Table 3.1 The four response outcomes of signal detection.	49
Table 4.1 Global statistical properties of the four road stimuli (The MIRA test).....	60
Table 4.2 Global statistical properties of the two road stimuli measured (Michelin test).....	64
Table 4.3 Global statistical properties of the eight road stimuli measured (The Uxbridge test)	71
Table 5.1 Geometric dimensions of the steering wheel rotational vibration test rig.....	75
Table 5.2 Physical characteristics of the group of pre-test participants involved in the laboratory experiments (n=8).....	78
Table 5.3 Steering wheel test rig stimulus reproduction accuracy for four scaled steering signals (using six scale values 0.8, 0.9, 1.0, 2.0, 3.0 and 4.0), three repetitions of each of the 24 stimuli were performed (n=8).....	78
Table 5.4 Physical characteristics of the group of test participants involved in the laboratory experiments (n=15).....	79
Table 6.1 Physical characteristics of the two groups of test participants involved in the laboratory experiments (n=15).....	90
Table 6.2 The <i>r.m.s.</i> acceleration values (m/s^2) of the five frequency bandwidth stimuli used for producing the laboratory test stimuli.....	91
Table 6.3 The <i>r.m.s.</i> acceleration values (m/s^2) of the un-manipulated and manipulated stimuli used for producing the laboratory test stimuli.	98
Table 7.1 Physical characteristics of the group of test participants involved in the laboratory experiment (n=15).....	107
Table 7.2 Global statistical properties of the three road stimuli used for producing the laboratory test stimuli to measure the effect of compression and expansion on the human detection.....	110
Table 8.1 Physical characteristics of the groups of test participants involved in the laboratory experiments (n=15).....	119
Table 8.2 Number of transient events identified in each wavelet group (WG) using different TTL values for all three stimuli used for producing the laboratory test stimuli.....	122
Table 8.3 Number of bump events extracted (NBE) from the original stimuli and the number of bump events that were reinserted (NBR) into the test stimuli using four time compression ratios.	128
Table 9.1 Physical characteristics of the group of test participants involved in the laboratory experiment (n=15).....	138
Table 9.2 Number of bump events extracted (NBE) from the original stimuli and the number of bump events that were reinserted (NBR) into the test stimuli.....	140

NOMENCLATURE

a	Scale dilation parameter ($a > 0$)
$a(t)$	Instantaneous acceleration value of a time series (m/s^2)
a_p	Acceleration amplitude (stimulus intensity)
A_k	Amplitude of the k_{th} harmonic
b	Time translation parameter
C_ψ	Admissibility wavelet condition
d'	Detectability index value
f	Frequency
f_k	Discrete frequency value (Hz)
f_s	Sampling frequency
Δf	Frequency step
G_{xx}	Auto-power spectral density of a time series [$(\text{m/s}^2)^2/\text{Hz}$]
$j k m n$	Variable integers
m	Mean value
M	Number of sampled values in a bump event
n	Stevens' power exponent
n_d	Number of averages
N	Number of data points (samples)
$p(x)$	Probability density function of a time series
$P(x)$	Probability distribution of a time series

$r.m.s.$	Root mean square (m/s^2)
$S(f_k)$	Power Spectral density of the random Gaussian process $y(t)$ corresponding to the frequency of the k_{th} harmonic f_k
t	Time (s)
T	Duration of a time series (s)
Δt	Sampling period (s)
W_h	Weighting filter for hand-arm vibration according to (ISO 5349)
W_s	Weighting filter for steering wheel hand-arm vibration
$W_\psi(a,b)$	Coefficients of the continuous wavelet transform
$W_\psi(m,n)$	Coefficients of the discrete scaled wavelet
x	Sampled variable
x_j	Instantaneous value of a time series at sample j
$x_{j\max}$	Maximum instantaneous value in a time series (m/s^2)
\bar{x}	Mean value
$x(t)$	Instantaneous value of a time series (m/s^2)
$X(\omega)$	Fourier transform dataset
y	Random Gaussian variable
$y(t)$	Random Gaussian process
Z	Z scores values
$\phi(t)$	Phase of a time series (degrees)
γ	Kurtosis (dimensionless)
λ	Skewness (dimensionless)
π	Mathematical constant equal to 3.1416
σ	Standard deviation (m/s^2)
σ_x^2	Variance of a time series (m/s^2)
ψ	Sensation Magnitude (Steven's Power Law)
$\psi(t)$	Wavelet function
$\psi_{a,b}(t)$	Scaled version of the base wavelet for the continuous wavelet transform
$\psi_{m,n}(t)$	Scaled version of the base wavelet for the discrete wavelet transform
ω	Angular frequency (s^{-1})

Σ	Denotes ‘the summation of’
*	Denotes the complex conjugate of a quantity
ARB	Anti-Roll Bar
ASA	Auditory Scene Analysis
ASTM	American Society for Testing and Materials
BS	British Standards
CF	Crest Factor
CR	Compression Ratio
CS	Coil Spring
CWT	Continuous Wavelet Transform
DAT	Digital Audio Tape
dBFS	Decibel Full Scale
DFT	Discrete Fourier Transform
dTi	Turbocharged diesel direct injection system
DW	Double Wishbone
Efi	Electronic Fuel injection fuel system
EHPS	Electro-Hydraulic Power Steering
EPS	Electric Power Steering
FFT	Fast Fourier Transform
FHC	Fixed-Head Coupé
HPS	Hydraulic Power Steering
I	Independent
I.M.S.	Independent and Macpherson strut
ISO	International Organization for Standardization
LIVM	Low Impedance Voltage Mode
LMS	Leuven Measurement Systems
LTM	Long Term Memory
MIRA	Motor Industry Research Association
MNMS	Mildly Non-stationary Mission Synthesis
NBE	Number of Bump Extracted
NBR	Number of Bump Reinserted
OWT	Orthogonal Wavelet Transform
OICA	International Organization of Motor Vehicle Manufacturers
PAS	Power Assist Steering

PES	Perception Enhancement Systems
PDF	Probability Density Function
R	Radial
ROC	Receiver Operating Characteristic
SAL	Saloon Sedan
SBW	Steer-By-Wire
SKE	Signal-Known-Exactly
SKS	Signal-Known-Statistically
SM	Sensory Memory
STD	Standard Deviation
STFT	Short Time Fourier Transform
STM	Short Term Memory
TB	Torsion Bar
TDF	Test Data File
TSD	Theory of Signal Detection
TTL	Threshold Trigger Level
VCA	Voltage-Controlled Amplifier
VDV	Vibration Dose Value
WG	Wavelet Group
WL	Wavelet Level
WM	Working Memory
WT	Wavelet Transform
WVD	Wigner-Ville Distribution
4Li	Four-Link

1. Automotive Steering Vibration as a Research Problem

Vibration stimuli reach automobile drivers by means of the pedals, the gearshift, the seat, the floor and the steering wheel, being this last one the principal sensory link between the driver and the automobile (Amman et al., 2005; Bianchini, E., 2005; Giacomini and Abrahams, 2000; Pak et al., 1991). In this context the word stimuli is taken to mean something external that elicits or influences a psychological activity or response on the part of the subject (Oxford English Dictionary, 2000). According to this definition, vibrational stimuli could help to the driver in the interpretation of many things including the type of road surface, the presence of water or snow, tyre slip and the dynamic state of subsystems such as the engine, the steering and the brakes (Giacomini and Woo, 2004). The stimuli are perceived, compared to models from long term memory and interpreted, with the consequent interpretation then influencing decision making.

Automobile manufacturers dedicate significant attention to noise and vibration suppression (Harrison, 2004) since high levels of noise and vibration for many people mean less vehicle quality and greater discomfort, but have they thought about the information that people receive through both sound and vibration? Many scenarios can be imagined in which the suppression of stimuli can result in a suppression of information. For many years, psychologists, cognitive scientists, and others have established the relation between stimuli and information (Newell, 1990, Simon, 1979, Gibson, 1969, Gibson and Gibson, 1955; Loomis, and Lederman, 1996). Given the above, the question of what information an automobile subsystem should transmit to the driver is not a simple one.

People attach great value to vision and to hearing due to the roles they play in making them aware of their surroundings. Therefore much research has been performed to understand the way in which people interpret the world through these two senses. The sense of touch is, however, a different matter because people often underestimate the role of touch in their perception of the world. In many cases, as it was stated above, touch could play the main role in the interpretation of an event. Loomis and Lederman (1996) have suggested that touch facilitates or makes possible virtually all motor activity, permits the perception of nearby objects, supports the understanding of spatial layout when viewing is not feasible, and informs of object properties such as temperature which are not accessible by means of the other senses. In this context, haptic perception has been defined by Loomis and Lederman (1996) as “the tactual perception in which both the cutaneous sense and kinesthesia convey significant information about distal objects and events”. Most tactually based perceptual and motor activity involves both cutaneous and kinesthetic information. The cutaneous sense is considered as the faculty of touch, while kinesthesia is considered instead to provide information about the relative positions and movements of the parts of the body as well as about muscular effort. Of specific interest to the automobile driver is the haptic information which is transmitted to the driver by means of the steering wheel vibration.

With the advent of electronically assisted steering and ‘by-wire’ technologies the question of what stimuli should reach the driver assumes great importance (Bretz, 2001; Jurgen, 1999; Ueki et al., 2004). From a comfort point of view, less steering vibration should be judged as better. Existing methodologies for estimating vibrational comfort (hand-arm or whole-body) based on the use of frequency weightings (ISO 5349-1, 2001; BS 6842-1, 2001), as well as those methodologies for evaluating vehicle drivability (Schoeggel, 2001) are all structured in such a way as to suggest that less vibration should be judged as better. This may not be appropriate in the case of information perceived by means of the steering wheel vibration, however, since scenarios can be imagined in which an increase in vibration level can help to clarify the nature of the road surface or the vehicle dynamic state (Giacomin and Woo, 2004). Although it is clear that not all vibration must be retained to clarify to the driver the environmental conditions, it is probable that some of the vibration must be maintained. Given the above, a methodology for quantifying the human ability to cognitively detect a road surface appears useful. Such a methodology could evaluate how people assimilate the information transmitted by means of the

vibrational stimuli occurring in automobile subsystems. Towards this goal several laboratory-based experiments were performed in order to achieve a first methodology for identifying which are the parameters or features used by the drivers to detect the road surface type. The experimental results are useful for both future steer-by-wire systems and also for current steering power systems.

Studies have shown that the global performance of a coupled person-machine system can be improved when certain low level perceptual and cognitive functions are assigned to the machine (Quek and Petro, 1993). In the past it has been argued that technology dehumanized life, but as people become committed to person-enhancing objects, this argument will need to be revisited. Making technology personable will entail learning about the human being. In the coming decades, converging technologies promise to increase significantly people's level of understanding, transform human sensory and physical capabilities, and improve interactions between mind and tool (Turkle, 2002; Roco and Bainbridge, 2002). The automotive steering is one important example of a person-machine interface which requires further research and understanding.

1.1 Automotive Steering System Architectures

Steering is the term applied to the collection of components, linkages, etc. which allow an automobile or other type of vehicle to follow a course determined by its driver. Gillespie (1992) stated that the most conventional steering arrangement is to turn the front wheels using a hand-operated steering wheel which is positioned in front of the driver, via the steering column, which may contain universal joints to allow it to deviate from a straight line. Two variants of conventional steering system are in common use, these being, the rack and pinion steering (see Figure 1.1) and the ball-and-nut steering. The latter is used when higher steering forces are required. Both systems are purely mechanical, with the steering wheel turning the pinion gear which moves the rack from side to side. As shown in Figure 1.1 this motion applies steering torque to the kingpins of the steered wheels via the tie rods and a short lever arm called the steering arm.

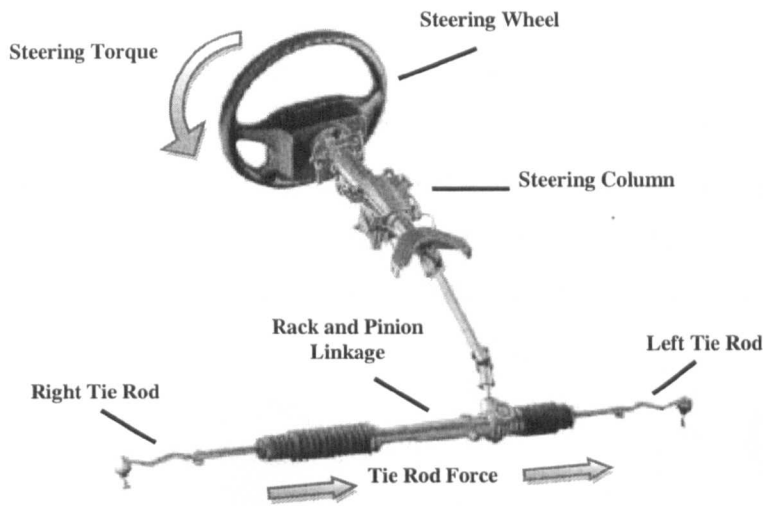


Figure 1.1 Mechanical Steering System (Adapted from Wolfgang, 2000).

Power steering is defined by the Bosch Automotive Handbook (2004) as “a system for reducing the steering effort on automobiles by using a power source to assist in turning the wheels”. Three types of power steering system are currently in mass production (Wolfgang, 2000; Ueki et al., 2004):

- 1) Hydraulic Power Steering (HPS),
- 2) Electro-Hydraulic Power Steering (EHPS), a hybrid system, and
- 3) Electric Power Steering (EPS).

For many years power steering technology has consisted of HPS which is based on the components of the mechanical steering systems with the addition of hydraulic pressure supplied by an engine-driven pump (Wong, 2001; Wang et al., 2005) as shown in Figure 1.2. These systems achieve a high level of performance in terms of ride and handling, cost and comfort.

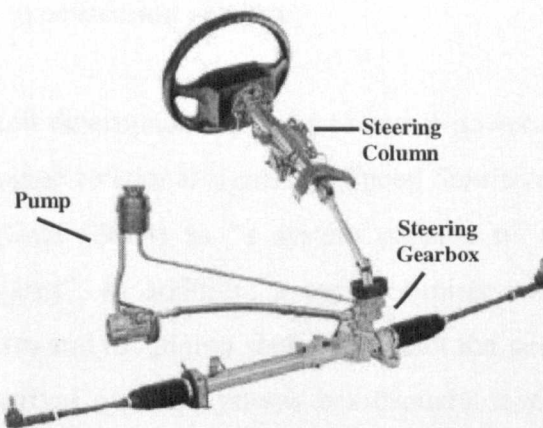


Figure 1.2 Hydraulic Power Steering System (Adapted from Wolfgang, 2000).

Current steering systems are more and more based on the use of electrical components. This is mainly because of two reasons: energy saving and installation simplification by modular design. In the case of EHPS systems such as the one shown in Figure 1.3a, the hydraulic pump is driven by an electric motor and runs independently from the engine. Since the speed of the pump is not subjected to the wide range of engine speeds, this reduces the power demand of the system and maintains all the basic properties of a hydraulic system.

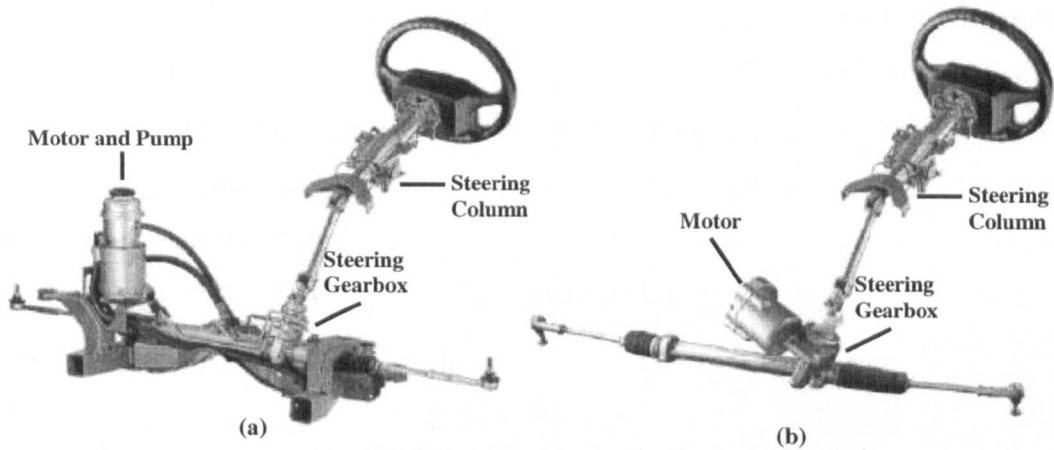


Figure 1.3 Current Steering Systems (Wolfgang, 2000): (a) Electro Hydraulic Power Steering System and (b) Electric Power Steering System.

EPS system as shown in Figure 1.3b consists of (Ueki et al., 2004):

- 1) a torque sensor located in the steering gearbox;
- 2) an electronic control unit which calculates signals from the torque sensor and supplies the necessary energy to the motor;
- 3) a motor that conveys an assisting force to a pinion shaft through a reduction gear mechanism; and
- 4) a rack-and-pinion type steering gearbox.

The electronic control unit determines the speed sensitive power assistance by processing the vehicle speed and engine rotational signals. A Speed Sensitive Power Steering (SSPS) system is defined by Ueki (2004) as “a system capable of adjusting steering force according to vehicle speed”. In addition, a torque limiter is positioned between the reduction gear mechanism and the pinion shaft, to protect the gear mechanism from road surface pressure. The arrival of EPS systems has brought several advantages. Electric actuation is a proven technology which offers several benefits including reliability, energy

efficiency and precise controllability (Iles-Klumpner et al., 2005). EPS is currently being applied widely in order to reduce fuel consumption and decrease installation costs.

In recent years important efforts have also been made in the area of by-wire technologies. The automotive industry is introducing decoupled actuators in order to improve driving comfort and safety and to reduce automobile cost by means of the greater design and installation flexibility offered by these systems. Steer-By-Wire (SBW) is a technology which replaces the mechanical interface between the steering wheel and the vehicle front wheels. SBW system has no direct mechanical link between the steering angle input of the driver and the direction in which the road wheels turn, as shown in Figure 1.4. Wires relay signals from the automobile's steering wheel to its front wheels by means of an electrically actuated motor.

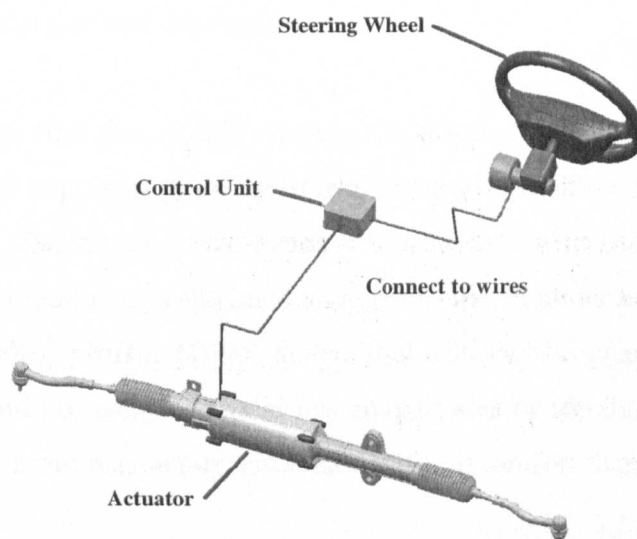


Figure 1.4 A steer by-wire system in an automobile.

Steer by wire systems offer a number of advantages in terms of packaging, noise performance and occupant crash protection due to the elimination of the steering column. The advantages also open the possibility for an alternative to the traditional steering wheel (Ward and Woodgate, 2004).

1.2 Discomfort Caused by Automotive Steering Vibration

Discomfort has been defined as any perceived disturbance to the well being of the subject (Costa, 1997; Griffin, 1990; Quehl, 2001). It is normally assumed that discomfort is associated with poor biomechanical factors (joint angles, muscle contractions, pressure

distribution) that produce feelings of pain, soreness, numbness, fatigue, and the like. Discomfort can often be alleviated by eliminating physical constraints. However, the elimination of physical constraints does not necessarily produce comfort (Griffin, 1990; Quehl, 2001). Comfort, instead, is defined by the Oxford English Dictionary (2000) as “the state of being physically relaxed and having a pleasant life”. The optimal condition of comfort can be defined as the neutral sensory condition, corresponding to the absence of discomfort stimuli. Researchers have questioned the common, unidimensional, definition of discomfort and comfort as representing the opposites of a continuous bipolar scale which ranges from a state of extreme discomfort through a neutral state to a state of extreme comfort (Quehl, 2001). Even though some motions may be the source of pleasure or satisfaction, and hence produce no discomfort, according to Griffin (1990) the study of human vibration has mainly concerned the extent to which motions are responsible for displeasure, dissatisfaction and discomfort.

As was stated in the first part of this chapter, the discomfort caused by vibration of the steering wheel is an important property for the acceptability of an automobile (Harrison, 2004). Vibration is transmitted to the hands and arms by means of the steering wheel. It may also be transmitted through the hand and arm to the shoulder and beyond (Giacomin and Abrahams, 2000). Griffin (1990) stated that automobile steering wheel vibration exposure of the hand normally occurs at low magnitudes or for short durations, and that these exposures are more reasonably associated with discomfort than injury or disease.

According to Reynolds and Angevine (1977) hand-arm vibration (HAV) occurs when the palm of the hand or the fingers are in contact with a vibrating surface. HAV often occurs along three translational axes, it may differ at the two hands, and it may vary along the length of the tool or workpiece handle. Further, the dependence of vibratory discomfort upon vibration frequency differs for the various directions of vibration. The human hand has been shown to be capable to discriminating the motion along three axis (Miwa, 1967; Mishoe and Suggs, 1977; Reynolds and Keith, 1977, Reynolds and Soedel, 1972).

The orientation of the coordinate system used to measure hand-arm vibration is normally be defined with reference to an appropriate basic-centric coordinate system (ISO 5349-1, 2001; BS 6842, 2001). This system is defined according to the orientation of the hand with respect to specific directions of the tool or workpiece (see Figure 1.5). According to

the BS 6842 (2001) measurements along the three axis should be made using an accelerometer which should be placed at or near the surface of the hand(s), the resulting signals being labelled as $a_{x,hw}$, $a_{y,hw}$, and $a_{z,hw}$.

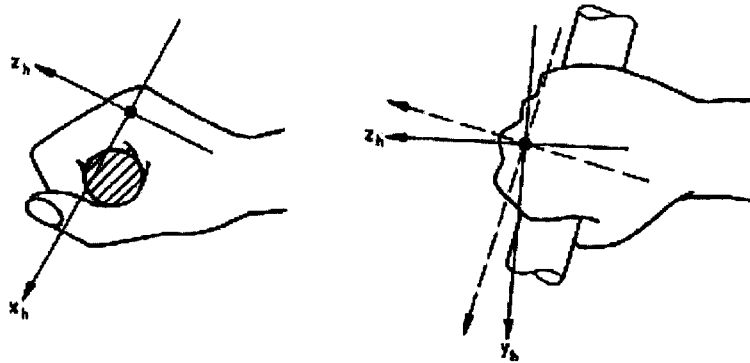


Figure 1.5 Coordinate system for the hand. Anatomical Coordinate System and Basic-centric Coordinate System (Adapted from ISO 5349, 2001 and BS 6842, 2001).

In order to assess the vibration felt, the acceleration values are usually weighted according to the frequency and the direction in which the vibration is applied. Frequency weightings are applied to convert the physical input acceleration into the human perceived acceleration. ISO 5349-1 (2001) and BS 6842 (2001) specify frequency weighting W_h for use along the standardized axis of measurement. The same frequency weighting is used for each of the three axes of vibration at the point of entry to the hand. Figure 1.6 shows how W_h is defined by the hand-transmitted vibration standards (ISO 5349-1, 2001 and BS 6842, 2001).

The evaluation of steering wheel vibrational discomfort by means of the W_h has often been performed in the automobile industry (Pak et al., 1991; Isomura et al., 1995). However, Giacomini et al. (2004) proposed a frequency weighting for evaluating the human subjective discomfort response to the rotational vibrations specifically encountered in automobiles. Figure 1.6 shows the comparison between the proposed frequency weighting W_s and the standard weighting W_h . The comparison suggests important differences, with a particularly note worthy point being the lower human sensitivity to vibration indicated by W_h at frequencies which are lower than 6.3 Hz.

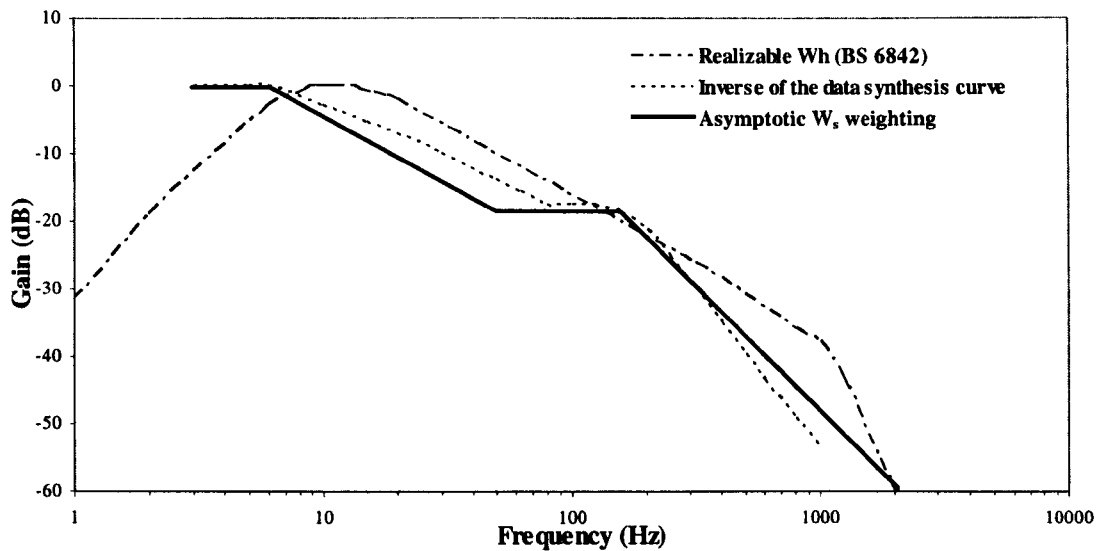


Figure 1.6 Comparison between the proposed frequency weighting W_s for rotational steering wheel vibration and frequency weighting W_h (Adapted from Giacomini et. al, 2004).

The magnitude of a vibration can be quantified by either, its displacement, its velocity or its acceleration. For practical convenience, the vibration intensity is commonly expressed in terms of acceleration, which is normally expressed in meters per second squared (m/s^2). BS 6842 (1997) requires that the vibration magnitude be calculated as an average value of frequency-weighted acceleration, using a root mean square (*r.m.s.*) acceleration value. The measurement of the *r.m.s.* acceleration is convenient because accelerometers are currently the cheapest and most widely utilised transducers, and instrumentation for the calculation of *r.m.s.* values is readily available.

Besides the magnitude, frequency, direction and duration of an applied vibration the subjective discomfort is also effected by the posture and orientation of the hand-arm and body (BS 6842, 2001), which may cause differences in the response of the same person on different occasions (intra subject variability).

The field of psychophysics (Geschieder, 1997) provides perceptual response models which are applicable to all sensory modalities including vibration. Psychophysical theory suggests that the most basic relation between vibration level and discomfort is given by the Steven's power law:

$$\psi = k a_p^n \quad (1.1)$$

where ψ is level of sensation, a_p is the acceleration amplitude (stimulus intensity), k is a constant which depends on the specific measurement scale used to define the sensation and on the units used to express the acceleration, and finally, n is the exponent that determines the increase in feeling. The well-known Steven's Power Law has been used in many research studies to model the human subjective response to both whole-body vibration (Hacaambwa and Giacomini, 2005) and to hand-arm vibration (Ajovalasit and Giacomini, 2005).

1.3 Feel and Information Arising from Automotive Steering Vibration

The top design priorities for power-assisted steering are traffic safety and driving discomfort. Legal limits of steering-assistance attempt to define safety standards; more power assistance eases control of the automobile, but excessive assistance leads to lack of 'feel' for the road, in other words, to lack of information. The driver's feeling during steering is related to characteristics such as the steering torque, yaw rate and lateral acceleration generated according to the steering angle. Fujinami et al. (1995) states that the steering feel is classified accordingly into the three categories: steering effort; steering returnability; and steering torque. Steering roughness and steering feel are major aspects in which automobile manufacturers can distinguish their products with respect to their competitors (Verhoeff et al., 2004).

Although there are several points of contact between the driver and the automobile through which the driver perceives vibration, the steering wheel is commonly considered the most important source of feedback information. This is due to the great sensitivity of the skin tactile receptors of the hand (Lee, 1998; Morioka, 1999), as well as the lack of intermediate structures such as shoes and clothing which can act to attenuate the transmission of vibrational stimuli to the driver.

In this context 'feel' is taken to mean something that people perceive by the sense of touch. It can be assumed that drivers 'feel' the road through the mechanical link to the wheels. For example, a grooved pavement makes the wheels vibrate, hence the mechanical links between the wheels and steering wheel vibrate in turn. Similarly, the mechanical links provide a certain feel to the steering wheel when the driver turns it. In the case of a steer-by-wire system which needs to emulate the feel of a traditional

mechanical steering system, it must use sensors on the wheel hub and suspension components and its electrical motor to produce realistic and informative steering wheel motion. That requires an active system which is constantly changing its response based on the road conditions.

According to both Verhoeff et al. (2004) and Giacomini (2005) the main challenge for electrical steering systems and for steer-by-wire systems is to achieve a steering feel similar or better than that of conventional systems. The idea should be to re-create the driving feel by providing feedback.

1.4 Perception Enhancement for Automotive Steering Systems

Giacomini (2005) has stated that the concept of Perception Enhancement Systems (PES) “emerges from the observation that not all machine emissions are informative, and that only certain cognitively-relevant features from the environment have meaning for humans”. In this light, the goal is therefore to design engineering systems which selectively amplify the key environmental phenomena so that humans can better interact with their machines.

Giacomini (2005) proposed a definition for an automotive steering perception enhancement system as any device which optimises the feedback to the driver of information about the interaction between the automobile and its surrounding environment. Such a system treats the data from an information theoretic point of view, and optimises the person-machine interface so as to make the vehicle feel more like an extension of the driver’s body. Such a system might be composed of electronic systems (see Figure 1.7) which have the function of identifying the significant vibration stimuli, occurring at the tyres and suspensions, which are required by the driver, and of transferring and transforming the stimuli in order to optimise detection and awareness (Giacomini and Woo, 2004).

A question that requires further research is: what steering hardware and software is required to achieve ‘the highest possible rate of detection of the current driving situation and of the dynamic state of the automobile’? The answer is not a simple one, but it can be suggested that such a system would necessarily require measurement sensors, electronics

for signal processing, machine intelligence and actuators for delivering stimuli to the automobile driver. If the system is designed based on knowledge of the human psychophysical and cognitive response, a steering perception enhancement system for an automobile can be achieved.

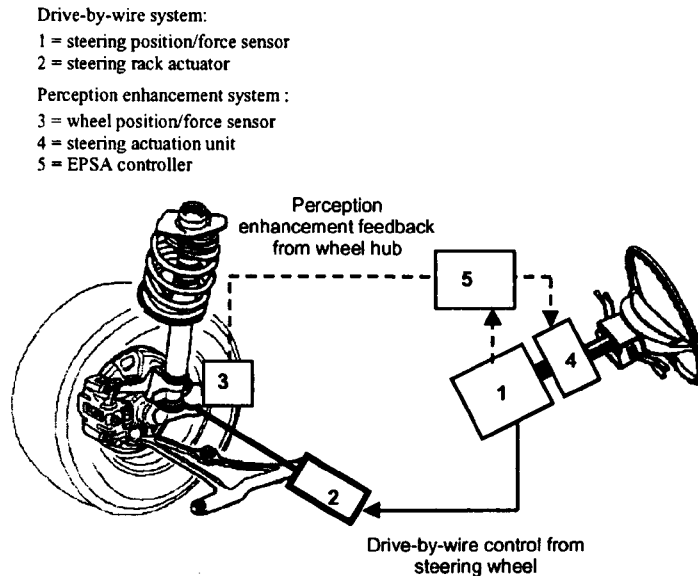


Figure 1.7 An approach of a perception enhancement system for a ‘by-wire’ steering (Giacomin and Woo, 2004)

1.5 The Objectives of the Research

According to Lakoff (1987) the technical specifications for interfaces such as Perception Enhancement System depend critically on the perceptual and cognitive characteristics of humans. Focussing on human steering perception, three questions naturally arise which can be defined as the issue of scale, the issue of frequency distribution and the issue of transient events. A detailed understanding of how human situational awareness changes as a function of the steering vibration scale, frequency distribution and transient events is required in order to define the technical specifications for an automotive steering perception enhancement system.

In order to understand the issues involved road surface detection was chosen as a test of the human cognitive response to steering wheel vibration. Road surface information is often gathered by means of the vision sense modality, but many driving scenarios exist in which the steering vibration feedback plays the leading role in the detection task. Night

time driving or driving in fog or rain are examples of situations in which the tactile perception can become dominant.

The detection problem may be of relevance to the designers of both traditional and by-wire steering systems since careful considerations are and will be necessary when choosing the specifications of the steering feedback for each driving condition. When considering current steering system technology in road vehicles, quantities of primary interest are the feedback gains and the feedback bandwidth over which the steering systems should operate. Particularly, the feedback frequency band over which the steering systems should operate may be of great importance since some by-wire steering actuators do not reach high response frequencies.

Since the human nervous system pays great attention to high amplitude event it might be the case that the human cognitive mechanism to detect road type uses individual transient features of the time history. The possibility of measuring the sensitivity of the human detection task to changes in the number or scale of individual transient events of the vibration stimuli offers to steering designers information which could be used to design the feedback characteristics of the steering system. Knowledge about human reactions to individual characteristics of the transient events would permit designers to tailor the system so as to optimise the useful information carrying events.

In order to investigate the relationship between steering vibration and the human detection of the road surface type, several research objectives were defined to:

1. Determine the effect of steering wheel acceleration magnitude on the human ability to detect road surface type, adopting the theory of signal detection as the analytical framework for the analysis.
2. Determine how the human detection of road surface type improves or degrades as a function of the frequency distribution of the steering acceleration signal, adopting the theory of signal detection as the analytical framework for the analysis.

3. Determine if signal transformations used in the field of music such as compressors or expanders improve or degrade the detection of road surface type, adopting the theory of signal detection as the analytical framework for the analysis.
4. Determine how the human detection of road surface type improves or degrades as a function of the number and size of the individual transient events which are contained in the steering acceleration signal, adopting the theory of signal detection as the analytical framework for the analysis.
5. Define a first set of guidelines for the feedback properties which an automotive system should have.

2. Signal Processing Methods

The primary goal of this chapter is to provide an introduction to the definitions, techniques and algorithms from the field of digital signal processing which are fundamental towards the understanding of the experiments performed during the research which is described in this thesis.

2.1 Classification of signals

McClellan et al. (2003) defines signals as patterns of variations that represent or encode information. For most purposes a signal can be defined simply as a mathematical function

$$y = f(x) \quad (2.1)$$

which can be classified into the categories of deterministic and random (Newland, 1993; Peebles, 1993; Mallat, 1998; Kudritzki, 2001). According to Newland (1993) a deterministic signal is one which is fully predictable given the existence of underlying physical laws while Peebles (1993) defines a random signal as a time waveform that can be characterized only in some probabilistic manner. A generally accepted system of signal classification is presented in Figure 2.1.

A deterministic signal can further be characterized as being periodic or a non periodic. A signal is periodic if it repeats with a characteristic period for all time. A signal is non periodic, instead, if it only exist for a finite time range (transient signal) or when one or more of the signal statistical parameters change with time (aperiodic). Periodic signals can further be characterized by having one single frequency (sinusoidal signal) or being a superposition of two or more harmonic waves (complex periodic). When the value of the

excitation at a given time cannot be fully predicted, the excitation is instead said to be non deterministic or random.

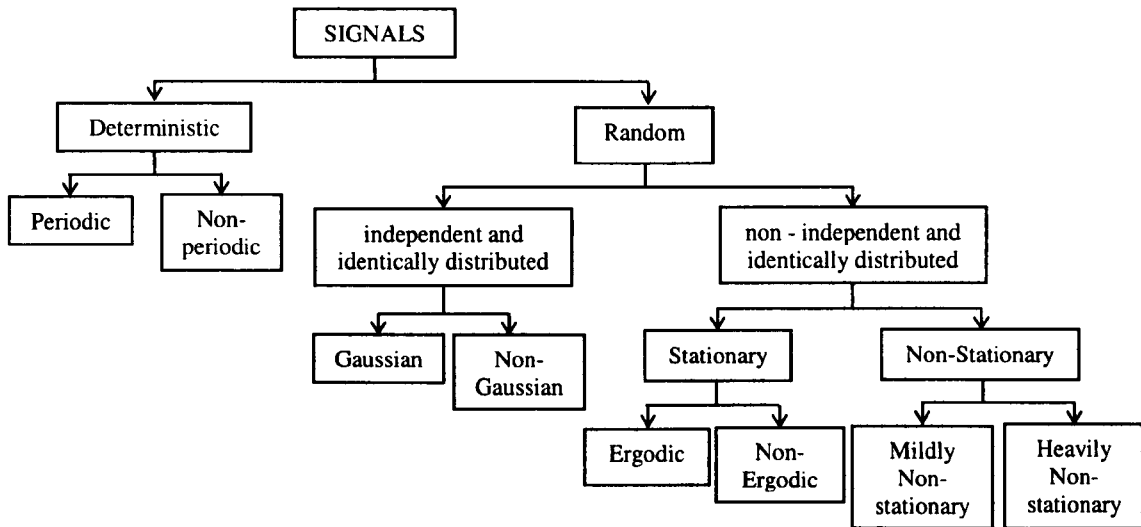


Figure 2.1 The classification of random signals.

2.1.1 The Random Process

The term random or stochastic refer to a general class of time waveforms which is frequently encountered in practical systems. The term ‘stochastic’ is derived from the Greek word for ‘by trial and error’ or ‘hit and miss’. Such a signal can be described only in terms of a probability distribution and of statistical averages computed over the ensemble of the sample records representing the random process. The probability distribution $P(x)$ for a random process is defined as (Bendat and Piersol, 1986):

$$P(x) = \int_x^{x+dx} p(x) dx \quad (2.2)$$

where $p(x)$ is the Probability Density Function (PDF) expressing the probability that the random variable takes a value between x and $x + dx$.

2.1.1.1 The Gaussian Distribution

A commonly used model of a stationary random process is the Gaussian distribution, which occurs when random signal amplitudes follow the well known ‘bell-shaped’ probability distribution illustrated in Figure 2.2.

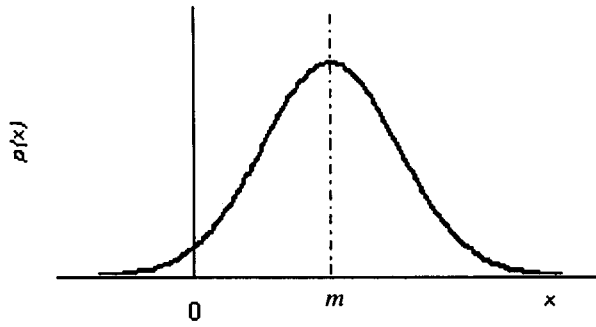


Figure 2.2 The Gaussian distribution

In this case the distribution of amplitudes is described by the mathematical expression

$$p(x) = \frac{1}{\sqrt{2\pi}\sigma} \exp^{-(x-m)^2/2\sigma^2} \quad (2.3)$$

where $p(x)$ is the probability of occurrence of the amplitude x and where m and σ are constants (the mean value and the variance, respectively). Newland (1993) suggests that the *normal* or *Gaussian* probability distribution is extensively used in random vibration theory to approximate the characteristics of random excitation. The function is symmetric about the mean value m , where it achieves its maximum value.

2.1.1.2 Stationarity and Ergodicity

A stationary random process is defined by Newland (1993) as one for which the probability distribution obtained for a sample data ensemble does not depend on time. According to Bendat and Piersol (1986) stationary signals exhibit constant statistical properties across the signal length. Specifically, global statistics such as the mean value, the root mean square value, the variance and the standard deviation value are independent of time. The statistics of non-stationary signals, on the other hand, are highly dependant on the measure of time. If only the mean and standard deviation are constant, a signal is considered to be weakly stationary. A process in which all probability distributions are invariant with time is considered to be strictly stationary.

Another term for describing a random process is that of ergodicity. An ergodic random process is one for which the ensemble averages can be exchanged for the time averages (Harris and Ledwidge, 1974; Peebbles, 1993). An ergodic signal is one for which a single sample, or single experimental measurement, is statistically representative of all possible measurements. Ergodicity is a very restrictive form of stationarity, and it is often difficult

to prove that it constitutes a reasonable assumption in many physical situations. Nevertheless, a process is often assumed to be ergodic in practice in order to simplify problems. It is important to note however that if a process is ergodic it must also be stationary. Harris and Ledwidge (1974) have stated that all ergodic processes are stationary, but that the converse is not necessarily true.

According to Giacomini et al. (1999) non-stationary signals can be further divided into two categories, mildly non-stationary and heavily non-stationary. Figure 2.3 presents automobile steering acceleration signals which exhibit stationary, mildly non-stationary and heavily non-stationary characteristics.

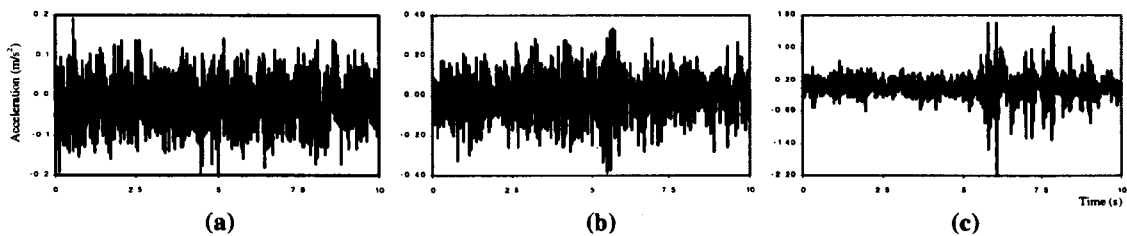


Figure 2.3 Examples of a stationary and non-stationary time histories: (a) stationary Gaussian signal (Highway Surface), (b) Mildly Non-stationary signal (Speed Circuit Surface) and (c) Heavily Non-stationary signal (Bump).

A mildly non-stationary signal is defined by Priestley (1988) as a random process with stable mean, variance and root-mean-square values for most of the record, but with short periods of changed signal statistics due to the presence of transient behaviour. A heavily non-stationary signal is defined in a similar manner to mildly non-stationary signals, but is characterised by the presence of more transient events.

2.2 Global Signal Statistical Parameters

Many authors have suggested the use of global signal statistics for the purpose of summarising and classifying random signals (Bendat and Piersol, 1986; Erdreich, 1986). In the field of vibro-acoustics the most commonly used statistics are the mean value, the standard deviation (SD) value, the root-mean-square (*r.m.s.*) value, the skewness value, the kurtosis value, the Crest Factor (CF) value and the Vibration Dose Value (VDV).

For a time series sampled for a period of time T_s at f_s samples per second, with a total of $N=T_s \cdot f_s$ sampled data values $x(i)$, the global statistical parameters are defined as follows.

2.2.1 Mean Value and Standard Deviation Value

The mean value \bar{x} is given by,

$$\bar{x} = \frac{1}{N} \sum_{j=1}^N x_j \quad (2.4)$$

while for the same time series the Standard Deviation (SD) value σ is given by,

$$\sigma = \left\{ \frac{1}{N} \sum_{i=1}^N [x(i) - \bar{x}]^2 \right\}^{1/2} \quad (2.5)$$

The mean and the SD value are considered the first and the second statistical 'moments' of the random process.

2.2.2 Root Mean Square Value

The overall energy associated with a signal is normally quantified by means of the root-mean-square (*r.m.s.*) value. For a time series, the *r.m.s.* value is defined as

$$r.m.s. = \left\{ \frac{1}{N} \sum_{j=1}^N x_j^2 \right\}^{1/2} \quad (2.6)$$

In the case of a zero mean process, the standard deviation and the *r.m.s.* are equal.

2.2.3 Skewness Value

The skewness value λ of a random process is defined as the average of the instantaneous vibration values cubed. In dimensionless form it is defined as

$$\lambda = \frac{1}{N} \sum_{j=1}^N \left(\frac{x_j - \bar{x}}{\sigma} \right)^3 \quad (2.7)$$

In the case of a normal distributed random process with zero mean, the skewness value results as zero. The skewness, which is a third statistical moment, characterises the degree of asymmetry of a distribution around its mean value. As illustrated in Figure 2.4, a positive skewness indicates a distribution with an asymmetric tail extending toward more

positive values, while a negative skewness indicates a distribution with an asymmetric tail extending toward more negative values.

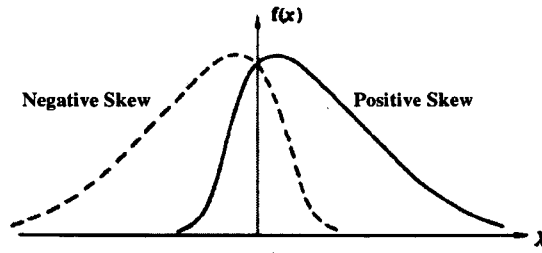


Figure 2.4 Comparisons of Skewness (Adapted from Harris and Ledwidge, 1974).

2.2.4 Kurtosis Value

The kurtosis value γ of a random process is defined as the average of the fourth power of the instantaneous vibration values and can be expressed in dimensionless form as

$$\gamma = \frac{1}{N} \sum_{j=1}^n \left(\frac{x_j - \bar{x}}{\sigma} \right)^4 \quad (2.8)$$

Kurtosis is highly sensitive to outlying data and as such can be thought of as the relative ‘peakedness’ of the vibration signal as shown in Figure 2.5. The importance of kurtosis as a metric is because it helps to quantify the extent of departure from stationary Gaussian distribution, for which the kurtosis value should be approximately 3.0. Higher kurtosis values indicate that there are more extreme values present in the data than would be expected from a Gaussian distribution (Harris and Ledwidge, 1974; Mallat, 1998; Newland, 1993).

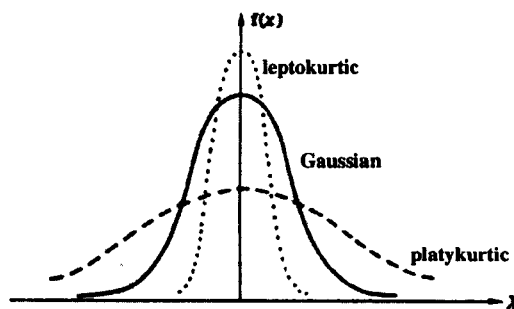


Figure 2.5 Comparisons of Kurtosis (Adapted from Harris and Ledwidge, 1974).

2.2.5 Crest Factor Value

The Crest Factor (CF) is defined as the ratio of the maximum instantaneous value of a sampled signal and the calculated *r.m.s.* value.

$$CF = \frac{x_{j\max}}{r.m.s.} \quad (2.9)$$

Crest factors can be either positive or negative depending on the sign of the maximum instantaneous value. For a *Gaussian* distribution the crest factor should normally lie in the range 3.5 to 4.5.

2.2.6 Vibration Dose Value

In signal processing applications involving the evaluation of human exposure to vibration, the vibration dose value is commonly used. The vibration dose value (VDV) of an acceleration time series is given by

$$VDV = (T_s \cdot \gamma)^{1/4} \cdot \sigma = \left[\frac{T_s}{N} \sum x^4(t) \right]^{1/4} \quad (2.10)$$

The evaluation of vibration severity is defined in the British Standards (BS EN 590, 2005; ISO 8041, 2005) as

$$VDV = \left[\int_0^T a^4(t) dt \right]^{1/4} \quad (2.11)$$

where T is the duration over which the VDV value is determined and $a(t)$ is the instantaneous acceleration. The VDV value provides a cumulative measure of the vibration exposure. From equation 2.10 it can be noted that exists a close correspondence between kurtosis and the VDV.

2.3 Frequency Domain Analysis

2.3.1 The Fourier Transform

Spectral analysis is widely used to analyse vibration signals (Piersol, 1992; Rahnejat, 1998). The mathematical function used to transform a time data series $x(t)$ into the frequency domain is called the Fourier Transform. The Fourier transform is used to convert a non-periodic function of time, $x(t)$, into a continuous function of frequency. The Fourier Transform of $x(t)$ is defined by the expression

$$X(\omega) = \int_{-\infty}^{+\infty} x(t) e^{-i\omega t} dt \quad (2.12)$$

where $i = \sqrt{-1}$ and ω is called the frequency variable, which is in units of rad/s in SI units. From a Fourier transformed dataset $X(\omega)$ it is also possible to reverse the transformation by obtaining its inverse;

$$x(t) = \int_{-\infty}^{+\infty} X(\omega) e^{i\omega t} d\omega \quad (2.13)$$

Equations 2.12 and 2.13 are called the Fourier Transform pairs, and they exist if $x(t)$ is continuous and integrable as defined by the admissibility condition

$$\int_{-\infty}^{+\infty} |x(t)| dt < \infty \quad (2.14)$$

2.3.2 The Discrete Fourier Transform (DFT)

Frequency analysis is concerned with the estimating of the spectrum of a random process $x(t)$ by analysing the discrete time series (see Figure 2.6) obtained by sampling a finite length of the sample function.

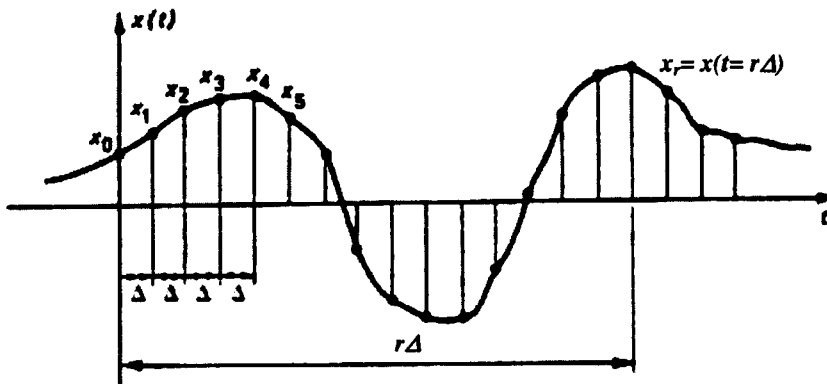


Figure 2.6 Sampling a continuous function of time at regular intervals (Newland, 1993).

In most applications the Fourier transform is applied to sampled data on a digital computer. The digital interpretation of the Fourier transform is called the Discrete Fourier Transform (DFT) and is defined for N discrete samples of $x(t)$ as

$$X(\omega) = \frac{1}{N} \sum_0^{N-1} x(t) e^{-i\omega t/N} \quad (2.15)$$

for $\omega = 0, 1, 2, \dots, N-1$. The inverse of the discrete Fourier transform is defined by

$$x(t) = \sum_0^{N-1} X(\omega) e^{i\omega t/N} \quad (2.16)$$

for $x = 0, 1, 2, \dots, N-1$. Again, the continuity and differentiability of the underlying processes are necessary conditions for the existence of the transform and of its inverse.

2.3.3 The Fast Fourier Transform (FFT)

The DFT makes possible the computer implementation of the Fourier Transform, but it is not efficient. The number of complex multiplications and additions required to implement equations 2.15 and 2.16 is proportional to the square of the number of data points N . For every $X(\omega)$ which is calculated, it is necessary to use all $x(0), \dots, x(N-1)$ data points.

It has been shown, however, that the decomposition of equation 2.15 can be achieved using a number of multiplication and addition operations which is proportional to $N \log_2 N$. The decomposition procedure in question is called the Fast Fourier Transform (FFT) algorithm. The FFT works by partitioning the full sequence x_r into a number of shorter sequences, it then combines together in a way which takes advantage of the symmetry of the matrix of reduction operations so as to yield the full DFT of x_r .

If the full sequence x_r (see Figure 2.7a) is partitioned into two shorter sequences y_r and z_r (Figure 2.7b), two half sequences are yielded. The half sequence are expressed as $y_r = x_{2r}$ and $z_r = x_{2r+1}$ when $r=0,1,2,\dots, (N/2 - 1)$.

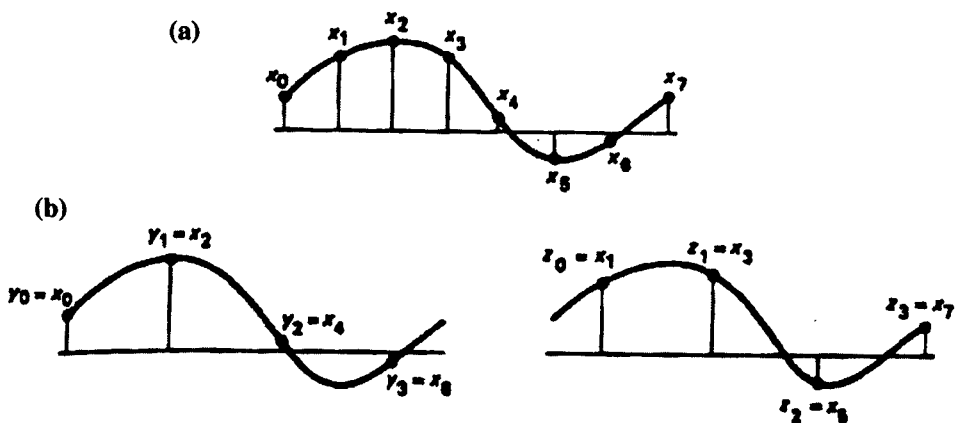


Figure 2.7 Partitioning the sequences x_r into two half sequences y_r and z_r (Newland, 1993).

The DFT's of these two short sequences, Y_k and Z_k , after simplification of the expression 2.15 are found to be

$$Y_k = \frac{1}{(N/2)} \sum_0^{N/2-1} y_r e^{-\frac{i\omega r}{(N/2)}} \quad k = 0, 1, 2, \dots, (N/2-1)$$

$$Z_k = \frac{1}{(N/2)} \sum_0^{N/2-1} z_r e^{-\frac{i\omega r}{(N/2)}} \quad (2.17)$$

Returning to the DFT of the original sequence and considering rearranging the summation into two separate sums similar to those occurring in equation 2.17, the resultant equation is the heart of the FFT method, mathematically expressed as

$$X_k = \frac{1}{2} \left\{ Y_k + e^{-\frac{i\omega r}{N}} Z_k \right\} \quad (2.18)$$

A useful representation in the case of random vibration signals is the autospectral density function which is commonly referred to as the Power Spectral Density (PSD) (Bendat and Piersol, 1986). The PSD represents the mean squared value as a function of frequency. It avoids the problem that random signals, producing a continuous frequency spectra, have the signal energy measured within a certain frequency band which depends on the width of that band (Bendat and Piersol, 1986). Because the Fourier Transform (equation 2.15) is computed only on one time interval, the spectrum is not typical of the complete time history. Averaging of the spectra from different intervals of the signal is thus necessary in order to obtain a more accurate representation. The PSD of a time series is thus defined as:

$$G_{xx}(f) = \frac{2}{n_d T} \sum_{i=1}^{n_d} |X_i(f, T)|^2 \quad f > 0 \quad (2.19)$$

where $X_i(f, T)$ is the FFT of the signal computed over the i^{th} data interval of duration T and n_d is the number of averages used in the calculation. The segment duration T determines the frequency resolution $\Delta f = 1/T = 1/N_{data} \cdot f_s$ for the FFT computation, and is normally chosen based on the characteristics of the type of data being analysed.

2.4 Time-Frequency Domain Analysis: The Wavelet Transform

The averaging process associated with the methods described in the previous sections can lead to a loss of information regarding the transient events present in the signal. An

extension of the classical analysis which is based on the assumption of the stationarity of the signal, to the analysis of a signal whose characteristics change in time, leads to the definition of time-frequency analysis (Piersol, 1992; Newland, 1994; Mallat, 1998). The most commonly used forms of time-frequency analysis are the Short Time Fourier Transform (STFT) (Hodges et al., 1985; Lim and Witer, 2000), the Wigner-Ville Distribution (WVD) (Staszewski et al., 1997) and the Wavelet Transform (Li et al., 1999). Of these methods, the wavelet transform has the advantage of a linear representation and offers the advantage of a multi-resolution analysis over the time-frequency plane (Mallat, 1998).

The wavelet transform is a linear transformation that decomposes a given function $x(t)$ into an infinite number of localised functions $\psi(t)$ called wavelets. Wavelets are mathematical tools for the analysis of non-stationary signals which perform multi-resolution analysis in both the time and frequency domains (Chui, 1992; Newland, 1994; Mallat, 1998). Wavelets have advantages over traditional Fourier methods in analyzing physical situations where the signal contains discontinuities, abrupt changes and sharp spikes (McHutchon, 2005). A wavelet is a function which adheres to the following admissibility condition (Chui, 1991; Mallat, 1998).

$$0 < C_{\psi} = \int_{-\infty}^{+\infty} \frac{|\Psi(f)|^2}{f} df < \infty \quad (2.20)$$

where $\Psi(f)$ is the Fourier transform of $\psi(t)$. To guarantee that this integral is finite the wavelet function must be defined in such a way that $\Psi(0)$ is equal to zero, such that the wavelet has a mean value of zero. If $\Psi(0)$ is zero the function is continuously differentiable, then the admissibility condition reduce to the condition that the wavelet function be of finite energy, meaning

$$\int_{-\infty}^{+\infty} |\psi(t)| dt < \infty \quad (2.21)$$

The transform based on wavelets trades resolution in a manner that varies over the time-frequency plane, in contrast to other type of analysis in which time-frequency resolution is uniform. The wavelet transform has a wide variety of applications including time-frequency analysis, graphical and audio data compression, noise filtering, feature extraction and fault detection (Wang and Mc Fadden, 1995; Lee and White, 2000).

Depending on the type of information that is required, two different forms of the wavelet transform are used: the Continuous Wavelet Transform (CWT) and the Orthogonal Wavelet Transform (OWT).

2.4.1 The Continuous Wavelet Transform

The Continuous Wavelet Transform (CWT) is a linear transformation that decomposes an arbitrary signal $x(t)$ of one variable into a superposition of elementary functions of two variables a and b . The CWT is based upon a family of equally shaped functions which can be generated from a basis wavelet by means of dilating and translating. The continuous wavelet transform is defined by the expression

$$W_{a,b}(t) = \frac{1}{\sqrt{a}} \psi \left(\frac{t-b}{a} \right), \quad a > 0, b \in \mathfrak{R}. \quad (2.22)$$

where $\psi(t)$ is a fixed function called the ‘mother wavelet’ which is localized both in time and frequency. A family of time-frequency functions is obtained by scaling $\psi(t)$ by a ; and translating $\psi(t)$ by b . The most commonly used mother wavelet is the Morlet wavelet:

$$\psi(t) = e^{j\omega_b t} e^{-t^2/2} \quad (2.23)$$

where ω_b is the wavelet frequency. The Morlet wavelet is a common choice for the mother wavelet because it permits a direct frequency interpretation of the scale parameter and because it is the function that is most compact in the time-frequency plane (Lee and White, 2000; Staszewski, 1998). The idea of the CWT is to decompose a signal $x(t)$ into wavelet coefficients $(W_x^\psi)(a,b)$ using the basis of wavelet functions $\psi(t)$. This decomposition can be expressed mathematically as

$$W_x^\psi(a,b) = \frac{1}{\sqrt{a}} \int_{-\infty}^{\infty} x(t) \psi^* \left(\frac{t-b}{a} \right) dt \quad (2.24)$$

where $\psi(t)$ is an analysing or elementary wavelet and $\psi^*(\cdot)$ is the complex conjugate of $\psi(\cdot)$. Each value of the wavelet transform $W_x^\psi(a,b)$ is usually normalized by the factor $1/\sqrt{a}$. This normalization ensures the integrated energy given by each wavelet $\psi(t)$ is independent of the dilation value a .

2.4.2 The Orthogonal Wavelet Transform

The representation given by the continuous wavelet transform contains redundancy. A natural extension of continuous analysis is therefore the discretisation of time b' and scale a according to the relationship $a = a_0^m$, $b = na_0^n b_0$ where m and n are integers, $b_0 \neq 0$ is the translation step. This implies the construction of a time-scale grid (Daubechies, 1992), thus producing a discrete wavelet transform

$$W_\psi(m, n) = \int_{-\infty}^{\infty} x(t) \psi_{m,n}^*(t) dt \quad (2.25)$$

$$\text{where } \psi_{m,n}(t) = a_0^{-m/2} \psi^*(a_0^{-m} t - nb_0) \quad (2.26)$$

The higher the subsampling on this grid, the smaller the redundancy of the wavelet transform. When the wavelet functions $\psi_{m,n}(t)$ form a set of orthonormal functions, there is no redundancy present in the analysis. A discrete wavelet transform based on such wavelet functions is called an Orthogonal Wavelet Transform (OWT).

The orthogonal wavelet transform uses a different basis function in order to analyse non stationary data at varying resolutions by decomposing the signal into their frequency bands (Hubbard, 1996). Any arbitrary signal $x(t)$ can be represented as a weighted sum of orthogonal wavelets,

$$x(t) = \sum_m \sum_n W_\psi(m, n) \psi_{m,n}(t) \quad (2.27)$$

This shows that the analysed signal $x(t)$ can be represented as a sum of m wavelet levels given by,

$$x_m(t) = \sum_n x_n^m \psi_{m,n}(t) \quad (2.28)$$

$$x_m(t) = \begin{cases} a_0 \phi(t) & \text{for } m = -1 \\ \sum_n a_{2^m+n} \psi(2^m t - n) & \text{for } m = 0, 1, 2, 3, \dots \end{cases} \quad (2.29)$$

where the coefficients a_0, a_1, a_2, \dots quantify the amplitude of all contributing wavelets.

The sum of all levels recreates the original signal, i.e.,

$$x(t) = \sum_m x_m(t) a_1, \quad (2.30)$$

Although the wavelet levels are in the time domain, this orthogonal decomposition allows not only for time domain localisation of different events but also for frequency decomposition of different signal components (Steinwolf, et al., 2002). A vast literature exists treating the application of wavelets to damage detection (Staszewski and Tomlinson, 1994; Wang and Mc Fadden, 1995; Staszewski, et al., 1997) and to automotive vibration analysis (Giacomin, et. al., 1999; Staszewski, et. al., 1997; Lee and White, 2000).

2.5 Signal Processing Techniques used in Audio Mastering

Signal processing has become an increasingly important part of the world of music. Audio mastering makes use of the applied practices of signal processing to augment or modify an audio signal in either the analog or digital domain (Huber and Runstein, 2005; Katz, 2002). It is considered the last opportunity for fixing any problems in a music recording before an album is sent for manufacturing. Audio mastering has traditionally been considered more of an art than a science, because the optimal sound signal transformations depend on the desired emotional response of the listener (Katz, 2002).

Audio mastering typically involves a set of specific effects, some of the most common signal processing operations being:

- Analog to digital conversion
- Digital to analogue conversion
- Noise reduction
- Equalizers which are used to shape the tonal balance
- Compressors, limiters, expanders and gates which are used to adjust the dynamics of a mix.
- Addition of special effects

2.5.1 Gain Changers

An important step of the mastering process occurs when the signal level is adjusted in a music recording by means of dynamic range processors, such as compressors and

expanders. An example of waveforms before and after use of gain changers is presented in Figure 2.8. One of the benefits when the signal level is adjusted, it is achieved when a signal is boosted to regain maximum signal level becoming the low-level signals much more audible and understandable. The small difference among all the peaks (the highest points and the average levels) in the waveforms after mastering reduces drastically the difference between the loudest part and the quietest parts of the music recording enhancing it.



Figure 2.8 Comparison between waveforms before and after Mastering.

2.5.2 Compressors

Compressors can be considered systems for performing automated volume control. They are used to proportionately reduce the amplitude of a signal that rise above a known threshold level. When a compressor receives an abundance of signal level, it triggers an automatic level control to decrease the signal strength, resulting in a decrease in volume. When the amplitude of the signal reaches a certain level, it surpasses a user-set threshold. As signal exceeds this threshold, an amplifier turns the signal level down according to the compressor settings. The most common parameters to control for a compressor includes: the input signal level which determines how much signal is sent to the compressor's input stage; the threshold level is a setting which determines the level at which the compressor will begin proportionally reduce the incoming signal; the output signal level which determines how much signal will be sent to the device's output; and the slope ratio which determines the amount of input signal level that is needed to cause a decrease at the compressor's output (see Figure 2.9).

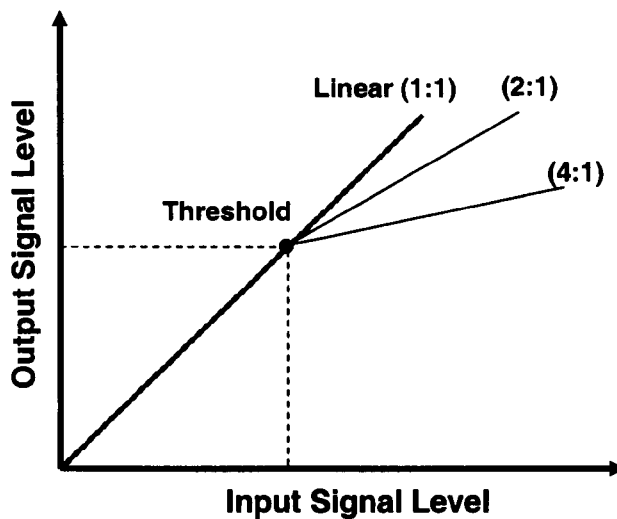


Figure 2.9 The output of a compressor is linear below the threshold and follows an input/output gain reduction ratio above this point (Adapter from Huber and Runstein, 2005).

When a compressor has extreme compression, with ratios large enough such as 10:1, 20:1 or more, the compressor becomes a limiter (see Figure 2.10). This kind of extreme compression results in an output signal level which does not appreciably alter as the input signal level changes. A limiter is used to keep signal peaks from exceeding a certain level in order to prevent the overloading of amplifier signals.

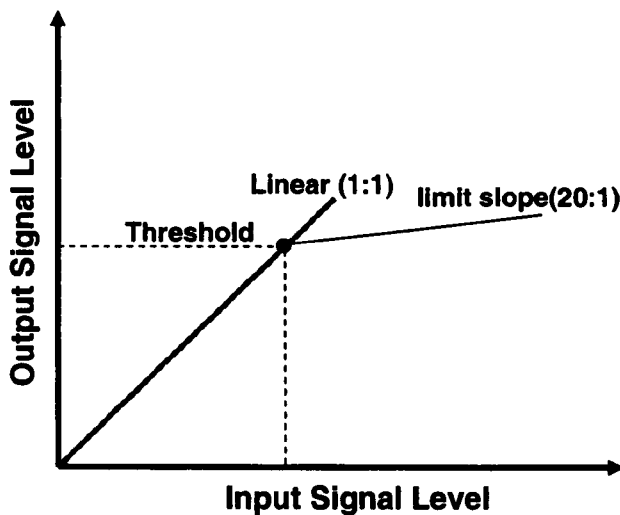


Figure 2.10 The output of a limiter is linear below the threshold and follows a high input/output gain reduction ratio (10:1, 20:1, or more) above this point (Adapter from Huber and Runstein, 2005).

2.5.3 Expander

An expander works in a similar way to a compressor, however, it works in an opposite manner. While with a compressor the signal over the threshold level is attenuated; for the expander the threshold is set and any part of the signal dropping below this threshold will be affected by the expander and this level will be raised. The expander therefore like the

compressor balances out the signal making it sound more professional. Expanders can be used to emphasize different parts of the signal levels from those affected by downward compressors. For example, upward expansion is great for restoring the liveliness of typical uninterested musical samples from samplers (Katz, 2002). The parameters which can be controlled for an expander are the same to those controlled for the compressor (see Figure 2.11). Both compressors and expanders have a voltage-controlled amplifier (VCA) circuitry, in the analog domain, in order to have the capability of turning the signal level. When the voltage level exceeds the threshold, in the case of the compressors, the signal level is decreased according to the processor settings, the opposite occur when the VCA circuitry is set as an upward expander.

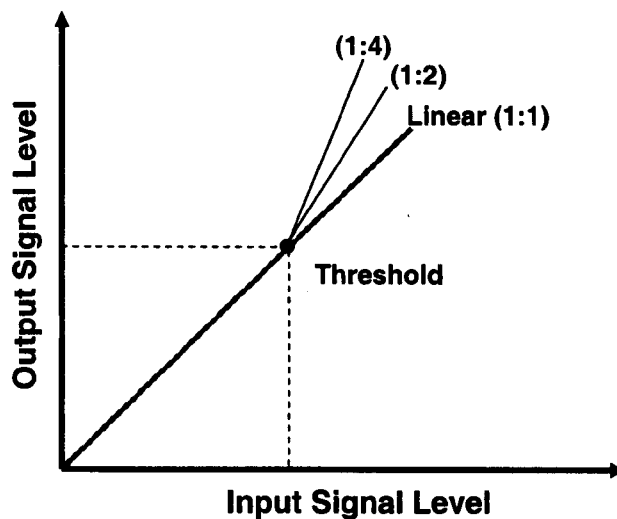


Figure 2.11 Typical expansion curves for expanders: output level versus Input level.

When the expansion ratio slope is low enough, as seen in Figure 2.12, it corresponds to extreme expansion and is often known as gating. This dynamic range processor allows a signal above a selected threshold to pass through to the output at unity gain and without signal level processing; however, once the input signal level falls below the threshold level, the gate acts as an infinite expander and effectively mutes the signal by fully attenuating. As presented in Figure 2.12 the output of a gate is linear above the threshold and follows an infinite expansion slope (is turned off) below this point (Huber and Runstein, 2005).

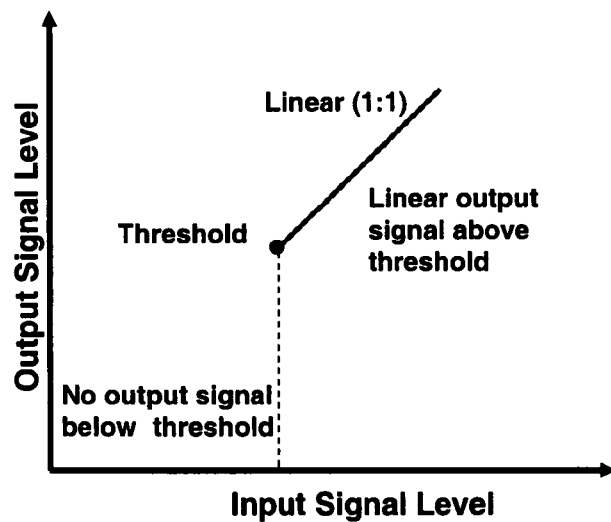


Figure 2.12 The output of a gate is linear above the threshold and follows an infinite expansion slope below this point gate (Huber and Runstein, 2005).

2.6 Signal Processing Techniques used in Vibro-acoustic Mission Synthesis

This section describes the signal processing fundamentals used into the Mildly Non-stationary Mission Synthesis (MNMS) algorithm. This algorithm was developed for the purpose of producing shortened vibration mission signals which are representative experimentally measured vibro-acoustic data. The algorithm uses the Discrete Fourier Transform (DFT), the Orthogonal Wavelet Transform (OWT) and bump (shock) extraction and reinsertion techniques.

2.6.1 The Mildly Non stationary Mission Synthesis Algorithm

The Mildly Non stationary Mission Synthesis Algorithm (MNMS) was developed to aid engineers in defining vibration mission signals for vehicle components (Giacomin et al., 1999). According to Giacomin “it represents a method of summarising mildly non stationary vibration records to obtain short mission signals that can be used for experimental or numerical testing purposes”. The MNMS algorithm creates mission signal by inserting characteristic bumps (shock events) from an original recorded signal into a synthesised background signal which equivalent to the underlying random Gaussian vibration of the original process. In this context the word ‘bump’ is taken to mean a high amplitude transient event which can cause the overall time history to deviate from a stationary Gaussian model. The output mission signals replicate the fundamental vibration characteristics of the input signal in terms of the fundamental global signal statistics such as *r.m.s.*, skewness, kurtosis, CF and the PSD (Giacomin et al., 1999; Grainger, 2001; Abdullah et al., 2004). The signal processing tools used in the MNMS algorithm are the

Discrete Fourier Transform (DFT), the Orthogonal Wavelet Transform (OWT) and data correlation functions. The algorithm consists of three main processing stages which are:

1. Application of the Discrete Fourier Transform (DFT) to the original vibration time history, and use of the resulting spectra to generate a short artificial background signal by means of Fourier inversion which has the same Power Spectral Density (PSD) as the input vibration data;
2. Application of the Orthogonal Wavelet Transform (OWT) to the steering vibration data, and grouping of wavelet levels to represent a small number of filter banks that subdivide the vibrational energy;
3. Identification of bump events within each wavelet group, and the reintroduction of bumps into the short Fourier background signal so as to peak correct it, returning a mission signal that replicates the non-Gaussian vibrational behaviour of the original steering vibration signal.

Each stage of the MNMS algorithm will be explained in depth into the next sections. The performance of the algorithm is dependent on the degree of non-stationary behaviour of the input road data. Giacomini et al. (1999) have published some results for seat guide vertical acceleration data, producing mission signals which are representative of the original road data in terms of PSD, r.m.s. value, kurtosis and crest factor values with mission signals statistics being typically within 5% of the input signal values in terms of r.m.s. and within 20% of the Kurtosis. Instead, Grainger (2001) has studied the algorithm's performance when it is applied to automobile wheel hub acceleration data containing a high number of high amplitude transient events. Results suggested the algorithm's performance is degraded when applied to wheel hub data containing increasing numbers of high amplitude transients with kurtosis and Crest Factors being underestimated by up to 60% in the worst case. On the other hand, Abdullah et al. (2004) applied the MNMS algorithm to fatigue mission synthesis of road vehicle suspension arm strain histories. For both strain time histories which were considered, all mission RMS values were found to be within the range $\pm 5\%$. For the kurtosis values, however, the tensile mean strain loading missions were in the range $\pm 25\%$ while the compressive means strain loading missions were in the range from -26% to 217%.

2.6.2 The First Stage: Synthetic Fourier Base Signal

The first stage in the MNMS algorithm is to synthesise a random time history which has the same PSD as the original vibration data. The Discrete Fourier Transform is used to obtain a spectral estimate of the vibration time history. Each frequency step value of the PSD is characterised by amplitude,

$$A_k = \sqrt{2\Delta f \cdot S(f_k)} \quad (2.31)$$

where $S(f_k)$ is the underlying PSD of the Gaussian signal, Δf is the frequency step and f_k is the frequency of the harmonic in question. The amplitudes A_k are used to generate a short synthetic signal which serves as the basis for constructing the vibration mission signal. The Fourier synthetic signal is generated from a Fourier series expansion using a large number N of harmonics, expressed as

$$x(t) = \sum_{k=1}^N A_k \cos(2\pi f_k t + \phi_k) \quad (2.32)$$

where the phase angles ϕ_k are chosen in a random manner, in-line with the traditional assumption of stationary Gaussian behaviour. The approach guarantees that the short test signal accurately reproduces the PSD of the original steering data.

2.6.3 The Second Stage: Wavelet Decomposition and Wavelet Level Grouping

In order to construct a vibration mission signal, high amplitude bump events from the original vibration data are identified and saved so as to be used later for correction of the synthetic background signal. For this purpose, the recorded vibrational data is separated into a number of frequency intervals, each of which is related to physical phenomenon that occurs during the motion, i.e. the resonance of the automobile body as an entire mass, torsion and bending of the chassis in multiple directions, tyre resonances, etc. By treating each of the constituent vibration components separately, the bump events occurring in the different frequency intervals do not cover each other or interfere with each other in any way during the signal processing. Figure 2.13 illustrates schematically the operations performed by the second stage of the MNMS algorithm.

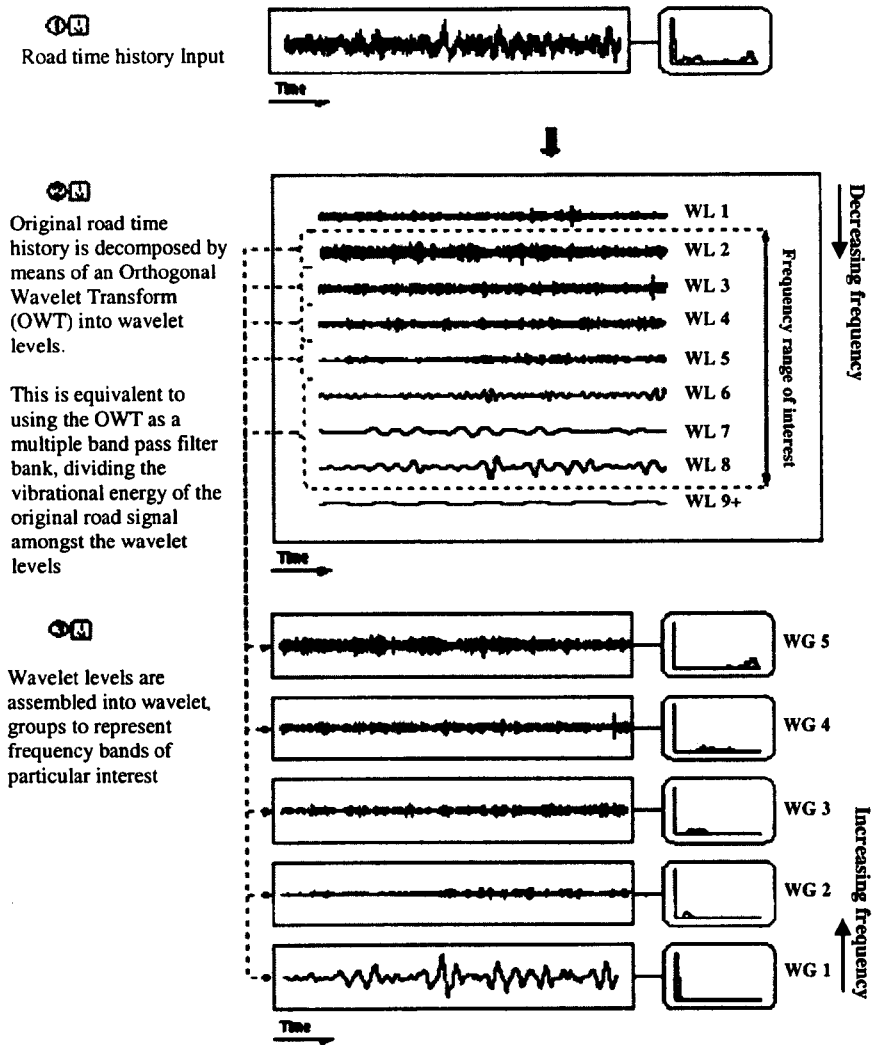


Figure 2.13 Schematic representations of the wavelet decomposition and grouping procedure (Adapted from Giacomini et al., 1999).

2.6.4 The third stage: bump event selection and processing

The third processing stage of the MNMS algorithm seeks to locate bump events in each wavelet group of the original vibrational data. These high amplitude events must be reinserted into the synthetic background history in order to ‘correct’ it, returning a mission signal that replicates the non Gaussian vibrational behaviour of the original vibration signal.

Bump events are identified by searching the wavelet group time histories for outlying data points which exceed a prescribed threshold, or trigger level, which must be defined manually individually for each wavelet group. Each trigger level is specified by the user in terms of a multiple of the standard deviation (*r.m.s.* value) of the wavelet group under consideration as illustrated in Figure 2.14(a).

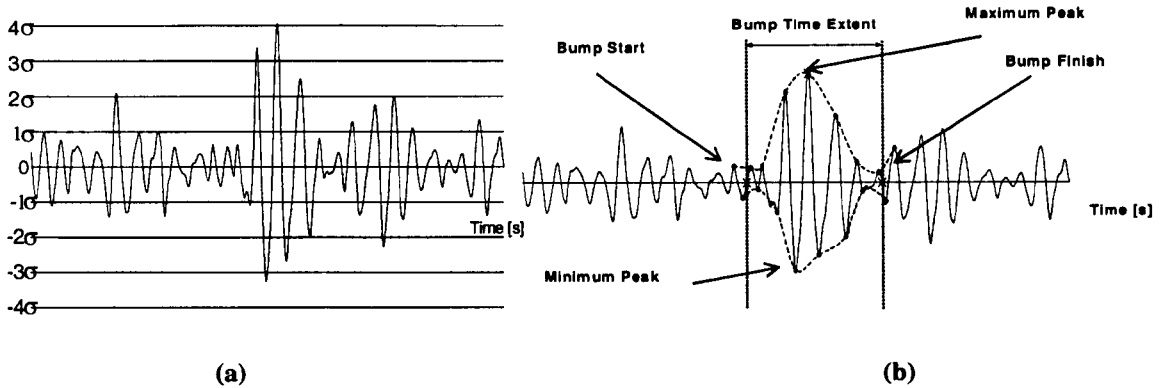


Figure 2.14 (a) Schematic diagram of bump identification using trigger levels and (b) Schematic diagrams of the determination of a temporal bump time extent (Adapted from Abdulla et al, 2004).

Once a bump event exceeding a specified trigger level has been identified, its time duration must be determined by the software algorithm. The determination of bump time extent is performed by means of a search which identifies the points at which the signal envelope inverts from decay behaviour. By considering the decay envelope at either side of the maximum peak of a transient, the end points of the bump can be defined as shown in Figure 2.14(b).

2.6.5 The Fourth Stage: Bump Reinsertion

After all the bumps have been identified in the respective wavelet groups the MNMS algorithm provides two methods for bump reinsertions which are: proportional reinsertion and maximum reinsertion.

2.6.5.1 Proportional Reinsertion

The proportional reinsertion introduces a number of bump events in proportion to the signal compression ratio (Giacomin et al., 1999). In this context, the compression ratio is defined as the ratio between the time extent of the original road signal and the time extent of the shortened mission sequence. After identifying and defining the time length of each bump the bumps were counted and sorted. For each wavelet group, each bump was ranked by its maximum peak amplitude (absolute CF) and then sorted by rank into descending order. Having sorted all bump events within their respective wavelet groups, bump events were selected for reintroduction into the synthetic signal wavelet groups by moving down the sorted list in steps equal to CR , the compression ratio. In doing this, bump events of various intensities appeared in the output mission signals.

2.6.5.2 Maximum Reinsertion

On the other hand, the maximum reinsertion introduces all bump events (beginning with the most severe) which can fit into the synthetic signal within the space available, in an attempt to more closely reproduce the kurtosis, or relative peakedness, of the original data. The scheme of non-proportional reinsertion leads to issues regarding the amount of space available in the synthetic signal with mission signal time compression. For the first (lowest frequency) wavelet group, not all of the smaller bumps can be fitted to the synthetic signal as the compression ratio increases because the base signal becomes saturated, and there is insufficient space available to fit all bumps. For the wavelet groups with higher dominant frequencies, most or all bumps can be fitted to the short test signals at high compression ratios as the transient events extracted from the original data wavelet groups are much shorter in duration.

2.6.5.3 Reinsertion correlation procedure

In order to reduce the impact of bump correction on the PSD of the synthetic Fourier background signal, each selected bump event is introduced at a location in time where the synthetic signal most closely resembles the transient event. This location is determined by means of a correlation procedure in which the bump event is moved along the whole time history of the synthetic signal, and the two signals are compared in terms of a root mean square difference at each position which is evaluated as

$$\sigma_{diff} = \left\{ \frac{1}{M} \sum_{j=1}^M (x_j - x_{Fourier,j})^2 \right\}^{-1/2} \quad (2.33)$$

where M is the number of data points of the bump event. The point in the background signal with the lowest root mean square difference (corresponding to the highest correlation) is selected as the insertion point, and the bump event of time extent $(M - 1)\Delta t$ then substitutes the similar event in the synthetic signal.

2.6.6 Synchronisation Procedures

After being decided the method of bump reinsertion the MNMS algorithm provides three different procedures to reinsert the bump event which are: non-synchronisation procedure, synchronisation procedure 1 and synchronisation procedure 2 (see Figures 2.15 to 2.17).

2.6.6.1 Non-synchronised procedure

The non-synchronised procedure treats each wavelet group independently assuming that transient events occurring in one wavelet group bear no relation to those of another (see Figure 2.15). Firstly, the synthetic signal is decomposed and grouped according to the wavelet grouping strategy applied to the original vibration data. Bumps are then reinserted independently at the point of closest similarity (highest correlation) between the transient events and their respective wavelet groups of the synthetic Fourier signal.

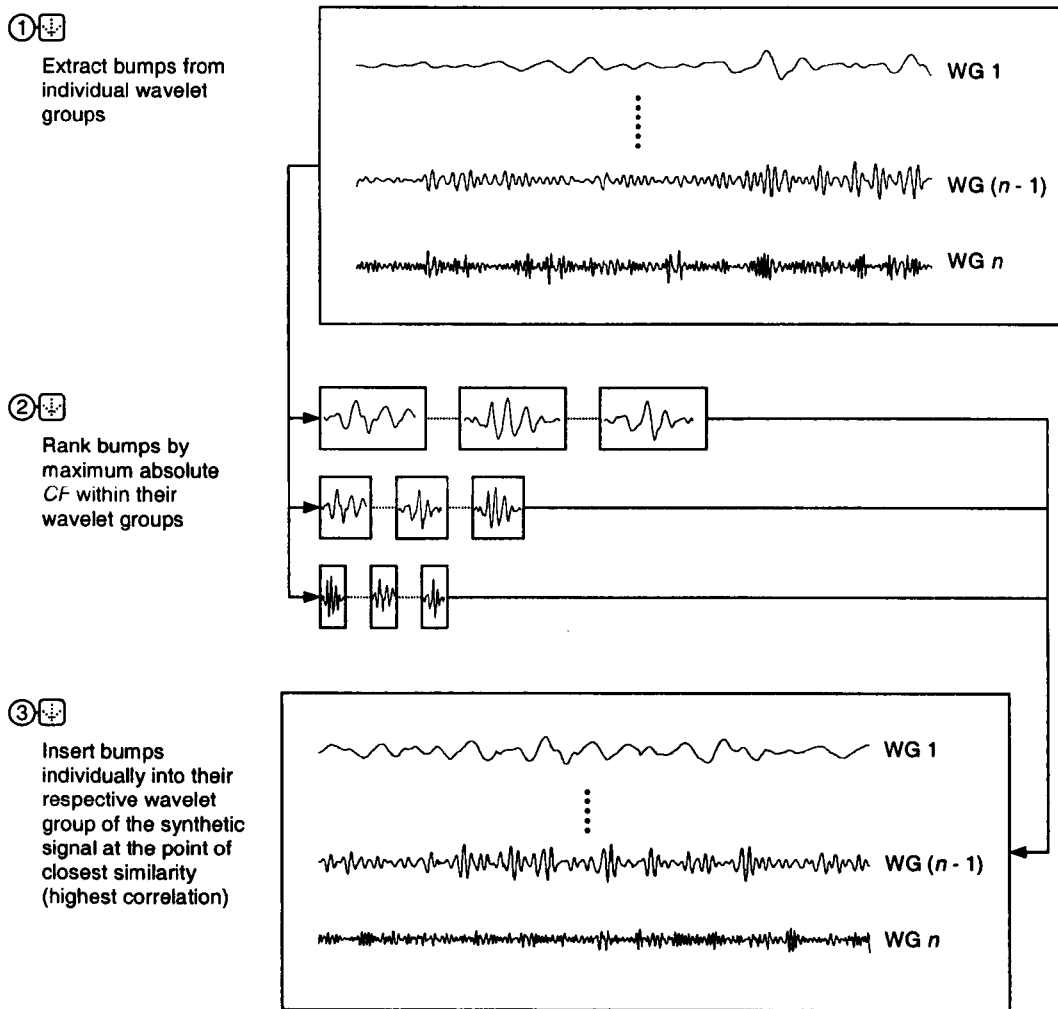


Figure 2.15 Non-synchronised bump reinsertion procedure (Adapted from Giacomini et al., 1999).

2.6.6.2 Synchronisation procedure 1: wavelet group synchronisation

The synchronisation procedure 1 involves the synchronisation of bump events across wavelet groups (see Figure 2.16). The logic behind this method is the observation that a single sharp road irregularity will approximate an impulse function. In the frequency domain energy would be present in the input spectrum up to a critical cut-off frequency. For an input signal of this type, the vibrational energy would be spread across many, if

not most, wavelet groups. The bump events in the various wavelet groups would therefore be expected to occur together (in time). Because of this, non-synchronised reinsertion of such events would smooth the peaks of the overall mission time history, formed by the summation of the peak corrected wavelet groups, and would not correctly represent the characteristics of the original road data.

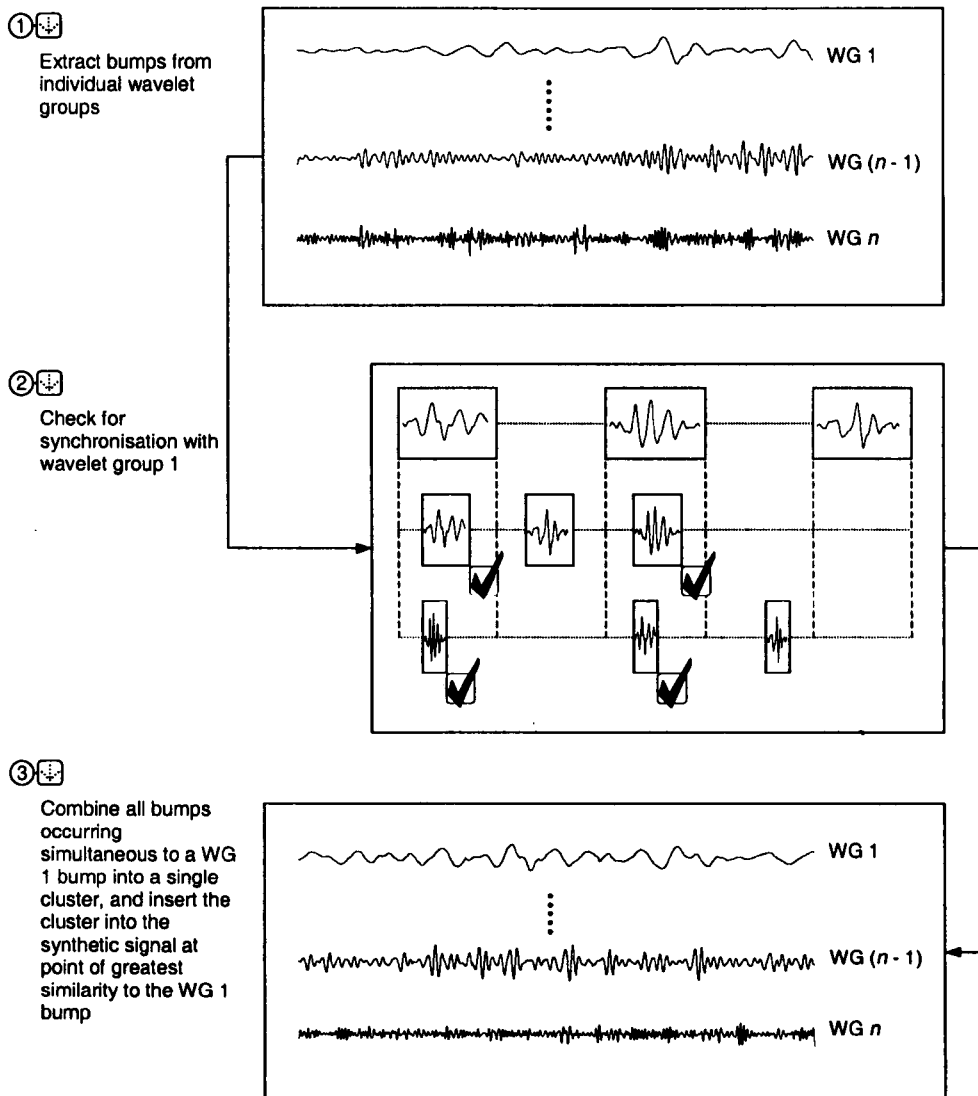


Figure 2.16 Synchronised bump reinsertion procedure 1 (Adapted from Giacomini et al., 1999).

Synchronisation procedure 1 attempts to alleviate this problem by reinserting together (in time) those bump events from various wavelets groups that occur simultaneously, due to impulsive inputs to the vehicle owing to road irregularities. Wavelet group 1, which spans the lowest frequency range under consideration, is used as the basis for the synchronisation check. Specifically, the check returns a positive result if the sampled point of the maximum peak of a transient is located within the limits of a wavelet group 1

bump event. A negative result is returned if a bump is found not to be synchronised with any of the lowest frequency (group 1) transients. All bumps from wavelet groups 2 and above that are found to occur at the same time as a wavelet group 1 event are then clustered together with that bump. These clusters of synchronised bumps are reinserted into their respective groups of the synthetic Fourier signal at the point of closest similarity between each wavelet group 1 transient and wavelet group 1 of the synthetic Fourier signal. Independent bumps, which have returned a negative result for synchronisation, are then fitted in the remaining unoccupied space in each of the Fourier wavelet groups.

2.6.6.3 Synchronisation procedure 2

The synchronisation procedure 2 involves reinsertion into the Fourier signal of whole segments of the original overall time history (see Figure 2.17). This procedure is considered the most conservative of the bump reinsertion strategies in which has been retained all of the original amplitude and phase relationships of a bump event extracted from the original data.

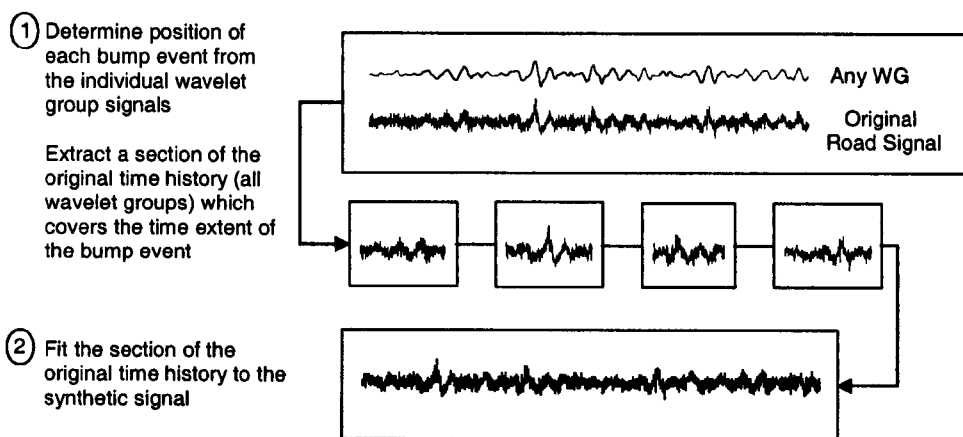


Figure 2.17 Synchronised bump reinsertion procedure 2 (Adapted from Giacomini et al., 1999).

Synchronisation procedure 2 firstly identifies bump events on a wavelet group by wavelet group basis in the same way as the previous two procedures. The procedural difference involved is in defining the length of a bump, and the subsequent cutting operation to remove the transient events from the overall time history. The start and finish points of all bumps identified within the individual wavelet groups are firstly compared, and bumps that overlap are concatenated to define a single transient event in the overall time history. Complete segments are removed from the original vibration data time history, rank them by peak Crest Factor, and finally, reintroduce them one by one into the *overall* synthetic

Fourier signal utilising a least-squares correlation procedure. By reinserting a segment of the original time history which has been identified as owing to the presence of shock transients, issues regarding the synchronisation of individual bump events are bypassed thus preserving all of the original amplitude and phase relationships of the original data.

2.6.7 Mission Synthesis Results

The flow chart for the complete MNMS algorithm as it is shown in Figure 2.18. User inputs can be performed either directly from terminal or by means of a parameter file. The program is written in Salford Software (Fortran), and runs on Windows-compatible PCs.

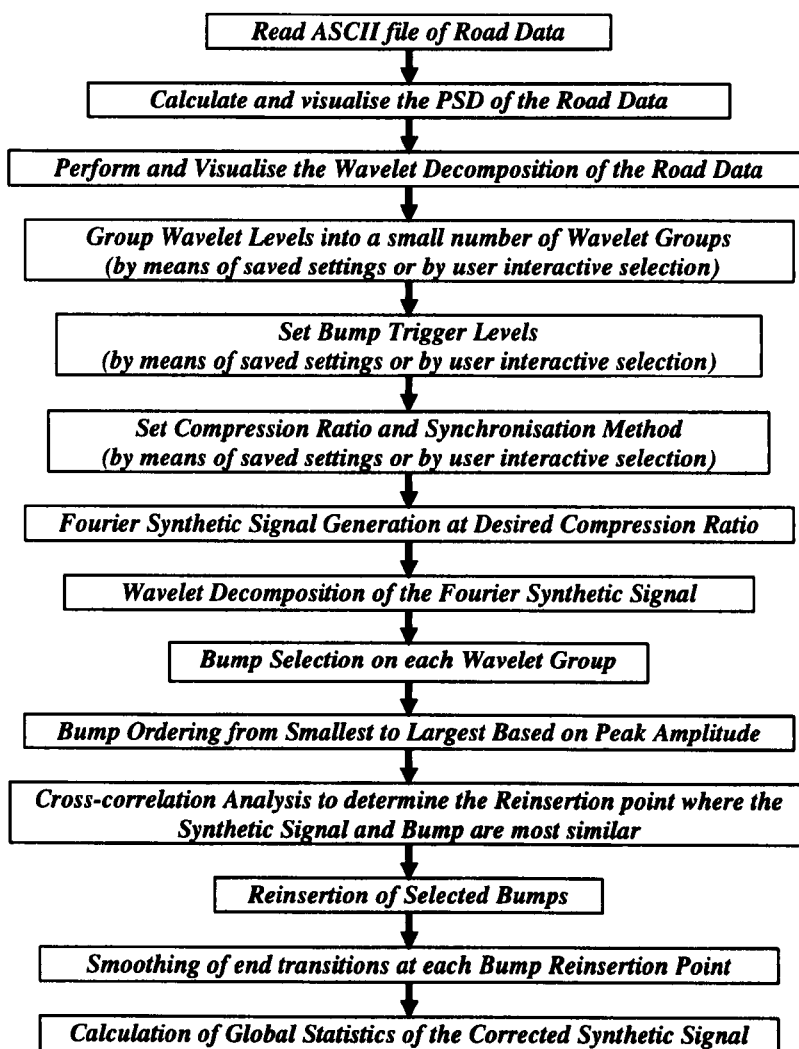


Figure 2.18 MNMS algorithm flowchart (Adapted from Giacomini et al, 1999).

3. Considerations from Human Cognition

The goal of this chapter is to provide an introduction to the definitions from the field of human cognition which are fundamental towards the understanding of the experimental protocols used during the research, as well as to the methods used when evaluating the experimental responses in this thesis.

3.1 Human Perception

How people understand, process and collect the information depends on how it is compared against information already stored in memory (Kosslyn et al., 1994; Mc Adams et al, 1993). Human cognition is a set of complex and interactive processes (Loomis and Lederman, 1998) because each cognitive system is intertwined and interacts with a range of other systems. Cognitive processes involve perceptual processes by which a stimulus is detected. The stimulus can be perceived as a discrete event or as a stream of events.

According to Dror (2005) perceptual mechanisms can be adjusted in terms of sensitivity thresholds, stimulus segmentation and other parameters. Therefore, much of what humans perceive is dependent on the perceiver rather than the object of perception (Dror and Dascal, 1997). The way in which a vibrational stimulus is experienced depends therefore upon several factors amongst are the person's past experiences, the person's memory and on a large variety of other psychological variables.

The mind and the brain are dynamic systems that play active roles in how people perceive and detect. Human perception depends on a range of factors, such as mental states, which play a critical role in how perceptual information is processed. Hopes, fears, and

expectations affect what people detect. There are numerous phenomena that can illustrate how the mind plays an active role in how humans perceive and construct reality, such as motivation, wishful thinking, cognitive dissonance, self-fulfilling prophecies, and confirmation bias (Darley and Gross, 1983; Snyder et al., 1977).

Dror (2005) stated that there are different people, with different experiences, different brains and different sensory mechanisms. This entails that people have different perceptions. Even if people perceive the exact same thing, that percept is not necessarily a true and accurate reflection of the 'objective reality'. This individualization of perception derives from the active nature of cognition and the wide range of factors that affect what and how people perceive.

3.2 Human Memory

Human memory is normally categorised as being of one of three different classes, these being Sensory Memory (SM), Short Term Memory (STM) and Long Term Memory (LTM) (Anderson, 1980; Baddeley, 1986; Tulving, 1972). Human memory is a series of systems which store and retrieve information gathered through the senses. The systems range in storage duration from fractions of a second to a whole lifetime, in capacity from tiny buffers to vast storage areas of the long term memory system (Miller, 1956). Atkinson and Shiffrin (1968) assumed that the progress of information through these stores can be referred to as the Information Processing Model, which is presented in Figure 3.1.

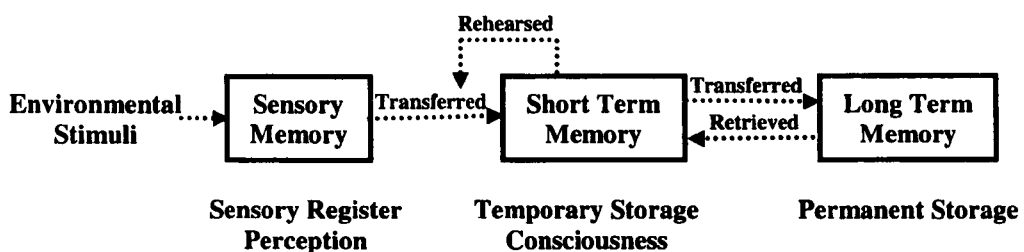


Figure 3.1 The flow of information through the memory system as proposed by Atkinson and Shiffrin (1968).

Sensory Memory (SM) is taken to mean a holding system where information from the environment enters the human information processing system. Modality specific sensory registers exist in SM, and their function is to perceive information from the environment. Miller (1956) stated that the sensory information store has unlimited capacity, and reacts

to both visual and auditory information. Norman (1970) assumed that these registers have the capacity to transform physical environmental stimuli into physiological representations. In this form information is capable of being temporarily retained in the memory system.

Within Short Term Memory (STM) there are three basic subdivisions: iconic memory, acoustic memory, and working memory (WM) (McMahon and McMahon, 1982). Iconic memory refers to the ability to hold visual images, while acoustic memory refers to the ability to hold sounds. Webster's New World Medical Dictionary (2006) defines working memory as "a system for temporarily storing and managing the information required to carry out complex cognitive tasks such as learning, reasoning, and comprehension". This term came into use with the publication of the book *Plans and the Structure of Behavior* by Miller, Galanter, and Pribram (1960). Baddeley (2002) has described the use of this term and its applications. Working memory is regarded as the major information processor responsible for both high-level cognitive processing, such as constructing mental models, integrating different mental representations, and short-term maintenance of information involved in those processes (Baddeley, 1986; Miyake and Shah, 1999). However, working memory has a very limited capacity and duration when people are dealing with unfamiliar information. For example, according to an accepted cognitive theory people are assumed to have a limited capacity of around seven chunks (Miller, 1956), where the term chunk is taken to mean a familiar pattern which is stored in LTM for no longer than several seconds (Brown, 1958; Peterson and Peterson, 1959).

The Webster's New World Medical Dictionary (2006) defines long term memory as "a system for permanently storing, managing, and retrieving information for later use. Items of information stored as long-term memory may be available for a lifetime". Anders (2002) stated that LTM is characterized by a lack of restrictions in two critical respects. Firstly, LTM has the capability to store information in a relatively permanent manner, and secondly, it seems to have a vast, virtually unlimited capacity to store information. People are generally unaware of the vast bulk of information they have stored in LTM because this information does not enter into conscious awareness until required. When certain information is required, it is retrieved back into consciousness from LTM stores. The knowledge is stored in LTM in the form of hierarchically organized, domain-specific structures called schemas (Simon, 1974). In this context schemas can be generally viewed

as cognitive constructs that allow people to treat multiple elements of information in terms of larger higher-level units. The performance of LTM suggests that people continually store enormous amounts of information.

3.3 Parameters Affecting Decision Making

Decisions are the outcomes that result from assessing and evaluating factors, while decision making is defined by Simon (1957) as the cognitive process leading to the selection of a course of action among alternatives. These decisions are affected by the way in which the decisions are made. A decision maker is thought to act according to his or her understanding of the given situation; therefore the source of any error is to be found in the person's previous knowledge or in the logical process followed when reaching the decision. Often, decisions are said to be made based on instinct or intuition (Bannister and Remenyi, 1999). Limitations of knowledge, personal experience, habits, cognitive ability, culture or religious system can represent obstacles towards reaching a decision. However, the effects on the decision making process and the relationships between these factors are not fully understood.

Decision Making can be categorized as either rational decision making, which is considered a logical process, or judgment decision making, which is considered a non-logical (Simon, 1967a). In the first case a decision maker is considered as an expert, in other words, the person who has all the knowledge relevant to make a decision. It is assumed that the rational decision maker uses this information to form assessment criteria which are used to assess decision alternatives. In this case, the decision maker seeks to optimize his or her decision alternatives (Simon, 1967b). On the other hand, judgment decision making deals with intuition and instinct (Simon, 1987). Moreover, for both types of decision making there exist a number of cognitive and environmental influences which affect the final decision. Among these are:

1. **Information bias.** This can occur when a subject is asked to choose among alternatives which he or she has had previous experience of Russo et al. (1998) affirmed that subjects unconsciously distort information. In his study, he found that the formation of preferences occurs without instruction and this led to subsequent predecisional distortion of product information.

2. **Cognitive biases.** This can occur when the amount of information available exceeds a decision maker's cognitive processing limits (Duhaime and Schwenk, 1985). A decision maker is often unable to cope with all the information relevant to a decision, so he or she simplifies the decision making process by applying cognitive filters or biases.
3. **Time Stress.** Time constraints can have a critical influence on a decision process (Orasanu and Martin, 1998). The level of time stress within a situation dictates the level of mental processes incorporated into the decision process. Relative to the amount of information presented, Wright (1974) notes that under high time stress, decision-making performance deteriorates when more rather than less information is provided. In high time stress situations people tend to restrict their range of focus on the environmental cues. Manipulating a large amount of data is not consistent with human information processing capability, especially under stress (Stokes, et al, 1992).
4. **Risk.** According to Miller (2006) the perception of risk is a feeling which is psychologically linked to emotion, and these emotions are affected by how decisions are framed. According to Miller's decision making theory, a choice is the result of a weighting between a risk and an expected gain.
5. **Uncertainty.** The level of uncertainty surrounding a decision creates a bias that alters the way in which information is gathered and the decision is made. Uncertainty is the perceived gap between the information available and the information a decision maker wants to have (Buchanan and Kock, 2000). Uncertainty influences both the decision maker and the outcome of the decision.

3.4 Theory of Signal Detection

Theory of Signal Detection (TSD) is an approach which facilitates the quantification of how people behave in detection situations (Tanner and Swets, 1954). TSD emerged as a method for investigating the assumption that expectancy and payoff have a significant influence on people in detection situations. Described in detail by Green and Swets (1966), TSD is a model based on statistical decision theory and certain ideas about electronic signal detecting devices. The starting point for signal detection theory is the assumption that nearly all reasoning and decision making takes place in the presence of some uncertainty. There are many applications for the Theory of Signal Detection in the

fields of sensory detection (Palmer, 1994), recognition memory (Yonelinas et al., 1996) and monitoring (De Carlo, 2003).

Theory of Signal Detection is applicable in any situation which can be considered to consist of two discrete states of the world, signal and noise, which cannot be easily discriminated (Green and Swets, 1966). In the detection situation, the observer must first make an observation (x) and then make a decision about the observation. On each trial, the observer must decide whether x is due to a signal which is present in a noise background or to the noise alone. According to Gescheider (1997), when the signal is weak the decision becomes difficult and errors are frequent. Figure 3.2 represents graphically two distributions describing the random variation of the noise and of the signal plus noise. Since the signal is added to the noise, the average sensory observation magnitude will be greater for the signal plus noise distribution than for the noise distribution. When the distributions are essentially the same, as seen in Figure 3.2 where a signal plus noise distribution is indicated by a dotted line, they greatly overlap and the decision making becomes difficult due to the lack of separation between the two stimuli.

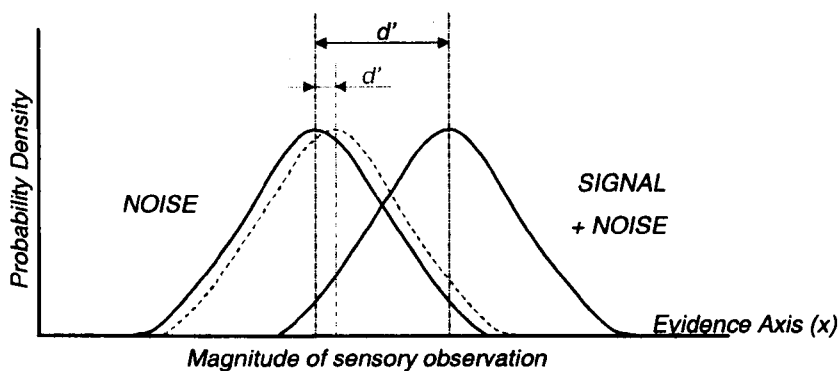


Figure 3.2 Theoretical probability distributions of a “noise” and of a “signal – plus – noise” for two different values of signal strength (Adapted from Baird and Noma, 1978).

The conceptual innovation of TSD was to consider as part of the testing and analysis the effects of cognitive factors such as an observer’s expectations and desires (Baird and Noma, 1978).

3.4.1 Ideal Observers

Research has demonstrated that if a subject is attempting to maximize signal identification the best decision strategy that he or she could employ would be that of an *ideal observer* (Baird and Noma, 1978; Lapsley Miller, 1999). The concept of an ideal observer (Lawson

and Uhlenbeck, 1950; Peterson et al., 1954) originated from detection tasks such as those involved in radar operation. The ideal observer is a mathematical theory of a detection task where the signal to be detected is noise degraded, and the observation of the signal is limited to a finite period of time. The aim of the theory is to determine to what extent noise limits the detection of the signal.

In order to behave as an ideal observer a subject must have stored in memory the signal and noise distributions, or have some other way to gain access to them. In particular, an ideal observer maps the external stimulus (a “noise” or a “signal plus noise”) onto a value x on the evidence axis and determines the probability of obtaining x from a noise and signal plus noise distribution, independently. The detectability of the signals is quantified by measuring how the errors are traded off as a function of the subject’s. The TSD assumes that an observer establishes a particular value as a cut-off point, or criterion, and that the decision is determined by whether a particular observation is above or below the criterion. According to Green and Swets (1966) no observer can make perfect detections of a signal masked by noise if there is overlap between the evidence distributions associated with a noise and a signal plus noise events, an example in this context was presented in Figure 3.2 when a signal plus noise distribution is drawn with a dotted line.

Peterson et al. (1954) derived the theory of Signal Detection and showed that the optimal observer used the likelihood ratio decision axis, or a decision axis strictly monotonic with likelihood ratio, as a basis for decisions about the existence of the signal. If the signal is known to the observer exactly, and the observer can transform the evidence to a quantity monotonic with likelihood ratio, then the observer is considered to be an ideal Signal–Known–Exactly (SKE) observer. If the observer does not have an exact representation of a signal, or if the observer is unable to use information about some property of a deterministic signal, the observer is considered to be a signal–known–statistically (SKS) observer.

The early radar engineers considered the ideal observer as a mathematical theory that predicted the best possible performance for a particular class of signals, with particular restrictions on the information the observer had about the signals (Peterson et al., 1954). When the theory was extended to psychophysics, the emphasis changed. Unlike engineers, psychophysicists were not interested in designing detection systems but were

trying instead to understand existing biological systems that did not necessarily perform ideally, and whose internal processes were usually inaccessible.

3.4.2 Detectability Measure, d'

According to Theory of Signal Detection (TSD) the separation of the noise and the signal plus noise distribution along the evidence axis is an indication of the level of sensory discrimination. In this context the term detectability refers to how well a stimulus can be discriminated from a noise, thus an observer with a high sensitivity is one who can easily distinguish a stimulus. The detectability measure normally adopted in TSD is known as the d' , which is determined by the separation between the mean of a noise and a signal-plus-noise distributions, as shown in Figure 3.2.

When an observer is asked to chose between the two possible states (noise and signal-plus-noise) during the course of a sensory exposure the combination of two stimulus and two response categories produces a 2x2 matrix (see Table 3.1). It involves four classes of joint events which are labelled as hits, misses, false alarms, and correct rejections.

Table 3.1 The four response outcomes of signal detection.

		Responses	
		Yes	No
Stimulus	Signal +Noise	<i>Hit</i> (Correct detection)	<i>Miss</i> (Incorrect rejection)
	Noise	<i>False alarm</i> (Incorrect detection)	<i>Correct rejection</i> (Correct denial)

Figure 3.3 shows the relations between the presence and absence of a stimulus, random variability and the decision criterion. The separation between the means of the two standardized distributions is a measure of detectability which indicates how well the subject can discriminate between the two events, and it is denoted as d' . The detection task is easier for cases characterized by large separations and/or small variances.

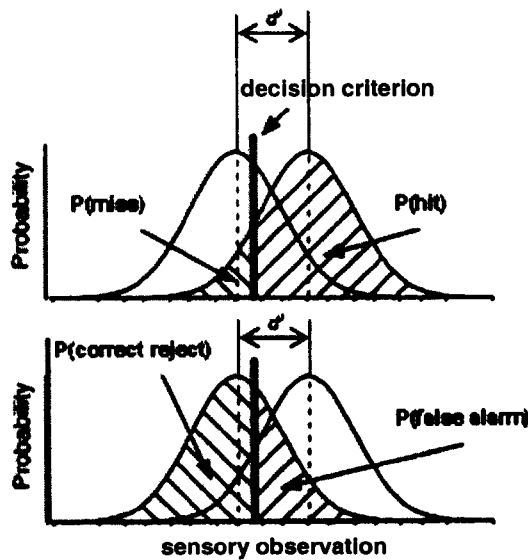


Figure 3.3 The signal detection diagram (Adapter from Heeger, 2003).

For experimental protocols in which observers are requested to provide a simple “yes” or “no” response, the detectability index d' can be estimated from the experimentally determined hit rates and false alarm rates by means of the associated Z score values (see Appendix C.1) using the relations below (Gescheider, 1997). The Z transformation converts a hit or false alarm rate to a Z score (i.e. to standard deviation units). A rate of 0.5 is converted into a Z score of 0, larger rates into positive Z scores, and smaller rates into negative ones.

$$P(\text{hit}) = \frac{\text{"number of yes" counted during signals present}}{\text{number of signals}} \quad (3.1)$$

$$P(\text{false alarm}) = \frac{\text{"number of yes" counted during signals present}}{\text{number of non - signals}} \quad (3.2)$$

$$Z_n = 1.0 - P(\text{false alarms}) \quad (3.3)$$

$$Z_{sn} = 1.0 - P(\text{hit}) \quad (3.4)$$

$$\text{where } d' = Z_n - Z_{sn} \quad (3.5)$$

Figure 3.4 presents an example of distributions of a “noise” and a “signal-plus-noise” expressed in Z scores values. Once the $P(\text{hit})$ and $P(\text{false alarm})$ are determined, the location of the criterion in both distributions is found by the subtraction of the $P(\text{hit})$ and $P(\text{false alarm})$ from 1.0 and converting this value in Z scores (see Equations 3.3 and 3.4).

The value of d' , a measure of the observer's sensitivity to the signal, is found by subtracting Z_{SN} from Z_N (see Equation 3.5).

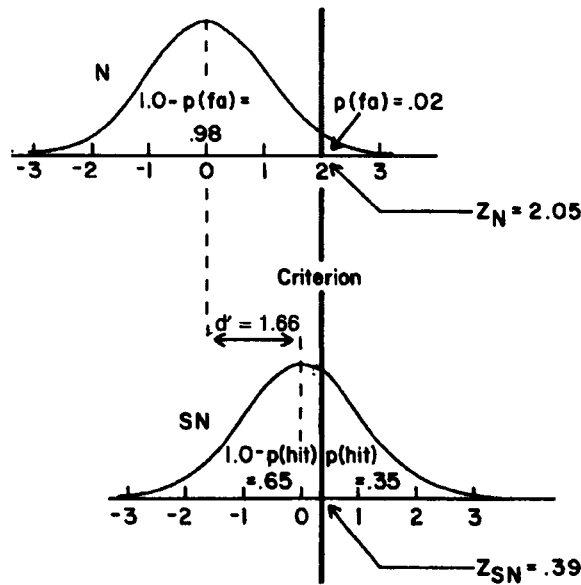


Figure 3.4 Distributions of a “noise” and a “signal plus noise” expressed in Z score values (Gescheider, 1997).

3.4.3 The ROC curve

One of the most important concepts to come out of the Theory of Signal Detection (TSD) is the Receiver Operating Characteristic (*ROC*) curve (Green and Swets, 1966; Swets, 1973) which was initially named an isosensitivity curve by Luce (1963) because all points on the curve have the same sensitivity value. The ROC graphs are two-dimensional graphs in which hit rate is plotted on the y-axis and false alarm rate is plotted on the x-axis (see Figure 3.5).

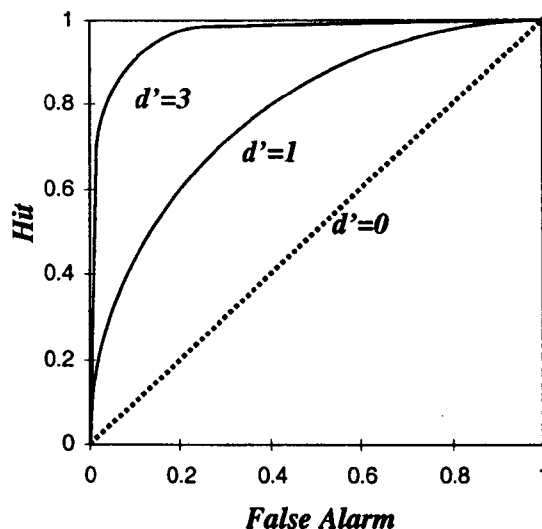


Figure 3.5 ROC curves for different detection criteria.

The ROC curve summarises the observer's performance as a function of the observer's decision criterion for all possible criteria (Green and Swets, 1966). As an example, Figure 3.5 shows different ROC curves in which detectability index values range from 0 to 3.0. An individual ROC curve reflects the response of an observer to a single strength of signal. If signal strength is increased, the ROC curve will have a more pronounced bow, as seen in Figure 3.5. If signal strength is decreased, the ROC curve becomes flatter and approaches the 45-degree diagonal line. Thus the amount of bow in the curve serves as a measure of the perceived signal strength. Variations in the observer's criterion result in different points along the ROC curve (see Figure 3.6). A single ROC curve is therefore a representation of detection performance for a situation characterised by a constant detectability index d' between a noise and a signal plus noise, but by changing values of the receiver detection criterion. Figure 3.6 presents the relationship between an individual ROC data point and the position of a noise and a signal plus noise distributions. The points on the curve indicate the mapping of hits and false alarms for different positions of the observer's criterion, while the dotted diagonal line represents the case where $d'=0$, when a noise and a signal-plus-noise distributions are identical.

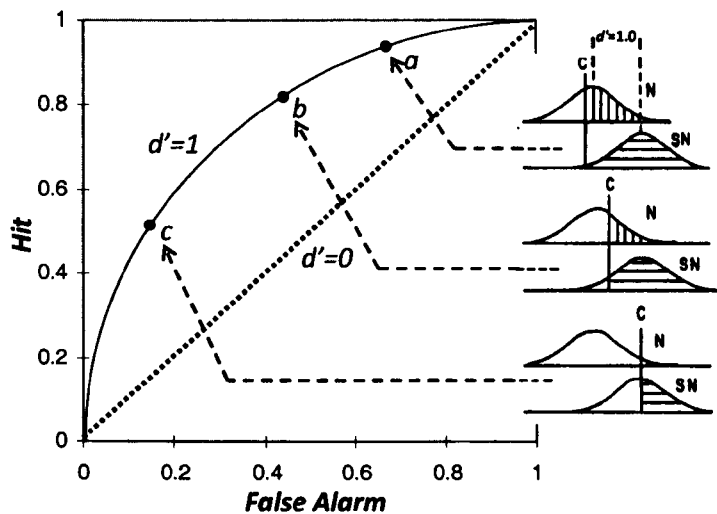


Figure 3.6 ROC curve for the signal plus noise and the noise distribution shown ($d'=1$) obtained over different observer's criterion.

Algebraically, an ROC curve is calculated by solving Equation 3.5 which means different curves represent different values of detectability index. The prediction of the Theory of Signal Detection states that if a subject in a discrimination experiment produce a (False-alarm, Hit) pair which belongs on a particular ROC curve (i.e. [0.2, 0.6], $d'=1$), the same

subject should be able to display any other (False-alarm, Hit) pair on the same curve (i.e. $[0.4, 0.8]$, $d'=1$) (Macmillan and Creelman, 2005).

Discrete observers are those whose outputs produce only a (False-alarm, Hit) pair which corresponds to a single point in the ROC space similar to those shown in Figure 3.7. Using the ROC point method each observer sets a criterion value which will determine a point in the ROC space. Points appearing close to the left-hand side upper corner of the ROC space are associated with classifications characterised by only a few false positive errors, while points appearing on the right-hand side lower corner are associated with classifications producing frequent false alarms.

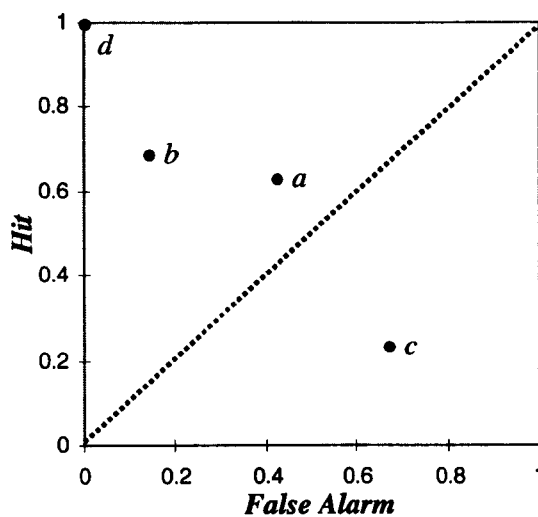


Figure 3.7 A basic ROC points graph showing four observers' pair responses.

4. Steering Vibration Measured from Road Testing

The objective of this chapter is to describe the steering wheel acceleration data which was used in the research presented in this thesis. As stated in Chapter 1, steering wheel vibration can be considered an important source of information to the driver (Pak et al., 1991). The acceleration level and spectral content of steering wheel vibration depend on several factors including the direction of vibration, the nature of the road surface, the dynamic characteristics of the tyres, the automobile speed and the design of the vehicle main suspension and steering mechanism. Vibrational energy at the steering wheel can reach frequencies of up to 300 Hz (Giacomin et al., 2004) and vibrational modes of the steering wheel and column can produce large resonant peaks in the steering wheel power spectrum at frequencies from 20 to 50 Hz (Pottinger et al., 1986).

Steering wheel acceleration data from tests performed on several road surfaces and several automobiles were used during the research described in this thesis to provide a wide statistical base of signals from which to define test stimuli. In particular, signal analysis was applied to quantify the typical statistical variation which occurred in the steering wheel vibration when driving over different road surfaces. Variations in the magnitude of the steering acceleration signals are chiefly caused by variations of the road roughness and by variations of the automobile speed (Gillespie and Sayers, 1983; Rouillard and Sek, 2002), where road roughness has been defined by the ASTM E1364-95 (2005) as “the deviation of a surface from a true planar surface with characteristic dimensions that affect vehicle dynamics, ride quality, dynamic loads, and drainage”. While the data presented in this chapter cannot be considered to be a definitive scientific analysis of road vehicle vibration, the values obtained can be considered to be typical of

the automotive vibration problem, thus useful for the purpose of defining specific laboratory-based experiments which can be considered representative of the automobile environment.

4.1 Experimental Vibration Tests

Before performing any laboratory tests of human ability to detect road surface type, or of human sensitivity to changes in the statistical properties of the steering acceleration signals, typical test stimuli from real automobiles had to be selected which could serve as the base stimuli for use in the research.

From a review of the available literature treating automotive vibration and from a review of the aims and objectives of the planned experimentation it was decided that the group of steering acceleration signals which could be used to study the human ability to detect road surface type should satisfy a set of logical conditions which can be summarised as the following:

1. The stimuli should come from normal production automobiles of the most commonly encountered manufacturers such as Ford, Renault, Toyota and Volkswagen and from the most commonly encountered market segments defined by the International Organization of Motor Vehicle Manufacturers, "Organisation Internationale des Constructeurs d'Automobiles" (OICA, 2008).
2. The stimuli should have been produced by commonly encountered road surfaces such as city asphalt, pave', potholes, bumps, country asphalt and smooth motorway surfaces, so as to be representative of ordinary driving conditions (Giacomin and Gnanasekaran, 2005).
3. The automobile test speeds should be reasonable values which are commonly used when driving over each specific type of surface (Department of Transport, 2006).
4. Where possible, the choices described by points 1 through 3 above should be made in such a way as to be as close as possible to the values used by the testing programmes of the major European automobile manufacturers, given their vast experience in the field of testing.
5. Where possible, the choices described by points 1 through 3 above should be made in such a way as to widen the amplitude range, the frequency range and the frequency distribution of the stimuli so as to produce the widest operational envelope of test stimuli.

4.2 MIRA Tests

Some of the steering wheel acceleration signals used in the research were provided by MIRA (Motor Industry Research Association). These acceleration measurements were performed at MIRA's proving ground in Nuneaton, Warwickshire, UK, which has a comprehensive range of circuits and facilities which are used to carry out a wide range of tests (MIRA Ltd, 2006).

4.2.1 Acceleration Measurement

Acceleration measurements were made at the automotive steering wheel. The measurement point was on the surface of the steering wheel at the 60° position (two o'clock position) with respect to top centre. This location coincides with a typical grip position of the driver's hand when holding an automotive steering wheel (Giacomin and Gnanasekaran, 2005).

All data were measured using an accelerometer which was clamped to the steering wheel measurement position by means of a mounting bracket of sufficient stiffness to guarantee accurate measurements to frequencies in excess of 500 Hz. The steering wheel acceleration time histories were digitally acquired using a PC-based digital data acquisition system running MIRA's own in-house software. The data acquisition system was placed inside the vehicle, and the data acquisition was triggered by the driver when driving over each road surface at a single constant speed. The sensors used in the road test data acquisition were Kyowa model AS-5GB accelerometers. The calibration of the MIRA measurement equipment was guaranteed by regularly scheduled calibration tests and by an internal quality assurance scheme.

4.2.2 Automobile Specifications

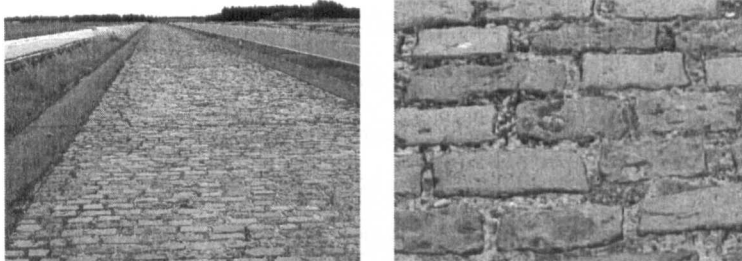
The automobile used by MIRA during the experimental vibration test was an Audi A4 model year 2000, type 4/5S SAL (4 doors, 5-speed manual transmission, saloon sedan). The engine was a turbocharged diesel 4-cylinder 1.8L with an EFi (Electronic Fuel injection) fuel system. The Audi A4 steering system was a rack and pinion Power Assist Steering (PAS) (see Chapter 1). The front suspension was an independent, four-link, double wishbone, and anti-roll bar (commonly abbreviated as I.4Li.DW.ARB.), while the rear suspension was an independent, trapezoidal link and anti-roll bar (commonly abbreviated as I.TzLi.ARB.). The front and rear tyres specifications were P195/65 R 15

meaning tyres from a passenger car (P), nominal section width in mm of 195, an aspect ratio of 65 for the ratio of the height to the total width of the tyre, Radial (R) construction of the fabric carcass of the tyre and a rim diameter in inches of 15.

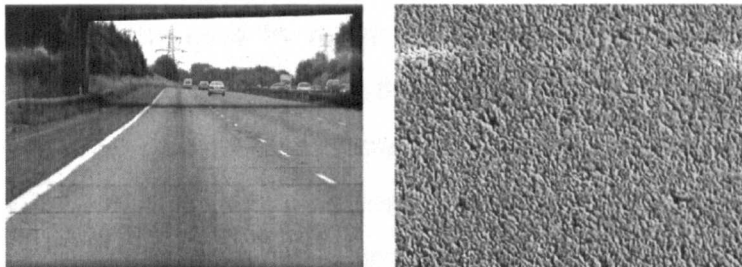
4.2.3 Description of Road Surfaces

The road surfaces used to measure the test stimuli were a Cobblestone surface, a Concrete surface, a Low Bump and a Tarmac surface. Figure 4.1 presents the four road surfaces as viewed from directly above and as seen from a distance as when driving, along with the automobile velocity at which they were measured.

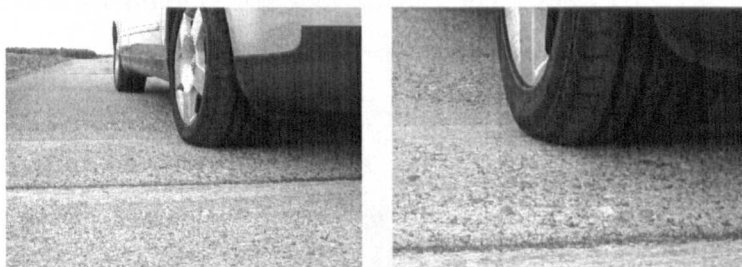
Cobblestone Road (vehicle speed 30 Km/h)



Concrete Road (vehicle speed 96 Km/h)



Low Bump (vehicle speed 50 Km/h)



Tarmac Road (vehicle speed 96 Km/h)

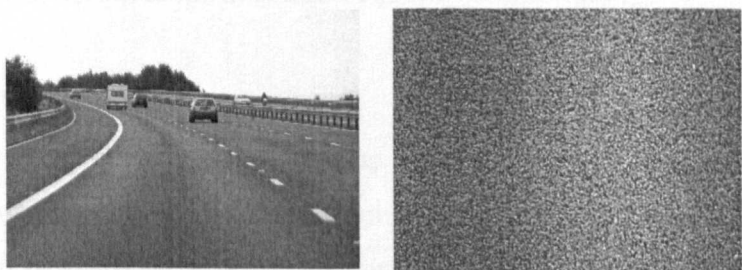


Figure 4.1 Road surfaces used by MIRA for their steering wheel vibration tests.

The four surfaces can be divided into two major categories, surfaces which produce a transient or impulsive input to the automobile and surfaces which produce a nearly stationary stochastic input (Giacomin and Masoero, 1993; Brucella et al., 1999; Rouillard et al., 2000). The first category includes the low bump which is basically an obstacle placed across a surface in the path of the automobile which produces an impulsive input. According to the Department of Transport (2006) in the UK this kind of obstacle is used in urban areas such as town centres, high streets, residential roads and in the vicinity of schools, therefore the automobile speed should be less than 40kph when driving over the obstacle.

The remaining surfaces measured by MIRA belong to the second category. The cobblestone surface is formed of rectangular stones such as those found in many Italian and French cities or in the city centre road surfaces in UK. The Department of Transport (2006) in the UK establishes a speed of less than 40kph to drive over such surfaces, the aim of this limit is to reduce vehicle speed due to the possible presence of vulnerable road users such as cyclists, children or the elderly. The concrete surface is formed by pieces of plain concrete which are coupled by means of expansion joints. The Tarmac surface, properly referred to as bituminous macadam or "Bitmac" for brevity, has the characteristic of being a smooth surface which is widely used to surface pavements, highways and even internal floors. The term bituminous refers to the product called bitumen which is produced by the oil-refining and petro-chemical industries, while the term macadam refers to the process of binding together smaller aggregates (BS 13108-1, 2006). The smoothness of the surface is determined by the aggregate type. The concrete surface and the tarmac surface are predominately used in non-built up areas or in built up areas where a higher speed is both safe and appropriate. Speeds above 90kph are common for these two types of road surfaces (Department of Transport, 2006). The four road surfaces measured by MIRA are of different nature thus they produce steering acceleration measurements of different amplitude and frequency distribution.

4.2.4 Signal Processing Analysis

Steering wheel tangential acceleration time histories were measured for the Audi A4 when driving over the four surfaces shown in Figure 4.1. For each road surface a 2 minute data recording was available from experimental testing. From each 2 minute recording a 10 second data segment of the tangential direction steering wheel acceleration time

history was extracted from each data set to serve as test stimuli. The individual segment for each surface type was selected such that the root mean square value, kurtosis value and power spectral density were statistically close to those of the complete 2 minute recording. Figure 4.2 presents the single 10 second time history segment of each of the four test roads.

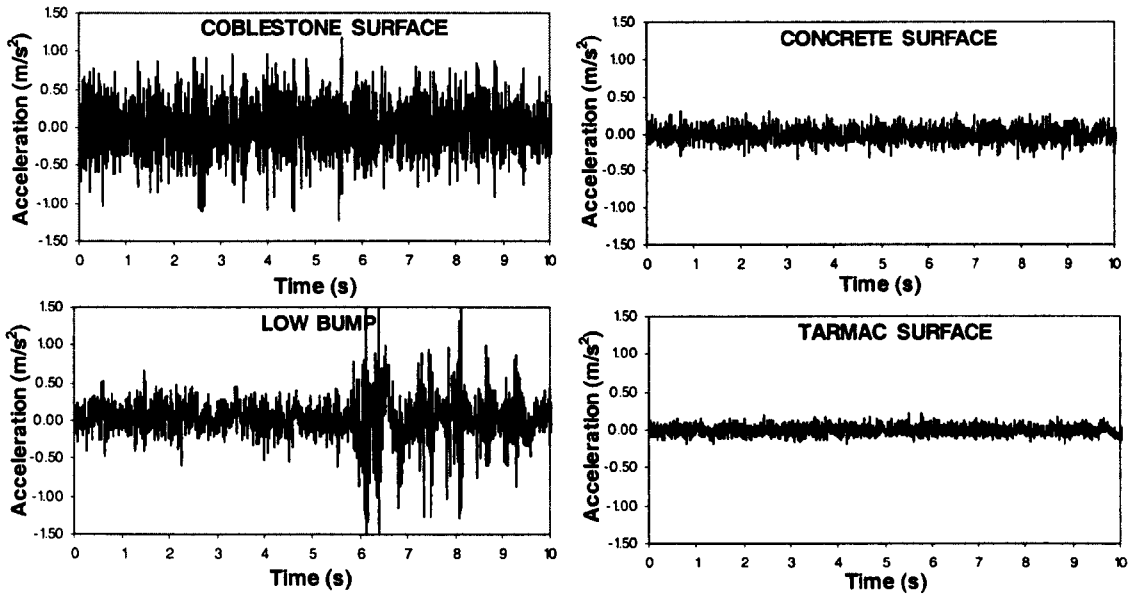


Figure 4.2 10 second segments of the tangential acceleration time history measured at the steering wheel for each of the four road surfaces (The MIRA test).

The global statistical properties calculated for the complete original 2 minute recording of each road surface is presented in Table 4.1 along with the automobile speed used during the measurement. The global statistical properties were calculated using the equations described in Chapter 2 (see Equations from 2.6 to 2.10). Results from Table 4.1 suggest that vibration at the steering wheel achieved root mean square (*r.m.s.*) acceleration levels from a minimum of 0.056 m/s^2 (for the tarmac surface) to a maximum of 0.287 m/s^2 (for the cobblestone surface). The kurtosis values were close to 3.0, suggesting a Gaussian distributed process, in all cases except for the low bump which had instead a kurtosis value of 12.672. The acceleration stimuli had skewness values which were close to 0.0 suggesting a Gaussian distributed process, in all cases except for the low bump which had a skewness value of -0.401. The maximum crest factor (CF) was obtained in the case of the low bump which produced a value of 7.485, while the minimum CF was found for the tarmac surface with a value of 3.872. Results for the vibration dose value (VDV) varied from $0.130 \text{ ms}^{-1.75}$ for the tarmac surface to $0.838 \text{ ms}^{-1.75}$ for the low bump.

Table 4.1 Global statistical properties of the four road stimuli (The MIRA test).

Type of Road Surface	<i>Global Statistics and Characteristics</i>					
	<i>r.m.s</i> (m/s ²)	Kurtosis (dimensionless)	Skewness (dimensionless)	CF (dimensionless)	VDV (ms ^{-1.75})	Speed (km/h)
Cobblestone	0.287	3.465	-0.002	4.710	0.736	30
Concrete	0.099	3.114	0.073	4.280	0.222	96
Low bump	0.216	12.672	-0.401	7.485	0.838	50
Tarmac	0.056	2.997	0.052	3.872	0.130	96

The power spectral density (PSD) of each of the two minute acceleration signals was calculated and the results are presented as Figure 4.3. Observation of the results suggests that the principal frequency content is mostly in the range from 0 to 80Hz for all four road surfaces. The highest peaks in the vibrational energy were found for the cobblestone surface, while the lowest peaks were found for the tarmac surface. The frequency distributions suggest that the higher peaks of energy correspond to the typical automobile resonance frequencies (Hamilton, 2000; Kulkarni and Thyagarajan, 2001; Pottinger and Marshall, 1986). The first region of resonance behaviour in the region from 0 to 5 Hz is common in any road data due to rigid body motion of the automobile chassis on the main suspensions. The second broader resonance region covering frequencies from 5 to 13 Hz can be associated with the behaviour of suspension units separately or with the rigid body motion of the engine/transmission unit. The third region resonance behaviour distributed between 13 and 22 Hz may reflect low frequency flexible body modes of the chassis. Finally, the fourth region from 22 to 100 Hz is probably mostly defined by higher-frequency modes of the chassis and by tire resonances (Giacomin and Lo Faso, 1993; Pottinger and Marshall, 1986).

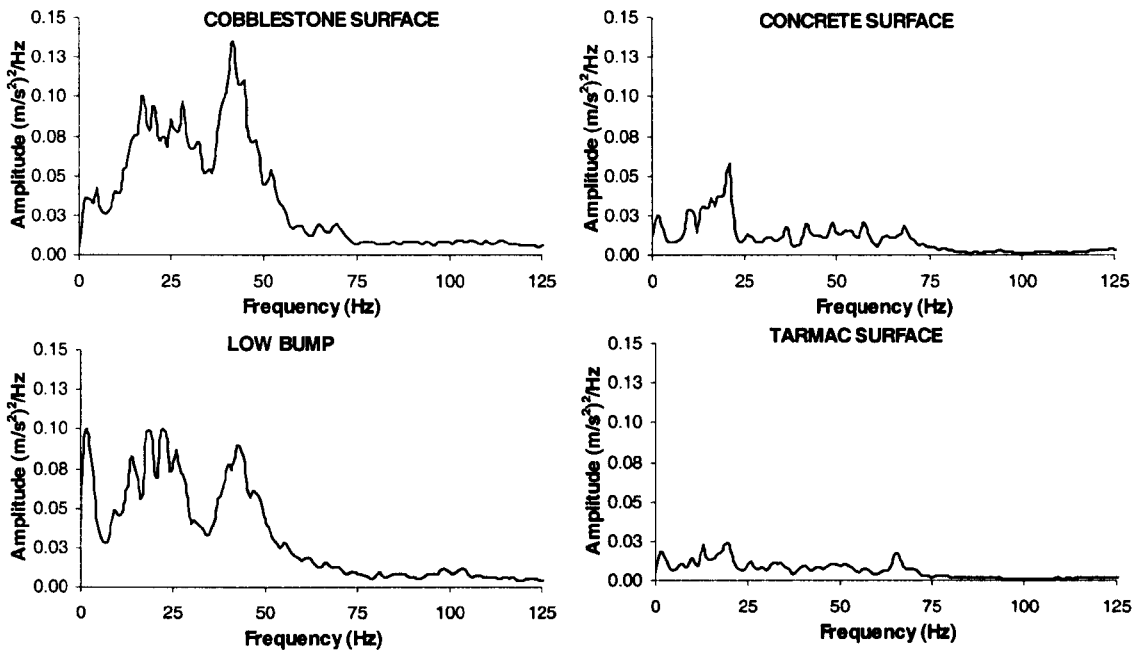


Figure 4.3 Power Spectral Densities (PSD) calculated from the four tangential acceleration time histories of the 2 minute duration which were measured at the steering wheel (The MIRA test).

4.3 Michelin Tests

Some of the steering wheel acceleration signals used in the research described in this thesis were provided by the Michelin Group. The acceleration measurements were performed at the Claremont-Ferrand proving ground in the province of Auvergne, France, which has a comprehensive range of circuits and facilities which are used to carry out a wide range of tests.

4.3.1 Acceleration Measurement

Acceleration measurements were made at the steering wheel in the same manner as the MIRA test which was described above in section 4.2.1. The steering wheel vibrations were measured by means of a tri-axial piezoresistive accelerometer (*Entran EGAS3-CM-25*). The acceleration signals were amplified by means of an *Entran MSC6* signal-conditioning unit, and stored using 6 channels of a Sony PC 216A Digital Audio Tape (DAT) recorder and monitored by a *Tektronix TDS 210* digital oscilloscope. The DAT sampling rate chosen for the vibration measurements was 5 kHz. The steering wheel acceleration time histories were digitally acquired using a PC-based digital data acquisition system running Michelin's own in-house software.

4.3.2 Automobile Specifications

The automobile used by Michelin during the acceleration measurements was a Renault Megane 1.9 dTi model year 1996, type 2+2 FHC (Fixed-Head Coupé), with 3 doors and a 5-speed manual transmission. The engine was a turbocharged diesel direct injection system (dTi) 4-cylinder 1.9 l. The Renault steering system was a rack and pinion Power Assist Steering (PAS). The front suspension was an independent and Macpherson strut (commonly abbreviated as I.M.S.), while the rear suspension was an independent (commonly abbreviated as I.). The front and rear tyre specifications were P175/65 R 14 (for tyre code description see section 4.2.2).

4.3.3 Description of Road Surfaces

The road surfaces used by Michelin to measure the steering wheel acceleration stimuli were officially named harsh surface and noise surface by the Michelin test centre. Figure 4.4 presents these two road surfaces as viewed from directly above, and as seen from a distance as when driving, along with the automobile test velocity. The harsh surface produced a transient or impulsive input to the automobile, while the noise surface produced a nearly stationary vibrational input.

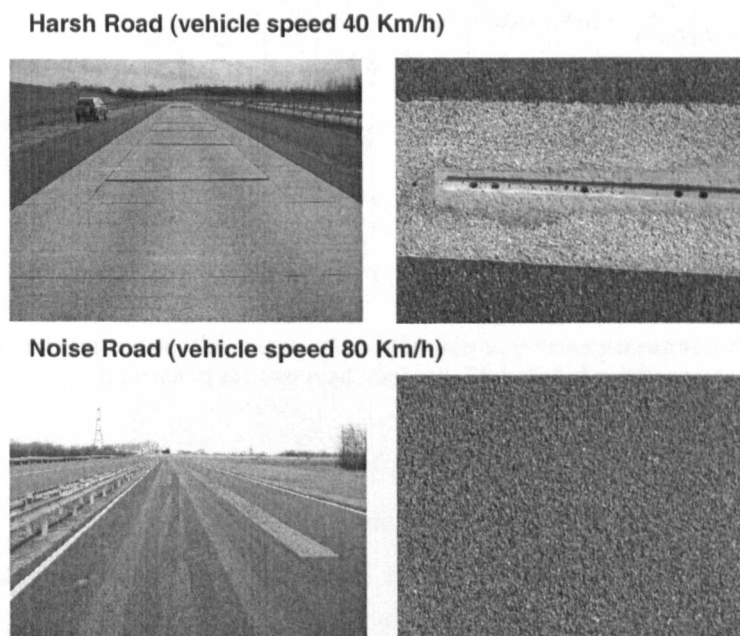


Figure 4.4 Road surfaces used by Michelin for their steering wheel vibration tests.

The harsh surface is a rectangular obstacle which produces impulsive input. This obstacle is basically a metal bar which is placed across an asphalt surface in the path of the

vehicle. The dimension of the bar is 100 mm in length by 25 mm in height. Given the nature of the bar, which resembles certain traffic calming measures adopted in cities, test speeds are normally less than 40 kph. The noise surface is a form of asphalt road which is widely encountered on pavements and highways. Speeds above 90kph are common for this kind of road surface. The two road surfaces were chosen because they represent a type of commonly encountered driving condition and because one of them, the harsh surface, produces great amounts of low frequency vibration while the other, the noise surface, produces great amounts of high frequency vibration.

4.3.4 Signal Processing Analysis

For each road surface a 1 minute data recording was available from experimental testing. A 10 second data segment of the tangential direction steering wheel acceleration time history was extracted from each data set to serve as test stimuli. The segments were selected such that the root mean square value, kurtosis value and power spectral density were statistically close to those of the complete recording. Figure 4.5 presents the time history segments selected for each of the road surfaces. As expected, different shapes and different acceleration levels are observed between the two road surfaces.

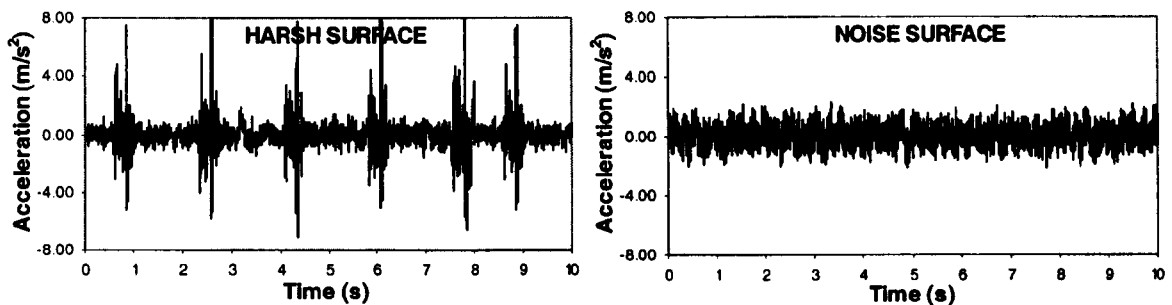


Figure 4.5 10 second segments of the tangential acceleration time history measured at the steering wheel for each of the two road surfaces (The Michelin test).

The global statistical properties calculated for the complete original 1 minute recording over each road surface is presented in Table 4.2 along with the automobile speed used during the measurement. Global statistical results were calculated using the equations described in Chapter 2 (see Equations from 2.6 to 2.10). Table 4.2 suggests that vibration at the steering wheel achieved root mean square (*r.m.s.*) acceleration levels of 0.710 m/s^2 for the noise surface and of 1.121 m/s^2 for the harsh surface. As occurs with Gaussian distributed processes, the noise surface had a kurtosis value close to 3.0 and a skewness value close to 0.0. The harsh surface, instead, produced a kurtosis value of 17.133 and a

skewness value of 0.986, which suggests that its acceleration data is not Gaussian distributed. The harsh surface also had the higher crest factor (CF) and VDV values compared with those obtained for the noise surface. The acceleration levels achieved for these two road surfaces were higher than those achieved in the MIRA measurements, where the acceleration level achieved by all the road surfaces was below 0.3 m/s^2 .

Table 4.2 Global statistical properties of the two road stimuli measured (Michelin test)

Type of Road Surface	Global Statistics and Characteristics					
	<i>r.m.s</i> (m/s^2)	Kurtosis (dimensionless)	Skewness (dimensionless)	CF (dimensionless)	VDV ($\text{ms}^{-1.75}$)	Speed (km/h)
Harsh	1.121	17.133	0.986	8.312	4.031	40
Noise	0.710	2.726	0.092	3.200	1.620	80

The power spectral density (PSD) calculated for each acceleration measurement is presented in Figure 4.6. As with the MIRA road surfaces (see section 4.2.4), the principal frequency content is in the range from 0 to 80 Hz for both road surfaces. The PSDs suggest that the highest peaks in the vibrational energy were found for the harsh surface, while lower peaks were found for the noise surface. The acceleration power spectral densities were found to be different between these two road surfaces, and also different from those produced by the MIRA road surfaces shown in Figure 4.3.

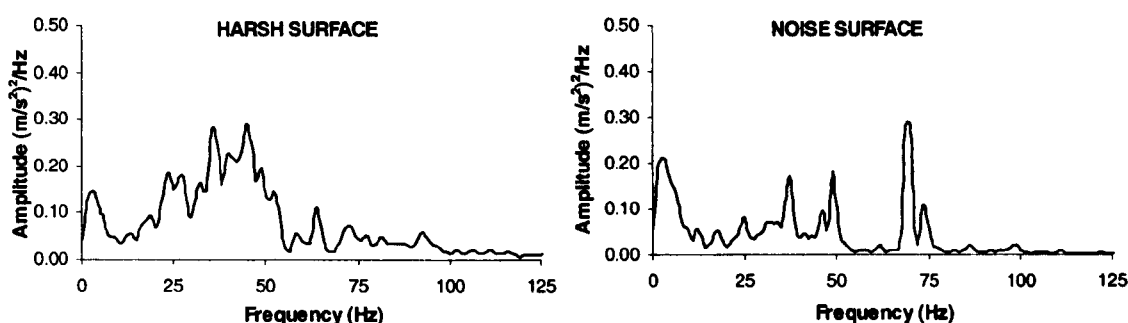


Figure 4.6 Power Spectral Densities (PSD) calculated from the two tangential acceleration time histories of the 2 minute duration which were measured at the steering wheel (The Michelin test).

4.4 Uxbridge Tests

In order to provide the widest possible statistical base of steering wheel acceleration signals a small number of measurements were also performed by the author over local roads whose characteristics differed from those which are typically found at the testing facilities of the motor vehicle manufacturers. The acceleration measurements were

performed over road surfaces in and around Uxbridge, West London, UK. The road surfaces were chosen due to their appearance and physical composition, which differed significantly from the MIRA and the Michelin road surfaces.

4.4.1 Acceleration Measurement

Acceleration measurements were made at the steering wheel as described previously in section 4.2.1. An example of the accelerometer position (two o'clock position) adopted for the Uxbridge measurements is presented in Figure 4.7. The direction of measurement for the steering wheel was taken along the tangential axis of the steering wheel.



Figure 4.7 Test measurements point for the accelerometer position at the steering wheel.

The steering wheel acceleration was measured by means of a SVAN 947 Sound and Vibration Level Meter and Analyser manufactured by SVANTEK Ltd., which uses a Low Impedance Voltage Mode (LIVM) accelerometer *3055B1*. The specifications of the accelerometer and the test equipment are provided in Appendix A. The accelerometer at the steering wheel measurement position was fixed by means of an aluminum clamp and mounting screws which guaranteed sufficient coupling stiffness to perform acceleration measurements in excess of 300 Hz. The geometrical dimensions of the steering wheel clamp are provided in Appendix B. The acceleration signals were stored using the SVAN 947 by means of its fast USB 1.1 interface (with 12MHz clock) which created a real time link for the application of the SVAN 947 as a PC front-end.

The SVAN 947 was run using a battery so as to eliminate electronic noise from vehicle systems. The sampling rate chosen for the acceleration measurements was 1 kHz. The rate of 1 kHz was sufficient to ensure that the acceleration stimuli were recorded with

adequate definition at the maximum frequency of interest of 512 Hz. The maximum analysis frequency of 512 Hz was chosen based on the assumption that the vibrational energy transmitted to the steering wheel can reach frequencies of up to 300 Hz when driving over certain road asperities and that the largest resonances are presented in the frequency range from 20 to 50 Hz (Pottinger and Marshall, 1986). The recorded signals were reacquired and analyzed at the Perception Enhancement Systems Laboratory by means of the *T-MON* module of the *LMS CADA-X 3.5E* software (LMS International, 2002), where signals were read as WAV files, transferred and converted to TDF (Test Data File) files into the LMS software. The signals were then resample at 512 Hz.

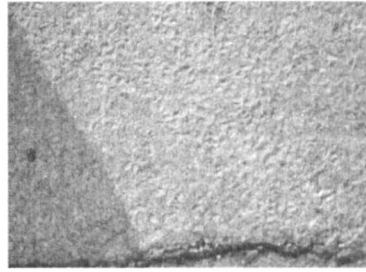
4.4.2 Automobile Specifications

The automobile used for the steering wheel tangential acceleration acquisition was a VW Golf 1.9 TDI model year 2005, type 5/5S HBK (5 doors, 5-speed manual transmission, Hatchback). The engine was a turbocharged diesel direct injection (TDI) 4-cylinder 1.9l. The steering system was a rack and pinion Power Assist Steering (PAS). The front suspension was an Independent, Macpherson Strut, Coil Spring with an Anti-Roll Bar (commonly abbreviated as I.MS.CS.ARB), while the rear suspension was an Independent, Torsion Bar, Coil Spring with an Anti-Roll Bar (commonly abbreviated as I.TB.CS.ARB.). The front and rear tyres specifications were P205/55 R 16 (for tyre code description see section 4.2.2).

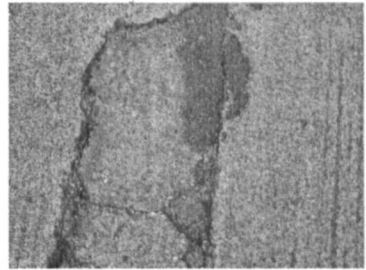
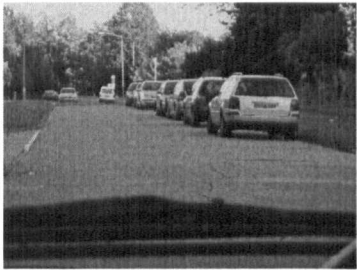
4.4.3 Description of Road Surfaces

The eight road surfaces were used for the steering acceleration tests are shown in Figure 4.8. They were named by the author as: Broken, Broken Concrete, Broken Lane, Bump, Cat's eyes, Cobbleston city, Country Lane and Motorway.

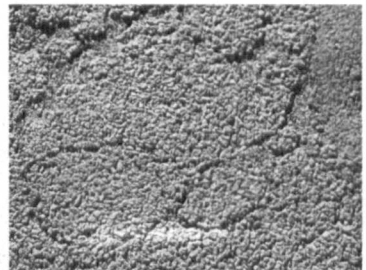
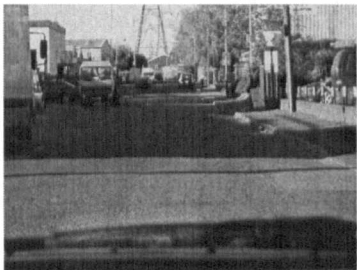
Broken (vehicle speed 40 Km/h)



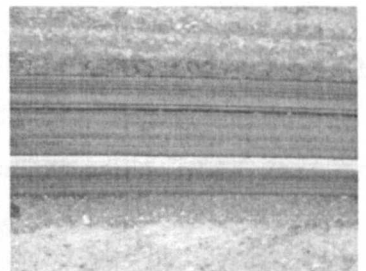
Broken Concrete (vehicle speed 50 Km/h)



Broken Lane (vehicle speed 40 Km/h)



Bump (vehicle speed 60 Km/h)



Cats-rhs (vehicle speed 40 Km/h)

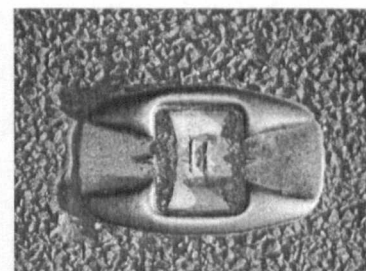
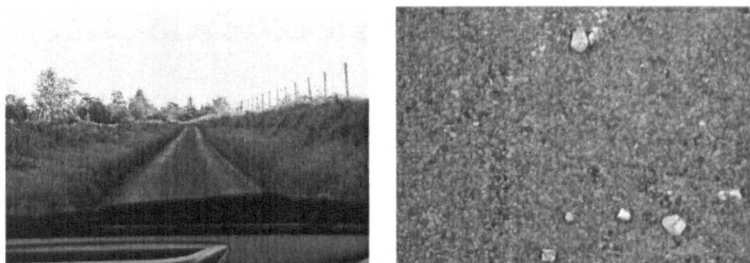
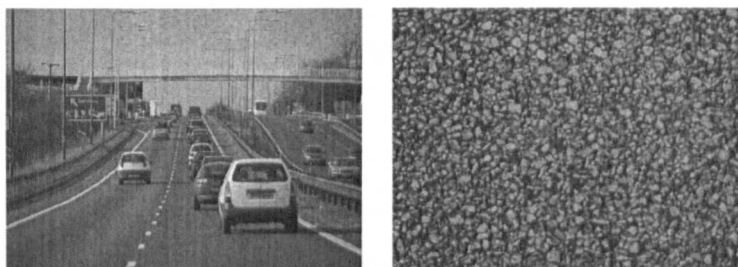


Figure 4.8 Road surfaces used by the author for the Uxbridge steering wheel test.

Country Lane (vehicle speed 40 Km/h)



Motorway Road (vehicle speed 110 Km/h)



Cobblestone City Road (vehicle speed 40 Km/h)

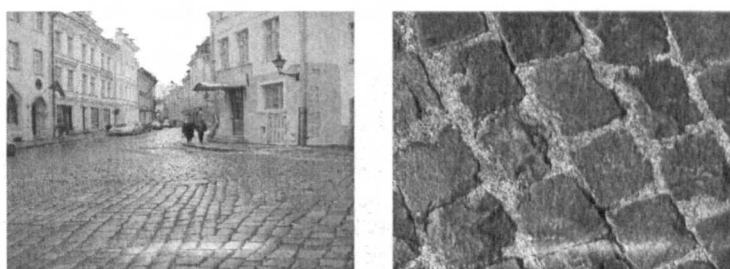


Figure 4.8 Road surfaces used by the author for the Uxbridge steering wheel test (continuation).

Damaged surfaces such as the Broken, Broken Concrete and Broken Lane are asphalt or concrete surfaces which are commonly found in many areas in the UK. The Bump and the Cat's eyes are types of surfaces which produce impulsive input, and as stated in previous sections of the chapter are basically obstacles placed across a surface in the path of the automobile in order to force drivers to either decrease the speed (i.e. bump) or to avoid to lane changing (i.e. cat's eyes). Speeds to drive over damaged surfaces can reach levels of up to 50kph, while the speed in the case of surfaces with obstacles such as the cat's eyes depends on the type of road surface on which they are placed (Department of Transport, 2006).

The country lane surface and the motorway surface are asphalt road surfaces which produce a nearly stationary acceleration signal. The country lane surface, which is commonly found in rural areas, is a type of road where stones and pieces of wood can be found across the asphalt surface. According to the Department of Transport, in the UK the speed limit in rural areas can vary from 32 kph to 50 kph. The motorway surface, on the

other hand, is a smoother type of asphalt road. The speed limits to drive over this kind of road surface can reach levels of up to 110 kph in the UK.

The cobblestone city surface has similar characteristics to those found for the cobblestone surface which was described in section 4.2.3. The city cobblestone surface is formed of rectangular stones and is the kind of surface which is found in many city centres in the UK. The recommended speed to drive over this road surface is less than 40kph for safety and security purposes (Department of Transport, 2006).

4.4.4 Signal Processing Analysis

Steering wheel tangential acceleration time histories were measured using a VW Golf automobile which was driven over the eight surfaces shown in Figure 4.8. For each road surface a 1 minute data recording was made. Figure 4.9 presents the 10 second data segment which was extracted from the tangential direction steering wheel acceleration time history of each data set so as to serve as test stimuli. The segments were selected such that the root mean square value, the kurtosis and the power spectral density were statistically close to those of the complete recording. From Figure 4.9 it can be observed that each road surface achieved a rather different acceleration level.

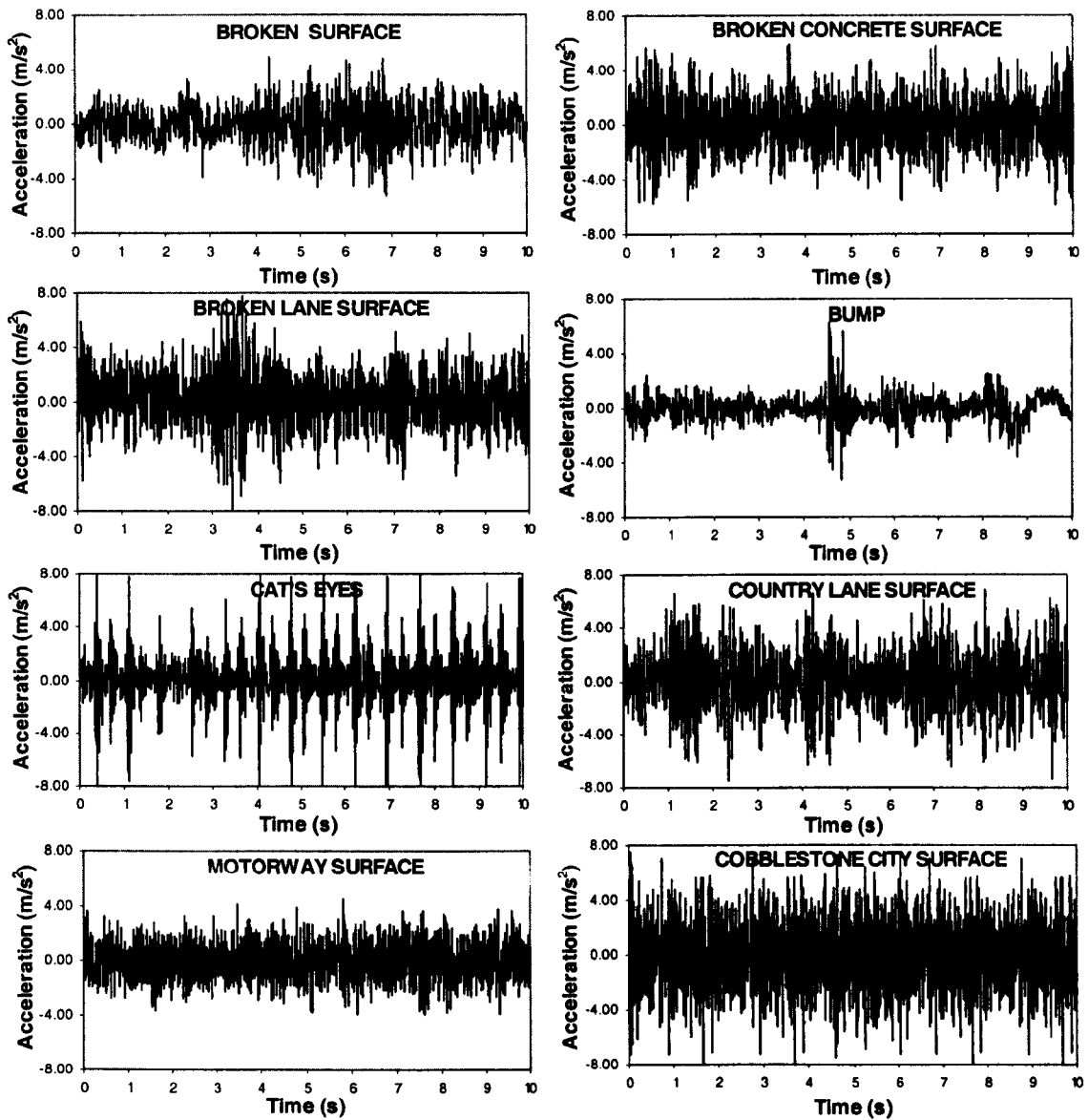


Figure 4.9 10 second segments of the tangential acceleration time history measured at the steering wheel for each of the eight road surfaces (The Uxbridge test).

Table 4.3 presents the global statistical properties determined from the data of each of the road surfaces. Root mean square (*r.m.s.*) acceleration levels from a minimum of 1.147 m/s^2 (for the motorway surface) to a maximum of 2.355 m/s^2 (for the broken lane surface) were found. Kurtosis value larger than 3.0 were found for those road surfaces which produced an impulsive input to the vehicle subsystems (i.e. the bump and the cat's eyes), while the remaining road surfaces had kurtosis values close to 3.0. The largest skewness value was found for the cat's eyes surface with a value of -0.266 , while the remaining road surfaces had skewness values close to 0.0. The bump had the highest crest factor (CF) at approximately 7.330, and the cat's eyes had the highest VDV at approximately $5.946 \text{ ms}^{-1.75}$. The root mean square (*r.m.s.*) acceleration levels achieved with these eight

road surfaces were higher than those achieved for both the MIRA test and the Michelin test.

Table 4.3 Global statistical properties of the eight road stimuli measured (The Uxbridge test)

Type of Road Surface	<i>Global Statistics and Characteristics</i>					
	<i>r.m.s</i> (m/s ²)	Kurtosis (dimensionless)	Skewness (dimensionless)	CF (dimensionless)	VDV (ms ^{-1.75})	Speed (km/h)
Broken	1.230	3.775	-0.048	3.920	3.200	40
Broken Concrete	2.028	3.210	0.010	3.360	4.127	50
Broken Lane	2.355	3.630	-0.030	4.400	4.380	40
Bump	1.860	7.660	-0.056	7.330	2.655	60
Cat's Eyes	2.048	6.800	-0.266	4.260	5.946	40
Country Lane	2.180	3.630	-0.030	4.400	4.897	40
Motorway	1.147	3.080	0.030	3.550	2.783	110
Paveb	2.161	3.423	-0.078	3.462	5.377	40

Power spectral densities (PSD) were calculated for the eight acceleration measurements and are shown in Figure 4.10. The principal frequency content is in the range from 0 to 80 Hz as was previously seen in the MIRA and Michelin tests. The highest peaks in the PSD energy were found for the cat's eyes surface, while the lowest peaks were found for the motorway surface and the broken surface. The acceleration PSDs were found to be different across the eight road surfaces, and also different from those produced by the MIRA road surfaces and the Michelin road surfaces, as seen in Figure 4.3 and Figure 4.6.

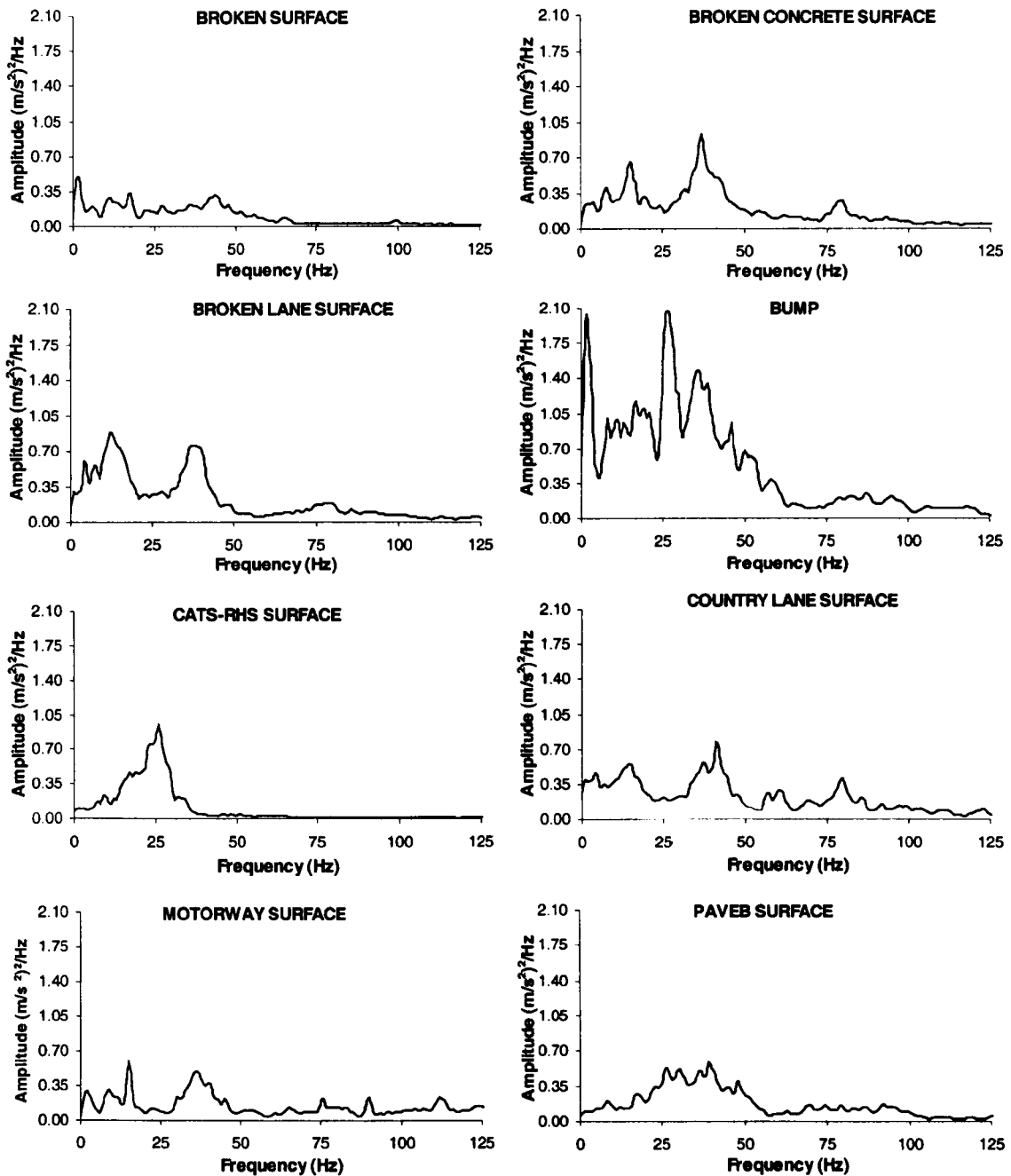


Figure 4.10 Power Spectral Densities (PSD) calculated from the four tangential acceleration time histories of the 1 minute duration which were measured at the steering wheel (The Uxbridge test).

4.5 The Selected Steering Wheel Vibration Stimuli

Although the data presented in this chapter cannot be considered to be a definitive scientific analysis of road vehicle vibration, the values obtained can be considered to be typical of the automotive vibration problem, thus useful for the purpose of defining specific laboratory-based experiments which can be representative of the automobile environment. The selected group of test stimuli provide data sets which achieved the five

criteria established at the beginning of the chapter in order to obtain steering wheel vibration to use in the study of human ability to detect road surface type.

The global statistical properties of all fourteen road surfaces analysed in this chapter and summarised in Tables 4.1 to 4.3 showed that although the majority of the road surfaces obtained statistical values close to those observed for a Gaussian distributed process, differences are presented across all road surfaces in two of their main statistical values. These differences were presented for the root mean square value and for the VDV value. Figure 4.11 presents the distribution of the fourteen road surfaces based on these two statistical properties which suggested that the steering wheel acceleration data from the tests performed in this chapter provided a wide statistical based of signals. Due to they are covering a wide range of root mean square (*r.m.s.*) acceleration levels from a minimum approximately of 0.06 m/s^2 to a maximum approximately of 2.4 m/s^2 , and also a wide range of VDV values from a minimum approximately of $0.13 \text{ ms}^{-1.75}$ to a maximum approximately of $6.00 \text{ ms}^{-1.75}$.

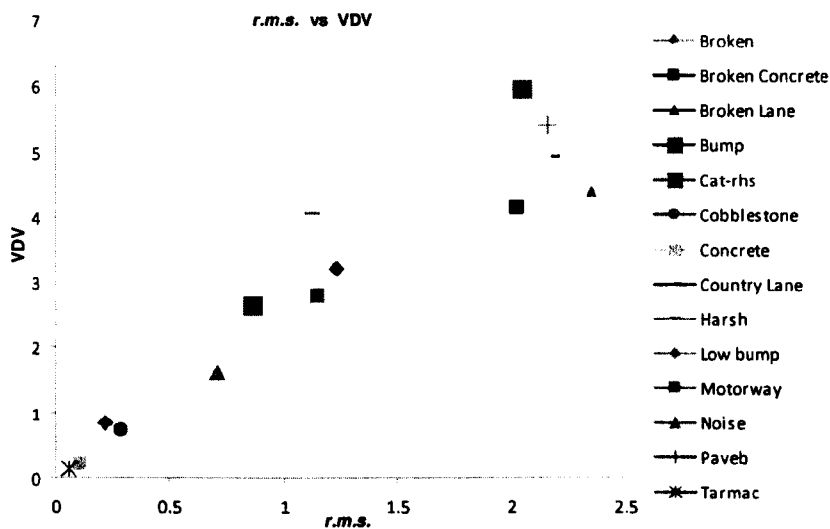


Figure 4.11 Distribution of the statistical values of the fourteen road surfaces: *r.m.s.* acceleration level against VDV value.

5. Test to evaluate the Effect of Steering Wheel Acceleration Magnitude on the Human Detection

Due to the lack of scientific literature concerning human cognitive detection in vibrational scenarios, the possible influence of several factors had to be evaluated so as to understand the mechanisms involved. The experimental testing activities described here were performed in order to measure the sensitivity of the human detection task to changes in the primary characteristic (scale) of the steering wheel acceleration stimuli. The main objectives of the study were:

- To measure the percentage of correct detection of the road surface type and the detectability index d' based on steering wheel vibration.
- To measure the percentage of correct detection of the road surface type and the detectability index d' based on steering wheel vibration when it has been scaled.
- To verify if one single scale value could improve the human detection for all road surface types.

The results of the experiment tests were plotted using the Theory of Signal Detection as the analytical framework and were summarised by means of both the detectability index d' and receiver operating curve (ROC) points.

5.1 Experimental Apparatus

5.1.1 Test Facility Specifications

The test facility adopted in this study for applying rotational vibration to a seated test subject used an existing steering wheel test rig, shown in Figure 5.1a, which was built in the Perception Enhancement Systems laboratory. A schematic representation of the steering wheel test rig and of the associated signal conditioning and data acquisition system is shown in Figure 5.1b.

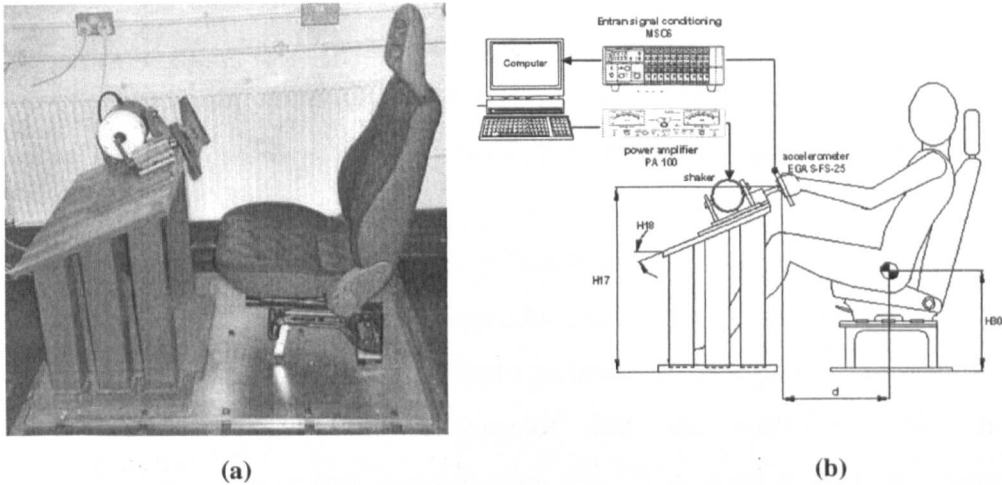


Figure 5.1 Steering wheel rotational vibration test facility

The rotational system consisted of a 325mm diameter aluminium steering wheel attached to a steel shaft which was in turn mounted to two SKF bearings. The shaft was connected to the electro-dynamic shaker head by means of a copper stinger-rod. Table 5.1 presents the main geometric dimensions of the test rig, which were chosen based on data from a small European automobile. The seat was fully adjustable in terms of horizontal position and back-rest inclination as in the original vehicle.

Table 5.1 Geometric dimensions of the steering wheel rotational vibration test rig

Geometric Parameter	Value
Steering column angle (H18)	23°
Steering wheel hub centre height above floor (H17)	710 mm
Steering wheel diameter (W9)	325 mm
Steering wheel tube diameter	25 mm
Horizontal distance from H point to steering wheel hub centre (d= L11-L51)	390–550 mm
Seat H point height from floor (H30)	275 mm

Rotational vibration was applied by means of a G&W V20 electro dynamic shaker driven by PA100 amplifier (Gearing & Watson Electronics Ltd, 1995). The steering wheel tangential acceleration was measured by means of an Entran EGAS-FS-25 accelerometer attached to the top left side of the wheel. The specifications of the accelerometer and of the vibration equipment are provided in Appendix C. The accelerometer signal was amplified by means of an Entran MSC6 signal conditioning unit (Entran Devices Inc., 1991). Control and data acquisition are performed by means of the LMS TMON software system coupled to a DIFA SCADASIII unit (LMS International, 2002). The car seat was directly taken from a 1997 Fiat Punto and was fully adjustable in terms of horizontal position and back-rest inclination as in the original vehicle. Test rig usage conformed to the health and safety recommendations of British Standards Institution BS7085 (2001).

5.1.2 Accuracy of the Steering Wheel Test Rig

In order to determine the stimuli reproduction accuracy of the test rig facility an evaluation was performed. The procedure evaluated the complete chain composed of the LMS software, the front end electronics unit, the electro-dynamic shaker, the accelerometer and the signal conditioning unit. The accuracy of the target stimuli reproduction was quantified by measuring the *r.m.s.* difference between the actuated signal and the target signal. Steering vibration stimuli to be used as the target signals were selected from four of the fourteen base stimuli described in Chapter 4 (tarmac, concrete, cobblestone and low bump). Six copies of each of the four selected acceleration time histories were constructed by rescaling the data using factor values of 0.8, 0.9, 1.0, 2.0, 3.0 and 4.0 obtaining a total of 24 target signals. The *r.m.s.* values of the target calibration stimuli ranged from a minimum of 0.045 m/s^2 (*r.m.s.*) to a maximum 1.116 m/s^2 (*r.m.s.*). Pretesting revealed that the power spectral densities of the reproduced stimuli did not match the target values due to the frequency response of the shaker and the bench mechanical components. Also, a maximum *r.m.s.* acceleration level difference between the actuated signal and the target signal was found to be approximately 32%.

Digital filters were therefore defined which compensated the effect of the frequency response of the shaker and mechanical components. A digital filter is an analytical expression which can transform a sampled, discrete-time signal to reduce, enhance or compensate certain aspects of the signal (Lyons, 2004; Strum and Kirk, 1988). As an example of the process, Figure 5.2 presents the PSD of the target stimuli and of the test

rig response signal for a cobblestone surface at the original scale value of 1.0 for both the non-filtered (Figure 5.2a) and the filtered (Figure 5.2b) steering signals. Figure 5.2 suggests that the energy level and distribution is almost the same when a digital filter is applied to compensate the signal. In this case, *r.m.s.* acceleration level difference between the actuated signal and the target signal was found to be less than 3%.

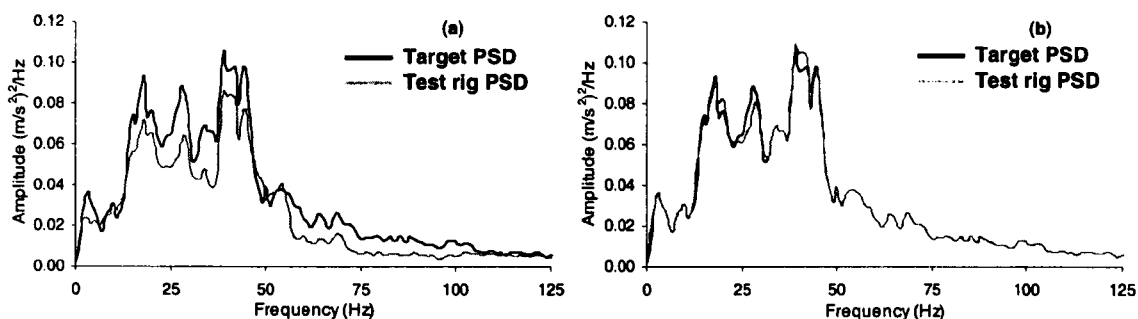


Figure 5.2 Use of compensator digital filter:
a) Comparison between target and test rig acceleration PSDs before filtering
b) Comparison between target and test rig acceleration PSDs after filtering.

Each of the 24 target stimuli was filtered and used in a pre-test in order to calculate the absolute maximum percentage of error between the *r.m.s.* acceleration level of the target signal and the actuated signal. Each stimulus was used three times during which the actuated acceleration response was recorded by means of the Entran EGAS-FS-25 accelerometer placed on the top left side of the steering wheel. Eight participants were used in the pre-test process so as to consider also the possible differences in bench response which are caused by differences in impedance loading on the steering wheel from people of different size. The subjects who participated in the acceleration magnitude experiment consisted of 4 males and 4 females. The physical characteristics of the group are summarised in Table 5.2, the mean values and standard deviations of all three measures can be seen to be near the UK population values for the height and mass. Results presented in Table 5.3 suggested that the maximum percent of error was found to be less than 5% for all stimuli used in the pre-test. This value is less than just noticeable difference for human perception of hand-arm vibration.

Table 5.2 Physical characteristics of the group of pre-test participants involved in the laboratory experiments (n=8)

Characteristics	Mean	STD	Minimum	Maximum
Age (years)	29.25	3.92	24	37
Height (m)	1.71	0.10	1.58	1.82
Mass (kg)	70.13	9.51	55	85

(STD) Standard Deviation

Table 5.3 Steering wheel test rig stimulus reproduction accuracy for four scaled steering signals (using six scale values 0.8, 0.9, 1.0, 2.0, 3.0 and 4.0), three repetitions of each of the 24 stimuli were performed (n=8)

Steering Acceleration Stimuli from different road type	Scale Factor Value	Original Signal (r.m.s.) m/s ²	Actuated Signals (r.m.s.) m/s ²	Absolute Maximum Percent Error (%)
			Mean Subjects (n= 8)	
TARMAC	0.8	0.045	0.044	2.22
	0.9	0.050	0.050	0.00
	1.0	0.056	0.058	3.57
	2.0	0.112	0.113	0.89
	3.0	0.168	0.167	0.60
	4.0	0.224	0.225	0.45
CONCRETE	0.8	0.079	0.079	0.00
	0.9	0.089	0.087	2.25
	1.0	0.099	0.101	2.02
	2.0	0.198	0.198	0.00
	3.0	0.298	0.296	0.67
	4.0	0.397	0.396	0.25
COBBLESTONE	0.8	0.223	0.229	2.69
	0.9	0.251	0.259	3.19
	1.0	0.279	0.282	1.08
	2.0	0.558	0.543	2.69
	3.0	0.837	0.803	4.06
	4.0	1.116	1.109	0.63
BUMP	0.8	0.240	0.235	2.08
	0.9	0.260	0.254	2.31
	1.0	0.272	0.274	0.74
	2.0	0.564	0.563	0.18
	3.0	0.780	0.801	2.69
	4.0	1.075	1.099	2.23

5.2 Experiment to Measure the Effect of Acceleration Magnitude

By measuring the sensitivity of the human detection task to changes in the primary characteristics of the scale of the steering acceleration stimuli the research attempted to define one of the basic dynamic characteristics that an automotive steering system should have in order to be capable of applying low level perceptual assistance to the driver. A

natural question which arises in the case of the steering system is if one single, fixed, feedback gain is optimal and improves the human detection for all road surface types.

A group of four road surfaces was selected to be tested in the study, which were: a Tarmac surface, a Concrete surface, a Cobblestone surface and a low bump. These road surfaces were selected in order to remain consistent with a previous study by Giacomini and Woo (2004). Due to the lack of information in this field it was considered important to perform a check and validation of the previous results obtained by Giacomini and Woo.

5.2.1 Test Subjects

The experiment involved the participation of 15 university staff and students. Upon arriving in the laboratory each participant was issued information and a consent form as well as an explanation about the experimental method and the laboratory safety features. Age, gender, height, and mass data were then collected and each participant was also requested to state whether he or she had any physical or mental condition which might effect perception of hand-arm vibration, and whether he or she had ingested coffee within the 2 hours previous to arriving in the laboratory. No participant declared any condition which might affect the perception of hand-arm vibration, and none declared having ingested coffee prior to their tests. The subjects who participated in the acceleration magnitude experiment consisted of 8 males and 7 females. The physical characteristics of the group are summarised in Table 5.4, the mean values and standard deviations of all three measures can be seen to be near the UK population values for the height and mass, but lower than the mean and standard deviation of the UK population in age.

Table 5.4 Physical characteristics of the group of test participants involved in the laboratory experiments (n=15)

Characteristics		Mean	STD	Minimum	Maximum
Age	(years)	27.73	5.06	20	40
Height	(m)	1.71	0.08	1.57	1.82
Mass	(kg)	71.67	10.87	55	90

(STD) Standard Deviation

5.2.2 Test Stimuli

The stimuli actuated at the wheel during experiment consisted of scaled signals taken from all four road surface types. Six scale factors were used for this purpose, which are 0.8, 0.9, 2.0, 3.0 and 4.0. The selection of these scale factors was based on the results from previous experiment carried out by Giacomini and Woo (2004) in which the authors selected scale values of 0.6, 0.8, 1.0, 4.0 and 7.0 so as to remain within the operational limits of the test equipment and to remain within realistic limits for real automobile. The *r.m.s.* acceleration values of the scaled stimuli ranged from a minimum of 0.045 m/s^2 (*r.m.s.*) to a maximum 1.116 m/s^2 (*r.m.s.*), all acceleration levels for the manipulated and un-manipulated stimuli were presented in Table 5.3. The mathematical operation of scaling was chosen so as to not affect spectral or phase relationships of the stimuli.

5.2.3 Test Protocol

Upon arriving in the laboratory each participant was asked to remove any articles of heavy clothing such as coats, and to remove watches or jewellery. He or she was asked to sit in the test rig and to adjust the seat so as to achieve a realistic driving posture. The participant was then asked to fix his or her eyes on a board directly in front of the test rig, which displayed a photograph of one of the four road surfaces which was being used in the test. Prior to commencing formal testing, the participant was provided an example of each of the four stimuli types which would be used later, in order to become acquainted with the detection task.

The detection task was to state by means of “yes” or “no” whether the actuated acceleration stimulus was from the road surface whose photograph was shown on the board directly in front of the test bench. When the response and the stimulus matched, the event was taken to be a correct detection. False alarms, on the other hand, were taken to be those situations when the participant responded “yes” to a stimulus which was not derived from the displayed road surface. During the course of the test no feedback was provided by the experimenter to the test participant at any point regarding whether the detection were correct or incorrect.

The experiment was performed in four parts, one for each road surface studied. Each involved five repetitions of each of un-manipulated and manipulated stimuli from the displayed road surface. In addition, twenty four stimuli were chosen randomly from the

stimuli sets of the other road surfaces which were used as background noise stimuli. The time duration of each individual test stimuli was chosen to be 10 seconds based on the knowledge that the tactile system of the hand does not present temporal integration properties below approximately 40 Hz (Gescheider et al., 1994). Six different series of nine acceleration stimuli were applied for each road surface type. In each series, each stimulus was separated from each other stimulus by a 5 second gap in which the participant was asked to state his or her judgment of road surface type. The order of stimuli presentation was fully randomised for each participant in each series in order to reduce learning effects. Each participant performed 54 detections for each road surface type, and a total of 216 detections in the complete experiment.

5.2.4 Results from the Experiment to Measure the Effect of Steering Wheel Acceleration Magnitude

Figure 5.3 presents the results obtained from the experiment to determine the effect of the steering wheel acceleration magnitude on the human ability to detect road surface type. The results are presented in terms of percent correct detection, from 0 to 100 percent. Percent correct detection is presented along the ordinate, while the scaled values are presented along the abscissa. The original base stimuli are labelled as x1.0 which means that all data points in the acceleration time history remain with the same acceleration magnitude since they are multiplied by the unity, while the five scaled values used are labelled as x0.8, x0.9, x2.0, x3.0 and x4.0. The percentage of correct detection responses for the four road surfaces were analysed in a between/within-subjects by means of the one factor repeated measures ANOVA. Statistical significance effect in the responses were found in all surfaces tested at a $p=0.01$ of significance level with a $F(5,70)$ value spanning from 7.76 to 38.51.

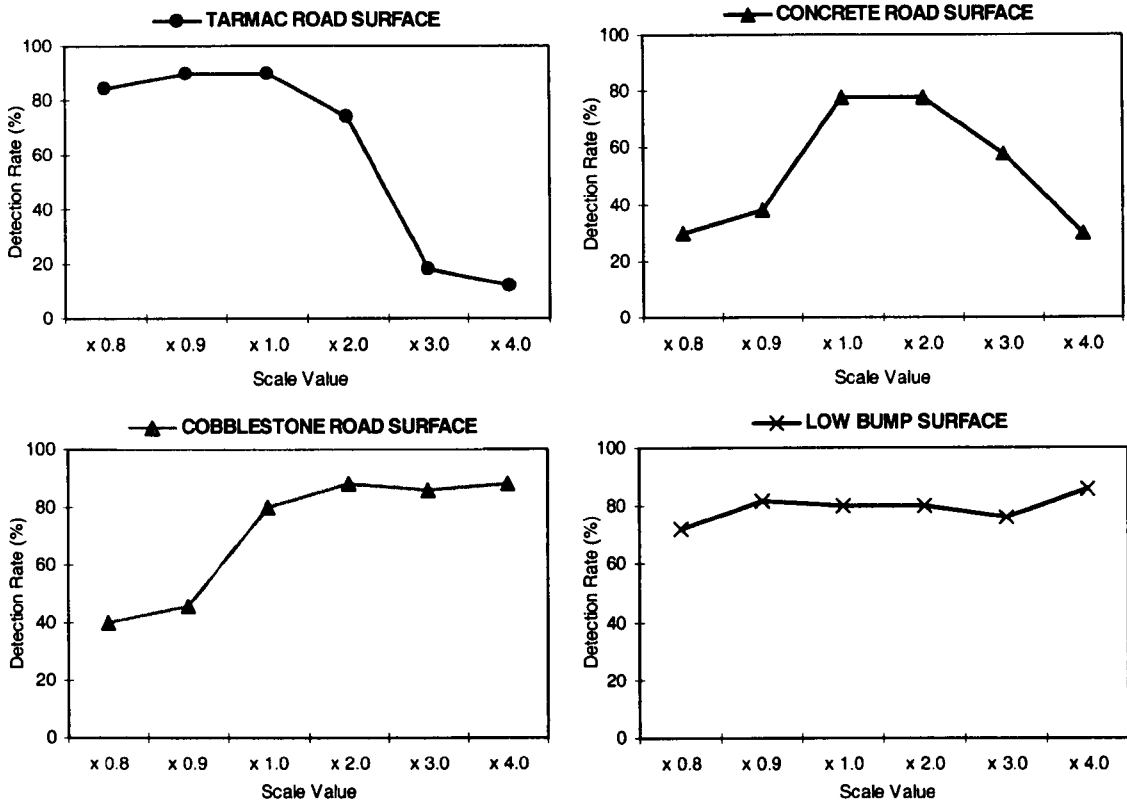


Figure 5.3 Results of the experiment to measure the effect of steering wheel acceleration magnitude on the human detection of road surface type in terms of percent correct detection (n=15).

As shown in Figure 5.3, the percentage of correct detection for the original base stimuli for the current experiment was approximately 90% for the tarmac stimuli, 78% for the concrete stimuli, 80% for the cobblestone stimuli and 79% for the low bump stimuli. These values can be compared to the values of approximately 82%, 46%, 48% and 60% respectively obtained by Giacomini and Woo (2004) for the same four surfaces. The higher percentages of correct detection found in the current study can be partially attributed to the fact that smaller and larger multiplication factors were used in the previous study (x0.6 and x7.0), thus creating a situation where the detection task was performed against a less complicated background noise. Nonetheless, the curves of percent correct detection from both experiments showed similar qualitative behaviour for each road surface tested.

As shown in Figure 5.3 by the results obtained for acceleration level x1.0, the use of the mathematical operation of scaling to manipulate the signals produced only mixed results. Although the Cobblestone stimuli, the Tarmac stimuli and the Concrete stimuli were categorised into the group of surfaces which produce a nearly stationary stochastic input to the automobile (section 4.2.3), three distinct behaviours can be identified from the

results of the three road surfaces: 1) The percentage of correct detection decreased for the Tarmac stimuli; 2) The percentage of correct detection increased and after decreased for the concrete stimuli; and 3) The percentage of correct detection increase for the cobblestone stimuli. The low bump road, instead, categorised into the group of surfaces which produce a transient or impulsive input to the automobile (section 4.2.3) increased the percentage of correct detection as a function of scale. The results show, however, that the percentage of correct detection of the low bump did not decrease below 73% at any scale factor tested. It suggests that the type of surfaces which produces transient or impulsive events are more easy to be detected by the driver due to the great attention that the human nervous system pays to high amplitude events.

Figure 5.3 suggests that a single, optimal, acceleration level does not exist which is valid for all road surfaces. The highest detection rate for the tarmac stimuli was found for scale factors of 0.9 and 1.0; this surface can be assumed to be representative of a category of surfaces whose correct detection is reduced by increases in the size of the acceleration stimuli. The highest detection rate for the concrete stimuli was found for acceleration level scaled by 1.0 and 2.0, while detection rates decrease with both increases and decreases in feedback gain. Important increases in correct detection occurred for the cobblestone stimuli and low bump stimuli for almost all scale factors greater than 1.0. The results for the cobblestone stimuli and for the low bump stimuli suggested that human memory and human expectations associate these two surfaces with large vibration amplitudes.

Current results are also presented in terms of detectability index d' value in Figure 5.4, from -1 to 3 determined from the hit and false alarm rates obtained from all sessions. Detectability index d' value is presented along the ordinate, while the scaled values are presented along the abscissa. Both the detection rate and the detectability results suggest similar human response to all stimuli types. For all road surfaces the result suggests that greater detection does not occur at the natural level of the steering acceleration measured in the road automobile.

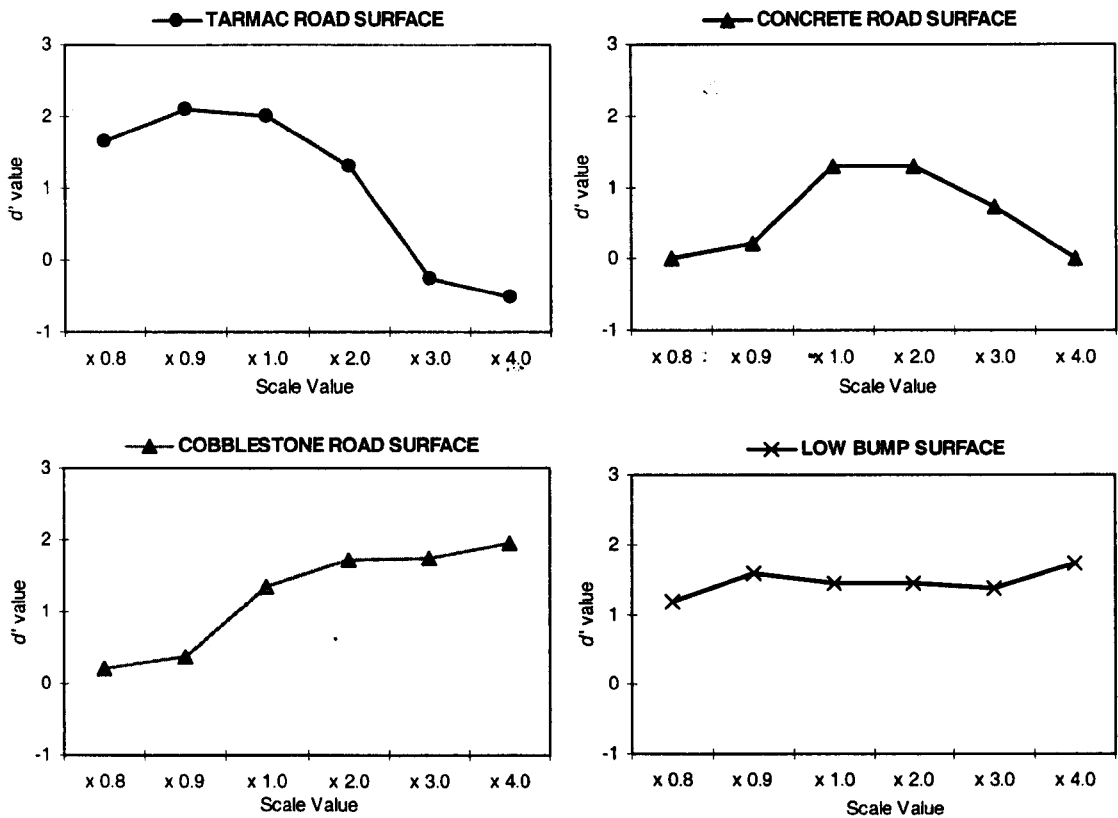


Figure 5.4 Results of the experiment to measure the effect of steering wheel acceleration magnitude on the human detection of road surface type in detectability index d' value ($n=15$).

As explained in section 3.4.3, the performance of each participant, specified as a hit rate and a false alarm rate, can also be represented as a single point on a receiver operating (ROC) space. Figures 5.5 to 5.8 present the ROC point graphs for the four surface stimuli and the six scale values used, in which each participant provides a single point into the ROC space as a result of his or her signal detection, having a total of 15 points for each ROC point graph.

Results from the Figure 5.5 to 5.8 confirms the improvement in detection where occurred at the level explained before for each stimuli. The tarmac stimuli results presented in Figure 5.5 suggest a decrease in detectability with the feedback gain in which the ROC points were found more close to the left-hand side lower corner of the ROC space, scale values of 0.90 and 1.0 were found the optimum for this type of road. The ROC points for the concrete stimuli (see Figure 5.6) were found more close to the left-hand side lower corner of the ROC space with both the decreased and increased of the feedback gain obtaining the highest detectability for the scale values of 1.0 and 2.0. The cobblestone and low bump results in Figures 5.7 and 5.8 suggest a progressive change in detectability with the feedback gain in which the ROC points were found more close to the left-hand side

upper corner of the ROC space. The data confirms the improvement in detection for the cobblestone stimuli and low bump stimuli were occurred for all scale values greater than 1.0. The results suggest that the long term memory model used by average drivers to judge road surface type does not have a single and optimum signal scale value for all road types, thus the optimal scale value appears to depend on the type of road surface.

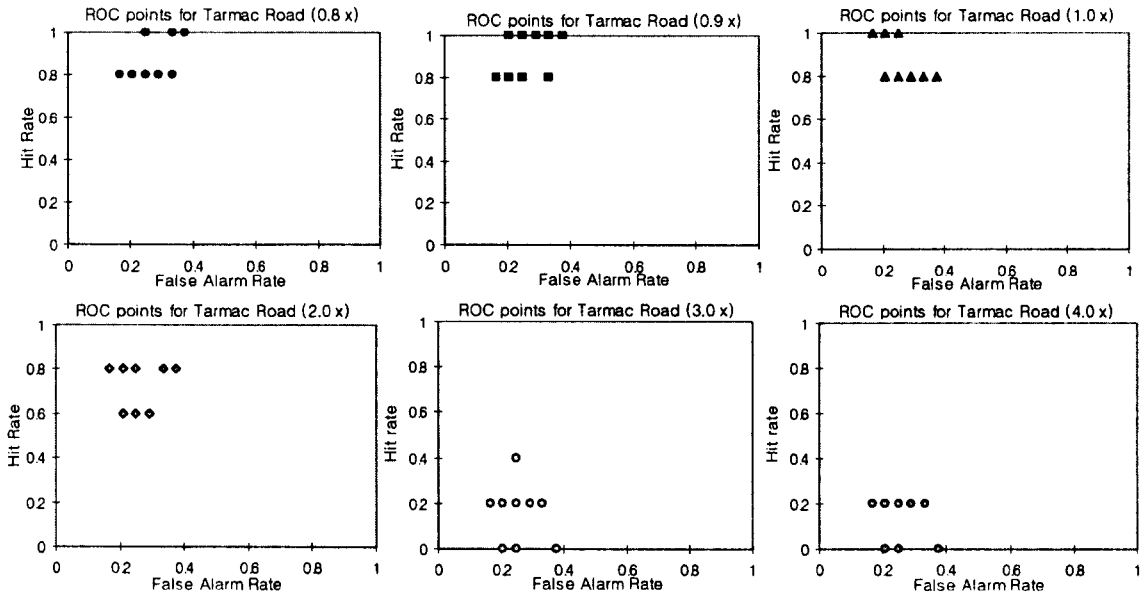


Figure 5.5 ROC points of tarmac surface for the laboratory experiment to measure the effect of steering wheel acceleration magnitude on the human detection of road surface type (n=15).

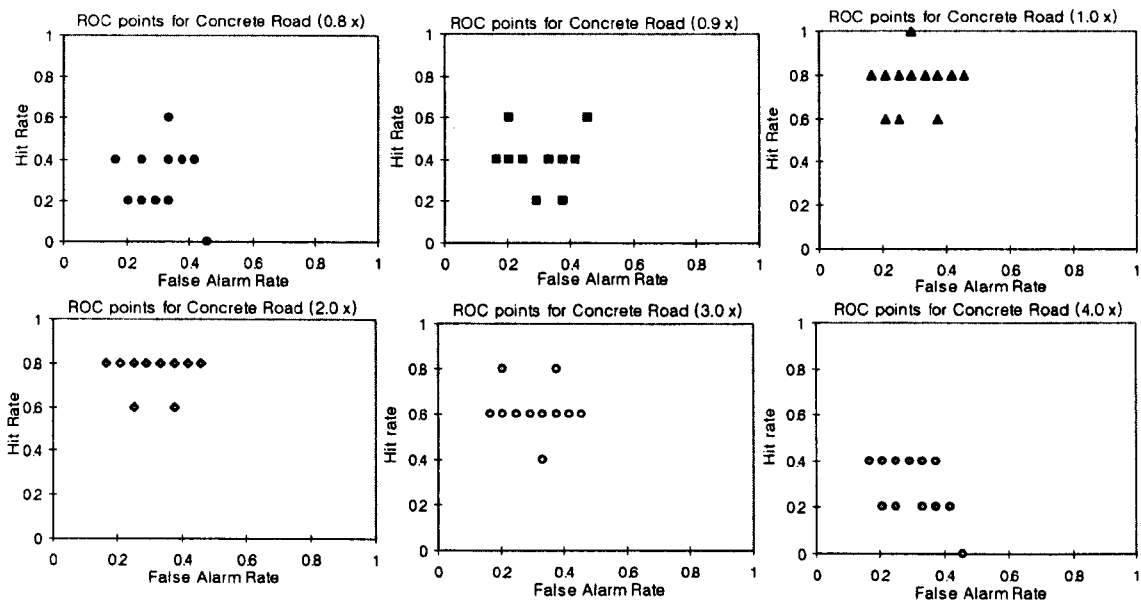


Figure 5.6 ROC points of concrete surface for the laboratory experiment to measure the effect of steering wheel acceleration magnitude on the human detection of road surface type (n=15).

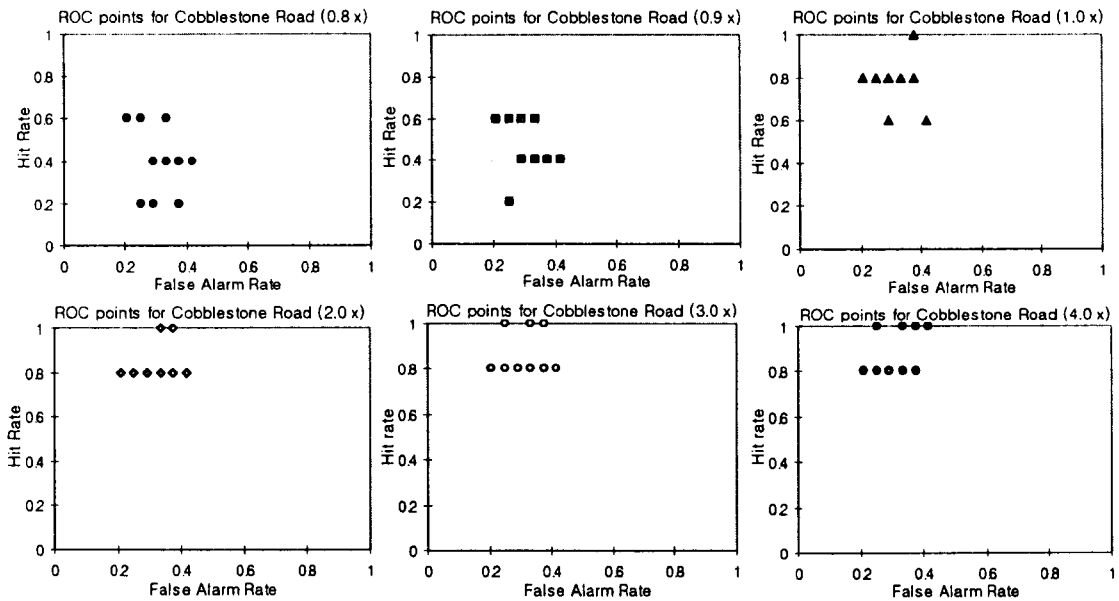


Figure 5.7 ROC points of cobblestone surface for the laboratory experiment to measure the effect of steering wheel acceleration magnitude on the human detection of road surface type (n=15).

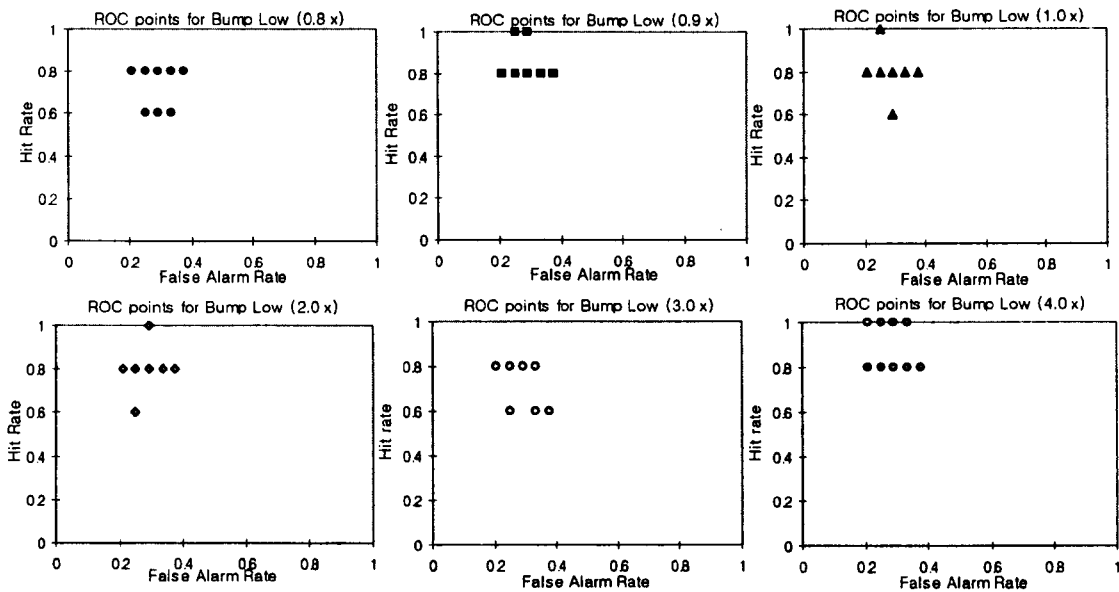


Figure 5.8 ROC points of low bump surface for the laboratory experiment to measure the effect of steering wheel acceleration magnitude on the human detection of road surface type (n=15).

5.2.5 Observations and Discussion

Comparison of the current results to similar data previously published by Giacomini and Woo (2004) suggests similarities. The curves of percent correct detection which are presented in the current study show similar qualitative behaviour to the curves obtained by Giacomini and Woo as a function of overall signal scale. For example, the monotonic improvement in detection rate as a function of increasing scale value found for the cobblestone surface in this study mirrors the monotonic increase obtained in the previous

study as a function of overall signal scale, but with small changes in detection across the various test conditions. The changes in detection can be partially attributed to the fact that smaller and larger multiplication factors were used in the previous research by Giacomini and Woo, thus creating a situation where the detection task, in the current study, was performed against a less complicated background noise.

The results of both the previous study reported by Giacomini and Woo (2004) and the current study suggest that the manipulation of steering wheel vibrational feedback can improve driver detection of the road surface and that correct detection is not strictly optimum at the natural acceleration level encountered in automobiles. This aspect of the detection problem may be of relevance to the designers of both traditional and by-wire steering systems since careful considerations appears to be necessary when choosing the target level of steering feedback for each driving condition. The results suggested that a single, fixed, feedback gain from the automobile to the steering wheel will result optimal in only a small number of driving conditions and that individual road surface types appear to require individual signal manipulation settings.

The optimum acceleration magnitude for detection appeared to be related to the cognitive model or cognitive interpretation mechanism which the participants associated with the surface in question (Giacomini and Gnanasekaran, 2005). As described above, at least three memory models, or categories, of road surface type appear to exist. Human perceptual characteristics and the human a priori knowledge of the road surface produce detection characteristics which are not simply related to the test stimuli in terms of amplitude. The complexity of the measured response suggests the need of further research to determine the optimal range of feedback gains for steering systems.

6. Test to determine the Effect of Steering Wheel Acceleration Frequency Distribution on the Human Detection

This chapter describes experimental testing activities performed in order to measure the effect of frequency bandwidth and the effect of the vibrational energy distribution, on the human ability to detect road surface type based on steering wheel vibration. The reason for studying both effects was the need to identify which energy band is most used by drivers to detect road surface type. Conceptually similar studies have been performed in the field of the Auditory Scene Analysis (ASA) (Bregman, 1999; Wright, 1986) and in the field of Music (Plomp and Levelt, 1965) using stimuli in which an important modification arising from the influence of critical bands. Results of studies in these fields suggest that human hearing has the ability to decompose a stimulus into separate neural patterns which approximately represent the different frequencies bands in the signal (Moore and Patterson, 1986). The research which is described in this chapter was performed based on the assumption that if the decomposition into different frequency bands is an ability that the human being has when discriminating different sounds, this kind of ability can also be present in the case of haptic perception. Further, the research described in this chapter assumed that specific frequency bands of the vibrational energy of the steering wheel are being used by the human in the detection task of road surface type, and not the complete frequency spectrum. In order to investigate if different manipulations of the frequency content of the steering wheel acceleration stimuli could affect the decision making the main objectives of the study were:

- To measure the percentage of correct detection of the road surface type and the detectability index d' based on steering wheel vibration.
- To measure the percentage of correct detection of the road surface type and the detectability index d' based on steering wheel vibration when it has been filtered so as to have vibrational energy only in specific frequency intervals.
- To verify if one specific frequency band contains most of the vibrational information that the human uses to perform the detection for all road surface types.

The results of the experiment tests were plotted using the Theory of Signal Detection as the analytical framework and were summarised by means of both the detectability index d' and receiver operating curve (ROC) points.

6.1 Two experiments in the Detection of Road Surface Type

Two laboratory-based experiments were carried out in this chapter, the first experiment was called the effect of frequency bandwidth and the second the effect of elimination of vibrational energy. Both experiments were performed in the Perception Enhancement Systems laboratory in order to measure the human cognitive response to changes in the steering wheel acceleration frequency distribution. The test facility used to perform the laboratory experiments was the same which was previously described in this thesis in section 5.1.1.

6.1.1 Test subjects

For each of the two experiments an independent group of 15 individuals was tested. The test groups consisted of university staff and students. Upon arriving in the laboratory each participant was issued information and a consent form as well as an explanation describing the experimental method and the laboratory safety features. Age, gender, height, and mass data were then collected, and the participant was requested to state whether he or she had any physical or mental condition which might affect perception of hand-arm vibration, and whether he or she had ingested coffee within the 2 hours previous to arriving in the laboratory. No test participant declared any condition which might affect the perception of hand-arm vibration, and none declared having ingested coffee prior to their tests.

The participants in the frequency bandwidth experiment (First Experiment) consisted of 11 males and 4 females, while the participants in the vibrational energy distribution experiment (Second Experiment) consisted of 9 males and 6 females. Table 6.1 presents the mean, standard deviation (STD), minimum and maximum values of age, height and mass encountered in the test groups. The values can be considered relatively representative of UK drivers in all values except age, which is below the natural average.

Table 6.1 Physical characteristics of the two groups of test participants involved in the laboratory experiments (n=15)

Characteristics	Mean	STD	Minimum	Maximum
Frequency Bandwidth Experiment				
Age (years)	27.10	5.50	18	42
Height (m)	1.69	0.04	1.58	1.82
Mass (kg)	72.00	11.10	54	85
Vibrational Energy Experiment				
Age (years)	27.20	4.50	17	40
Height (m)	1.75	0.06	1.55	1.92
Mass (kg)	72.60	12.70	52	95

(STD) Standard Deviation

6.2 Experiment to Measure the Effect of Frequency Bandwidth

This experiment involved steering acceleration stimuli which were modified by means of digital low-pass filters (Hamming, 1989; Strum and Kirk, 1988). Different cutoff frequencies were selected with this purpose which should span in the range from 0 to 100 Hz due to the principal frequency content of the steering signals was normally found in that range (see Chapter 4).

The results from the previous experiment (in Chapter 5) which investigated the effect of steering wheel acceleration magnitude suggested that human perceptual abilities and the human a priori knowledge of the road surface produce detection characteristics which are not simply related to the test stimuli in terms of magnitude. At least three memory models, or categories, of road surface type appear to exist. The results for the Cobblestone surface and the Tarmac surface suggested that detection varied inversely for these two stimuli sets which are also supported by the work of Giacomini and Woo (2004). Detection of the cobblestone surface improved with increases in stimuli level while the opposite was true of the tarmac surface.

A natural question which therefore arises is whether the detection of these two stimuli also varies as a function of the frequency bandwidths. Based on the above the cobblestone surface and the tarmac surface were chosen to be studied in the new experiment which had the objective of measuring the effect of frequency bandwidth on the human detection task of road type. In a similar study Giacomini and Woo (2005) defined a minimum bandwidth requirement of approximately 0 to 60 Hz, which is required by drivers for the detection task.

6.2.1 Test Stimuli

Each of the two steering wheel time histories was low-pass filtered by means of digital Butterworth filters which were constructed in the LMS[®] TMON software (LMS TMON, 2002) and applied to each original stimulus. For each of the two original stimuli frequency bandwidths of 0-20 Hz, 0-40 Hz, 0-60 Hz, 0-80 Hz and 0-100 Hz were achieved. A total of 10 filtered test stimuli were therefore produced. The *r.m.s.* acceleration values of the five frequency bandwidth test stimuli used in the laboratory test are presented in Table 6.2.

Table 6.2 The *r.m.s.* acceleration values (m/s^2) of the five frequency bandwidth stimuli used for producing the laboratory test stimuli.

<u>Frequency Bandwidth</u>	<u>Tarmac</u>	<u>Cobblestone</u>
0-20 Hz	0.029	0.112
0-40 Hz	0.038	0.204
0-60 Hz	0.044	0.266
0-80 Hz	0.046	0.268
0-100 Hz	0.047	0.269

6.2.2 Test Protocol

Upon arriving in the laboratory each participant was asked to remove any articles of heavy clothing such as coats, and to remove watches or jewellery. He or she was asked to sit in the test rig and to adjust the seat so as to achieve a realistic driving posture. The participant was then asked to fix his or her eyes on a board directly in front of the test rig, which displayed a photograph of one of the two road surfaces which was being used in the test. Prior to commencing formal testing, the participant was provided an example of each of the two stimuli types which would be used later, in order to become acquainted with the detection task.

The experiment was performed in two parts, one for each road surface studied. Each part involved five repetitions of each test stimuli (presented in Table 6.2) from the displayed road surface. In addition, twenty five stimuli were chosen randomly from the stimuli sets of the other road surfaces which were used as background noise stimuli. The time duration of each individual test stimuli was chosen to be 10 seconds (as explained in section 5.3.2). Five different series of ten acceleration stimuli were applied to evaluate each road surface type. In each series, each stimulus was separated from each other stimulus by a 5 second gap in which the participant was asked to state by “yes” or “no” whether the actuated acceleration stimulus was from the road surface whose photograph was shown on the board directly in front of the test bench. When the response and the stimulus matched, the event was taken to be a correct detection. False alarms, on the other hand, were taken to be those situations when the participant responded “yes” to a stimulus which was not derived from the displayed road surface. The order of stimuli presentation was fully randomised for each participant in each series in order to reduce learning effects. Each participant performed 50 detections in each part of the experiment, for a total of 100 detections in a complete experiment.

6.2.3 Results from the Experiment to Measure the Effect of Frequency Bandwidth

Figure 6.1 presents the results obtained from the experiment to determine the effect of frequency bandwidth on the human ability to detect road surface type. In Figure 6.1a the results are presented in terms of percent correct detection from 0 to 100 percent while in Figure 6.1b the results are presented in terms of detectability index d' , as a function of the frequency bandwidth of the stimuli (0-20 Hz, 0-40 Hz, 0-60 Hz, 0-80 Hz and 0-100 Hz). For each frequency bandwidth the hit rate was taken to be the proportion of “yes” responses obtained from the stimuli which were actually derived from the road surface shown on the board. The false alarm rate was taken to be the proportion of “yes” responses obtained from the stimuli which were not derived from the road surface shown on the board. The detection responses for the two road surfaces were analysed in a between/within-subjects by means of the one factor repeated measures ANOVA. Statistical significance effect in the responses were found in both surfaces tested at a $p=0.01$ of significance level with a $F(4,56)$ value of 28.4 and 11.57 for the cobblestone stimuli and the tarmac surface stimuli, respectively.

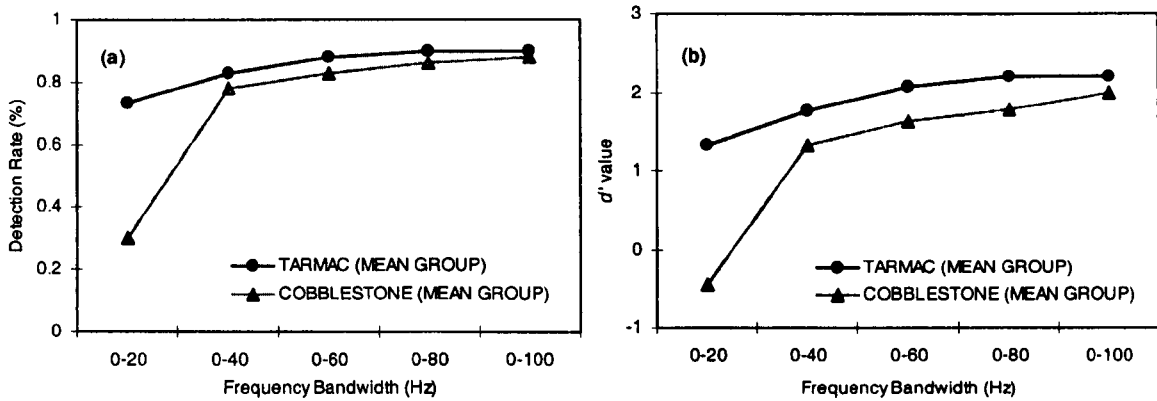


Figure 6.1 Results of the experiment to measure the effect of steering wheel acceleration frequency bandwidth on the human detection of road surface type (n=15), in terms of: (a) Percent correct detection rate and (b) detectability d' value detection.

As shown in Figure 6.1, the results suggest a monotonically increasing relationship between the detectability and bandwidth, detection of both road surfaces having improved with increases in the bandwidth of the vibration stimuli. The greater the maximum frequency range, the greater the percent detection and the detectability value.

When reinforced by the presence of visual and/or acoustic stimuli it may be possible that correct detection might be achieved at bandwidths less than the 60 to 80 Hz suggested by the current findings. Nevertheless a bandwidth in excess of 60 Hz appears necessary for driving conditions in which tactile feedback alone is relied upon for surface detection.

Figures 6.2 and 6.3 present the Receiver Operating Characteristic (ROC) points obtained for the 15 test participants for the cobblestone and the tarmac surface stimuli, respectively. Figures 6.2 and 6.3 suggest a progressive change in detectability with bandwidth. Average hit rates exceeded 80% for the both cobblestone and the tarmac stimuli when the bandwidth used covered the frequency range from 0 to 60 Hz. The results suggest that the long term memory model used by average drivers to judge road surface type contains information to oscillatory frequencies in excess of 60 Hz. While qualitatively similar, the small differences between the two data sets suggest that the energy content associated with the higher frequencies was more important towards correct detection of the cobblestone surface than of the tarmac surface.

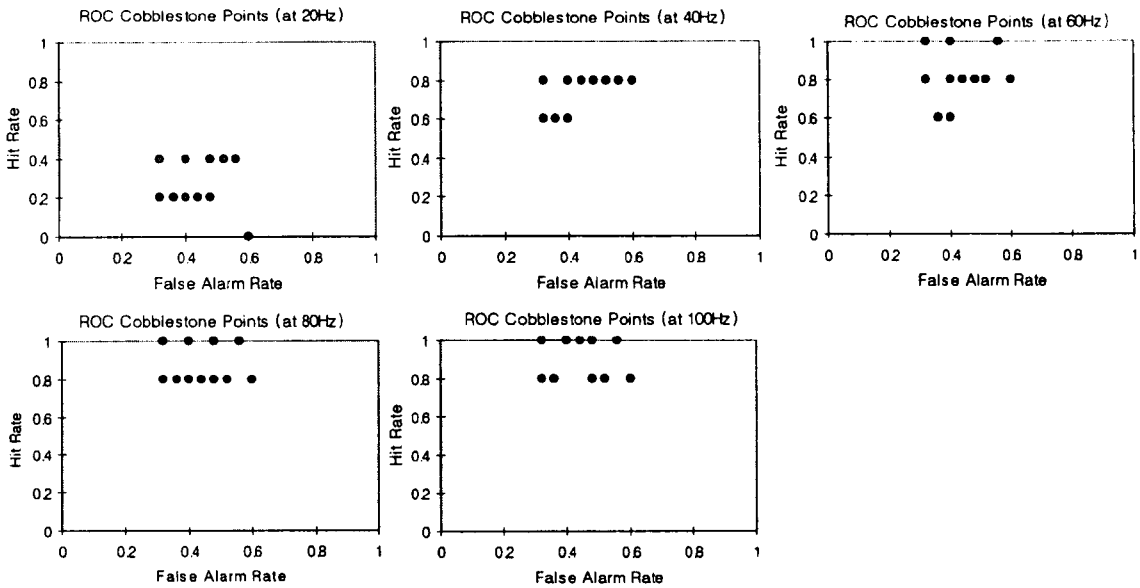


Figure 6.2 ROC points of cobblestone surface for the laboratory experiment to measure the effect of steering wheel acceleration frequency bandwidth on the human detection of road surface type (n=15).

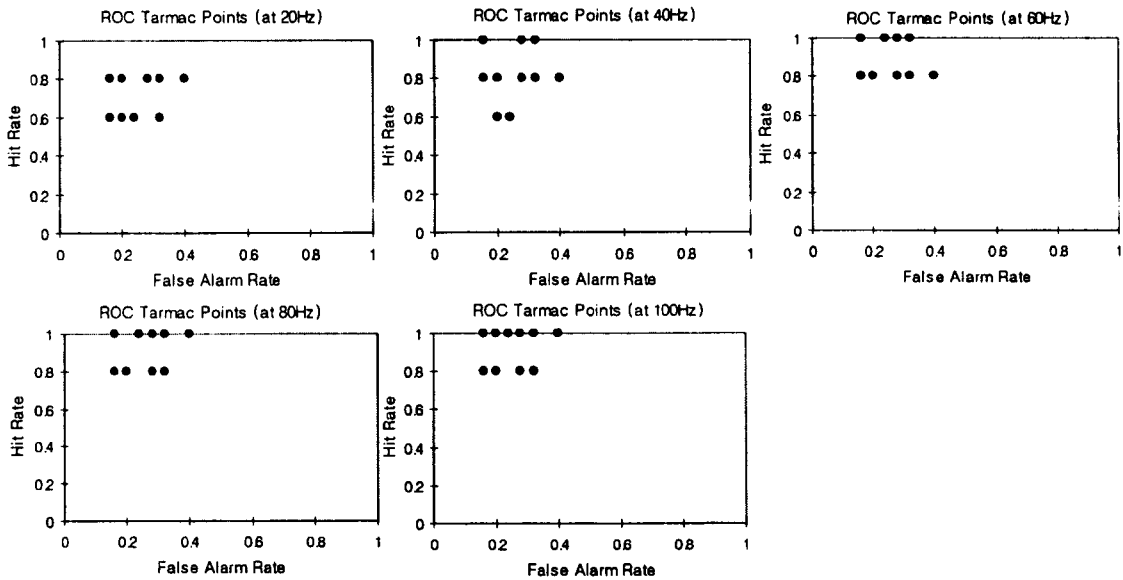


Figure 6.3 ROC points of tarmac surface for the laboratory experiment to measure the effect of steering wheel acceleration frequency bandwidth on the human detection of road surface type (n=15).

6.2.4 Observations and Discussion

In the tests performed to measure the human detection of road surface type based on steering wheel acceleration magnitude, the human detection was found to follow one of three general patterns: improve with increasing acceleration amplitude, degrade with increasing acceleration amplitude, or degrade with any change (greater or lower) away from the natural acceleration level measured in the road vehicle. The road surface types used in this experiment were chosen because they followed the first two of these patterns, meaning the two less intuitive results (see Chapter 5). For these two road surfaces the

detection results suggest that the perceptual and cognitive mechanisms used by the test participants required vibrational information up to frequencies in excess of 60 Hz in order to permit accurate detection in situations where detection relies solely on the tactile sense modality, the same finding obtained by Giacomini and Woo (2005). The results of the frequency bandwidth experiment therefore provide a clear indication of the bandwidth used by humans to judge road surface type when driving current production automobiles. Bandwidths of less than 60 Hz are to be considered detrimental to human detection, and to any information metrics that can be developed for the automobile steering system. This point may be of relevance to the designers of steering systems since the current frequency content of those systems are often less than 40 Hz (Jurgen, 1999; Sugiyama et al., 2006).

Although the results of this experiment suggested that bandwidths of less than 60 Hz are detrimental to human detection, it did not clarify how variations of the distribution of vibrational energy within the overall bandwidth might affect the detection task. As noted in Chapter 4, the principal frequency content at the steering wheel for all road types is normally in the frequency range from 0 to 80 Hz. However, different roads produce different shapes and levels along the complete frequency spectrum, in which some frequency bands are found to have higher energy than others. A natural question is therefore whether any one frequency band within the range from 0 to 60 Hz is more important than others.

6.3 Experiment to Measure the Effect of the Vibrational Energy Distribution

In order to isolate critical bands of steering wheel vibrational energy a test was performed in which individual bands were eliminated from the overall steering wheel signal. By identifying which bands created most damage to the human detection task when eliminated it would be possible to isolate the most important energy region. The selection of the bands to be eliminated was based on the approximate locations of the higher peaks of vibrational energy. The assumption was made that the highest peaks of vibrational energy would most likely have been the result of resonances in the automobile's systems, and that the elimination of information from one of the most important subsystems might deny the driver an important source of information about the road.

6.3.1 Test Stimuli

Three road surfaces were selected for use in testing which were a motorway surface, a broken concrete surface and a broken lane surface. Each of the three original steering wheel time histories was high-pass filtered and band-pass filtered (Hamming, 1989; Strum and Kirk, 1988) by means of digital Butterworth filters which were constructed in the LMS[®] TMON software (LMS TMON, 2002) and applied to each original stimulus. Figure 6.4 presents the five frequency ranges from the steering wheel acceleration spectrum which were selected for elimination of vibrational energy, for each of the original base stimuli. Selected frequency ranges were from 0-6, 6-13, 13-27, 27-60 and 60-150 Hz for the motorway stimuli, 0-6, 6-12, 12-27, 27-53 and 53-150 Hz for the broken concrete stimuli and 0-6, 6-9, 9-22, 22-58 and 58-150 Hz for the broken lane stimuli. Each band can be considered an important subdivision of the vehicle's vibrational energy, which is dominated by one specific frequency which is associated with one specific vehicle subsystem.

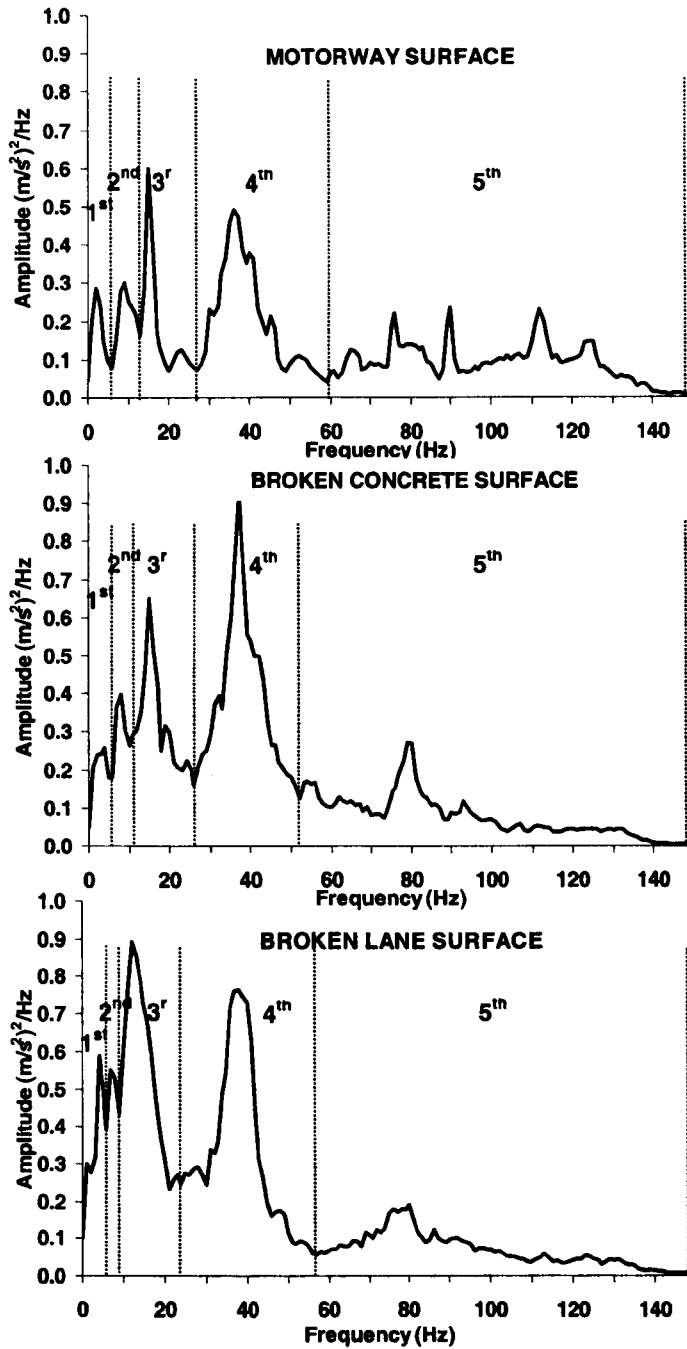


Figure 6.4 Power spectral densities of the experimentally acquired steering wheel acceleration signals, along with the frequency intervals selected for consideration for each type of road.

As an example of the high-pass filtering and band-pass filtering, Figure 6.5 presents power spectral density (PSD) graphs of the un-manipulated and manipulated motorway stimuli. A total of 18 test stimuli were obtained. The *r.m.s.* acceleration values (m/s^2) for all un-manipulated and manipulated test stimuli used in the laboratory test are presented Table 6.3.

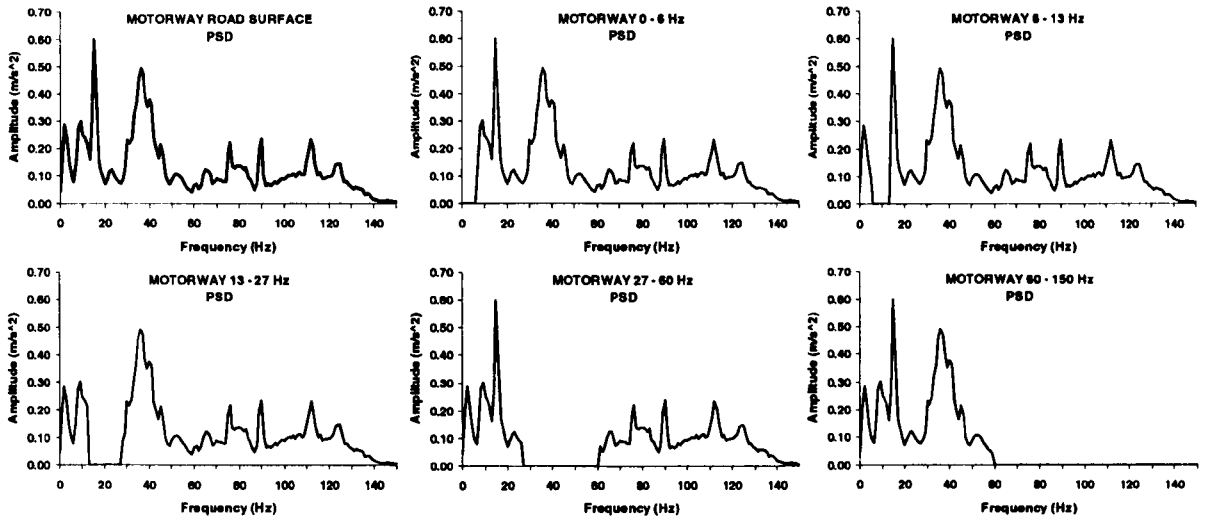


Figure 6.5 Laboratory test stimuli for the Motorway road surface that were produced by means of digital Butterworth high-pass and band-pass eliminating filters.

Table 6.3 The *r.m.s.* acceleration values (m/s^2) of the un-manipulated and manipulated stimuli used for producing the laboratory test stimuli.

Road Surface Type	Original	1st Frequency Interval	2nd Frequency Interval	3rd Frequency Interval	4th Frequency Interval	5th Frequency Interval
Motorway (M)	1.15	1.09	1.07	1.04	0.83	0.99
Broken Concrete (C)	2.03	1.91	1.87	1.73	1.26	1.83
Broken Lane (BL)	2.36	2.13	2.05	1.88	1.95	2.22

6.3.2 Test Protocol

Upon arriving in the laboratory each participant was asked to remove any articles of heavy clothing such as coats, and to remove watches or jewellery. He or she was asked to sit in the test rig and to adjust the seat so as to achieve a realistic driving posture. The participant was then asked to fix his or her eyes on a board directly in front of the test rig, which displayed a photograph of one of the three road surfaces which was being used in the test. Prior to commencing formal testing, the participant was provided an example of each of the three stimuli types which would be used later, in order to become acquainted with the detection task.

The experiment was performed in three parts, one for each road surface studied. Each part involved five repetitions of each of the five high-pass filtered and band-pass filtered stimuli and of the original base stimuli for each type of road, plus a further 24 stimuli chosen randomly from the stimuli sets described in Chapter 4 which acted as background

noise. The time duration of each individual test stimuli was chosen to be 10 seconds. Six different series of nine acceleration stimuli were applied to evaluate each road surface type. In each series, each stimulus was separated from each other stimulus by a 5 second gap in which the participant was asked to state by “yes” or “no” his or her judgment of road surface type so as to indicate if the experimental stimulus seemed to be from the road which was displayed during the test. The order of stimuli presentation was fully randomised for each participant in each series in order to reduce learning effects. Each participant performed 54 detections for each road surface type, and a total of 162 detections in the complete experiment.

6.3.3 Results from the Experiment to Measure the Effect of the Vibrational Energy Distribution

Figure 6.6 presents the results obtained from the experiment plotted in terms of percent correct detection, from 0 to 100 percent. Percent correct detection is presented along the ordinate while the five different frequency ranges for each road are presented along the abscissa. The original base stimuli are labelled as O. For each frequency range, the hit rate was taken to be the proportion of “yes” responses obtained from the stimuli which were actually from the road surface which was shown on the board. The false alarm rate was taken to be the proportion of “yes” responses obtained from the stimuli which were not derived from the road surface which was being shown on the board. The percentage of correct detection responses for the three road surfaces were analysed in a between/within-subjects by means of the one factor repeated measures ANOVA. Statistical significance effect in the responses were found in all surfaces tested at a $p=0.01$ of significance level with a $F(5,70)$ value of 60.6, 43.3 and 65.73 for the broken concrete stimuli, the broken lane stimuli and the motorway stimuli, respectively.

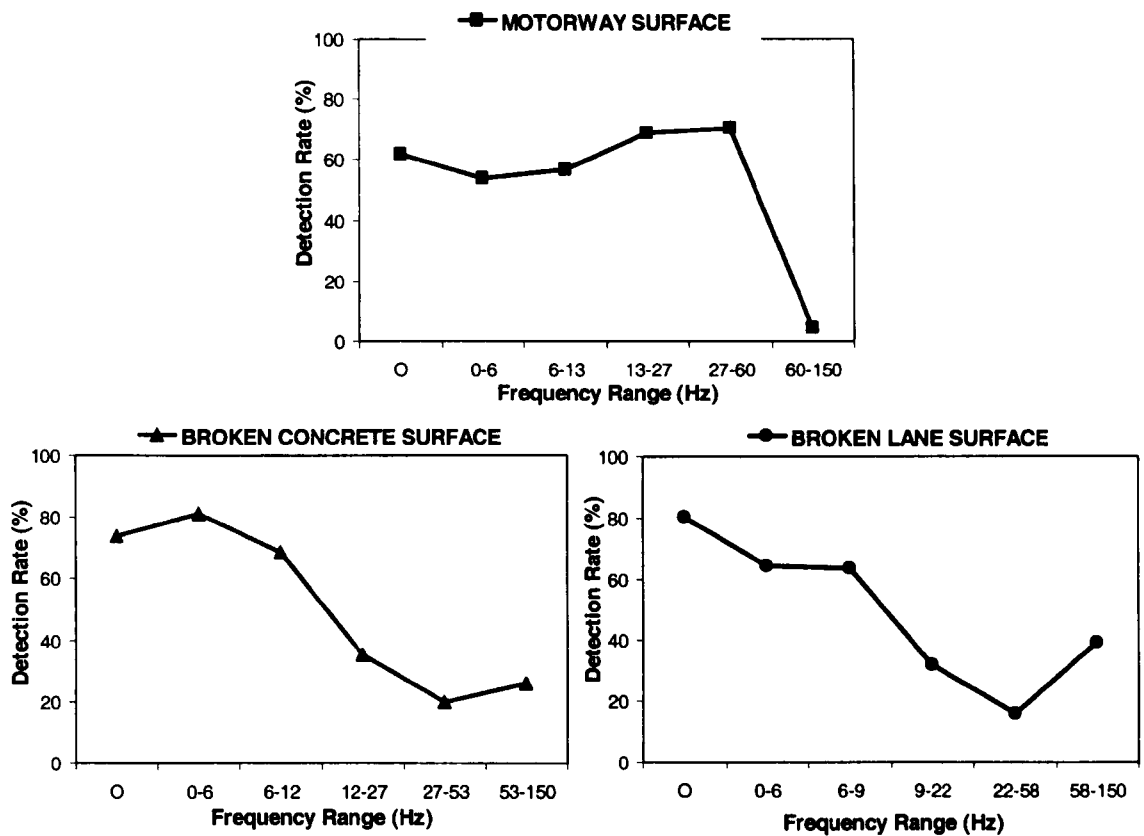


Figure 6.6 Results of the laboratory experiments regarding the effect of the vibrational energy distribution of the steering wheel acceleration signal on the human detection of road surface type (n= 15).

As shown in Figure 6.6, the percentage of correct detection for the original base stimuli for the current experiment was approximately 62% for the motorway stimuli, 74% for the broken concrete stimuli and 80% for the broken lane stimuli. The curves of correct detection as a function of the eliminated frequency interval for the broken concrete and broken lane stimuli showed similar qualitative behaviour, decreasing in detection until the 27Hz to 53Hz frequency interval for the broken concrete stimuli, and the 22Hz to 58Hz frequency interval for the broken lane stimuli. Qualitatively, the results from the motorway stimuli showed a very different behaviour from that of the other two test stimuli.

The results are also presented in terms of the detectability index d' value in Figure 6.7, from -1 to 2, determined from the hit and false alarm rates obtained from all sessions. Detectability index d' is presented along the ordinate, while the five frequency ranges eliminated for each road surface are presented along the abscissa. Both the detection rate and the detectability results suggest similar qualitative human response and suggest that

the frequency range from approximately 20 Hz until 60 Hz is playing a key role in the human cognitive detection of the road surface type for all three surfaces.

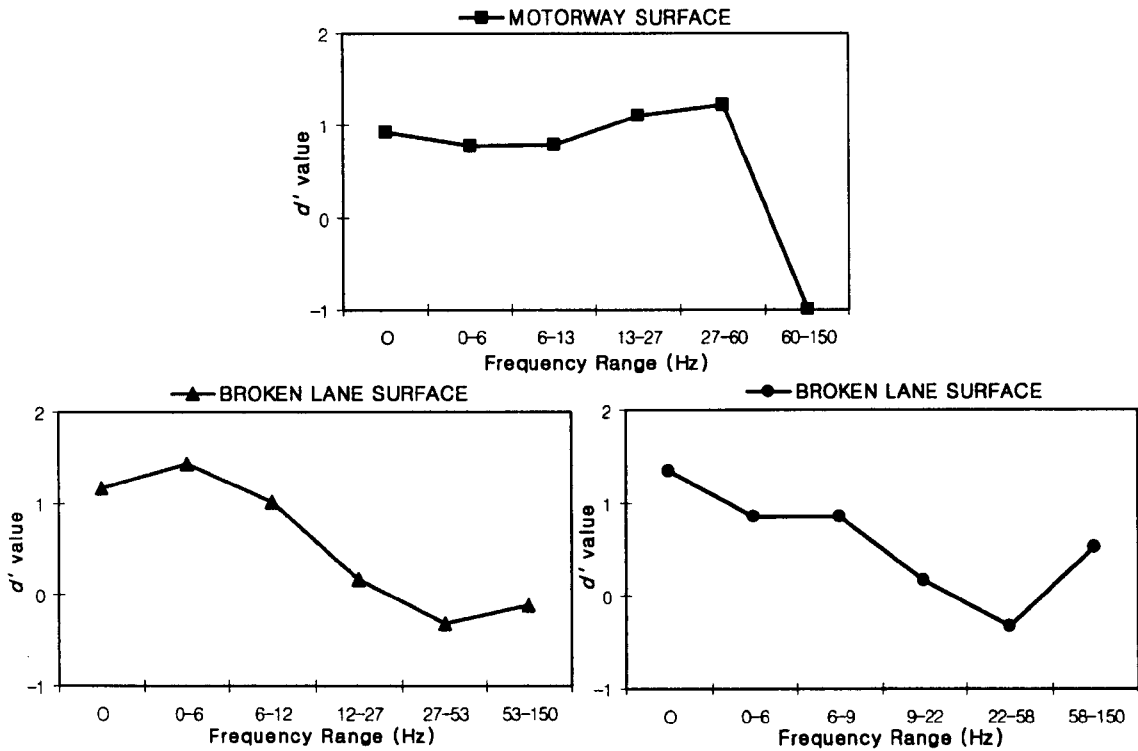


Figure 6.7 Results of the laboratory experiments regarding the effect of the vibrational energy distribution of the steering wheel acceleration signal on the human detection of road surface type (n= 15).

Figures 6.8 to 6.10 present the Receiver Operating Characteristic (ROC) points obtained for the 15 test participants for the motorway surface, the broken concrete surface and the broken lane surface. ROC point results suggest that the long term memory model used by average drivers to judge all three road surface types contains information at the frequency range approximately from 20 Hz to 60 Hz. The results suggest that this frequency range where the automobile has its column resonances, steering wheel resonances and chassis resonances seems critical to detection. Elimination of vibrational energy in the range from 20 to 60 Hz made it almost impossible to correctly detect broken surfaces (concrete and asphalt lane) while it dramatically improved detection of the smooth surface (motorway). Clearly, the energy in this band is very important towards determining the surface type.

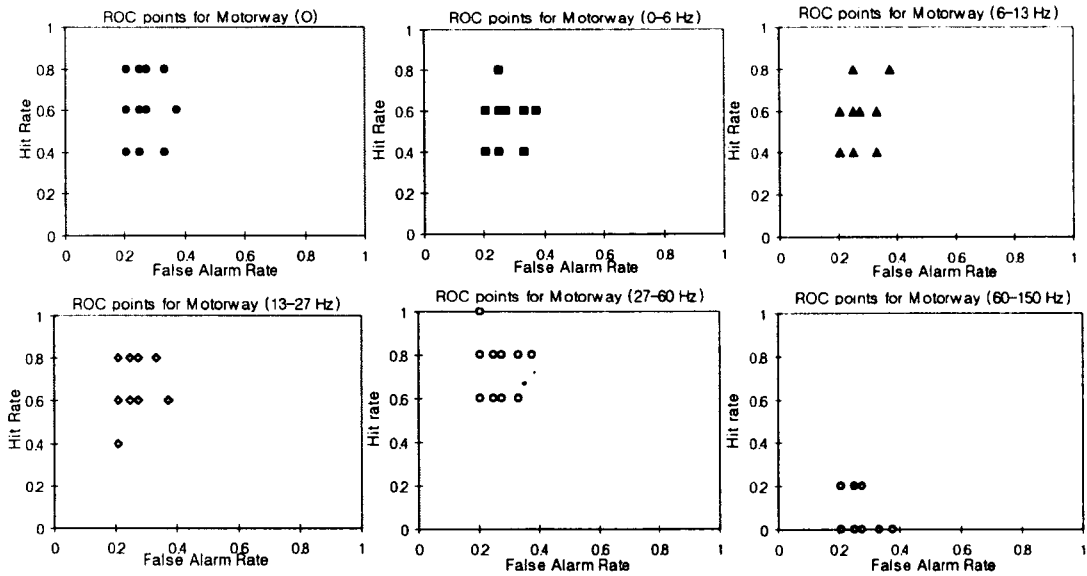


Figure 6.8 ROC points for the Motorway surface stimuli regarding the effect of the vibrational energy distribution of the steering wheel acceleration signal (n= 15)

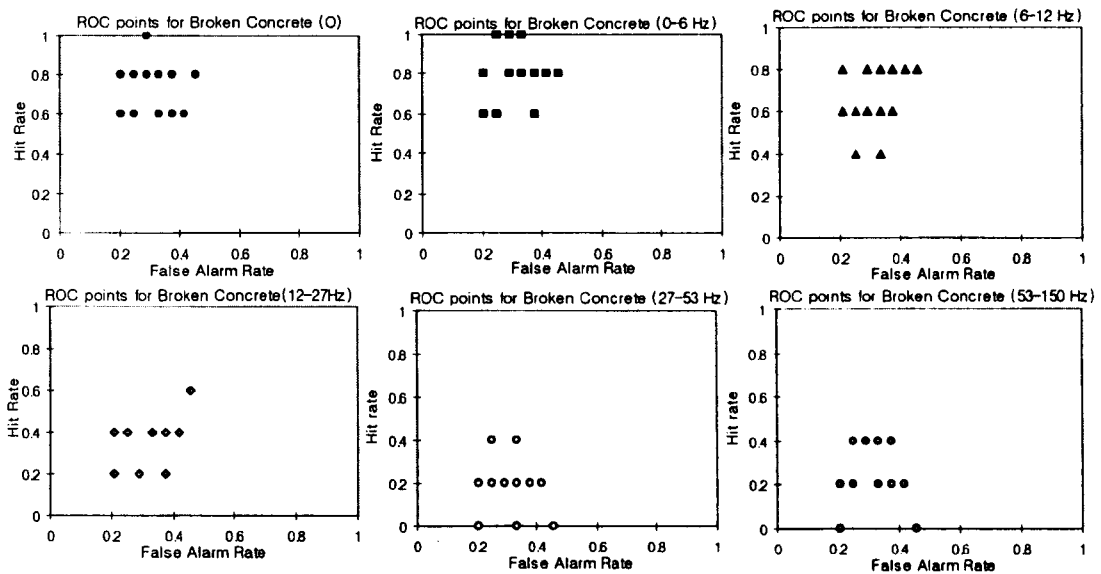


Figure 6.9 ROC points for the Broken Concrete surface stimuli regarding the effect of the vibrational energy distribution of the steering wheel acceleration signal (n= 15)

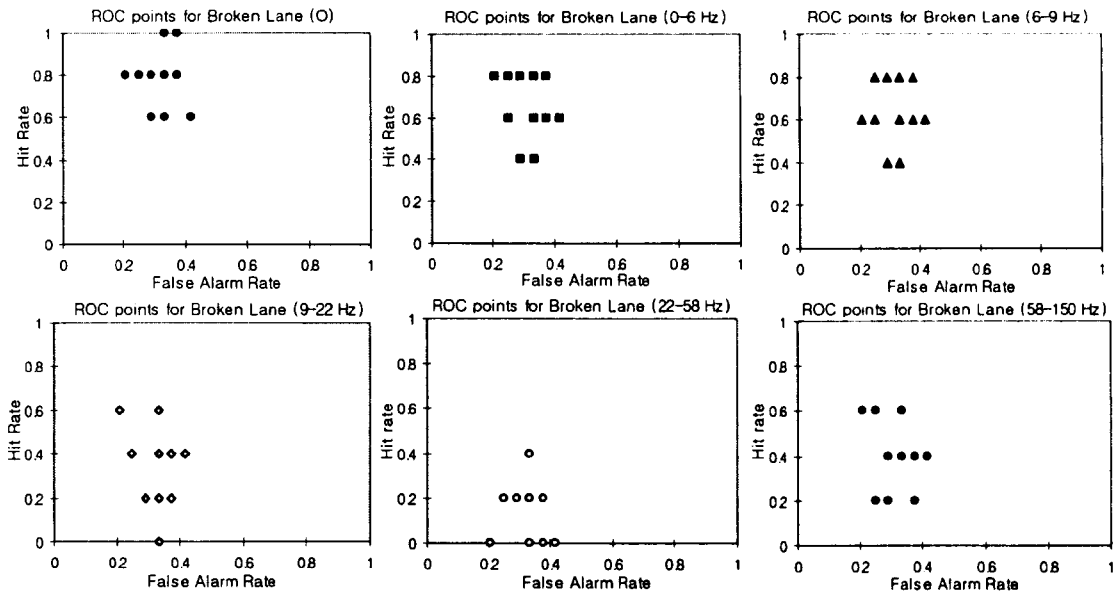


Figure 6.10 ROC points for the Broken Lane surface stimuli regarding the effect of the vibrational energy distribution of the steering wheel acceleration signal ($n= 15$)

6.3.4 Observation and Discussion from the Experiment to Measure the Effect of Vibrational Energy Distribution

The detection rate of less than 100 percent for all three road surface types suggests the difficulty of achieving fully accurate detection in a laboratory task in which several key stimuli, notably the acoustical stimuli, are absent. Notwithstanding the less than perfect environmental reproduction, the results of the vibrational energy distribution suggest that the frequency range from approximately 20 Hz until 60 Hz played a key role in the human cognitive detection of the road surface type for all three surfaces. The effect of the elimination of energy distribution results show some qualitative similarities to those obtained by the bandwidth experiments (Giacomin and Woo, 2005) in which the elimination of high frequency energy from the steering wheel vibration signal was found to have a detrimental effect on road surface type detection. In the effect of bandwidth experiment carried out by Giacomin and Woo (2005) and also in this thesis was stated that the long term memory model used by average drivers to judge road surface type appeared to contain information to oscillatory frequencies in excess of 60 Hz. The effect of vibrational energy distribution results suggest that the elimination of energy in the frequency range from 20 to 60 Hz seems helpful towards the detection of surfaces which are expected to have low level of energy content, but that it is greatly detrimental for those road surfaces which are expecting to have high level of energy content, since much more of this energy is found in this band.

Considering no a-priori knowledge of the possible meaning of the vibration energy in the 20 to 60 Hz band, it would appear from the results that eliminating one of the intervals which contains the greatest amount of vibration energy in current production automobiles can be said to deprive the driver an important source of driving information, and thus an important source of steering feel.

A-prior information about this frequency band includes, however, the knowledge that it normally contains more than one resonance of the steering system (tyres, front suspensions, steering column, steering wheel, etc.) thus elimination of this band would appear to remove important feedback to the driver about the dynamic state of those subsystems (Giacomin and Lo Faso, 1993; Pottinger and Marshall, 1986). Given the resonance behaviours of the automobile in the 20 to 60 Hz frequency band, it may be the case that in current production automobiles the frequency band provides a focus and a principal source of driver perception.

The findings may be interpreted as suggesting that road surface, steering and suspension in the 20 to 60 Hz frequency interval provide vital clues to automobile drivers regarding the roads over which they drive and the dynamic response of the vehicle. Steering feel may be compromised by any reductions in vibrational energy at the steering wheel in this interval.

7. Test to determine the Effect of Compression and Expansion of the Steering Wheel Acceleration Signal

This chapter describes a set of experimental testing activities performed in order to measure the effect of signal compression or expansion on the human ability to detect road surface type based on steering wheel acceleration signals. The reason for studying this effect was the interest in determining if some effects used in the music field to enhance perception could improve also the steering stimuli for the detection task. As explained in Chapter 2, compressors and expanders manipulate stimuli above a critical threshold level. Such effects, compression and expansion, are used in the field of the music to enhance recordings (Eargle, 1995; Huber and Runstein, 2005; Katz, 2002) by selectively reducing or increasing the audio levels such that the louder passages are made softer, or the softer passages are made louder, or both. The research which is described in this chapter was performed based on the assumption that if the use of these effects enhances the human perception of music sound signals then it might also prove beneficial in the case of steering wheel acceleration signals. In order to investigate if different manipulations above a critical threshold level of the steering wheel acceleration stimuli could affect the decision making, the main objectives of the study were:

- To measure the percentage of correct detection of the road surface type and the detectability index d' based on steering wheel vibration.
- To measure the percentage of correct detection of the road surface type and the detectability index d' based on steering wheel vibration when it has been either compressed or expanded.

- To verify if the manipulation of the stimuli above a critical threshold level by either compressing or expanding could improve the human detection for all road surface types.
- To verify if only one single compressor factor or expander factor could improve the human detection for all road surface types.

The results of the experimental tests were plotted using the Theory of Signal Detection as the analytical framework and were summarised by means of the detectability index d' value.

7.1 Experiment to Measure the Effect of Compression and Expansion of Steering

Wheel Acceleration Signals

A laboratory-based experiment was performed in the Perception Enhancement Systems laboratory in order to measure the human cognitive response to compression or expansion of the steering wheel acceleration signals. The test facility used to perform the laboratory experiment was the same which was previously described in this thesis in section 5.1.1. The mathematical operation of compressing and expanding does not affect the spectral or phase relationships of the stimuli.

Steering vibration from three road surfaces was selected to perform the current laboratory experiment, which were: a Tarmac surface, a Concrete surface and a Cobblestone surface. This selection was based on the assumption that possibly the test stimuli used in Chapter 5 did not need to be re-scaled in their complete acceleration time histories in order to improve the human detection task. Possibly manipulation of their acceleration level above a threshold value would prove more beneficial.

7.1.1 Test subjects

A group of 15 individuals was tested who were all university staff and students. Upon arriving in the laboratory each was issued an information and consent form. Verbal explanation was also provided about the experimental method and the laboratory safety features. Age, gender, height, and mass data were then collected and the participant was requested to state whether he or she had any physical or mental condition which might affect perception of hand-arm vibration, and whether he or she had ingested coffee within the 2 hours previous to arriving in the laboratory. No test participant declared a physical

or cognitive condition which might affect the perception of hand-arm vibration, and none declared having ingested coffee prior to their tests.

The subjects who participated in the compression and expansion of the steering acceleration signals test consisted of 9 males and 6 females. Table 7.1 presents the mean, standard deviation (STD), minimum and maximum values of age, height and mass encountered in the test. None of the characteristics deviate substantially from 50th percentile characteristics except age, which was substantially lower than the national average.

Table 7.1 Physical characteristics of the group of test participants involved in the laboratory experiment (n=15)

Characteristics		Mean	STD	Minimum	Maximum
Age	(years)	24.13	4.39	20	37
Height	(m)	1.69	0.07	1.57	1.81
Mass	(kg)	73.13	6.83	58	85

(STD) Standard Deviation

7.1.2 Test Stimuli

In order to make use of compressors or expanders some parameters had to be defined. These were: a critical threshold level, a compressor factor and an expander factor. In this context, the critical threshold level is defined as the amplitude level above which reduction or amplification begins to occur, while the compressor and the expander factors are the ratio of input to output above the threshold level (Eargle, 1995; Huber and Runstein, 2005; Katz, 2002). According to Katz (2002) in the field of music the threshold value would be from -20 to -10 dBFS (decibel Full Scale) which is considered the range where most of the musical movements take place. In the case of steering wheel vibration a human detection threshold value has never been defined in the research literature. The research described here adopted as threshold level three values ($\pm 3\sigma$, $\pm 2\sigma$, $\pm \sigma$) which were based on the standard deviation σ of the acceleration values of the signal in m/s^2 . Figure 7.1 shows schematically the adopted values above which reduction or amplification was performed.



Figure 7.1 Standard deviation values used as critical threshold levels above which gain reduction or amplification was performed.

According to Katz (2002) common factor values used for music enhancement are approximately 0.40 when compressing and 1.10 when expanding. Considering that compressor and expander factors used to enhance music might be expected to be different from those which could enhance perception of the steering vibration, a range of different factor values were selected for the steering wheel test stimuli. Scale values of 0.40, 0.60, 0.80 and 0.90 were selected as compressor factors, while 1.10, 1.50, 2.00 and 2.50 were selected as expander factors. Both selected ranges include those factor values which usually enhance music as stated above (0.40 and 1.10).

The stimuli actuated at the wheel during the experiment consisted of the compressed and expanded signals taken from all three road surface types. The stimuli were manipulated above the three critical threshold level values by means of the four compressor factors and also the four expander factors. As an example of this process, Figure 7.2 shows the effect of various compressors or expanders applied to the tarmac surface when the critical threshold level is taken to be the three standard deviation values of the data points composing the steering acceleration time history. Figure 7.2 suggests that the use of a compressor greatly reduces the acceleration level of the stimuli and the peakedness, while the use of expanders greatly increases the acceleration level of the stimuli and also the peakedness.

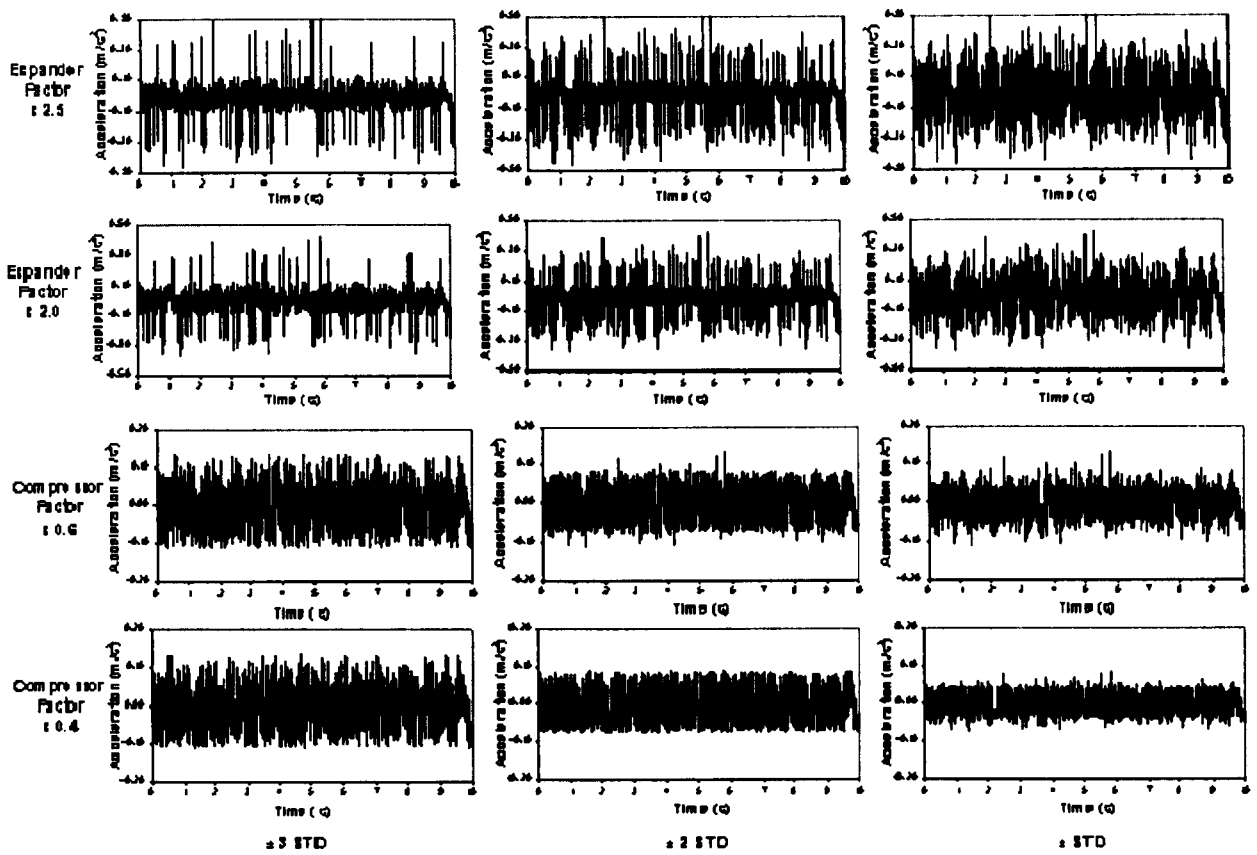


Figure 7.2 The effect of various compressor and expander factors used at the tarmac stimuli when the critical threshold levels are taken to be the three standard deviation values.

Table 7.2 presents the global statistical properties determined from the un-manipulated and the manipulated stimuli of each of the three road surfaces selected for the current experiment. As expected from the acceleration time histories presented in Figure 7.2, the global statistical properties of the manipulated stimuli changed drastically as their acceleration time histories were manipulated by means of compressors and expanders. The kurtosis value, which measures the peakedness of the probability distribution of the acceleration time histories, increased when the steering signals were manipulated by means of expander factors. The kurtosis value for the original base stimuli changed from a value close to 3.0 to a kurtosis value above 15.0 in some cases. On the other hand, when the steering signals were manipulated by means of compressor factors the kurtosis value decreased, in some cases achieving values below to 2.0. Such kurtosis values are more close to the expected value for a sine wave of 1.50 than the value expected of a random vibration signal. The remaining global statistical properties such as the *r.m.s.* acceleration value, skewness value, crest factor value and the VDV value changed in some cases by more than a factor of 2.0 when expanders were applied while decreasing by more than a half when compressors factors were applied, as seen in Table 7.2.

Table 7.2 Global statistical properties of the three road stimuli used for producing the laboratory test stimuli to measure the effect of compression and expansion on the human detection.

Type of Road Surface		Global Statistics and Characteristics					
		r.m.s (m/s ²)	Kurtosis (dimensionless)	Skewness (dimensionless)	CF (dimensionless)	VDV (ms ^{-1.75})	
COBBLESTONE		0.287	3.465	-0.002	4.710	0.736	
Expander	±3 STD	x 2.50	0.429	15.666	-0.086	6.869	1.519
		x 2.00	0.383	10.593	-0.057	6.163	1.229
		x 1.50	0.342	6.044	-0.025	5.170	0.955
		x 1.25	0.325	4.332	-0.009	4.537	0.834
	±2 STD	x 2.50	0.585	7.908	0.023	5.046	1.743
		x 2.00	0.486	6.823	0.022	4.852	1.398
		x 1.50	0.393	5.214	0.017	4.500	1.057
		x 1.25	0.350	4.208	0.013	4.214	0.892
	± STD	x 2.50	0.741	3.753	-0.015	3.980	1.834
		x 2.00	0.596	3.679	-0.011	3.960	1.468
		x 1.50	0.452	3.529	-0.004	3.918	1.101
		x 1.25	0.380	3.391	0.001	3.877	0.918
Compressor	±3 STD	x 0.90	0.305	2.861	0.012	3.482	0.705
		x 0.80	0.300	2.644	0.017	3.144	0.681
		x 0.60	0.292	2.437	0.026	2.422	0.650
		x 0.40	0.287	2.436	0.033	2.467	0.637
	±2 STD	x 0.90	0.296	2.783	0.003	3.594	0.679
		x 0.80	0.282	2.450	0.000	3.350	0.627
		x 0.60	0.257	2.015	-0.006	2.750	0.545
		x 0.40	0.239	1.977	-0.008	1.978	0.503
	± STD	x 0.90	0.283	3.036	0.008	3.759	0.663
		x 0.80	0.255	2.875	0.011	3.698	0.591
		x 0.60	0.202	2.434	0.012	3.497	0.450
		x 0.40	0.154	1.907	0.001	3.065	0.322
CONCRETE		0.099	3.144	0.073	4.280	0.222	
Expander	±3 STD	x 2.50	0.141	12.752	0.089	5.280	0.473
		x 2.00	0.123	9.282	0.091	4.832	0.382
		x 1.50	0.107	5.719	0.079	4.157	0.295
		x 1.25	0.100	4.204	0.067	3.702	0.255
	±2 STD	x 2.50	0.190	6.247	-0.096	3.915	0.533
		x 2.00	0.156	5.620	-0.054	3.806	0.427
		x 1.50	0.124	4.606	-0.001	3.597	0.323
		x 1.25	0.109	3.900	0.027	3.419	0.271
	± STD	x 2.50	0.228	3.492	-0.027	3.263	0.553
		x 2.00	0.183	3.444	-0.013	3.250	0.443
		x 1.50	0.138	3.342	0.009	3.223	0.332
		x 1.25	0.116	3.245	0.027	3.197	0.277
Compressor	±3 STD	x 0.90	0.092	2.771	0.043	2.900	0.211
		x 0.80	0.090	2.545	0.036	2.633	0.203
		x 0.60	0.087	2.329	0.023	2.049	0.191
		x 0.40	0.085	2.350	0.014	2.105	0.186

	± 2 STD	x 0.90	0.089	2.748	0.056	3.005	0.204
		x 0.80	0.084	2.435	0.057	2.833	0.186
		x 0.60	0.075	1.974	0.043	2.383	0.158
		x 0.40	0.068	1.907	0.002	1.759	0.141
	\pm STD	x 0.90	0.086	2.983	0.062	3.120	0.200
		x 0.80	0.077	2.859	0.076	3.080	0.178
		x 0.60	0.061	2.495	0.104	2.944	0.135
		x 0.40	0.045	1.981	0.114	2.637	0.095
TARMAC			0.056	2.997	0.052	3.872	0.130
Expander	± 3 STD	x 2.50	0.080	12.693	-0.549	6.786	0.268
		x 2.00	0.070	8.981	-0.348	6.161	0.217
		x 1.50	0.062	5.416	-0.127	5.245	0.168
		x 1.25	0.058	3.999	-0.023	4.642	0.147
	± 2 STD	x 2.50	0.110	6.332	-0.124	4.940	0.310
		x 2.00	0.091	5.647	-0.090	4.792	0.248
		x 1.50	0.072	4.561	-0.032	4.514	0.187
		x 1.25	0.063	3.827	0.011	4.277	0.158
	\pm STD	x 2.50	0.133	3.485	0.081	4.076	0.323
		x 2.00	0.107	3.424	0.077	4.059	0.259
		x 1.50	0.081	3.303	0.071	4.023	0.194
		x 1.25	0.068	3.191	0.068	3.988	0.162
Compressor	± 3 STD	x 0.90	0.054	2.748	0.094	3.604	0.124
		x 0.80	0.053	2.566	0.118	3.264	0.120
		x 0.60	0.051	2.408	0.149	2.529	0.114
		x 0.40	0.050	2.442	0.157	2.588	0.112
	± 2 STD	x 0.90	0.052	2.687	0.090	3.737	0.119
		x 0.80	0.049	2.396	0.116	3.515	0.109
		x 0.60	0.044	1.999	0.162	2.941	0.094
		x 0.40	0.040	1.990	0.190	2.159	0.085
	\pm STD	x 0.90	0.050	2.901	0.066	3.886	0.117
		x 0.80	0.045	2.768	0.068	3.833	0.104
		x 0.60	0.036	2.395	0.081	3.653	0.079
		x 0.40	0.027	1.920	0.127	3.254	0.056

7.1.3 Test Protocol

Upon arriving in the laboratory each participant was asked to remove any articles of heavy clothing such as coats, and to remove watches or jewellery. He or she was asked to sit in the test rig and to adjust the seat so as to achieve a realistic driving posture. The participant was then asked to fix his or her eyes on a board directly in front of the test rig, which displayed a photograph of one of the three road surfaces which was being used in the test. Prior to commencing formal testing, the participant was provided an example of each of the three stimuli types which would be used later, in order to become acquainted with the detection task.

The experiment was performed in six parts, two for each road surface investigated. For each road surface, the first part of the experiment corresponded to the study of the compressed stimuli and the second part to the study of the expanded stimuli. Each part involved five repetitions of each un-manipulated and manipulated test stimuli from the displayed road surface. In addition, twenty five stimuli were chosen randomly from the stimuli sets of the other road surfaces, and were used as background noise stimuli.

The time duration of each individual test stimuli was chosen to be 10 seconds. Six different series of fifteen acceleration stimuli were applied in each part of the experiment. Each stimulus was separated from each other stimulus by a 5 second gap in which the participant was asked to state by “yes” or “no” his or her judgment of road surface type so as to indicate if the experimental stimulus seemed to be from the road which was displayed during the test. The order of stimuli presentation was fully randomised for each participant in each series in order to reduce learning effects. Each participant performed 90 detections in each part of the experiment, for a total of 540 detections in a complete experiment.

7.1.4 Results from the Experiment to Measure the Effect of Compression and Expansion of Steering Wheel Acceleration Signals

The laboratory-based experiment results from the group of 15 people are presented in Figure 7.3. These results show the effect which compression or expansion of the steering acceleration stimuli has on the human ability to detect road surface type. The results of Figure 7.3 are presented in terms of percent correct detection, from 0 to 100 percent. The graphs are organised according to the three threshold levels used in the laboratory experiment (± 3 STD, ± 2 STD and ± 1 STD). Percent correct detection is presented along the ordinate, while the compressor and expander factors are presented along the abscissa. The original base stimuli are labelled as x1.0, which means that all data points of the acceleration time histories above the critical threshold level remain without change, since they are either compressed or expanded by the value of unity. The four compressor factors used are labelled as x0.40, x0.60, x0.80 and x0.90, while the four expander factors used are labelled as x1.10, x1.50, x2.00 and x2.50. The percentage of correct detection responses for the three road surfaces were analysed in a between/within-subjects by means of the one factor repeated measures ANOVA. Statistical significance effect in the

responses were found in all surfaces at a $p=0.01$ of significance level with a $F(4,56)$ value spanning from 5.01 to 320.77.

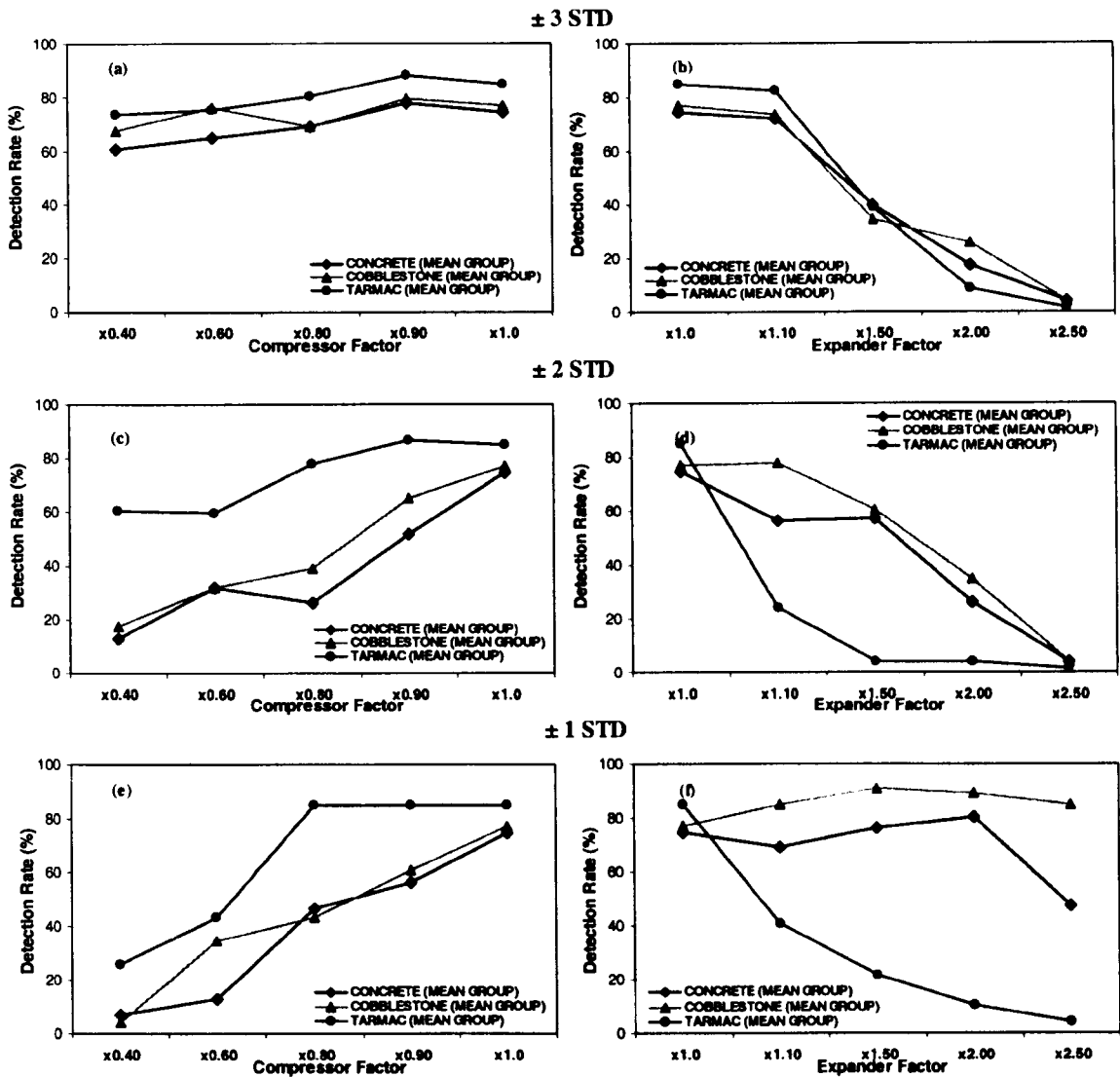


Figure 7.3 Results of the experiment to measure the effect of compression and expansion of the steering wheel acceleration signals on the human detection of road type in percent correct detection ($n=15$) where:
 (a, b) Results at threshold level of ± 3 STD
 (c, d) Results at threshold level of ± 2 STD
 (e, f) Results at threshold level of ± 1 STD

As shown in Figure 7.3, the percentage of correct detection for the original base stimuli was approximately 85% for the tarmac stimuli, 75% for the concrete stimuli and 78% for the cobblestone stimuli. These values can be compared to the values of approximately 90%, 78% and 80% respectively obtained for the same road surface type in Chapter 5. The small differences between these results, less than 5% for all road types, suggests that the tests described in this chapter did not deviate substantially from the research described in previous chapters of this thesis. The small differences may be due to small changes in the group of test subjects or in the environmental conditions.

Figure 7.3 suggests that a single, optimal, threshold level above which the stimuli can be manipulated by either compression or expansion exists which is valid for all three road surfaces that were investigated. It was found at the ± 3 STD threshold level when the stimuli are compressed by a factor of 0.90. This result can suggest that, similarly to the case of music, the compression of the highest peaks by a small factor makes the stimuli clearer to be detected. However, the percentage difference of less than 7% between the detection rate of the original stimuli (x1.0) and that of the stimuli which was compressed by a factor of 0.90 is not large in magnitude.

Similarly to the effect of scale/gain which was studied in Chapter 5, the highest detection rate for the tarmac stimuli was approximately of 90%, which was achieved when the stimulus was compressed by a factor of 0.90. In the (scale/gain) study the detection of the concrete surface and the cobblestone surface rescaled by factor of 0.90 produced detection rates of approximately 40%, while in the current study the detection rate was 78% for the concrete stimuli and 80% for the cobblestone stimuli using the same compressor factor of 0.90.

The use of expanders in the tarmac road surface at any threshold level only produced a detriment to detection. This surface can be assumed to be representative of a category of surfaces whose correct detection is reduced by increases in the size of their acceleration stimuli. For the concrete stimuli, instead, an improvement in detection occurred when the stimuli was expanded by a factor of 1.5 and 2.0 above a ± 1 standard deviation. Increases in correct detection also occurred for the cobblestone stimuli when expanded for almost all factors greater than 1.0 above a ± 1 standard deviation. The results for the concrete stimuli and cobblestone stimuli suggest that human memory associates the stimuli for these surfaces with large vibration amplitudes, however improvements in detection only seems to be achieved when almost all the data points in the time history are expanded.

These results are also presented in Figure 7.4 in terms of detectability index d' value as a function of the three threshold levels used in the laboratory experiment (± 3 STD, ± 2 STD and ± 1 STD). Results oscillate from -2 to 2 determined from the hit and false alarm rates obtained from all sessions. Detectability index d' value is presented along the ordinate,

while the scaled factors are presented along the abscissa. Both the percentage of detection rate and the detectability results suggest similar human response to all stimuli types.

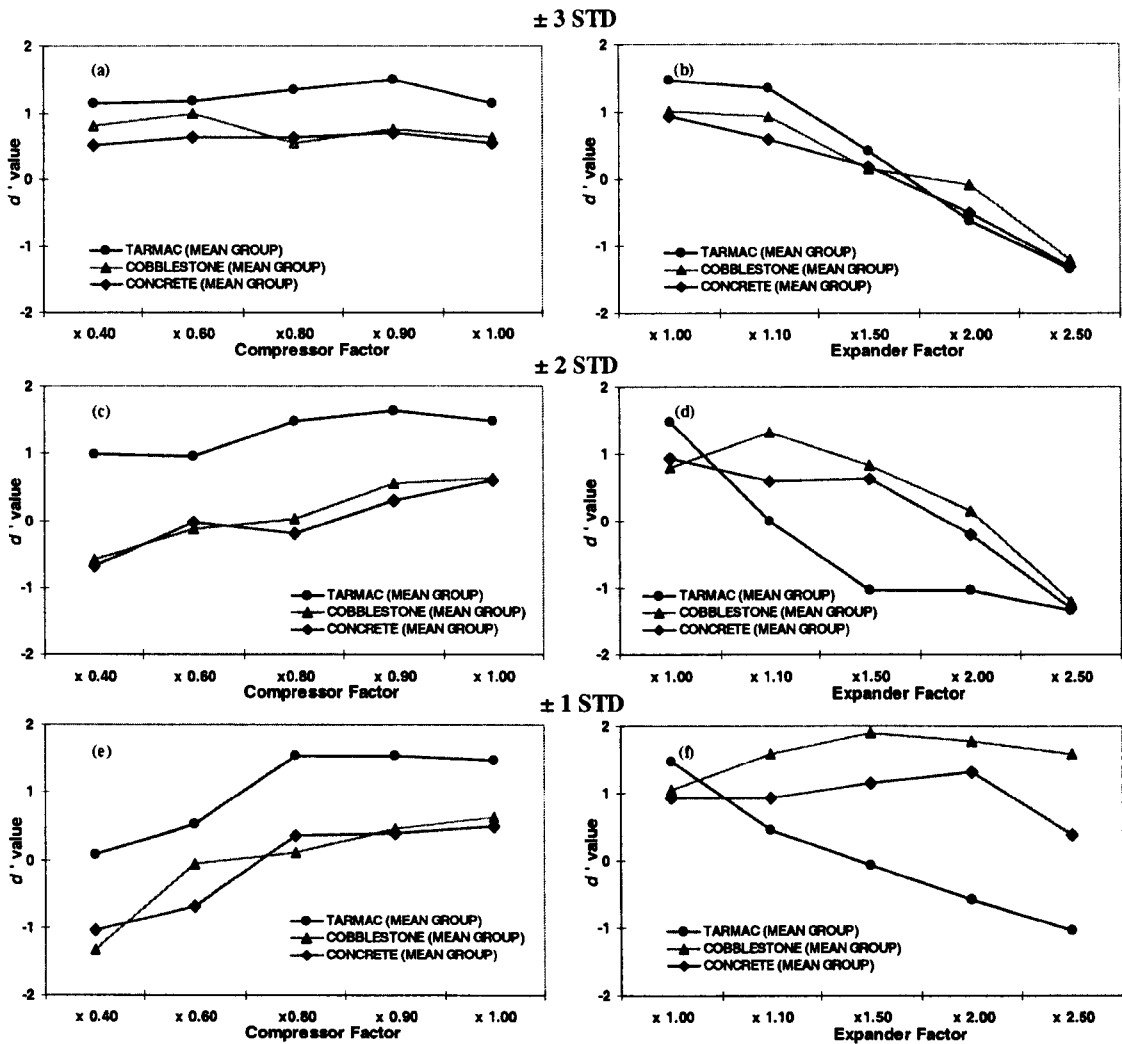


Figure 7.4 Results of the experiment to measure the effect of compression and expansion of the steering wheel acceleration signals on the human detection of road type in detectability index d' value ($n=15$) where:
(a, b) Results at threshold level of ± 3 STD
(c, d) Results at threshold level of ± 2 STD
(e, f) Results at threshold level of ± 1 STD

Appendix D.1 presents the Receiver Operating Characteristic (ROC) points obtained for the 15 test participants for the tarmac surface, the concrete surface and the cobblestone surface.

7.1.5 Observations and Discussion

For the three road surfaces investigated in the experiment the results suggested that the effect of compression or expansion of the steering wheel acceleration signals can lead to improvements in the detection task for all surfaces at a single and a fixed compression factor. This finding suggests that the assumption made at the beginning of the chapter

could be confirmed and that the use of these effects could also enhance the human perception in the case of steering wheel acceleration signals. However, the percentage difference of less than 7% between the detection rate of the original stimuli and that of the stimuli which was compressed by a factor of 0.90 suggests that more research is required. since the simple operation of either compression or expansion of the complete steering wheel acceleration signal does not produce extremely large changes in detection rate of the road surface. If very large improvements are required, a more selective process for defining the parts of the signal which should be amplified or reduce would seem necessary.

The music literature (Izotope, 2004; Katz, 2002) suggests the need to listen to the music when selecting what to compress or expand. The overall quality of the result of the transformation is directly judged by a listener. From the results found in the current study, it suggested that something similar must be applied to the steering stimuli in order to enhance the human road detection. It seems that the way in which the compressors and expanders are used to manipulate the steering stimuli must be carefully controlled according to the human cognitive mechanism used to detect the road surface. The results suggest that the situation is not as simple as choosing an arbitrarily threshold level above which compressors or expanders manipulate the stimuli, but that this threshold level should be carefully selected based on the expected human responses.

8. Test to determine the Effect of Steering Wheel Acceleration Transient Events on the Human Detection

According to the literature the term of transient event is used to describe dynamic events which are short in duration (Exarchos et al., 2006; 2006; Giacomini et al., 1999; Oikonomou et al., 2007; Tzallas et al., 2004) compared to the underlying long term changes in the signal. In the study of vibrational stimuli a transient event is considered to be a sudden increase in vibration which occurs for a short period of time, sometimes less than a fraction of a second, in an acceleration time history (Giacomini et al., 1999; Grainger, 2001; Steinwolf et al., 2002). Such events are detected as deviations from stationarity which exceed a specific threshold level. The presence of high-amplitude transient events is common in time histories of road vehicle vibration when the vehicle is driven over rough road surfaces. Even those road surfaces which appear smooth at first sight will often have rougher points which produce transient events.

This chapter describes experimental testing activities performed in order to measure the effect of transient event frequency content and scale on the human detection of road surface type by means of steering wheel vibration. The steering acceleration stimuli were manipulated by means of the mildly non-stationary mission synthesis (MNMS) algorithm (Giacomini et al., 1999) in order to produce test stimuli which were selectively modified in terms of the number, and size, of transient vibration events they contained. A natural question which arises in the case of the steering system is whether short, sharp, transients of the kind that occur when driving over cracks or stones have an effect on the detection of road surface type. The research which is described in this chapter was performed based

on the assumption that transient events could be features from which drivers receive information to detect road surface type. In this context the term of information is taken to mean something that people get from the environment, or something that a machine tells them they did not know before (Garner, 1962). In order to investigate if different manipulations in the number and the size of transient events could affect the decision making the main objectives of the experimental activities described in this chapter were:

- To measure the percentage of correct detection of the road surface type and the detectability index d' based on steering wheel vibration.
- To measure the percentage of correct detection of the road surface type and the detectability index d' based on steering wheel vibration when it has been manipulated in the number of the transient events by means of the MNMS algorithm using different compression ratios.
- To verify if one single compression ratio could produce mission signals which contain most of the informative transient events that the human uses to perform the detection for all road surface types.
- To measure the percentage of correct detection of the road surface type and the detectability index d' based on steering wheel vibration when it has been manipulated in the size of the transient events by means of the MNMS algorithm using different scale factors.
- To verify if one specific scale factor could re-size transient events in order to improve the human detection for all road surface types.

The results of the experiment tests were plotted using the Theory of Signal Detection as the analytical framework and were summarised by means of the detectability index d' value.

8.1 Three experiments in the Detection of Road Surface Type

Three laboratory-based experiments were carried out in this chapter. The first experiment investigated the effect of threshold trigger level, the second experiment investigated the effect of the number of the transient events and the third experiment investigated the effect of the scale of the transient events. All three experiments were performed in the Perception Enhancement Systems laboratory. The test facility used to perform the

laboratory experiments was the same which was previously described in this thesis in section 5.1.1.

8.1.1 Test subjects

For each of the three experiments a group of 15 individuals was tested. The test groups consisted of university staff and students. Upon arriving in the laboratory each participant was issued information and a consent form and an explanation was provided which described the experimental method and the laboratory safety features. Age, gender, height, and mass data were then collected, and the participant was requested to state whether he or she had any physical or mental condition which might affect perception of hand-arm vibration, and whether he or she had ingested coffee within the 2 hours previous to arriving in the laboratory. No participant declared any condition which might affect the perception of hand-arm vibration, and none declared having ingested coffee prior to their tests.

The participants in the threshold level experiment (First Experiment) consisted of 8 males and 7 females, while the participants in the number of the transient events experiment (Second Experiment) and the participants in the scaling of the transient events experiment (Third Experiment) consisted of 9 males and 6 females. Table 8.1 presents the mean, standard deviation (STD), minimum and maximum values of age, height and mass encountered in the test groups. The values can be considered relatively representative of UK drivers in all values except age, which is below the natural average.

Table 8.1 Physical characteristics of the groups of test participants involved in the laboratory experiments (n=15)

Characteristics	Mean	STD	Minimum	Maximum
Threshold Level Experiment				
Age (years)	24.60	5.74	20	37
Height (m)	1.71	0.08	1.60	1.95
Mass (kg)	72.33	8.44	58	90
Number of transient events				
Scale of transient events				
Age (years)	28.20	3.98	22	33
Height (m)	1.72	0.05	1.60	1.8
Mass (kg)	72.60	4.64	59	80

(STD) Standard Deviation

8.2 Experiment to Evaluate the Effect of Threshold Level on the Human Detection of Road Surface Type

One of the most fundamental and important variables in the MNMS algorithm is the Threshold Trigger Level (TTL). In MNMS, transient event identification is achieved in each wavelet group time history by means of a user selected threshold trigger level that is specific to the wavelet group. Variations of this value result in a change in the number of the transient events identified and extracted from the wavelet groups, and therefore, a change in the transient events reinserted back into the synthetic Fourier signal. The purpose of this laboratory-based experiment was to investigate the optimum value for the threshold level for each road surface type, so as to establish if a single value would prove optimal for all road surface types.

8.2.1 Test Stimuli

Three road surfaces were selected for use in testing. They were a broken concrete surface, a broken lane surface and a cobblestone surface. Each of the three steering wheel time histories was manipulated by means of the MNMS algorithm. A feature which is specific to MNMS is a wavelet grouping stage which permits the user to group individual wavelet levels into larger regions of significant energy, as illustrated in the PSD plots of Figure 8.1, where each wavelet group (WG1, WG2, etc.) is formed of two or more automatically generated wavelet levels. For all three acceleration stimuli used in the current study, the signal was automatically divided into 12 wavelet levels, which were then grouped based on user inputs into 5 wavelet groups. As shown in Figure 8.1 the wavelet groups were ordered from the lowest frequency to the highest frequency for simplicity.

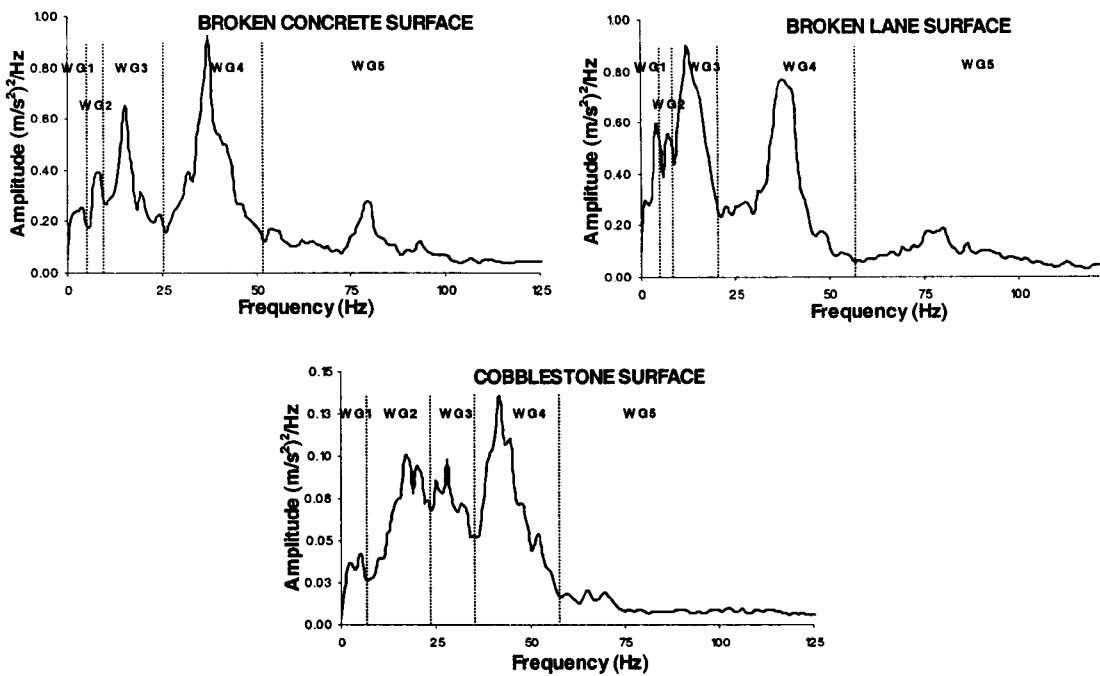


Figure 8.1 Power Spectral Densities (PSD) of the experimentally acquired steering wheel acceleration signals, showing the wavelet groups chosen for use in the current study.

Threshold trigger level (TTL) values of 2.4, 2.6, 2.8, 3.0, 3.2 and 3.4 were chosen so as to produce mission signals for use as test stimuli. Table 8.2 presents the number of transient events identified in each wavelet group using the six TTL values for each of the three road surfaces. The results suggest that the higher the TTL value, the lower the number of transient events identified into each wavelet group.

Once all transient events have been identified and extracted from all wavelet groups they are sorted by MNMS in descending order by maximum peak amplitude (absolute crest factor value). The transient event reinsertion method selected was maximum reinsertion, meaning synchronization procedure 2, which does not affect the amplitude and phase relationships within each bump event extracted from the original data (see section 2.6.6). Time compression ratio and bump scale factor were both set to the unity in order to produce mission signals without affecting the number, or size, of the transient events. Mission signals were then acquired into the LMS[®] TMON software in order to be tested (LMS TMON, 2002).

Table 8.2 Number of transient events identified in each wavelet group (WG) using different TTL values for all three stimuli used for producing the laboratory test stimuli.

SIGNALS		THRESHOLD TRIGGER LEVEL (TTL)					
		WG NUMBER	2.4	2.6	2.8	3.0	3.2
BROKEN CONCRETE	WG1	9	9	6	3	3	3
	WG2	15	6	6	6	3	3
	WG3	63	39	24	18	9	6
	WG4	87	60	36	27	9	6
	WG5	153	111	93	72	48	42
BROKEN LANE	WG1	12	9	3	3	0	0
	WG2	18	18	15	9	6	6
	WG3	36	21	21	15	6	6
	WG4	87	63	36	24	9	3
	WG5	158	122	87	60	48	27
COBBLESTONE	WG1	7	2	1	1	1	0
	WG2	16	11	6	3	2	0
	WG3	49	35	25	16	11	8
	WG4	80	58	36	25	17	12
	WG5	147	104	74	43	27	19

8.2.2 Test Protocol

Upon arriving in the laboratory each participant was asked to remove any articles of heavy clothing such as coats, and to remove watches or jewellery. He or she was asked to sit in the test rig and to adjust the seat so as to achieve a realistic driving posture. The participant was then asked to fix his or her eyes on a board directly in front of the test rig, which displayed a photograph of one of the three road surfaces which was being used in the test. Prior to commencing formal testing, the participant was provided an example of each of the three stimuli types which would be used later, in order to become acquainted with the detection task.

The experiment was performed in three parts, one for each road surface studied. Each part involved five repetitions of each of the manipulated test stimuli which were derived from the original road data and also the original stimuli from the displayed road surface. In addition, twenty five stimuli were chosen randomly from the stimuli sets of the other road surfaces which were used as background noise for the overall test. The time duration of

each individual test stimuli was chosen to be 10 seconds. Five different series of twelve acceleration stimuli were applied to evaluate each road surface type. In each series, each stimulus was separated from each other stimulus by a 5 second gap in which the participant was asked to state by “yes” or “no” his or her judgment of road type. The order of stimuli presentation was fully randomised for each participant in each series in order to reduce learning effects. Each participant performed 60 detections in each part of the experiment, for a total of 180 detections in a complete experiment.

8.2.3 Results from the Experiment to Evaluate the Effect of Threshold Trigger Level on the Human Detection of Road Surface Type

Figure 8.2 presents the experimental results plotted in terms of percent correct detection, from 0 to 100 percent. Percent correct detection is presented along the ordinate while the six different threshold trigger level (TTL) values are presented along the abscissa. The original base stimuli are labelled as O. For each TTL, the hit rate was taken to be the proportion of “yes” responses obtained from the stimuli which were actually derived from the presented road surface. The false alarm rate was taken to be the proportion of “yes” responses obtained from the stimuli which were not derived from the road surface which was being presented. The detection responses for the three road surfaces were analysed in a between/within-subjects by means of the one factor repeated measures ANOVA. Statistical significance effect in the responses were found in all the three surfaces tested at a $p=0.01$ of significance level with a $F(6,84)$ value of 21.19, 21.16 and 3.39 for the broken concrete stimuli, the broken lane stimuli and the cobblestone stimuli, respectively.

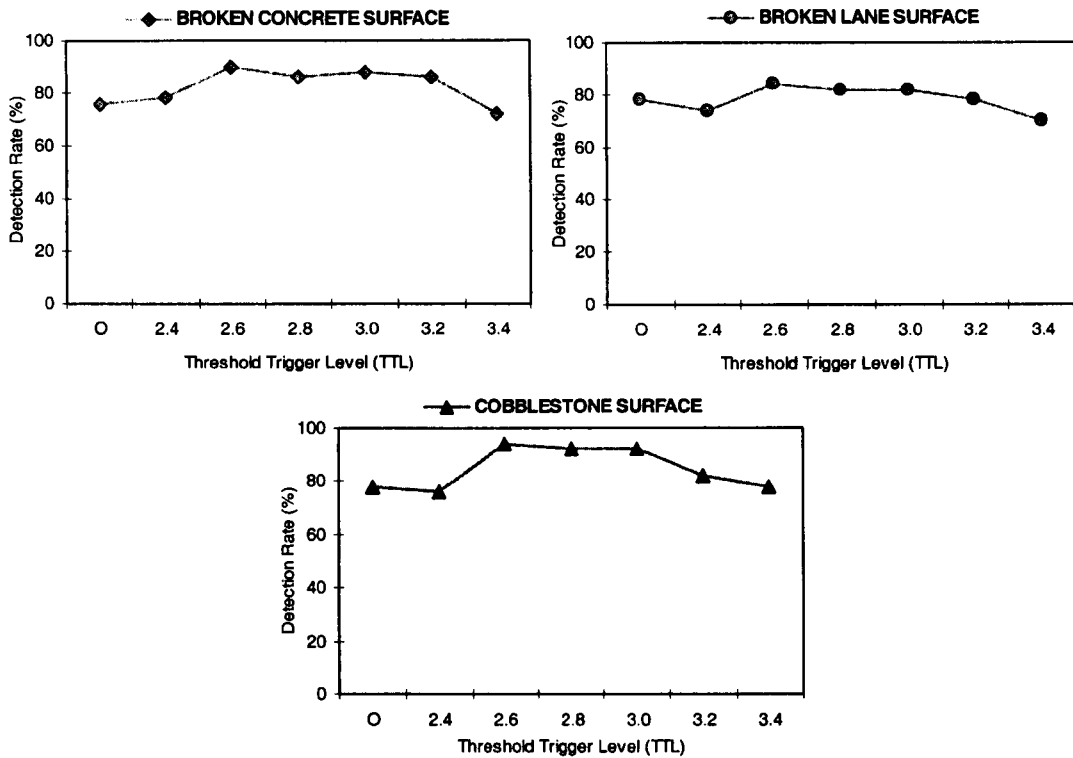


Figure 8.2 Results of the laboratory experiments regarding the effect of threshold level of the steering wheel acceleration signal on the human detection of road surface type in percent correct detection ($n= 15$).

As shown in Figure 8.2 the percentage of correct detection for the original base stimuli was approximately 78% for the broken concrete stimuli, 80% for the broken lane stimuli and 78% for the cobblestone stimuli. These values can be compared to the values of approximately 74%, 80% and 80% respectively obtained in previous experiments in Chapter 5 and 6. These results suggested a maximum difference in detection lesser to 5% for all three road surfaces. The results in Figure 8.2 suggest an improvement in detection when threshold trigger level (TTL) values from 2.6 to 3.2 were used to produce mission signals for all the three road surfaces. The use of TTL values lesser to 2.6 or greater to 3.2 seems to be detrimental to human detection.

The results are also presented in terms of the detectability index d' value in Figure 8.3, from 0 to 3, determined from the hit and false alarm rates obtained from all sessions. Detectability index d' is presented along the ordinate, while the six threshold trigger level (TTL) values are presented along the abscissa. Both the detection rate and the detectability results suggest similar qualitative human response and suggest that the bumps events identified and extracted in the range of TTL values from 2.6 until 3.2 are playing a key role in the human cognitive detection of the road surface type for all three surfaces.

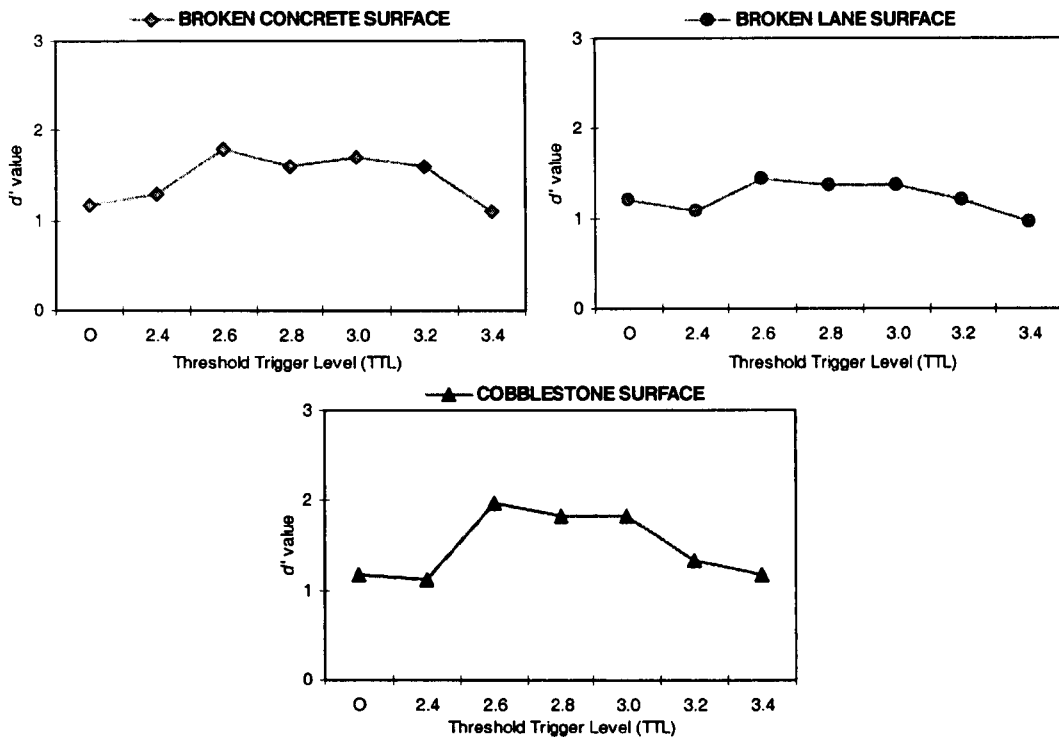


Figure 8.3 Results of the laboratory experiments regarding the effect of threshold level steering wheel acceleration signal on the human detection of road surface type in detectability index d' value ($n= 15$).

Both curves, the detection rate and the detectability present in the current study, show similar qualitative behaviour for all three road surfaces, decreasing in detection when the lesser threshold level was evaluated (2.4), increasing in detection in the range of TTL from 2.6 to 3.2, and then again decreasing in detection at the greater TTL of 3.4. The detection results suggest that the perceptual and cognitive mechanisms used by the average driver required vibrational information which content transient events with a standard deviation spanning from 2.6 to 3.2, which can permit accurate detection in situations where detection relies solely on the tactile sense modality. The identification of these TTL values may be of relevance in order to use the MNMS algorithm to manipulate steering stimuli.

The use of TTL values different to those found in the range from 2.6 to 3.2 seems to be detrimental to human detection for the three road surfaces studied. Current results suggest that possibly certain transient events in the original stimuli are not informative to the driver, and that their extraction and their reinsertion made the stimuli more complex to detect as seen in the case of a TTL value of 2.4, or some transient events are missed when TTL values are selected to be greater than 3.2.

Appendix D.2 presents the Receiver Operating Characteristic (ROC) points obtained for the 15 test participants for the broken concrete surface, the broken lane surface, and the cobblestone surface. ROC point results also suggest that an improvement in detection is found at threshold trigger level (TTL) values from 2.6 to 3.2 from each wavelet group. The results suggest that the transient events identified with TTL values spanning from 2.6 to 3.2 seem critical to the human detection: averaging hit rates exceeded 80% for the three road surfaces.

8.3 Experiments to Measure the Effect of the Number of Transient Events and the Scale of Transient Events

Laboratory-based experiments were conducted to evaluate the effect of the number and scale of transient vibration events on the human detection of road surface type by means of steering wheel vibration. The study used steering wheel tangential direction acceleration time histories which had been measured in a mid-sized European automobile that was driven over three different types of road surface. The steering acceleration stimuli were manipulated by means of the Mildly Non-stationary Mission Synthesis (MNMS) algorithm (section 2.6) in order to produce test stimuli which were selectively modified in terms of the number, and size, of transient vibration events they contained. Participants were exposed to both un-manipulated and manipulated steering wheel rotational vibration stimuli.

8.3.1 Test Stimuli

Three road surfaces were selected for use in testing which were a cobblestone surface, concrete surface and a tarmac surface. Each of the three steering wheel time histories was manipulated by means of the MNMS algorithm as described in section 8.2.1. The steering stimuli wavelet levels were grouped into larger regions of significant energy called wavelet groups as seen in Figure 8.4, where each wavelet group is formed of two or more automatically generated wavelet levels.

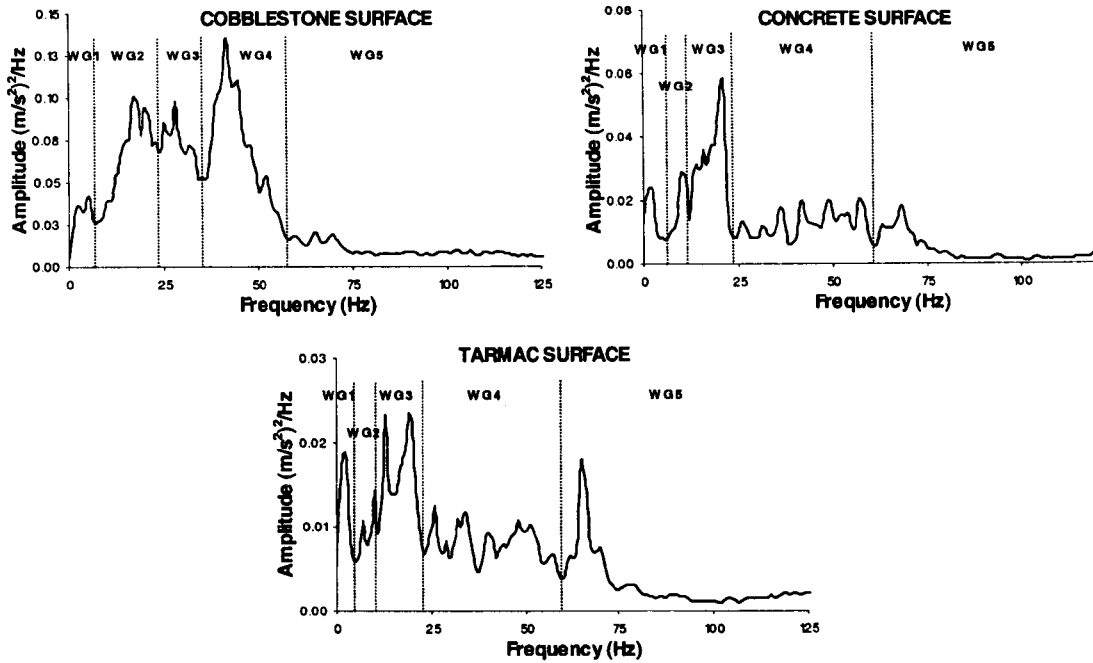


Figure 8.4 Power Spectral Densities (PSD) of the experimentally acquired steering wheel acceleration signals, showing the wavelet groups chosen for use in the study.

In the study the wavelet group trigger levels were chosen to be in the range from 2.6 to 3.2 standard deviations based on the findings of the previous experiment which is describe in section 8.2.

Test signals were produced from each of the three experimentally acquired base signals using four time compression ratios of 1.0, 2.0, 3.0 and 4.0 and five transient event scale factors of 0.8, 1.0, 2.0, 3.0 and 4.0. The transient event reinsertion method selected was maximum reinsertion, meaning synchronization procedure 2, which does not affect the amplitude and phase relationships within each the bump event which was extracted from the original signal (see section 2.6.6). Table 8.3 presents the number of bump events that were extracted (NBE) from the original stimuli and the number of bump events that were reinserted (NBR) into the test stimuli at the four time compression ratios (CR) selected for the study. Figure 8.5 presents the power spectral densities obtained for the original concrete road stimuli and for the test stimuli. The close correspondence of the curves of Figure 8.5 suggests that the energy distribution was accurately retained after manipulation by the MNMS algorithm.

Table 8.3 Number of bump events extracted (NBE) from the original stimuli and the number of bump events that were reinserted (NBR) into the test stimuli using four time compression ratios.

SIGNAL	Compression Ratio (CR)	Number of Bumps Extracted (NBE)	Number of Bumps Reinserted (NBR)
COBBLESTONE	1.0	53	53
	2.0		53
	3.0		53
	4.0		52
CONCRETE	1.0	53	53
	2.0		49
	3.0		48
	4.0		47
TARMAC	1.0	53	53
	2.0		53
	3.0		49
	4.0		44

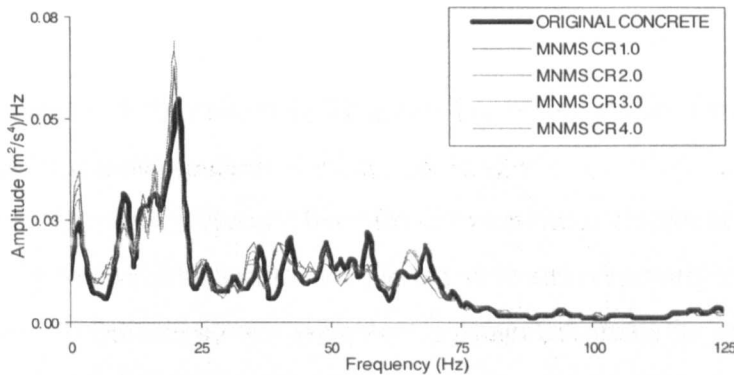


Figure 8.5 Power Spectral Density of the original concrete road base stimuli and of the test stimuli obtained using compression ratios of 1.0, 2.0, 3.0 and 4.0.

8.3.2 Test Protocol

Upon arriving in the laboratory each participant was asked to remove any articles of heavy clothing such as coats, and to remove watches or jewellery. He or she was asked to sit in the test rig and to adjust the seat so as to achieve a realistic driving posture. The participant was then asked to fix his or her eyes on a board directly in front of the test rig, which displayed a photograph of one of the three road surfaces which was being used in the test. Prior to commencing formal testing, the participant was provided an example of each of the three stimuli types which would be used later, in order to become acquainted with the detection task.

Both the experiment to determine the effect of the number of transient events and the experiment to determine the effect of the transient event scaling were performed in three

parts, one for each road surface studied. Each part involved five repetitions of each test stimuli from the displayed road surface. In addition, twenty five stimuli were chosen randomly from the stimuli sets of the other road surfaces, and were used to provide a noise background for the study.

The time duration of each individual test stimuli was chosen to be 10 seconds. Five different series of ten acceleration stimuli were applied to evaluate each road surface type for each test experiment. In each series, each stimulus was separated from each other stimulus by a 5 second gap in which the participant was asked to state by “yes” or “no” his or her judgment of road type. The order of stimuli presentation was fully randomised for each participant in each series in order to reduce learning effects. Each participant performed 50 detections in each part of the experiment, for a total of 150 detections in a complete experiment.

8.3.3 Results from the Experiment to Measure the Effect of the Number and Scaling of Transient Events

Figure 8.6 presents the results obtained from the experiment to determine the effect of the number of transient events. The results are plotted in terms of percent correct detection, from 0 to 100 percent. Percent correct detection is presented along the ordinate while the ratio of signal compression (the increases in the number of transient events) is presented along the abscissa. The original base stimuli are labelled as O, while the four compressed test stimuli are labelled as +1, +2, +3 and +4 to indicate the compression ratios from 1 to 4. For each compression ratio, the hit rate was taken to be the proportion of “yes” responses obtained from the stimuli which were actually from the presented road surface. The false alarm rate was taken to be the proportion of “yes” responses obtained from the stimuli which were not derived from the road surface which was being presented. The percentage of correct detection responses for the three road surfaces were analysed in a between/within-subjects by means of the one factor repeated measures ANOVA. Statistical significance effect in the responses were found in all the three surfaces tested at a $p=0.01$ of significance level with a $F(4,56)$ value of 6.70, 17.48 and 36.26 for the cobblestone stimuli, the concrete stimuli and the tarmac stimuli, respectively.

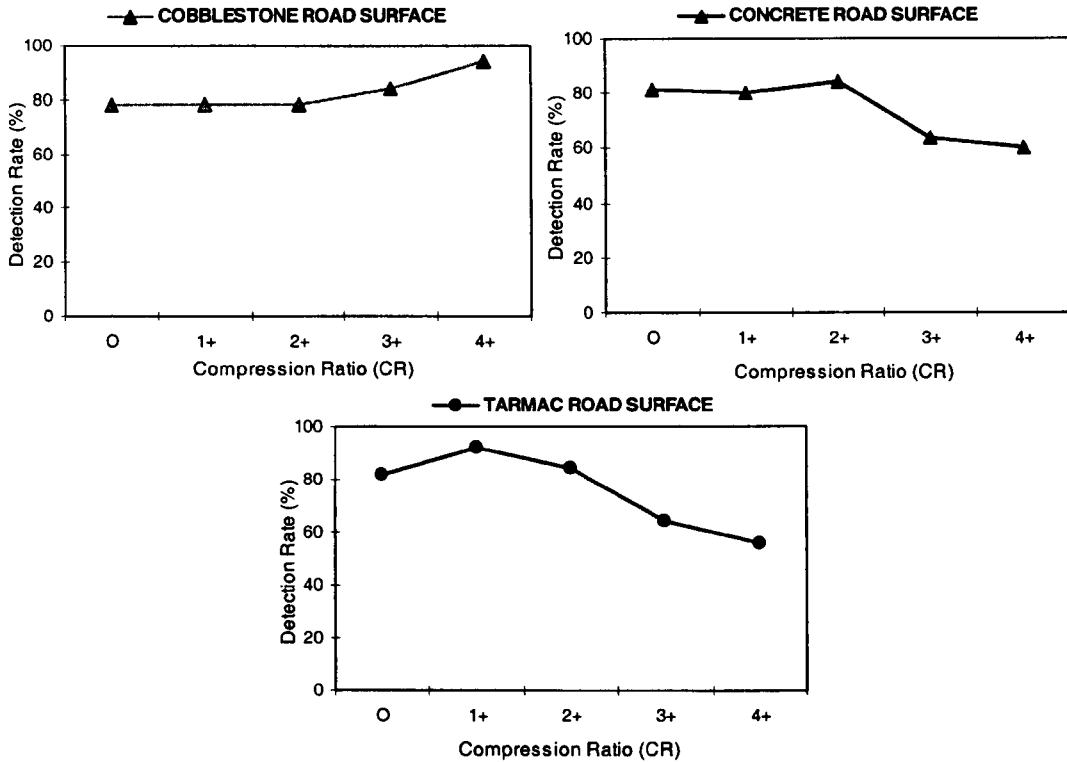


Figure 8.6 Results of the laboratory experiments regarding the effect of the number of transient events of the steering wheel acceleration signal on the human detection of road surface type plotted in terms of percent correct detection ($n= 15$).

As shown in Figure 8.6 the results obtained for a compression ratio of 1, which consists of the use of the MNMS algorithm to manipulate the signals without increasing the number of transient events, produced only mixed results. The percentage of correct detection remained constant for the cobblestone stimuli, decreased for the concrete stimuli and improved for the tarmac stimuli. This suggests that human detection of road surface type can be sensitive not just to the type, size and number of transient events in the signal, but also to their position in the stimulus time history since changes in the position is the main result of operating MNMS without any signal compression.

Figure 8.6 does suggest, however, the potential usefulness of controlling the transient events which are present in the steering vibration stimuli. Important increases in correct detection occurred for all compression ratios greater than 2 for the cobblestone stimuli, for compression ratio 2 for the concrete stimuli and for compression ratios of both 1 and 2 for the tarmac stimuli.

The results are also presented in terms of the detectability index d' value in Figure 8.7, from 0 to 3, determined from the hit and false alarm rates obtained from all sessions.

Detectability index d' is presented along the ordinate while the compression ratio values are presented along the abscissa. Both the detection rate and the detectability results suggest similar qualitative human response.

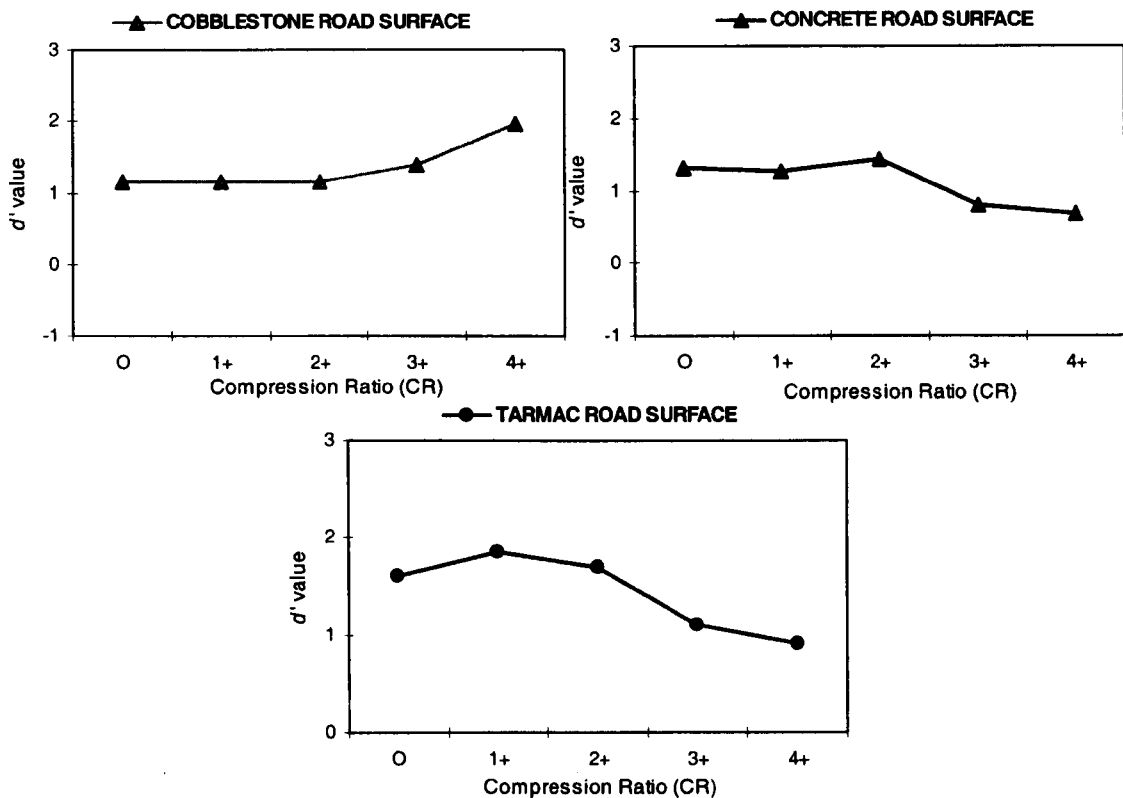


Figure 8.7 Results of the laboratory experiments regarding the effect of the number of transient events of the steering wheel acceleration signal on the human detection of road surface type plotted in terms of detectability index d' value ($n=15$).

Figure 8.8 presents the results obtained from the experiment to determine the effect of transient event scaling on the human ability to detect road surface type. The stimuli used in this experiment had a compression ratio of 2, which was chosen because it was the mean compression ratio considered in the current study. The results are again plotted in terms of percent correct detection, from 0 to 100 percent. The scale factors applied to the individual transient events (0.8, 1.0, 2.0, 3.0 and 4.0) by means of the MNMS algorithm are presented along the abscissa. The percentage of correct detection responses for the three road surfaces were analysed in a between/within-subjects by means of the one factor repeated measures ANOVA. Statistical significance effect in the responses were found in all the three surfaces tested at a $p=0.01$ of significance level with a $F(4,56)$ value of 18.82, 15.12 and 35.47 for the cobblestone stimuli, the concrete stimuli and the tarmac stimuli, respectively.

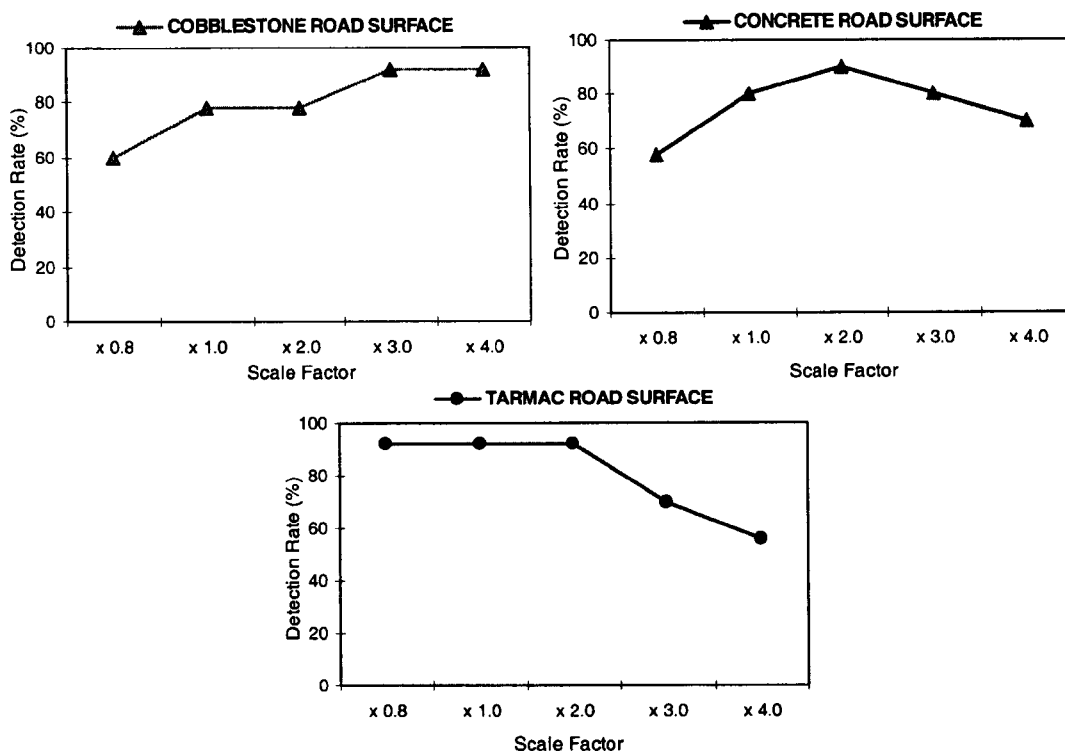


Figure 8.8 Results of the laboratory experiments regarding the effect of the transient events scaling of the steering wheel acceleration signal on the human detection of road surface type plotted in terms of percent correct detection (n= 15).

For the stimuli involving transient events which were maintained at their natural scale (x1.0), the percentages of correct detection were 75% for the cobblestone stimuli, 80% for the concrete stimuli and 92% for the tarmac stimuli. In the case of the cobblestone stimuli the optimum detection was achieved at the largest scale that was tested (x4.0), while for the concrete stimuli optimum detection occurred at the mean value (x2.0) and detection for the tarmac stimuli was optimum for the smallest scale values tested (x0.8). For all three road surface types, optimum detection occurred for stimuli having transient events which were different in size from those occurring naturally in the original stimuli.

The results are also presented in terms of the detectability index d' value in Figure 8.9, from 0 to 2, determined from the hit and false alarm rates obtained from all sessions. Detectability index d' is presented along the ordinate while the compression ratio values are presented along the abscissa. Both the detection rate and the detectability results suggest similar qualitative human response.

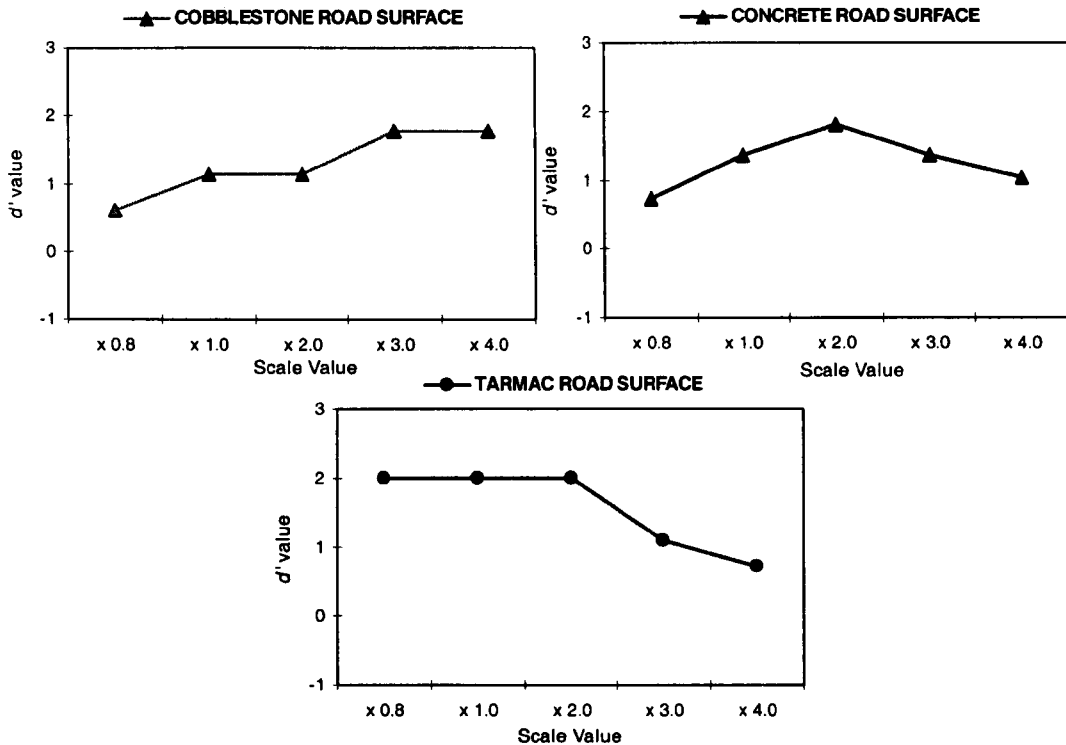


Figure 8.9 Results of the laboratory experiments regarding the effect of the transient events scaling of the steering wheel acceleration signal on the human detection of road surface type plotted in terms of detectability index d' value ($n=15$).

Appendix D.3 and D.4 present the Receiver Operating Characteristic (ROC) points obtained for the 15 test participants for the cobblestone surface, the concrete surface and the tarmac surface

8.3.4 Observations and Discussion

The findings suggest that steering wheel transient vibration events play a key role in human detection of road surface type. Improvements of up to 20 percentage points in the rate of correct detection were achieved by means of selective manipulation of the steering vibration stimuli. The results also suggest, however, that no single setting of the MNMS algorithm proved optimal for all road surface types which were investigated.

Comparison of these results to those of Chapter 5 relative to the study of the effect of gain/scale suggests similarities. The curves of percent correct detection which are presented here, both those as a function of transient event number, and those as a function of transient event scale, show similar qualitative behaviour to the curves obtained as a function of overall signal scale. The improvement in detection rate as a function of increasing compression ratio found for the cobblestone surface in this study mirrors the monotonic increase obtained as a function of overall signal scale in Chapter 5. Also, the

decrease in detection rate as a function of increasing the scale of the transient events found for the tarmac surface mirrors the monotonic decrease obtained as a function of overall signal.

Although the results of the test to measure the effect of the number of transient events suggested that there was no single time compression ratio (i.e. increase in the density of transient events in the signal) which was optimal for all of the road surface types which were investigated, the time compression value of 2 did nevertheless provide significant improvements for the concrete stimuli and for the tarmac stimuli while simultaneously providing reasonable results for the cobblestone stimuli.

Although the results of the test to measure the effect of the scaling of the transient events suggested that there was no single scale factor (i.e. increase or decrease of the size of the individual transient events in the signal) which was optimal for all of the road surface types which were investigated, the scale factor of 2.0 did nevertheless improve detection for the cobblestone stimuli and for the concrete stimuli while providing reasonable results for the tarmac stimuli.

An overall conclusion which can be hypothesised based on the results of the transient event number and scale experiments is that simple repetition or scaling of the individual transient events, performed as the only perception enhancement operation, does not provide universally optimal results. Doubling both the number and size of the transient events in the signal would be expected to produce improvements in the detection of many road surfaces, but these parameter settings are not sufficient to guarantee universally optimal perception enhancement. From the results of these experiments it would appear that selection and targeting of individual transient events is probably required in order to achieve universally optimal results. Possibly only a small number of transient events carry the main part of the road surface information to the driver, thus only those events should be scaled and repeated so as to achieve optimal results.

9. Experiment to determine the effectiveness of a first set of guidelines for automotive steering vibration feedback

The final test activity of the PhD research is presented in this chapter. It was performed based on the assumption that automotive steering vibration feedback can be optimised for the purposes of road surface detection by implementing the most promising feedback settings which were found in the various tests which are described in the previous chapters of this thesis. By collecting the best MNMS algorithm settings from the various individual tests of road surface detection it was expected that a simple first set of perception enhancement guidelines could be assembled for use with the automotive steering.

Based on the results described in the previous chapters of this thesis the parameter settings which can be applied to the Mildly Non-stationary Mission Synthesis (MNMS) algorithm so as to achieve general improvements in the rate of road surface detection include the following:

1. The steering vibration should contain transient events extracted from at least the key frequency band identified in the study of the effect of steering wheel acceleration frequency distribution of Chapter 6. The frequency band in question is the range from approximately 20 Hz to 60 Hz for the road surfaces studied.
2. Based on the results of the study of the effects of threshold trigger level (TTL) of Chapter 8, the steering vibration should contain transient events which are chosen

using a trigger value in the range from 2.6 to 3.2 standard deviations. If only the single frequency band described in point (1) above is manipulated, then only a single standard deviation value is required, which can be taken to be 2.6 based on the results of chapter 8.

3. The steering vibration signal should contain more transient events than would be expected from current practice with automobiles. Improvements in road surface detection can be achieved by implementing a compression ratio of 2.0 using the MNMS algorithm so as to double the number of transient events in the steering vibration signal as described in chapter 8.
4. The steering vibration signal should contain transient events which are scaled upwards so as to be larger than those which occur from current practice with automobiles. Improvements in road surface detection can be achieved by implementing a bump scale factor of 2.0 using the MNMS algorithm, as described in chapter 8.

In order to investigate the possible effectiveness of the first set of guidelines for automotive steering vibration feedback which are listed above, the experimental test activity described in this chapter had the following objectives:

- To measure the percentage of correct detection of the road surface type based on steering wheel vibration.
- To measure the percentage of correct detection of the road surface type based on steering wheel vibration when it has been manipulated according to the first set of guidelines for automotive steering vibration feedback.
- To verify if the automotive steering vibration feedback guidelines lead to general improvements in human detection for a wide range of road surfaces.

The results of the experimental tests were plotted using the Theory of Signal Detection as the analytical framework and were summarised by means of receiver operating curve (ROC) points.

9.1 Experiment to Measure the effect of the first set of guidelines for automotive steering vibration feedback

A laboratory-based experiment was conducted to evaluate the effect of a first set of guidelines for automotive steering vibration feedback on the human detection of road surface type. The study used steering wheel tangential direction acceleration time histories which had been measured in a mid-sized European automobile that was driven over ten different types of road surface. The original experimentally acquired steering acceleration stimuli were manipulated by means of the Mildly Non-stationary Mission Synthesis (MNMS) algorithm (section 2.6) in order to produce test stimuli which were selectively modified according to the steering feedback guidelines. For each steering acceleration stimuli a single manipulated test stimulus was produced. During the course of the experiment the participants were exposed to both un-manipulated and manipulated steering wheel rotational vibration stimuli.

9.1.1 Test Subjects

A group of 15 participants was tested who were all university staff and students. Upon arriving in the laboratory each participant was issued an information and consent form as well as a description of the experimental method and the laboratory safety features. Age, gender, height, and mass data were then collected, and each participant was requested to state whether he or she had any physical or mental condition which might affect perception of hand-arm vibration, and whether he or she had ingested coffee within the 2 hours previous to arriving in the laboratory. No test participant declared a physical or a cognitive condition which might affect the perception of hand-arm vibration, and none declared having ingested coffee prior to their tests.

The participants consisted of 9 males and 6 females. The physical characteristics of the group are summarised in Table 9.1. The mean value and the standard deviation of each of the three measures of age, height and mass can be seen to be near the UK population values except in the case of age, which was somewhat lower than the UK national statistics.

Table 9.1 Physical characteristics of the group of test participants involved in the laboratory experiment (n=15)

Characteristics		Mean	STD	Minimum	Maximum
Age	(years)	29.93	3.75	22	35
Height	(m)	1.69	7.66	1.58	1.8
Mass	(kg)	68.67	6.85	58	76

(STD) Standard Deviation

9.1.2 Test Stimuli

Ten road surfaces were selected for use in the experiment. They were a broken surface, a broken concrete surface, a broken lane surface, a cobblestone surface, a cobblestone city, a concrete surface, a country lane, motorway surface, a noise surface and a tarmac surface. Each of the ten steering wheel acceleration time histories was manipulated by means of the MNMS algorithm as described in section 8.2.1 based on the conditions established at the beginning of the chapter. The wavelet levels of the steering acceleration stimuli were grouped into three large regions of significant energy which are the wavelet groups WG1, WG2 and WG3 which are shown in Figure 9.1. Each wavelet group is formed of two or more automatically generated wavelet levels. WG2 is the wavelet group which contains the critical frequency range of 20 to 60 Hz.

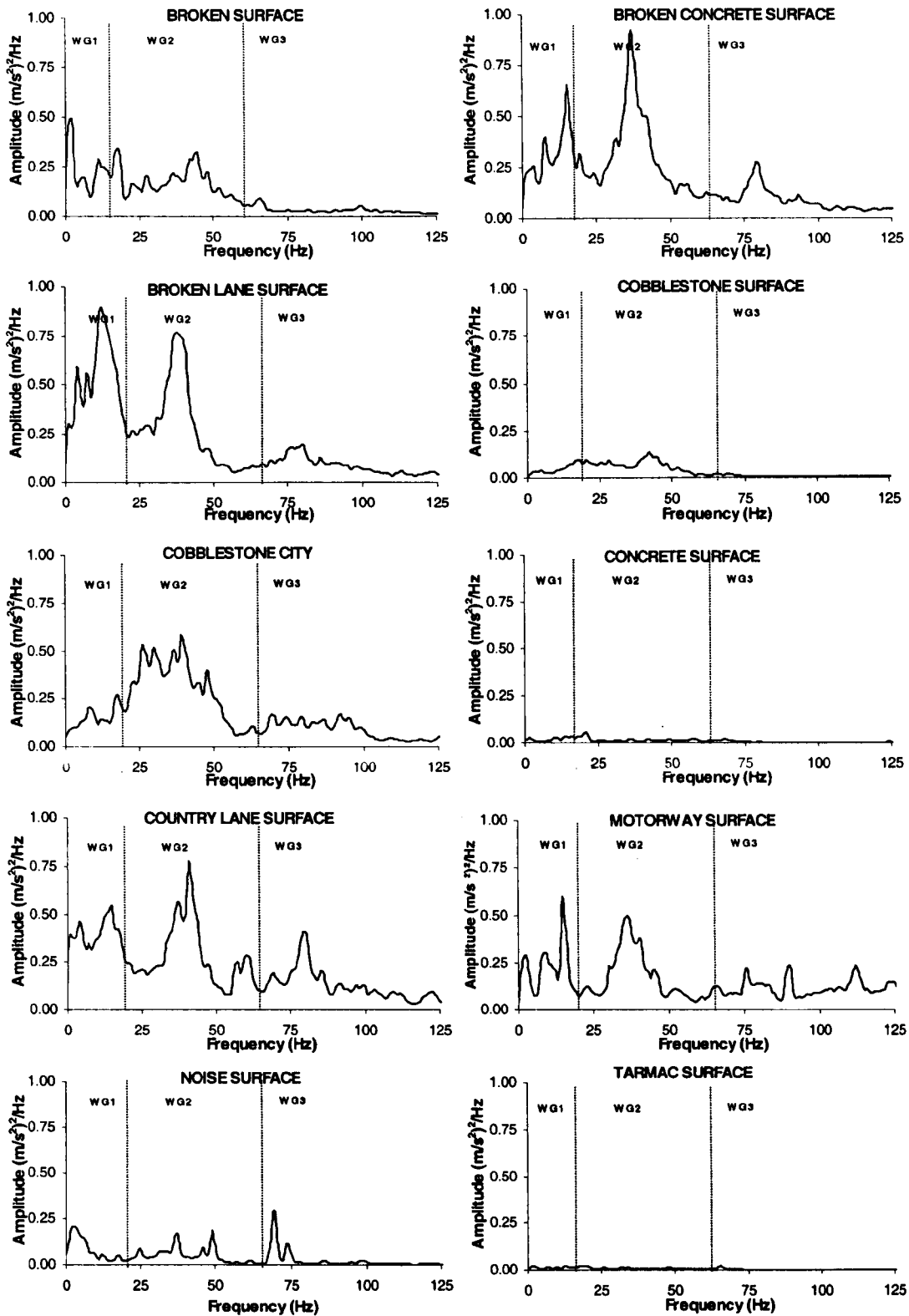


Figure 9.1 Power Spectral Densities (PSD) of the experimentally acquired steering wheel acceleration signals, showing the wavelet groups chosen for use in the experiment.

Although the steering acceleration stimuli wavelet levels were grouped into three wavelet groups, transient events (bumps) were only extracted from the wavelet group 2 (WG2). Manipulated stimuli were produced from each of the ten experimentally acquired signals

using: a threshold trigger level value of 2.6, a time compression ratio of 2.0 and a transient event scale factor of 2.0. The transient event reinsertion method selected was maximum reinsertion, meaning synchronization procedure 2, which does not affect the amplitude and phase relationships within each the bump event which was extracted from the original signal (see section 2.6.6). Table 9.2 presents the number of bump events that were extracted (NBE) from the original stimuli and the number of bump events that were reinserted (NBR) into the test stimuli.

Table 9.2 Number of bump events extracted (NBE) from the original stimuli and the number of bump events that were reinserted (NBR) into the test stimuli.

SIGNAL	Number of Bumps Extracted (NBE)	Number of Bumps Reinserted (NBR)
Broken	65	62
Broken Concrete	60	55
Broken Lane	63	60
Cobbleston	35	35
Cobbleston City	71	68
Concrete	35	33
Country Lane	60	60
Motorway	60	60
Noise	46	46
Tarmac	33	33

9.1.3 Test Protocol

Upon arriving in the laboratory each participant was asked to remove any articles of heavy clothing such as coats, and to remove watches or jewellery. He or she was asked to sit in the test rig and to adjust the seat so as to achieve a realistic driving posture. The participant was then asked to fix his or her eyes on a board directly in front of the test rig, which displayed a photograph of one of the ten road surfaces which was being used in the test. Prior to commencing formal testing, the participant was provided an example of each of the ten stimuli types which would be used later, in order to become acquainted with the detection task.

The experiment was performed in ten parts, one for each road surface studied. During each part of the experiment a photograph of a single road surface was displayed on the

board directly in front of the participant throughout the test. Each part involved five repetitions of the original experimentally acquired steering vibration stimuli from the road which was displayed on the board, and five repetitions of the optimised stimuli which had been developed through manipulation according to the steering feedback guidelines. In addition, ten other test stimuli were chosen from among the original or the optimised stimuli associated with the other nine road surfaces. The stimuli from the other road surfaces served to form the noise background for the study, against which the detections of the correct stimuli from the actual road were being made.

The time duration of each individual test stimuli was chosen to be 10 seconds. Two different series of ten acceleration stimuli were applied to evaluate each road surface type. In each series, each stimulus was separated from each other stimulus by a 5 second gap in which the participant was asked to state by “yes” or “no” whether the actuated acceleration stimulus was from the road surface whose photograph was shown on the board directly in front of the test bench. The order of stimuli presentation was fully randomised for each participant in each series in order to reduce learning effects. Each participant performed 20 detections in each part of the experiment, for a total of 200 detections in a complete experiment.

9.1.4 Results from the Experiment to Measure the Effect of the first set of guidelines for an automotive steering vibration feedback

Figure 9.2 presents a histogram containing the percent correct detection from both the original stimuli and the manipulated stimuli for each of the ten road surfaces investigated in the experiment. The percent correct detection is presented along the ordinate, while the name of the road surface is presented along the abscissa. For each un-manipulated or manipulated road surface stimulus the hit rate was taken to be the proportion of “yes” responses obtained from the stimuli which were actually from the presented road surface. The false alarm rate was taken to be the proportion of “yes” responses obtained from the stimuli which were not derived from the road surface which was being presented.

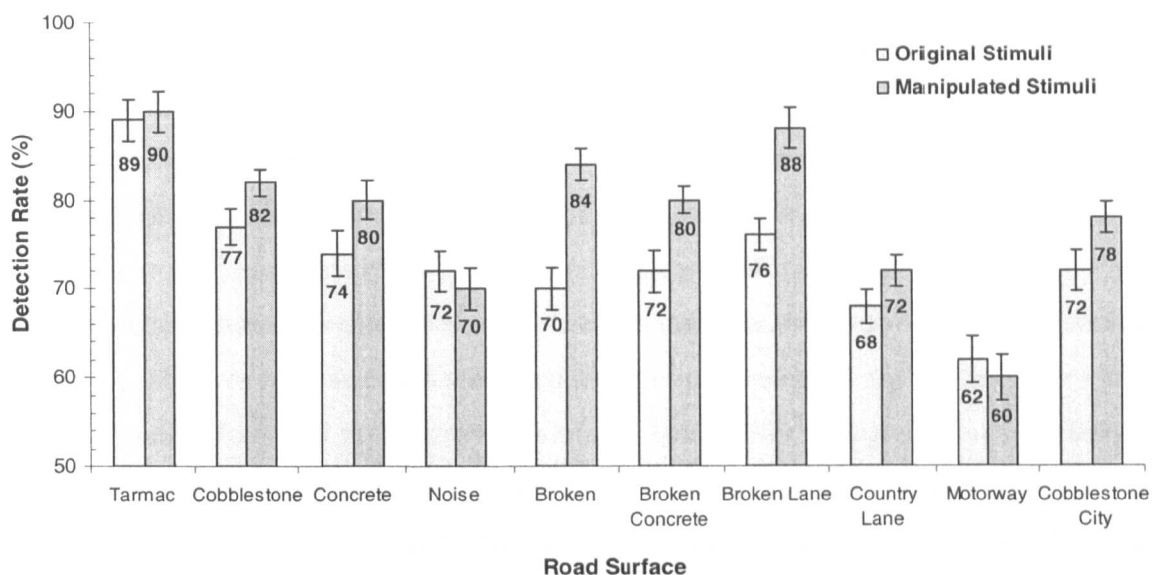


Figure 9.2 Results of the laboratory experiments regarding the effect of the first set of guidelines for automotive steering vibration feedback on the human detection of road surface type in terms of percent detection rate (n= 15).

As shown in Figure 9.2 the application of the first set of steering vibration feedback guidelines by means of the MNMS algorithm produced improvements in some cases of up to 14 percentage points in the rate of correct detection. Manipulation of the steering wheel acceleration stimuli by means of MNMS and the steering vibration feedback guidelines produced improvements in the rate of detection of 8 of the 10 road surfaces. The same manipulation lead to a degradation in detection in two of the road surfaces, i.e. the motorway surface and the noise surface.

The percentage of the correct detection responses for the ten road surfaces were analysed in a between/within-subjects by means of the one factor repeated measures ANOVA. Statistical significance effect in the responses were found in almost all surfaces which produced improvements in the detection rate at a $p=0.05$ of significance level with a $F(1,14)$ spanning from 5.385 to 10. Except for the tarmac stimuli in which no significant effect was found at a $p=0.05$ of significance level with a $F(1,14)$ equal to 1.0. Although the percentage of correct detection of the manipulated stimuli for both the motorway stimuli and the noise stimuli decreased in detection, it was not found to be significant at a $p=0.05$ of significance level.

Appendix D.5 presents the Receiver Operating Characteristic (ROC) points obtained for the 15 test participants for the ten surfaces investigated.

9.1.5 Observations and Discussions

Following the general pattern established in chapter 6 of this thesis, the improvements in correct detection were found to be a function of the amount of energy in the critical 20 to 60 Hz band. The 8 road surfaces which were each characterised by significant vibration energy in the 20 to 60 Hz band, and whose correct detection was found in chapter 6 of this thesis to depend critically on the 20 to 60 Hz band, all improved significantly when the steering vibration signal was optimised using the steering vibration feedback guidelines. The two road surfaces which contained little energy in the 20 to 60 Hz band, i.e. the noise surface and the motorway surface, both suffered degradation in detection due to the feedback guidelines only being applied to the critical 20 to 60 Hz band. For these two road surfaces, the critical 20 to 60 Hz band actually seems to contain little vibration energy and little useful information. Manipulation therefore appears to have complicated the detection task rather than simplify it. Extending the steering vibration feedback guidelines to the complete frequency range from 0 to 80 Hz would be expected to produce improvements in detection for all ten of the road surfaces.

10. Conclusions and Recommendations for Future Research

10.1 Summary of the Research Findings

The experimental activities described from chapter 5 to chapter 9 of this thesis were performed in order to answer questions about the human ability to detect road surface type based on steering wheel vibration and to use the findings to define a simple first set of perception enhancement guidelines could be assembled for use with the automotive steering. This chapter summarises the main findings and attempts to provide an answer to the objectives posed in the Chapter 1 in light of the experimental results.

- **The Issue of Steering Wheel Acceleration Magnitude.**

The effect that has the steering wheel acceleration magnitude of road surface road surface stimuli on the human ability to detect road surface type suggests that road detection is not strictly optimal at the natural vibration magnitude encountered in automobiles and that a single, fixed, feedback gain from the automobile to the steering wheel will result optimal in only a small number of driving conditions. The optimum vibration magnitude for detection appeared to be related to the characteristics of the cognitive mechanism model which the test participant associated with the surface in question. This aspect of the detection problem may be of relevance to the designers of both traditional and by-wire steering systems since careful consideration appears to be necessary when choosing the target magnitude of steering feedback for each driving condition.

- **The Issue of Steering Wheel Acceleration Frequency Distribution.**

The effect that has the frequency bandwidth of road surface stimuli on the human ability to detect road surface type suggests that an average hit rate of more than 80% for stimuli with vibrational energy at frequency up to 60-80 Hz. In this experiment the road surfaces investigated had the same behaviour, an improvement with increasing in frequency bandwidth. This may be of relevance to the designers of automotive steering systems since the current frequency contents of most steering systems are under 40 Hz.

The effect that has the vibrational energy distribution of road surface stimuli on the human ability to detect road surface type suggests that the frequency range from approximately 20 Hz until 60 Hz played a key role in the human cognitive detection of the road surface type for all three surfaces. The results show some qualitative similarities to those obtained by the bandwidth experiment in which the elimination of the high frequency energy from the steering wheel vibration signal was found to have a detrimental effect on road surface type detection. The results suggest that the elimination of energy in the frequency range from 20 to 60 Hz can improve the detection of surfaces which are expected to have little energy at low frequencies, but that it is greatly detrimental for those road surfaces which have much of their vibrational energy at high frequencies. Given the resonance behaviours of the automobile in the 20 to 60 Hz frequency band, it may be the case that in current production automobiles this frequency band provides a focus and a principal source of driver perception.

The findings may be interpreted as suggesting that road surface, steering, chassis and suspension in the 20 to 80 Hz frequency interval provide vital clues to automobile drivers regarding the roads over which they drive and the dynamic response of the vehicle. Steering feel may be compromised by any reductions or elimination in vibrational energy at the steering wheel in this interval.

- **The Issue of Steering Wheel Acceleration Compression and Expansion.**

The effect that has the steering wheel acceleration compression and expansion on human detection of road type suggests that a single, optimal, compression factor of 0.90 exists which was valid for all three road surfaces when the stimuli were compressed above the ± 3 STD threshold level. The results suggest that the compression of the highest peaks works acceptably for all test stimuli investigated, increasing the detection rate. It may be

the case that the highest peaks which occur in a steering wheel acceleration time history act as masking for parts of the steering acceleration stimuli which are vital clues for an automobile driver. Based on the current results it may be the case that the cognitive mechanism used by human to perceive steering vibration is similar to those used to perceive music. Although this result is one of the main findings in this research, further investigation is required in order to better understand the parts of the stimuli which need to be compressed or expanded so as to improve the human detection.

- **The Issue of the individual transient events which are contained in the Steering Wheel Acceleration Stimuli.**

The effect of the transient events, in terms of number and size, which are contained in the steering wheel acceleration stimuli, suggests that the manipulation of both the number and the size of the transient events played a role in improving the human detection of road surface type in driving situations. Improvements in the correct detection rate occurred for all the road surfaces which were tested (in some cases of up to 20 percentage points) suggest the potential usefulness of controlling the transient events which are present in the steering vibration stimuli with which some driving scenarios can be clarified. The results suggest, however, that no single time compression ratio and no single bump scale factor might work for all the road surface types, and that each road surface requires specific control in the number and scale of transient events they contain. From the results of these experiments it would appear necessary, as future research, to cluster and classify individual transient events. Possibly there are individual transient events within the complete time history with similar characteristics (i.e. time duration, amplitude, wave shape) which carry the main part of the road surface information to the driver. The repetition and re-scaling of such events in the steering stimuli might achieve optimal results for all driving scenarios.

- **Confirmation of the first set of guidelines for automotive steering vibration feedback.**

The implementation of the most promising feedback settings which were found in the various individual tests performed in this research suggests that similarly to the findings in Chapter 6, the correct detection of road type is a function of the energy contained in the frequency band investigated. The road surfaces which were characterised by significant vibration energy in the key 20 to 60Hz band all improved significantly (in some cases of

up to 14 percentage points) in detection when the steering vibration signal was optimised using the steering vibration feedback guidelines. While for the road surfaces which were characterised by little vibration energy in the key 20 to 60Hz band suffered reduced detection due to the feedback guidelines only being applied to the critical 20 to 60 Hz band. Extending the steering vibration feedback guidelines to the complete frequency range from 0 to 80 Hz might be expected to produce improvements in detection for all driving scenarios.

10.2 Research Limitations and Sources of Error

As with all research, there are limitations and sources of error which should be considered, the following is a discussion of some of the main issues:

- The first significant limitation was due to the lack of scientific literature concerning the human cognitive detection in vibrational scenarios, which made this study a real challenge. The fact of being one of the first studies to evaluate the human cognitive detection of road surfaces based on the feedback vibrations provided by the automobile steering wheel gives the opportunity to be the first to state the first findings in this field, but it also leads to difficulties in stimulus selection, protocol selection, and statistical analysis due to the lack of analogous studies. While logical motivations were applied to all test signal and protocol decisions during the course of the research, there are few studies in the literature which can be used to substantiate the choices which were made (Giacomin and Woo, 2004; Giacomin, 2005).
- The number and selection of the steering vibration stimuli used to perform the experimental test activities of the thesis (described in the Chapter 4) can be considered a research limitation. The author knows that there are several factors which cause a change in the dynamics of the automobile, consequently there are several factors which also cause changes in the steering wheel stimuli. Among them could be included:
 - the type of the automobile (i.e. sport, luxury, compact, lorry);
 - the type of engine (i.e. diesel, gasoline);
 - the suspension type;
 - the tyres pressure,
 - the driving speeds,

- the type of road surface,
- the environmental conditions, etc.

While this research attempted to achieve the most common driving conditions possible, a limitation of the present study is that the evaluation of the human detection of road type was performed using steering wheel stimuli obtained when only three different automobiles were driven over ten different road surfaces, at only one single speed for each driving condition. Since the purpose of the research was to identify any universally beneficial steering vibration transformations, the limitation of using only ten road surfaces and three automobiles may be a factor which must be considered when assessing the results. When a perception enhancement system (PES) for an automobile steering system can be defined, it should satisfy all driving conditions.

- When the findings of a study are based on laboratory experimental tests where humans are the test subjects, many questions emerge in the search of any source of error which might affect the results and consequently the findings of the research. This thesis has treated systematically the sources of error inherent in the various laboratory-based experiments such as: the calibration of the test facilities, the accuracy of the test stimuli reproduction and the test protocol employed during the test activity, which includes: instructions given to the participant, posture of the participant during the test, the number of repetitions of the test stimuli, the duration of each test stimulus, the way to judge each test stimulus and the environmental conditions. A significant effort was made to achieve the greatest possible repeatability in these parameters, thus the results should be considered reliable.

The fact of isolating the real context of the driving experience can be considered a source of error and a limitation of the research. However, the use of a real driving scenario to evaluate the steering wheel vibration can produce results influenced much more by other human senses (i.e. sight and auditory senses) instead of the sense of touch which is the aim of the current study. The author knows that in the environment of driving a real car each of the human senses is interlinked and can affect each other in the perception of what is see, hear or feel. Nevertheless, the isolation of the steering wheel vibration in this research was necessary in order to determine more clearly how

much information of the steering feel is store in the human memory and which are the features carrying the main part of the road surface information to the driver.

- The laboratory-based experiments in this research employed fifteen human test subjects. A natural question which arises is whether or not fifteen participants are enough to achieve the needed scientific accuracy. From the research literature available in the fields of whole-body vibration and hand-arm vibration, there is no study in which has been defined the number of test participants considered as satisfactory. Most of the studies performed in these fields to date represent the average responses of from least 6 to 15 test subjects. In the human whole-body vibration literature, Mansfield and Griffin (2000) investigated the effect of vibration magnitude on both the apparent mass of the seated body and the transmission of vibration to locations on the abdominal wall, the lumbar spine and the pelvis in which 12 male participants were exposure to whole-body vertical vibration. In the hand-arm transmitted vibration literature, Miwa (1967) established equal sensation curves for 10 male participants who held their palm flat against a plate which was vibrated sinusoidally in either the vertical or horizontal direction, while Morioka and Griffin (2006) established a family of equal sensation curves for 12 male participants who gripped with one hand a cylindrical handle which was vibrated sinusoidally in either the vertical, axial or horizontal directions. With respect to automotive steering vibration Giacomini et al. (2004) established equal sensation curves for 15 participants (10 males and 5 females) who held a rigid sinusoidally rotating steering wheel with both hands.

10.3 Suggested Future Research

Although an extensive number of test experiments were described in this research work, further investigation and test experiments are required in order to define the system specifications for a steering perception enhancement system for automobiles. A few important areas in which further research would be beneficial are listed below:

A selection of individual transient events. Individual transient events in the vibration time history appear to be an important source of information to the driver, and further research could attempt to categorise and classify these extracted events and to evaluate their effect on human cognitive response they produce. In order to achieve the possibility

of evaluating the information content of the vibration stimuli occurring in road vehicles, a number of measures could be developed to assess the informativeness of the transient events. These measures will be used as a criterion for transient event selection. The information theory (Shannon, 1959) assesses the information content of random variables and can be used as a criterion for event selection (see Figure 10.1). This information can be measured by the entropy calculation, which is estimated in terms of probability events. The results should provide a rudimentary “language” of automobile-driver communication.

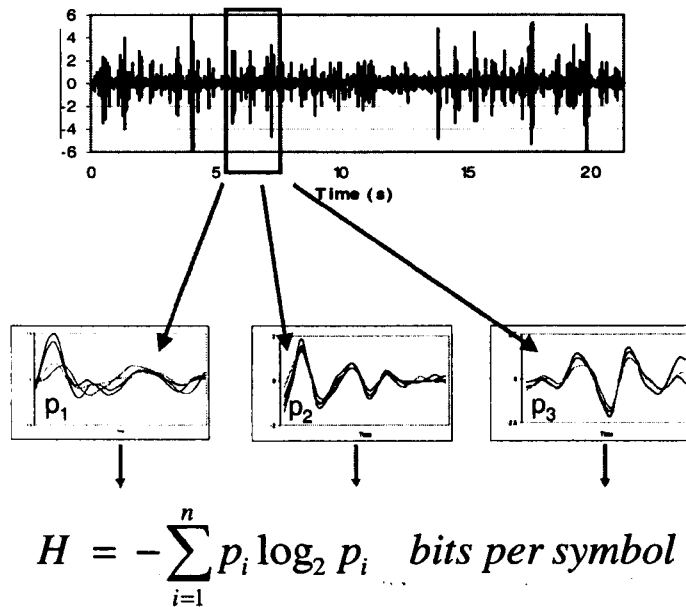


Figure 10.1 A possible basis for an automotive steering PES is an *Information Entropy* measure which is used in conjunction with a library of road features.

Performing of experimental tests using road surfaces which produce transient or impulsive input to the automobile. Most of the road surfaces employed in the studies described in this thesis are of type which produce a nearly stationary vibrational input to the automobile. However, there are still many driving scenarios which require to be studied, such as: bump events, cat eyes, joints, strips, harsh events, stone-on-the road, etc. Although, the shock events presented in these types of surfaces seem to be easily detected by the common driver, as it was reported in the results of the low bump surface (Chapter 5) either increasing or decreasing the magnitude level of the stimuli, the evaluation of the human cognitive detection of road surface which produce impulsive input to the automobile is still needed.

References

- Abdullah, S., Giacomini, J.A. and Yates, J.R., 2004. A mission synthesis algorithm for fatigue damage analysis, Proceedings of the IMechE, Part D - Journal of Automobile Engineering, Vol. 218, pp 243-258.
- Ajvalasit, M. and Giacomini, J. 2005, Human subjective response to steering wheel vibration caused by diesel engine idle, Proceedings of the IMechE, Part D - Journal of Automobile Engineering, Vol 219, No. 4, pp 499-510.
- Amman, S., Pielemeier, B., Snyder, D. and Toting, F., 2001. Road vibration investigation using the Ford vehicle vibration simulator. SAE Paper 2001-01-1572.
- Anders E., K. and Kintsch, W., 2002. Long-Term Working Memory. <http://www.ecs.soton.ac.uk/~harnad/Papers/Py104/ericsson.long.html>.
- Anderson, J. R., 1980. Cognitive psychology and its implications. San Francisco: W.H. Freeman, 1980.
- ASTM E1364 - 95(2005) Standard Test Method for Measuring Road Roughness by Static Level Method.
- Atkinson, R. C. and Shiffrin, R. M., 1968. Human memory: A proposed system and its control processes. In press on the psychology of learning and motivation: Advances in research and theory. New York: Academic Press, by K.W. Spence.
- Baddeley, A. D., 1986. Working memory. New York: Oxford University Press.
- Baddeley, A. D., 2002. Is Working Memory Still Working? European Psychologist, Vol. 7, No. 2, June, p. 85-97.
- Baird, J. C. and Noma, E., 1978. Fundamentals of Scaling and Psychophysics. Wiley Series in Behaviour.
- Bannister, F. and Remenyi, D., 1999. Instinct and Value in IT Investment Decisions. Occasional Paper Series, University of Wolverhampton.

- Bendat, J. S. and Piersol, A. G., 1986. Random data: analysis and measurement procedures. 2nd ed. New York: John Wiley and Sons, Inc.
- Bianchini, E., 2005. Active Vibration Control of Automotive Steering Wheels, Society of Automotive Engineers, SAE 2005-01-2546.
- Bregman, A. S., 1999. Auditory Scene Analysis: The Perceptual Organization of Sound. MIT Press.
- Bretz, E. A., 2001. By-Wire Cars Turn the Corner. IEEE Spectrum, April 2001. http://lees.mit.edu/public/In_the_News/By-Wire+Cars.pdf.
- British Standards Institution, BS EN 6842, 1987. Measurement and evaluation of human exposure to vibration transmitted to the hand. British Standards Institution, London.
- British Standards Institution, BS EN 7085, 2001. Safety aspects of experiments in which people are exposed to mechanical vibration and shock. London.
- British Standards Institution, BS EN 590, 2005. Human response to vibration - Measuring instrumentation. London.
- British Standards Institution, BS EN 13108-21, 2006. Bituminous mixtures. Material specifications. Factory production control.
- Bosch Automotive Handbook, 2004. 6th Edition, Plochingen: Robert Bosch GmbH.
- Brown, J., 1958. Some test of the decay theory of immediate memory. Quarterly Journal of Experimental Psychology, 10, 12-21.
- Buchanan, J. and Kock, N. 2000. Information overload: A decision making perspective. Proceedings of Multiple Criteria Decision Making 2000, Ankara.
- Bruscella, B., Rouillard, V., and Sek, M. A., 1999. Analysis of road profiles. J. Transp. Engrg., ASCE, 125(1): 55-59.
- Chui, C. K., 1992. Introduction to wavelets, Academic Press, New York USA.
- Costa, M., Enrietti, L. and Pasero, E., 1997. Application of data driven techniques to the prediction of seat comfort performance. <http://www.neuronica.polito.it/pub/ata97.pdf>.
- Darley, J. M., and Gross, P. H., 1983. A hypothesis-confirming bias in labeling effects. Journal of Personality and Social Psychology, 44: p. 20-33.
- Daubechies, I., *Ten Lectures on Wavelets*, SIAM, Philadelphia USA, 1992.
- De Carlo, L. T., 2003. Source monitoring and multivariate signal detection theory, with a model for selection. Journal of Mathematical Psychology 47: 292-303.
- Department of Transport, 2006. Speed Leaflet 2006. <http://www.dft.gov.uk>.

- Dodds, C. J. and Robson, J. D. (1973). The description of road surface roughness. *The Journal of Sound and Vibration*, Vol. 31, No. 2, pp. 175-183.
- Dror, I.E., 2005. Perception is far from perfection: The role of the brain and mind in constructing realities. *Brain and Behavioural Sciences* 28 (6): 763.
- Dror, I. E. and Dascal, M., 1997. Can Wittgenstein help free the mind from rules? The philosophical foundations of connectionism. In D. Johnson & C. Erneling Eds., *The Future of the Cognitive Revolution*, p. 217-226. Oxford University Press.
- Duhaime, I. M. and Schwenk, C. R., 1985. Conjectures on cognitive simplification in acquisition and divestment decision making. *Academy of Management. The Academy of Management Review* (pre-1986). vol. 10(2): p. 287-295.
- Eargle, J. M., 1995. *Music, Sound, and Technology*. Second Ed., International Thomson Publishing, Inc.
- Entran Devices Limited, 1991. *MSC Series Multi-channel Conditioning Unit. Instruction Manual*. Watford.
- Erdreich, J., 1986. A distribution based definition of impulse noise. *J. Acoust. Soc. Am.* 79(4): p. 990-998.
- Exarchos, T. P., Tzallas, A. T., Fotiadis, D. I., Konitsiotis, S. and Giannopoulos, S., 2006. EEG Transient Event Detection and Classification Using Association Rules. *IEEE Transactions on information technology in biomedicine*, Vol. 10, No. 3, July.
- Festinger, L. and Carlsmith, J. M. , 1959. Cognitive consequences of forced compliance. *Journal of Abnormal and Social Psychology*, 58: 203-210. In *Classics in the History of Psychology*, by Green, C. D. <http://psychclassics.yorku.ca/Festinger/>.
- Fujinami, H., Yamamoto, M. and Hisaoka, Y., 1995. Vehicle Response and Drivers' Feeling. *JSAE Technical Paper No. 9534379*
- Garner, W. R., 1962. *Uncertainty and structure as psychological concepts*. New York: Wiley.
- Gescheider, A. G., 1997. *Psychophysics The Fundamentals*, 3rd. edition, Lawrence Erlbaum Associates Publishers, London.
- Giacomin, J. 2005. Perception Enhancement for Steer-by-Wire Systems, *ATA. Ingegneria dell'Autoveicolo*, Vol. 58, No. 8/9, Sept./Oct.
- Giacomin, J. and Abrahams, O. 2000, Human fatigue due to automobile steering wheel vibration, *SIA Conference on Car and Train Comfort*, Nov. 15-16, LeMans, France
- Giacomin, J. and Gnanasekaran, S., 2005. Driver estimation of steering wheel vibration intensity: questionnaire-based survey. *Journal of the Engineering Integrity Society*. 18: p. 23-29.

- Giacomin and Lo Faso, 1993. Vibration survey of the Fiat Tempra and Fiat tipo. Fiat Report.
- Giacomin and Masoero, 1993. Advanced technologies for automotive seat evaluation and design (SED). Fiat Report.
- Giacomin, J. and Woo, Y.J., 2004. Beyond comfort: information content and perception. *Engineering Integrity*, Vol. 16, July, pp 8-16.
- Giacomin, J., Shayaa, M.S., Dormegnie, E. and Richard, L., 2004, Frequency weighting for the evaluation of steering wheel rotational vibration, *International Journal of Industrial Ergonomics*, Vol. 33, pp 527-541.
- Giacomin, J., Steinwolf, A. and Staszewski, W.J., 1999. A vibration mission synthesis algorithm for mildly non stationary road data, ATA 6th Int. Conf. on the New Role of Experimentation in the Modern Automotive Product Development Process, Florence, Italy.
- Gibson, E. J., 1969. Principles of perceptual learning and development. New York: Appleton-Century-Crofts.
- Gibson, J. J. and Gibson, E. J., 1955. Perceptual Learning: Differentiation or Enrichment? *Psychological Review* 62: 32-41.
- Gillespie, T. D., 1992. Fundamentals of vehicle dynamics. S.A.E. International, Warrendale Pennsylvania.
- Gillespie, T. D. and Sayers, M. W., 1983. Measuring Road Roughness and Its Effects on User Cost and Comfort: A Symposium, Papers presented at the symposium on Roughness Methodology, which was held on 7 Dec. 1983 in Bal Harbour, Florida. ASTM International.
- Grainger, J. J., 2001. Application of Mildly Nonstationary Mission Synthesis (MNMS) to Maserati Wheel Hub Road Data, M.Eng Dissertation, The University of Sheffield, United Kingdom.
- Green, D. M. and Swets, J. A., 1966. Signal detection theory and psychophysics, reprint edition. Los Altos, CA: Peninsula Publishing.
- Griffin, M. J. Handbook of Human Vibration. London: Academic, 1990.
- Hacaambwa, T. M. and Giacomin, J. 2005, Subjective response to seated fore-and-aft direction whole-body vibration, Accepted for publication by the *International Journal of Industrial Ergonomics*.
- Hamilton, D., 2000. Frequency domain considerations in vehicle design for optimal structural feel. SAE TECHNICAL PAPER SERIES 2000-01-1344
- Hamming, R.W., 1989. Digital filters. Third Ed., Prentice Hall International (UK) Ltd.

- Harris, R. W. and Ledwidge, T. J., 1974. Introduction to noise analysis. Pion Limited, London.
- Harrison, M., 2004. Vehicle Refinement, Controlling Noise and Vibration in Road Vehicles. Elsevier Butterworth-Heinemann.
- Heeger, D., 2003. Signal Detection Theory. <http://www.cns.nyu.edu/~david/sdt/sdt.html>.
- Hodges, C. H., Power, J. and Woodhouse, J., 1985. The use of sonogram in structural acoustics and an application to the vibrations of cylindrical shells. *Journal of Sound and Vibration*. 101: p. 203-218.
- Hubbard, B. B., 1996. *The World According to Wavelets*, A K Peters, Massachusetts.
- Huber, D. M. and Runstein, R. E., 2005. *Modern Recordings Techniques*. 6th Ed, Elsevier, Focal Press.
- Iles-Klumpner, D., Risticvic, M., Hartkorn, H. W., Lahm, G., Serban, I. and Boldea, I., 2005. Electric Actuation Technologies for Automotive Steering Systems, SAE TECHNICAL PAPER SERIES, 2005-01-1275.
- International Organization for Standardization, ISO5349-1, 2001. Mechanical Vibration - Measurement and assessment of human exposure to hand-transmitted vibration - Part 1: General guidelines, Geneva.
- International Organization for Standardization, ISO8041, 2005. Human response to vibration - Measuring instrumentation, Geneva.
- Isomura, A., Hara, T. and Kmiya, K. 1995, Human factors on driver's steering wheel operation: three parameters evaluating characteristics of driver's steering wheel operations, *JSAE Review*, Vol. 16, pp 388-410.
- Izotope, 2004. <http://www.izotope.com.html>
- Jurgen, R. K., 1999. *Electronic Steering and Suspensions Systems*, S.A.E. International, Warrendale Pennsylvania.
- Katz, R. A., 2002. *Mastering Audio: The Art and the Science*. 2nd Ed., Focal Press, 2002
- Kosslyn, S. M., Alpert, N. M., Thompson, W. L., Chabris, C. F., Rauch, S. L. and Anderson, A. K., 1994. Identifying objects seen from different viewpoints: A PET investigation. *Brain* 117: p. 1055-1071.
- Kudritzki, D. K., 2001. Road Tests Adopted to Analyse Cars' Vibrational Behaviour. SAE TECHNICAL PAPER SERIES 2001-01-1098.
- Kulkarni, K. B. and Thyagarajan, R. S., 2001. Optimizing the effects of body attachment stiffness on steering column in- vehicle modes. SAE TECHNICAL PAPER SERIES 2001-01-0041.

- Lapsley Miller, 1999. The role of bandwidth-duration product in the detectability of diotic signals. PhD thesis, Victoria University of Wellington, New Zealand
- Lawson, J. L., and Uhlenbeck, G. E., 1950. Threshold Signals, Vol. 24 of Radiation Laboratory Series McGraw-Hill, New York.
- Lee, S. I., 1998. Human sensitivity responses to vibrotactile stimulation on the hand: measurement of absolute thresholds. *J. Ergonomics Soc. South Korea*, 17(2), 1-10.
- Lee, S. K. and White, P. R., 2000. Application of wavelet analysis to the impact harshness of a vehicle. Proc. Instn. Mech Engrs, Vol 214 Part C.
- Li, D., Magnuson, D. S. K. and Jung, R., 2000. Application of wavelet analysis to the impact harshness of a vehicle. Proc. Inst. Mech. Engrs Part C. 214: p. 1331-1338.
- Lim, T. C. and Witer, A. J., 2000. Experimental characterization of engine crankshaft rumble noise signatures. *Applied acoustics*. 60: p. 45-62.
- LMS International, 2002. LMS Cada-X Fourier Monitor Manual. Revision 3.5E. Leuvan.
- Loomis, J. M. and Lederman, S. J., 1996. Tactual perception. *Handbook of Human Perception and Performance*, Wiley, NY.
- Lyons, R. G., 2004. Understanding digital signal processing. Second Ed., Prentice Hall, Pearson Education, Inc.
- Mallat, S., 1998. A wavelet tour of signal processing. London; San Diego: Academic Press.
- Macmillan, N. A. and Creelman, C. D., 2005. Detection Theory: A user's guide. Second Ed. Lawrence Erlbaum Associates, Inc.
- McClellan, J. H., Schafer, R.W. and Yoder, M., 2003. A Signal Processing First. Pearson Prentice Hall.
- McHutchon, M. A., Staszewski, W. J. and Schmid, F., 2005. Signal Processing for Remote Condition Monitoring of Railway Points. Blackwell Publising, Ltd., Strain 41, 71-85.
- McMahon, F. B., and McMahon, J. W., 1982. Psychology: The hybrid science, 4th Ed., Homewood, IL: The Dorsey Press.
- Meyer, Y., 1993. Wavelets: Algorithm and Applications, SIAM, Philladelphia USA.
- Miller, G. A., 1956. The magical number seven, plus or minus two: Some limits of our capacity for processing information. *Psychological Review*, 63, 81-97.
- Miller, G. A., Galanter, E., and Pribram, K. H., 1960. Plans and the structure of behavior. New York: Holt, Rinehart & Winston.

- Miller, G., 2006. The emotional brain weighs its options. *Science*, 313: 599-600.
- MIRA Ltd, 2006. <http://www.mira.co.uk/Facilities/TestFacilitiesProvingGround.htm>
- Mitchel, T. M., 1997. *Machine Learning*. Mc Graw-Hill International Editions.
- Miyake, A. and Shah, P., 1999. *Models of working memory: mechanisms of active maintenance and executive control*. Cambridge: Cambridge University Press, c1999
- Miwa, T. 1967, Evaluation methods for vibration effect, Part 3: Measurements of threshold and equal sensation contours on hand for vertical and horizontal sinusoidal vibrations, *Industrial Health*, Vol. 5, pp 213-220.
- Moore, B. C. J. and Patterson, R. D., 1986. *Auditory frequency selectivity*, NATO-ASI Series. Plenum, New York.
- Morioka, M., 1999. Effect of contact location on vibration perception thresholds in the glabrous skin of the human hand. In *Proceedings of 34th UK Group Meeting on Human Responses to Vibration*, 22–24 September (Ford Motor Company, Dunton, Essex).
- Mishoe, J. W. and Suggs, C. W., 1977. Hand-Arms Vibration Part II: Vibration Responses of The Human Hand. *Journal of Sound and Vibration* 53(4), 545-558.
- Newell, A., 1990. *Unified Theories of Cognition*, Harvard University Press.
- Newell, A., and Simon, H. A., 1972. *Human problem solving*. Englewood Cliffs, NJ: Prentice Hall.
- Newland, D. E., 1993. *Random vibrations, spectral and wavelet analysis*. Third edition, Longman Scientific and Technical, England.
- Norman, D. A., 1970. Introduction: Models of Human Memory. In D. A. Norman (Ed.), *Models of Human Memory* p. 1-15. New York: Academic Press.
- OICA, 2007. *World Motor Vehicle Production: World Ranking of Manufacturers 2007*. <http://oica.net/wp-content/uploads/world-ranking-2007.pdf>.
- Oikonomoua, V. P., Tzallas, A.T. and Fotiadis, D. I., 2007. A Kalman filter based methodology for EEG spike enhancement. *Computer methods and programs in biomedicine* 85: 101–108.
- Orasanu, J. and Martin, L., 1998. *Errors in Aviation Decision Making: A Factor in Accidents and Incidents*. NASA-Ames Research Center. HESSD '98.
- Oxford English Dictionary, 2000. *Oxford Advanced Learner's Dictionary Sixth edition*. Oxford: Oxford University Press.
- Palmer, J., 1994. Set-Size Effects in Visual Search: the Effect of Attention is Independent of the Stimulus for Simple Tasks. *Vision Res.* Vol. 34, No. 13: p. 1703-1721.

- Pak, C.H., Lee, U.S, Hong, S.C., Song, S.K., Kim, J.H and Kim, K.S, 1991. A study on the tangential vibration of the steering wheel of passenger car. *SAE Technical Paper Series*, Paper 912565, 961-968.
- Peruzzetto, P., 1988. Assessing the relative importance of hand vibration with respect to whole-body vibration. In United Kingdom and French joint Meeting on Human Response to Vibration. I.N.R.S., Vandoeuvre, France, 26-28 September, p. 1-11.
- Peterson, L. R., and Peterson, M. J., 1959. Short-term retention of individual items. *Journal of Experimental Psychology*, 58, 193-198.
- Peterson, W. W., Birdsall, T. G., and Fox, W. C., 1954. The theory of signal detectability. *Trans I.R.E.*, p. 171-212.
- Peebles, P. Z. Jr., 1993. *Probability, Random Variables, and Random Signal Principles*. McGraw-Hill International Editions, Third Ed.
- Piersol, A. G., 1992. Data Analysis:, in *Noise and Vibration Control Engineering: Principles and Applications*, L.L.a.V. Bernarek, I.L., Editor. John Wiley & Sons, Inc.: New York, chapter 3, p. 45-73.
- Plomp, R. and Levelt, W. J. M., 1965. Tonal consonance and critical bandwidth. *Journal of the Acoustical Society of America*, Vol. 38, p. 548-560.
- Pottinger, M.G. and Marshall, K.D., 1986. A Review of Tire/Pavement Interaction Induced Noise and Vibration, in the Tire Pavement Interface, ASTP STP 929, M.G. Pottinger and T.J. Yager, Editors. American Society for Testing and Materials: Philadelphia, p. 183-287.
- Priestley, M. B., 1988. *Non-linear and non-stationary time series analysis*. London: Academic Press, 1988.
- Quek, F. and Petro, M., Human-Machine Perceptual Cooperation, 1993. *Proceedings of the International Conference on Computer-Human Interaction INTERCHI'93: Human Factors in Computing Systems*, 123-130.
- Quehl, J., 2001. *Comfort studies on aircraft interior sound and vibration*. PhD Thesis, University of Oldenburg, Germany.
- Rahnejat, H., 1998. *Multi-body Dynamics: Vehicle, Machines and mechanisms*. Bury St Edmunds, UK: Professional Engineering Publishing Limited.
- Reynolds, D.D. and Soedel, W. 1972. Dynamic response of hand-arm system to sinusoidal input, *Journal of Sound and Vibration*, Vol. 21, No. 21, pp 339-352
- Reynolds, D. D. and Angevine, E. N. 1977. Hand-arm vibration, Part 2: Vibration transmission characteristics of the hand and arm, *Journal of Sound and Vibration*, Vol. 51, No. 2, pp 255-265.

- Reynolds, D.D. and Keith, R.H. 1977. Hand-arm vibration, Part 1: Analytical model of the vibration response characteristics of the hand, *Journal of Sound and Vibration*, Vol. 51, No. 2, pp 237-253.
- Roco, M.C. and Bainbridge, W.S., 2002. *Converging Technologies for Improving Human Performance: Nanotechnology, Biotechnology, Information Technology, and Cognitive Science (NBIC)*. NSF/DOC-sponsored report, 1-27.
- Russo, J. E., Meloy, M. G. and Medvec, V. H., 1998. Predecisional distortion of product information. *Journal of Marketing Research*, vol. 35(4): p. 438-451.
- Rouillard, V., Sek, M. A., and Bruscella, B., 2000. Classification of road surface profiles. *J. Transp. Engrg., ASCE*, 126(1): 41-45.
- Rouillard, V. and Sek, M. A., 2002. A statistical model for longitudinal road topography. *Road and Transport Research*, Vol. 11, No 3.
- Schoeggel, P. and Ramschak, E., 2000. Vehicle Driveability Assessment using Neural Networks for development, calibration and quality tests. SAE TECHNICAL PAPER SERIES 2000-01-0702.
- Shiffrin, R. M., and Schneider, W., 1977. Controlled and automatic human information processing: II. Perceptual learning, automatic attending, and a general theory. *Psychological Review*, 84, 127-190.
- Simon, H. A., 1957. *The Administrative Behavior*. New York: Free Press.
- Simon, H. A., 1957. *Models of Man*. New York: Wiley.
- Simon, H. A., 1967. Theories of decision-making in economics and behavioural science. In Alexis, M. and Wilson, C. Z., *Organizational Decision Making*, Prentice-Hall, New Jersey, p. 201-219.
- Simon, H. A., 1974. How big is a chunk? *Science*, 183, 482-488.
- Simon, H. A., 1979. Information processing models of cognition. *Annual Review of Psychology*, 30, 363-396.
- Simon, H. A. 1987. Making management decisions: The role of intuition and emotion. *The Academy of Management Executive*, vol. 1, no. 1, p. 57-63.
- Society of Automobile Engineers, 1974. *Vehicle Dynamics Terminology*. SAE J670e. Warrendale, PA.
- Steinwolf, A., Giacomini, J. and Staszewski, W.J., 2002. On the need for bump event correction in vibration test profiles representing road excitations in automobiles, *Proc. of the Instn. of Mech. Engrs, Part D, Journal of Automobile Engineering*, 216, D4, pp. 279-295.
- Staszewski, W. J., and Tomlinson, G., 1994. Application of the wavelet transform to fault detection in a spur gear. *Mechanical Systems and Signal Processing*, 8, 289± 307.

Staszewski, W. J., Worden, K., and Tomlinson, G., 1997. Time-frequency analysis in gearbox fault detection using wigner-ville distribution and pattern recognition. *Mechanical Systems and Signal Processing*, 11, 673± 692.

Staszewski, W. J., 1998a. Identification of non-linear systems using multi-scale ridges and skeletons of the wavelet transform, *Journal of Sound and Vibration*, 214(4): p. 639-658.

Staszewski, W. J., 1998b. Wavelet based compression and feature selection for vibration analysis. *Journal of Sound and Vibration*, 211(5): p. 735-760.

Stokes, A. F., Kemper, K. L. and Marsh, R., 1992. Time-stressed flight decision making: A study of expert and novice aviators (Tech. Rep. No. 4). Arlington, VA: Office of Naval Research.

Strum, R. D. and Kirk, D. E., 1988. *First Principles of Discrete Systems and digital signal processing*. Addison-Wesley Series.

Sugiyama, A., Kurishige, M., Hamada, H. and Kifuku, T., 2006. An EPS Control Strategy to Reduce Steering Vibration Associated with Disturbance from Road Wheels. SAE TECHNICAL PAPER SERIES 2006-01-1178.

Swets, J. A., 1973. The relative operating characteristic in psychology. *Science* 182: p. 990–1000.

Tanner, W. P. and Swets, J. A., 1954. A decision-making theory of visual detection. *Psychological Review*, 61: 401-409.

Tacer, B. and Loughlin, P.J., Nonstationary signal classification using the joint moments of time-frequency distributions, *Pattern Recognition*, 1998, 31, 11, pp. 1635-1641.

Turkle, S., 2002. Sociable technologies: enhancing human performance when the computer is not a tool but a companion. NSF/DOC-sponsored report, 122-140.

Tulving, E., 1972. Episodic and semantic memory. In: Tulving E., Donaldson W., eds. *Organization of Memory*. New York: Academic Press 1972.

Tzallas, A. T., Katsis, C. D., Karvelis, P. S., Fotiadis, D. I., Konitsiotis, S. and Giannopoulos, S., 2004. Classification of transient events in EEG recordings. Proceedings of the 2nd International Conference on Advances in Biomedical Signal and Information Processing. IEE 2004.

Ueki, N., Kubo, J., Takayama, T., Kanari, I. and Uchiyama, M., 2004. Vehicle Dynamics Electric Control Systems for Safe Driving. http://www.hitachi.com/ICSFiles/afiedfile/2004/11/26/r2004_04_104_3.pdf.

Verhoeff, L., Verschuren, R. and Zuurbier, J., 2004. Tire Force Estimation for Improved Steering Feel in EPAS and Steer - By -Wire. SAE TECHNICAL PAPER SERIES, 2004-05-0157.

- Vogel, W., 1965. Distribution of wavelengths and heights of various road surfaces. *Automobile Technische Zeitschrift*, Vol. 67, pp. 7-11.
- Wang, M., Zhang, N., and Misra, A., 2005. Sensitivity of Key Parameters to Dynamics of Hydraulic Power Steering Systems. *SAE TECHNICAL PAPER SERIES*, 2005-01-2389
- Wang, W., and Mc Fadden, P., 1995, Application of orthogonal wavelets to early gear damage detection. *Mechanical Systems and Signal Processing*, 9, 497± 507.
- Ward, D. and Woodgate, R., 2004. Meeting the challenge of drive-by-wire electronics, *Aerosystems International*. <http://mira.atalink.co.uk/articles/104>.
- Webster's New World Medical Dictionary, 2006. WebMD, Second Ed., JW. Wiley.
- Wright, J. K., 1986. Auditory Object Perception: Counterpoint in a New Context. McGill University, Master's thesis.
- Wright, P., 1974. The harassed decision maker: Time pressures, distractions, and the use of evidence. *Journal of Applied Psychology*, 59, 555-561.
- Wolfgang P., W. H., Gerhard R., P. D., and Blessing, P., 2000. Future Electrical Steering Systems: Realizations with Safety Requirements, *SAE TECHNICAL PAPER SERIES*, 2000-01-0822.
- Wong, T., 2001. Hydraulic Power Steering System Design and Optimization Simulation, *SAE TECHNICAL PAPER SERIES*, 2001-01-0479.
- Yonelinas, A. P., Dobbins, I., Szymanski, M. D., Dhaliwal, H. S. and King, L., 1996. Signal-Detection, Threshold, and Dual-Process Models of Recognition Memory: ROCs and Conscious Recollection. *Consciousness and Cognition* 5: 418-441.

APPENDIX A

Technical Specifications of Test Equipment

A.1 Technical Specifications of the equipment used to measure the steering wheel vibration for the Uxbridge test.

The technical specifications of the SVAN 947 Sound and Vibration Level Meter and Analyser manufactured by SVANTEK Ltd. are presented in Figures A.1 and A.2. The technical specifications of the Low Impedance Voltage Mode (LIVT™) accelerometer *3055B1* are presented in Figures A.3 and A.4.

SVAN 947 Sound & Vibration Analyser

The SVAN 947 is all digital, Type 1 sound level & vibration meter and analyser. It is intended for general acoustic measurements, environmental noise monitoring, occupational health and safety monitoring.

Three acoustic or vibration profiles can be measured in parallel with independently defined filters and RMS detector time constants (e.g. concurrent Impulse, Fast and Slow measurements are possible).

All required weighting filters (e.g.: A, C, W-Bxy, W-Bz or H-A) including the latest ISO 2631-1 standard are available with this instrument. RMQ detector enables direct measurement of the Vibration Dose Value.

The SVAN 947, using computational power of its digital signal processor, can perform real time 1/1 & 1/3 octave analysis including statistical calculations.

The high resolution FFT and pure tone detection options further extend the capabilities of this unit.

Fast USB 1.1 interface (with 12 MHz clock) creates real time link for the application of the SVAN 947 as a PC front-end.

Measurement results can be stored in large (8, 16 or 32 MB), non-volatile memory and easily downloaded to any PC using USB 1.1 or RS 232 interface and SvanPC software.

The SVAN 947 can be used in hard environmental conditions over the whole work day thanks to built-in rechargeable battery and robust, lightweight construction.

FEATURES

Sound Level Meter & Analyser

- noise measurements (Spl, Leq, SEL, Lden, TaktMax and statistics) with Type 1 accuracy
- parallel Impulse, Fast and Slow detectors for the measurements with A, C or Lin filters
- one measurement range 24 dB_A RMS - 140 dB_A PEAK in the SLM mode
- 1/1 and 1/3 octave real time analysis parallel to the SLM operation (optional)
- FFT calculation (1920 lines in real time up to 22.4 kHz) spectra parallel to the SLM operation (optional)

Vibration Meter & Analyser

- vibration measurements according to ISO 2631-1 with Type 1 accuracy (ISO 8041)
- parallel Peak, RMS (incl. MTVV) and RMQ (incl. VDV) measurements
- 1/1 and 1/3 octave real time analysis (optional)
- FFT calculation (1920 lines in real time up to 22.4 kHz) spectra parallel to the SLM operation (optional)

General

- internal buffer for logging more than two weeks of 1 sec RMS / Max / Peak results (8, 16 or 32 MB of non-volatile memory)
- USB 1.1 and RS 232 interfaces
- built-in rechargeable battery (operational time > 8 h)
- handheld, robust case
- light weight (only ca 600 grams)

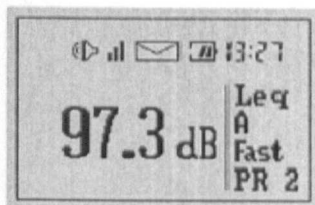


INSTRUMENTATION FOR SOUND & VIBRATION
MEASUREMENTS

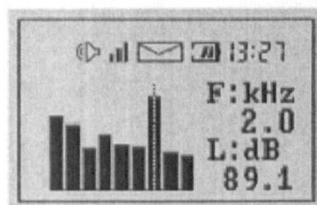
Figure A.1 SVAN 947 Sound and Vibration Level Meter and Analyser manufactured by SVANTEK Ltd. used for the experimental steering vibration measurements. Part I.

TECHNICAL SPECIFICATIONS

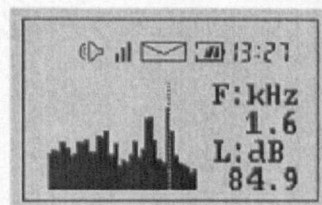
Sound Level Meter	Type 1: IEC 651, IEC 804 and IEC 61672-1 L _{eq} , L _{max} , L _{min} , L _{Peak} , Spl, SEL, Lden, L _{ms} , L _{ms} statistics; L _n (L ₁ -L ₉₉), Time History for all A, C, Lin (Z) filters in parallel
Vibration Meter	Type 1: ISO 8041 RMS, Peak, Max, Min, MTVV, VDV (RMQ), Time History
Sound & Vibration Analyser	Real time 1/1 & 1/3 octave (optional) analysis with statistics (spectra logging speed down to 2 ms), 1920-line FFT spectra calculated in the real time for 22.4 kHz and sub-bands with Hanning window (optional)
Input	TNC with IEPE power supply for the microphone preamplifier or accelerometer
Microphone Preamplifier Measurement Range	SV 12L From 22 dB _{A,RMS} (with 5 dB margin from noise) to 140 dB _{A,PEAK} or 0.1 ms ⁻² - 10000 ms ⁻² (with 3220B accelerometer)
Dynamic Range	120 dB (in the SLM mode), 100 dB (in the Vibration and Analyser mode), A/D conversion: 2 x 20 bits,
Frequency Range	10 Hz - 20 kHz for sound and 1 Hz - 20 kHz for vibration, sampling rate: 48 kHz
Weighting Filters	A, C and Lin (Type 1: IEC 651, IEC 804 and IEC 61672-1) and W-Bxy, W-Bz, W-Bc, H-A, W _k , W _c , W _d , W _j (ISO 8041 and ISO 2631-1)
1/1 Octave Filters	15 filters with centre frequencies 1 Hz - 16 kHz, Type 1- IEC 1260 (optional)
1/3 Octave Filters	45 filters with centre frequencies 0.8 Hz - 20 kHz, Type 1- IEC 1260 (optional)
RMS & RMQ Detectors	Digital True RMS & RMQ with Peak detection, resolution 0.1 dB, integration time programmable up to 24 h Time Constants: Slow, Fast, Impulse (in parallel) in SLM mode; from 100 ms to 10 s in the Vibration Meter mode (any three in parallel)
Microphone Accelerometer	SV 22 prepolarised 1/2" condenser microphone, sensitivity 50 mV/Pa 3220B (3.5 grams, 1 mV/ms ²) for the Hand Arm measurements; other IEPE accelerometers optional
Display	LCD 97x32 pixels plus icons with backlighting
Memory	8, 16 or 32 MB non-volatile (Flash type)
Analogue Output Interfaces	AC 0.5 V _{RMS} USB 1.1 and RS 232
Power Supply	Built-in rechargeable battery 4.8 V / 1.6 Ah External power supply 8 - 15 V _{DC} / 600 mA Internal battery operating time > 8 h
Environmental Conditions	Temperature from -10 °C to 50 °C Humidity up to 90 % RH, non condensed
Dimensions	328 x 82 x 42 mm (with microphone and preamplifier)
Weight	Approx. 0.6 kg with battery



Main result



1/1 octave spectrum



1/3 octave spectrum

Continuous product development and innovation is the policy of our company. Therefore, we reserve the right to change the specifications without prior notice.

SVANTEK Sp. z o.o., ul. Ks. Jana SITNIKA 1/68, 01-410 WARSAW, POLAND
phone/fax (+48 22) 828 80 39, (+48 22) 827 25 36
<http://www.svantek.com> e-mail: office@svantek.com.pl

Figure A.2 SVAN 947 Sound and Vibration Level Meter and Analyser manufactured by SVANTEK Ltd. used for the experimental steering vibration measurements. Part II.

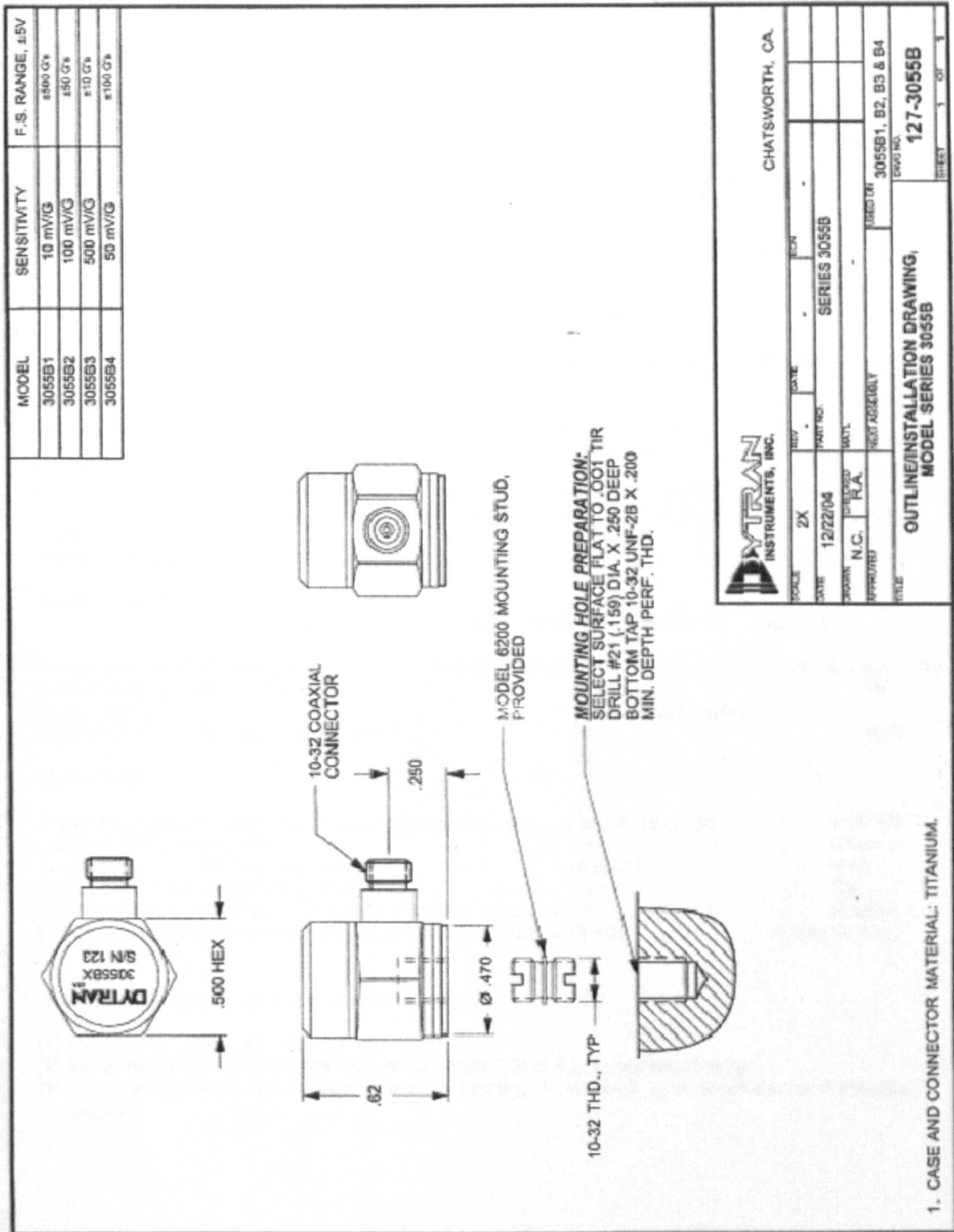


Figure A.3 Technical specifications for the LIVT™ accelerometer Series 3055B1 used for the experimental steering vibration measurements. Part I.

SPECIFICATIONS
MODEL SERIES 3055B LIVM ACCELEROMETERS

SPECIFICATION	VALUE				UNITS
PHYSICAL					
WEIGHT	10				Grams
SIZE, HEX x HEIGHT	.50 x 0.62				Inches
MOUNTING PROVISION	10-32 X .150 DEEP TAPPED HOLE				
CONNECTOR, RADially MOUNTED	10-32				Coaxial
MATERIAL, BASE, CAP & CONNECTOR	TITANIUM				
SEISMIC ELEMENT TYPE	CERAMIC, PLANAR SHEAR				
PERFORMANCE					
	MODELS				
	3055B1	3055B2	3055B3	3055B4	
SENSITIVITY, $\pm 5\%$ [1]	10	100	500	50	mV/g
RANGE F.S. FOR ± 5 VOLTS OUTPUT	± 500	± 50	± 10	± 100	g's
FREQUENCY RANGE, $\pm 5\%$ (all models)	1 to 10,000				Hz
RESONANT FREQUENCY, NOM. (all models)	35				kHz
ELECTRICAL NOISE FLOOR (25Hz-25kHz)	.0002	.00006	.00005	.0005	g's RMS
(1Hz-10kHz)	.0004	.0001	.0001	.0010	g's RMS
LINEARITY [2] (all models)	± 2				% F.S.
TRANSVERSE SENSITIVITY, MAX. (all models)	± 2				%
ENVIRONMENTAL					
	3055B1	3055B2	3055B3	3055B4	
MAXIMUM VIBRATION/SHOCK	600/3000	400/2000	200/1000	500/2000	\pm g's/g's PK
TEMPERATURE RANGE (all models)	-60 to +250				°F
SEAL, HERMETIC	Glass-to-metal/welded				
COEFFICIENT OF THERMAL SENSITIVITY	.06				%/°F
ELECTRICAL					
SUPPLY CURRENT/COMPLIANCE VOLTAGE RANGE [3]	2 to 20/+18 to +30				mA/Volts
OUTPUT IMPEDANCE, TYP.	100				Ohms
BIAS VOLTAGE, +10.5 VOLTS NOM.	+9 to +12				VDC
DISCHARGE TIME CONSTANT, NOM.	0.5				Sec
OUTPUT SIGNAL POLARITY FOR ACCELERATION TOWARD TOP					Positive
ELECTRICAL ISOLATION, CASE GROUND TO MOUNTING SURFACE					10 Meg Ω , min.

Accessories supplied: (1) Model 6200 mounting stud.

[1] Measured at 100 Hz, 1 G RMS per ISA RP 37.2.

[2] Measured using zero-based best straight line method, % of F.S. or any lesser range.

[3] Do not apply power to this device without current limiting, 20 mA MAX. To do so will destroy the integral IC amplifier.

Figure A.4 Technical specifications for the LIVT™ accelerometer Series 3055B1 used for the experimental steering vibration measurements. Part II.

APPENDIX B

Geometrical Dimensions of the steering wheel clamp for vibration measurements

B.1 Drawings of the geometrical dimensions of the steering wheel clamp used for vibration measurements.

Figures B.1 to B.3 present the drawings of the steering wheel mounting clamp which show the geometrical dimensions and also an ensemble drawing.

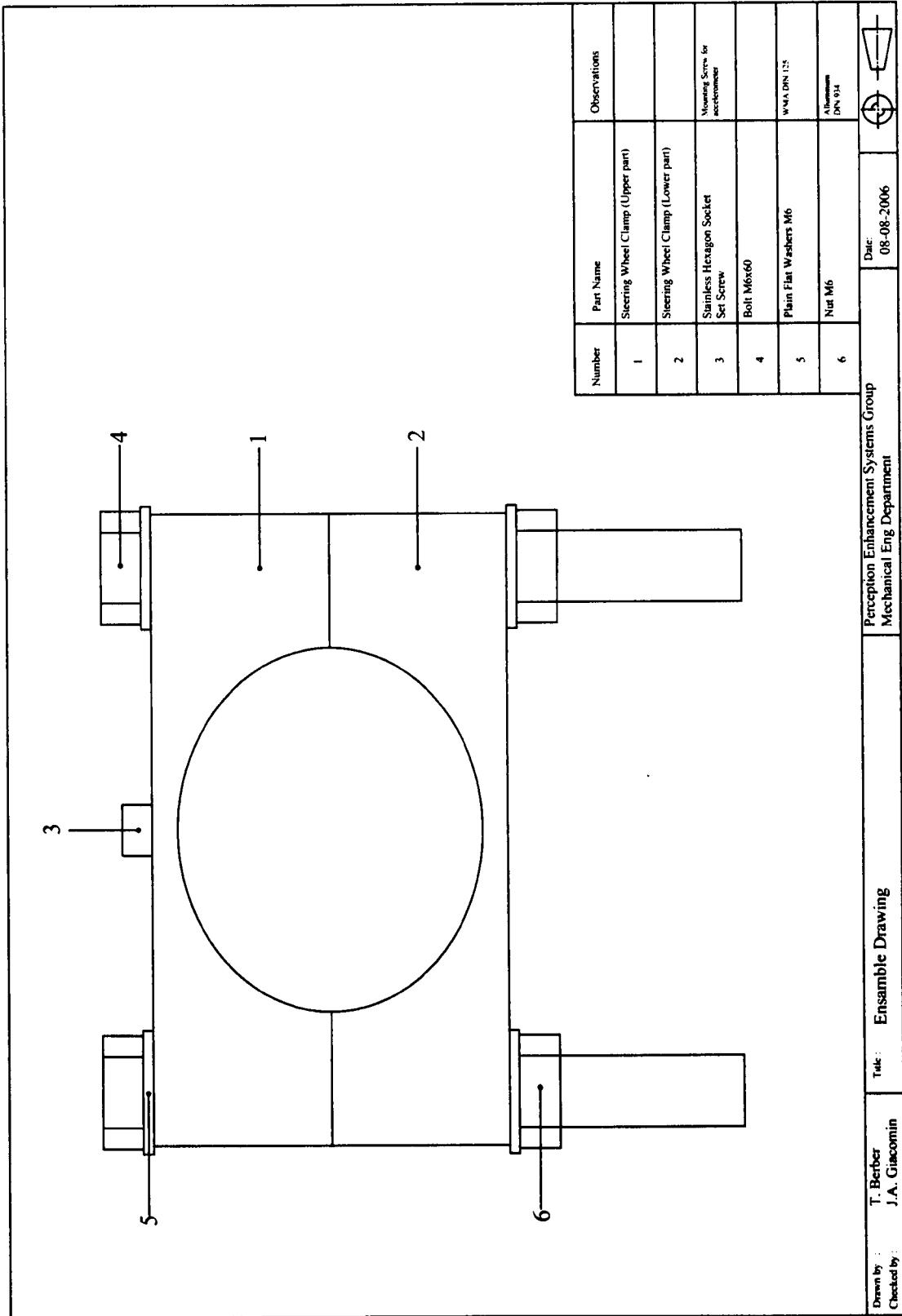


Figure B.1 Ensemble drawing of the steering wheel clamp used to measure the steering wheel vibration for the Uxbridge test.

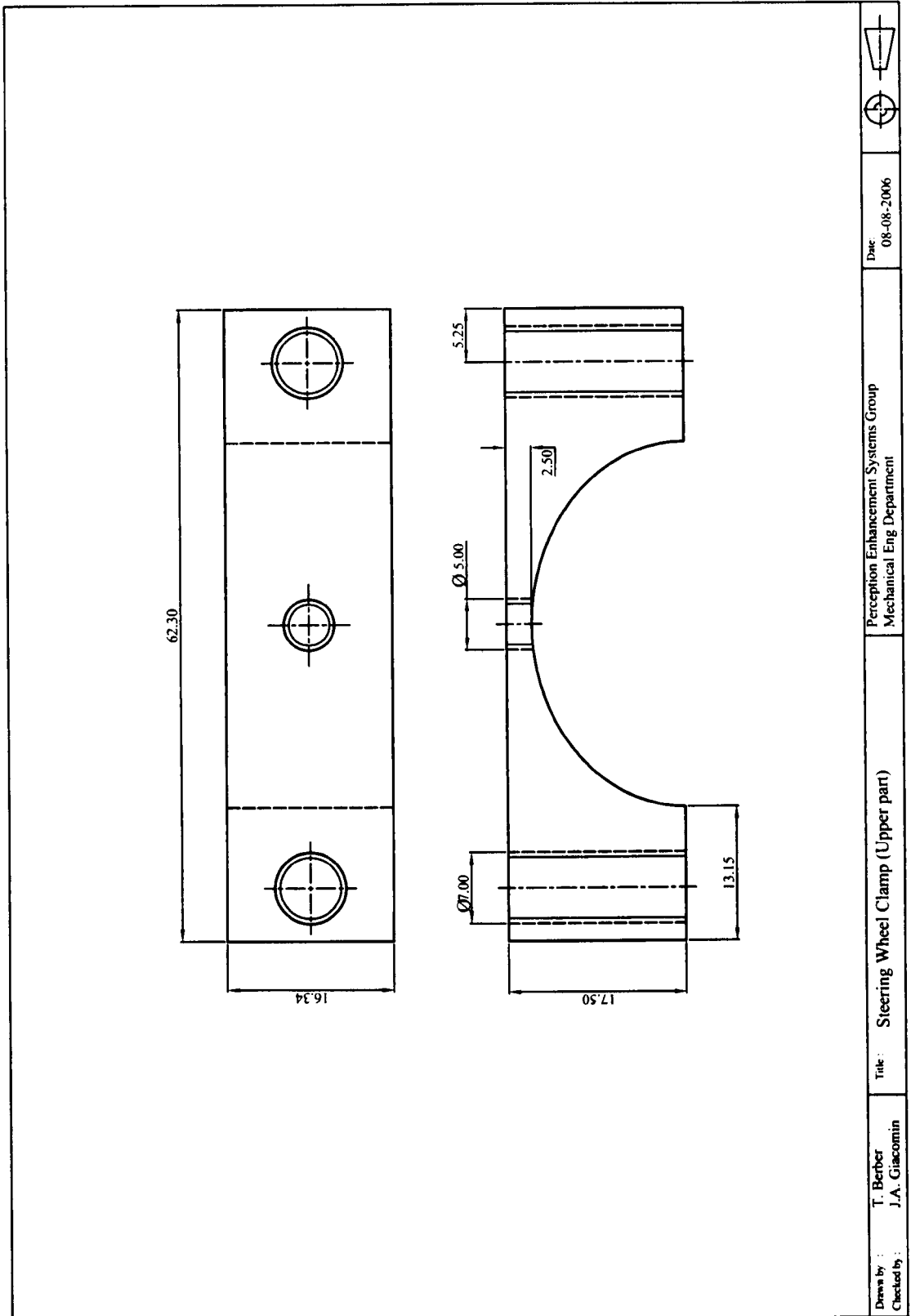


Figure B.2 Geometrical dimensions of the upper part of the steering wheel clamp used to measure the steering wheel vibration for the Uxbridge test.

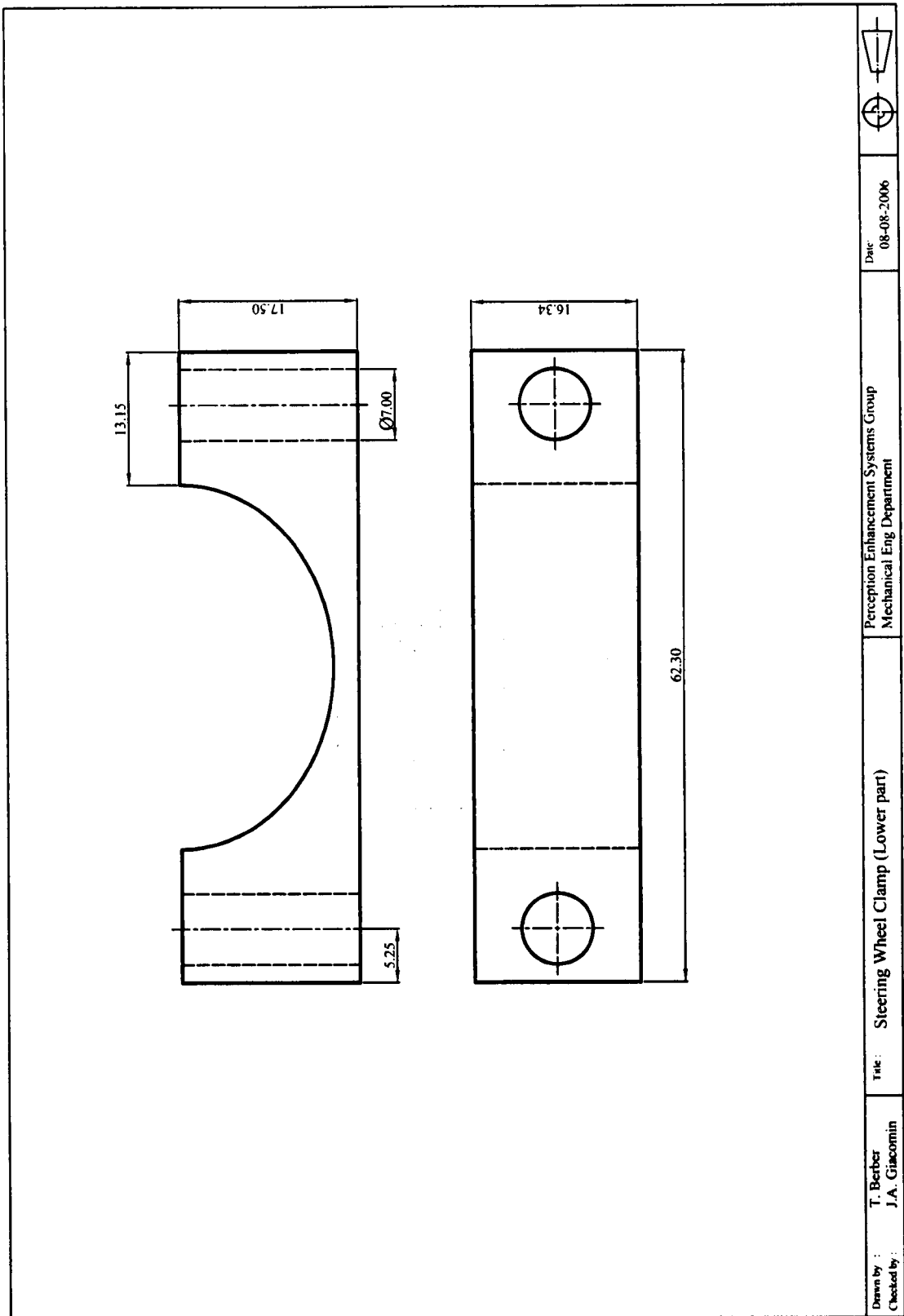


Figure B.3 Geometrical dimensions of the lower part of the steering wheel clamp used to measure the steering wheel vibration for the Uxbridge test.

APPENDIX C

Technical Specifications of Equipment used in the experimental laboratory tests

C.1 Description and Technical Specifications of the equipment used in the experimental laboratory test.

The monoaxial accelerometer which was placed on the rotational steering wheel test rig is presented in Figure C.1. Technical specifications of the accelerometer are presented in Figure C.2, while its certificate of calibration is presented in Figure C.3 in which is described the properties of the single axis of measurement.

The technical specification for the multi-channel signal conditioning MSC6 is presented in Figure C.4, while the technical specification for the power amplifier PA100E and the shaker V20 are presented in Figure C.5.

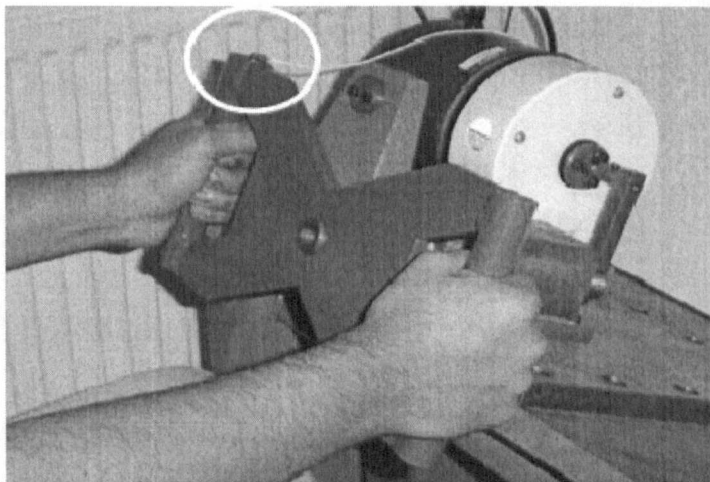


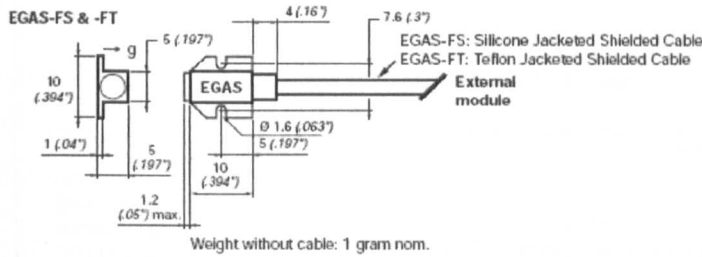
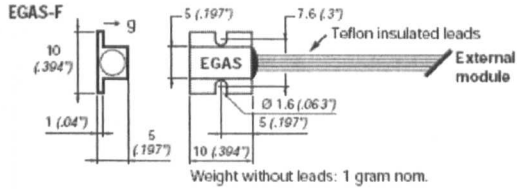
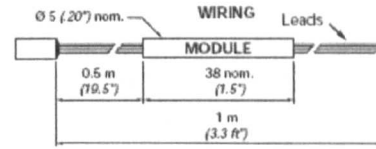
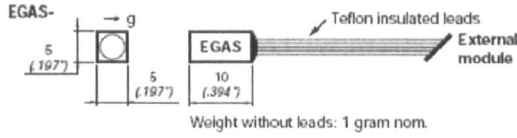
Figure C.1 Accelerometer position at the rotational steering wheel test rig, located on the top left side of the wheel.

EGAS Series Accelerometers



Miniature - Rugged

EGAS, EGAS-F, EGAS-FS & EGAS-FT



Dim: mm (inches)

EGAS Series

RANGES "FS"	OVERRANGE LIMIT	FREQUENCY RESPONSE $\pm 1/2$ dB nom./min.	NATURAL FREQUENCY nom.	SENSITIVITY mV/g nom.	OUTPUT "FSO" mV nom.
± 5	± 500	0 to 150/80 Hz	300 Hz	20	± 100
± 10	± 1000	0 to 200/120 Hz	400 Hz	10	± 100
± 25	± 2500	0 to 400/240 Hz	800 Hz	4	± 100
± 50	± 5000	0 to 600/350 Hz	1200 Hz	2	± 100
± 100	± 10000	0 to 900/500 Hz	1800 Hz	1	± 100
± 250	± 10000	0 to 1300/750 Hz	2600 Hz	0.4	± 100
± 500	± 10000	0 to 1750/1000 Hz	3500 Hz	0.2	± 100
± 1000	± 10000	0 to 2500/1500 Hz	5000 Hz	0.1	± 100
± 2500	± 10000	0 to 3500/2000 Hz	7000 Hz	0.04	± 100

EXCITATION: 15VDC
IMPEDANCE IN: 1300 Ω nom. typ.
IMPEDANCE OUT: 1500 Ω nom.
COMB. NON-LINEARITY & HYSTERESIS: $\pm 1\%$
TRANSVERSE SENSITIVITY: 2% max
DAMPING RATIO AT 20°C (70°F): 0.7 nom. (0.5 to 0.9)
OVERRANGE STOPS: Integral
THERMAL ZERO SHIFT: $\pm 1\text{mV}/50^\circ\text{C}$ ($\pm 1\text{mV}/100^\circ\text{F}$)
THERMAL SENSITIVITY SHIFT (TSS): $\pm 2.5\%/50^\circ\text{C}$ ($\pm 2.5\%/100^\circ\text{F}$)
OPERATING TEMPERATURE: -40°C to 120°C (-40°F to 250°F)
COMPENSATED TEMPERATURE: 20°C to 80°C (70°F to 170°F)
ZERO OFFSET AT 20°C (70°F): $\pm 15\text{mV}$ typ.

 www.entran.com	EGAS ACCELEROMETERS Miniature Rugged	Entran Sensors & Electronics USA: Fairfield, NJ UK: Garston, Watford, Herts, England Europe: Les Clayes-sous-Bois, France		
		SPECIFICATION EGASS001U	ISSUE PB0	PAGE 1 of 2

Figure C.2 Technical specifications for the monoaxial EGAS accelerometer used for the experimental laboratory tests.



CERTIFICATE OF CALIBRATION

Property of : P.O. : Entran FO : 21138

PLEASE READ OPERATING INSTRUCTIONS BEFORE POWERING UNIT

Model : EGAS-FT*-25-/L02M Axis : S/N : 899329
Type : ACCELEROMETER
Range : 25 g Do Not Exceed : 2500 g
Compensated Range : 20 to 80 °C Operating Range : -40 to 120 °C
Specifications : *: DIN type 7 pin connector to be wired to sensor for NSC.

Other characteristics according to : EGAS001E-A

CALIBRATION DATA

Non linearity ± Hysteresis ± CNL&N ± 1.00 %FSO
Th. zero shift ± 1.00 mV/50°C Thermal Sens. Shift ± 2.50 %/50°C
Zero (typ.) ± 15 mV
Ref. Temp. ± 22 °C (72°F)
Shunt Cal. with : KΩ across :
Sensitivity : 3.681 mV/g with Excitation : 15.0 V Max. : 18.0 V
Natural frequency : 740 Hz Damping : 0.66
Input ohms : 1368 Ω Output ohms : 1562 Ω
Cal Equip. : M65
Notes : ELECTROMAGNETIC COMPATIBILITY, RESIDENTIAL, COMMERCIAL AND LIGHT INDUSTRY.

WIRING

Connector : DIN 7b. Transducer to Comp. Module : Total length :
+In. : 1 +Out. : 5 Common mode : V output
-In. : 2 -Out. : 4 referenced to -Input =

*The calibrated values do not exceed the data sheet specifications, value shown is the data sheet value.
*Value given by manufacturing design.

The above instrument has been calibrated against a working standard which is directly traceable to a national standard.
All data interpreted per Entran Instruction Manuals unless otherwise indicated.

Control : S. COSTE [Signature] Date : 08/11/99

200718

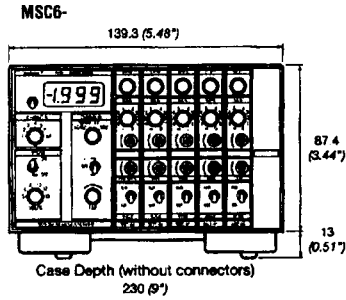
Table with 4 columns: Entran Devices, Inc. (Fairfield, NJ), Entran European Headquarters (Les Clayes-sous-Bois), Entran Limited (Watford, England), Entran Sensoren GmbH (Ludwigshafen).

Figure C.3 ENTRAN Certificate of calibration and specifications for the monoaxial EGAS accelerometer used to measure the steering wheel vibration test rig along the z-axis.

Specifications



MSC6



Dim: mm (inches)

Chassis with Power Supply

FOR A1 AMPLIFIERS:
FOR A2 AMPLIFIERS (Also accepts A1 amplifiers):
NUMBER OF CHANNELS:
POWER:
DISPLAY:
EXCITATION TO SENSOR (Common to all Channels):
INTERNAL CALIBRATION:

MSC6
Not Available
6
 115/220VAC ($\pm 10\%$, 45-440Hz) Switch Selectable (Optional 12/24 VDC)
 3 1/2 DIGIT LED, 1.999V or 19.99V Switchable
 Switchable: 5V, 6V, 8V, 10V, 12V and 15V
 $\pm 1\text{mV}$ through $\pm 10\text{V}$ continuously adjustable

Signal Conditioning Channels A1 & A2

OUTPUT:
AMPLIFIER GAIN (Switchable with fine control):
AMPLIFIER BANDWIDTH (-1dB):
ZERO OFFSET:

A1	A2
$\pm 10\text{V}$ or $\pm 2\text{V}$	4-20mA and $\pm 10\text{V}$ or $\pm 2\text{V}$
1 to 2000	10 to 10000
0 to 50KHz	0 to 1.5KHz
$\pm 40\text{mV}$ at input	$\pm 10\text{mV}$ at input

INPUT RANGE:
INPUT MODE:
INPUT IMPEDANCE:
OUTPUT TYPES:
OUTPUT IMPEDANCE FOR TAPE:
OUTPUT FOR GALVOS:
OUTPUT LINEARITY:
OPERATING TEMPERATURE:
INPUT CONNECTORS:
OUTPUT CONNECTORS:
CE CONFORMANCE:

5mV to 1.0V
 Full, Half or 1 Arm Bridge. Internal Bridge Completion
 1M Ω Differential
 Tape and Galvo
 0.5 Ω
 $\pm 10\text{mA}$ into 120 Ω
 0.05%
 0°C to 40°C (32°F to 104°F)
 DIN Type 7 Pin. with unwired mate
 D Type with unwired mate
 EN61010-1, EN 50081-1, EN 50082-1

	TITLE MSC INSTRUMENTATION Multi-Channel Signal Conditioning	Entran ENGLAND: Gerston, Watford, Herts. EUROPEAN HEADQUARTERS: Les Clayes-sous-Bois, FRANCE		
		SPECIFICATION NUMBER	ISSUE	PAGE
		MSCS0001E	01	1 of 2

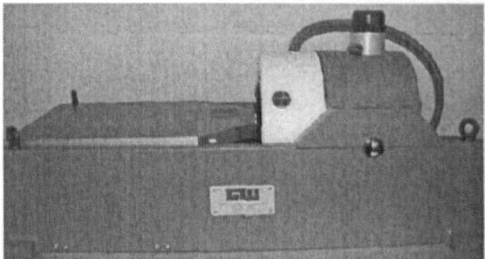
Figure C.4 Technical specification for the multi-channel signal conditioning MSC6.

Specifications

Parameter	Units	V2	V4	V20	V20
Power Amplifier		PA30E	PA30E	PA30E	PA100E
Sine force peak	N	9	17.8	53	100
Random force rms	N	3	5.9	17.6	33
Acceleration peak	g	91	91	32	60
Velocity peak	m/s	1.05	1.49	1.14	1.51
Displacement p-p	mm	2.5	5	10	10
Armature mass	kg	0.01	0.02	0.17	0.17
Armature diameter	mm	Spigot	Spigot	38	38
Suspension stiffness	kgf/mm	0.32	0.45	1.14	1.14
Cooling		Natural	Natural	Natural	Natural
System power utility	VA	100	100	100	200

Parameter	Units	V20	V55	V55	V55
Power Amplifier		PA300E	PA100E	PA300E	DSA1-1K
Sine force peak	N	155	142	310	444
Random force rms	N	58	50	110	160
Acceleration peak	g	90	28.9	63	90
Velocity peak	m/s	1.78	0.81	1.14	1.52
Displacement p-p	mm	10	12.7	12.7	12.7
Armature mass	kg	0.17	0.5	0.5	0.5
Armature diameter	mm	38	76.2	76.2	76.2
Suspension stiffness	kgf/mm	1.14	1.79	1.79	1.79
Cooling		Forced air	Natural	Forced air	Forced air
System power utility	VA	600	200	600	1000

Options
* Beryllium copper spiders for V2 and V4 shakers to reduce axial stiffness.
* Trunnions for models V4, V20 and V55.
* Constant current drive for modal applications.
* Three axis testing configurations for models V20 and V55.
* Metric/Imperial/American table threads.

Three Axis Testing with Small Shakers


Gearing & Watson Electronics Ltd

South Road, Hailsham, East Sussex, BN27 3JJ, United Kingdom
 Tel +44 (0)1323 846464 Fax +44 (0)1323 847550
 E mail: sales@gearing-watson.com Web: www.gearing-watson.com

Figure C.5 Technical specification for the power amplifier PA100E and the shaker V20 used during the experimental laboratory tests.

APPENDIX D

ROC points results for the laboratory experiments

D.1 ROC points for the laboratory experiment to measure the effect of steering wheel acceleration compression or expansion on the human detection of road surface type.

The Receiver Operating Characteristic (ROC) points results obtained for the 15 test participants for the tarmac surface, the concrete surface and the cobblestone surface when compressed and expanded are presented in Figures D.1 to D.18. Results are presented according to three threshold levels used in the laboratory experiment (± 3 STD, ± 2 STD and ± 1 STD).

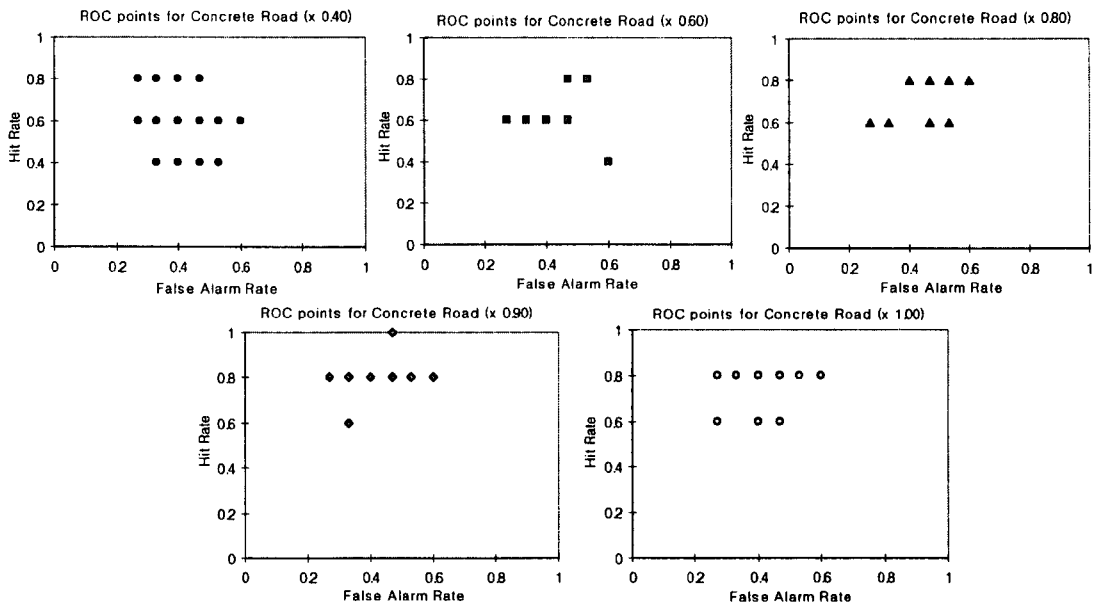


Figure D.1 ROC points of concrete surface for the laboratory experiment to measure the effect of steering wheel acceleration compression on the human detection of road surface type ($\pm 3\text{STD}$, $n=15$).

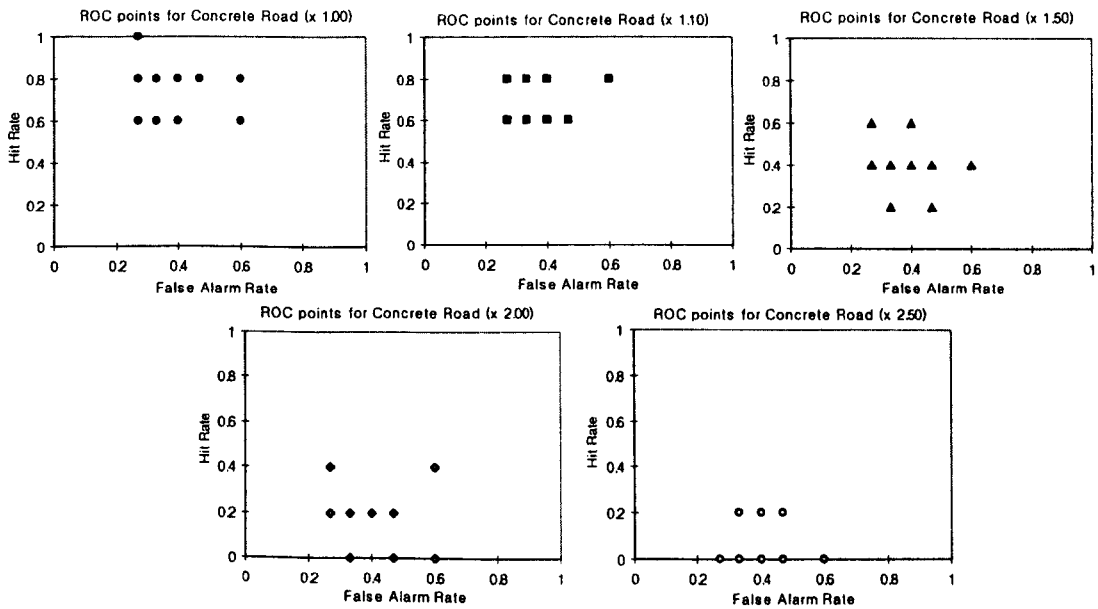


Figure D.2 ROC points of concrete surface for the laboratory experiment to measure the effect of steering wheel acceleration expansion on the human detection of road surface type ($\pm 3\text{STD}$, $n=15$).

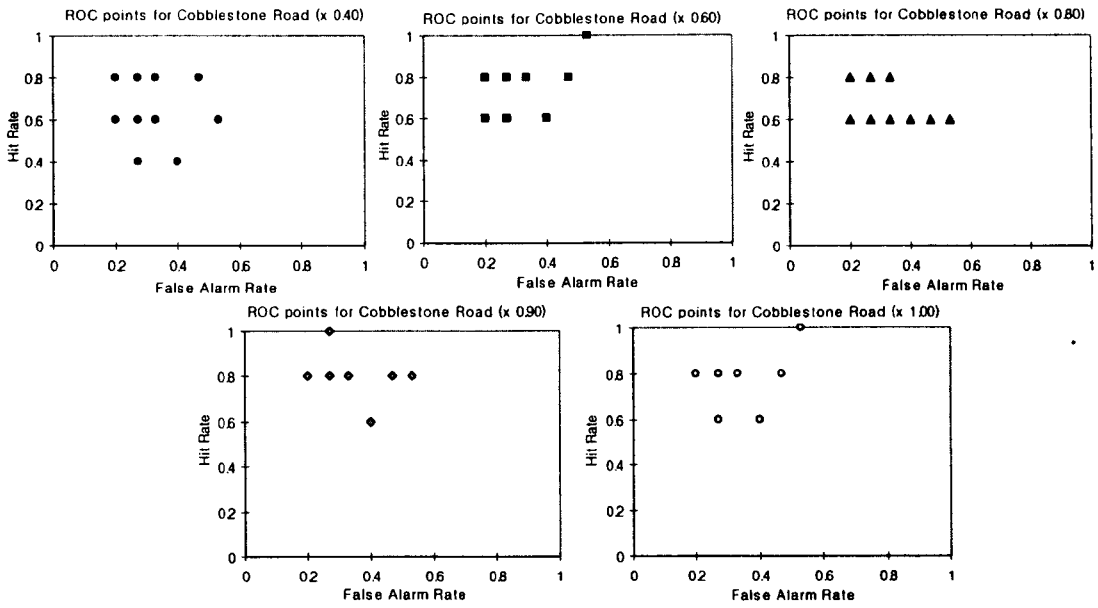


Figure D.3 ROC points of cobblestone surface for the laboratory experiment to measure the effect of steering wheel acceleration compression on the human detection of road surface type ($\pm 3\text{STD}$, $n=15$).

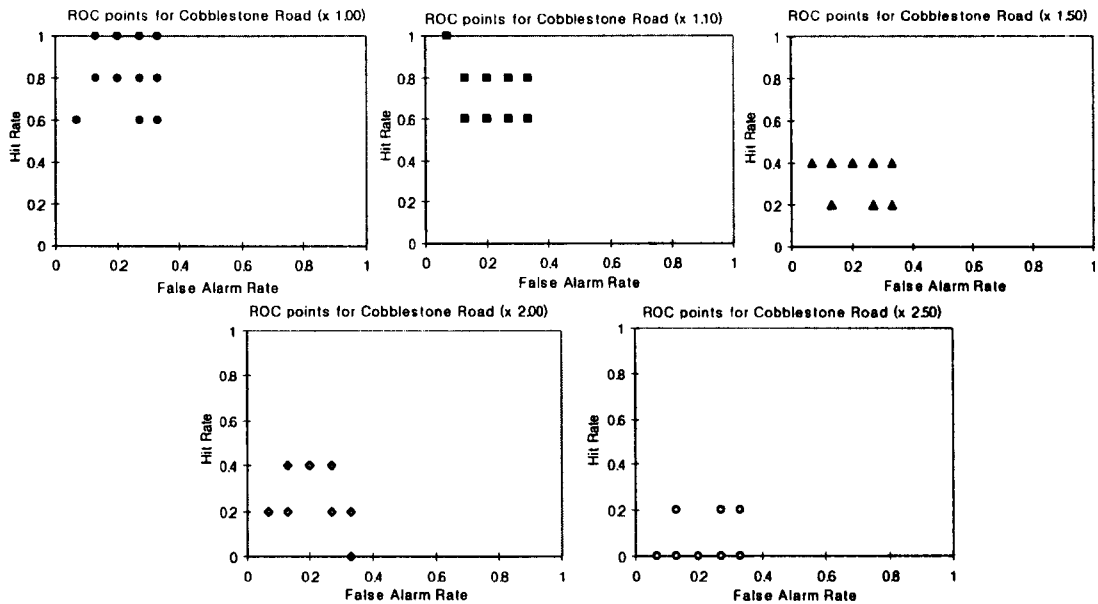


Figure D.4 ROC points of cobblestone surface for the laboratory experiment to measure the effect of steering wheel acceleration expansion on the human detection of road surface type ($\pm 3\text{STD}$, $n=15$).

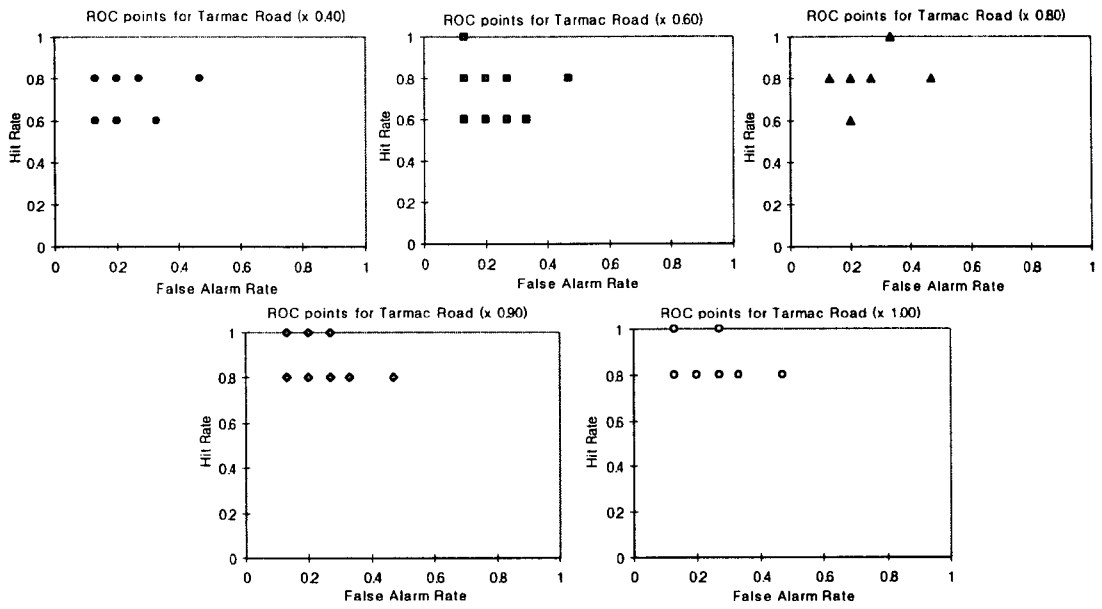


Figure D.5 ROC points of tarmac surface for the laboratory experiment to measure the effect of steering wheel acceleration compression on the human detection of road surface type ($\pm 3\text{STD}$, $n=15$).

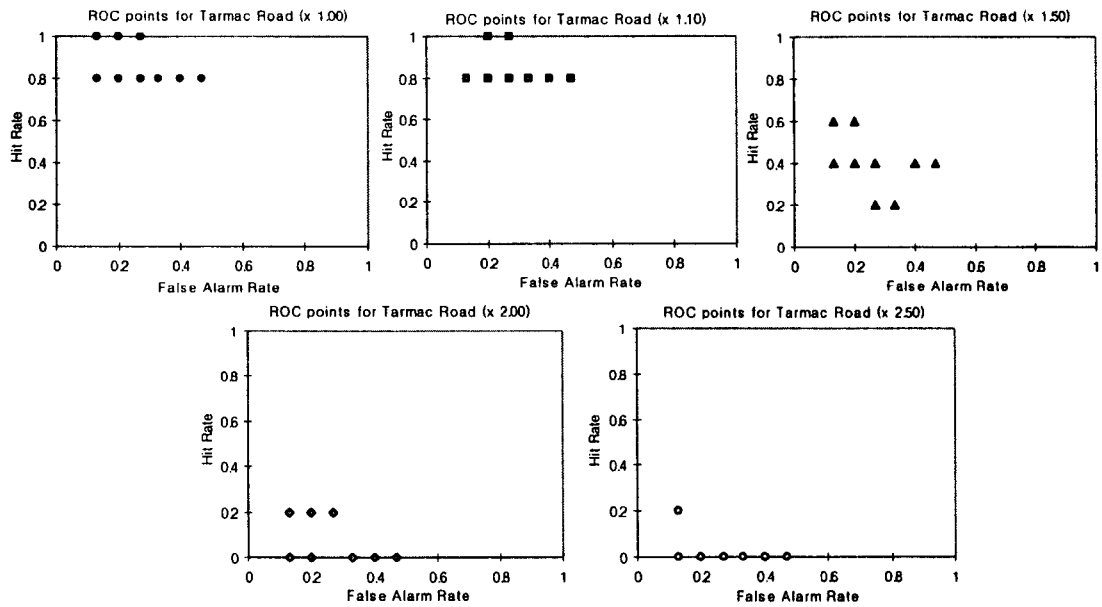


Figure D.6 ROC points of tarmac surface for the laboratory experiment to measure the effect of steering wheel acceleration expansion on the human detection of road surface type ($\pm 3\text{STD}$, $n=15$).

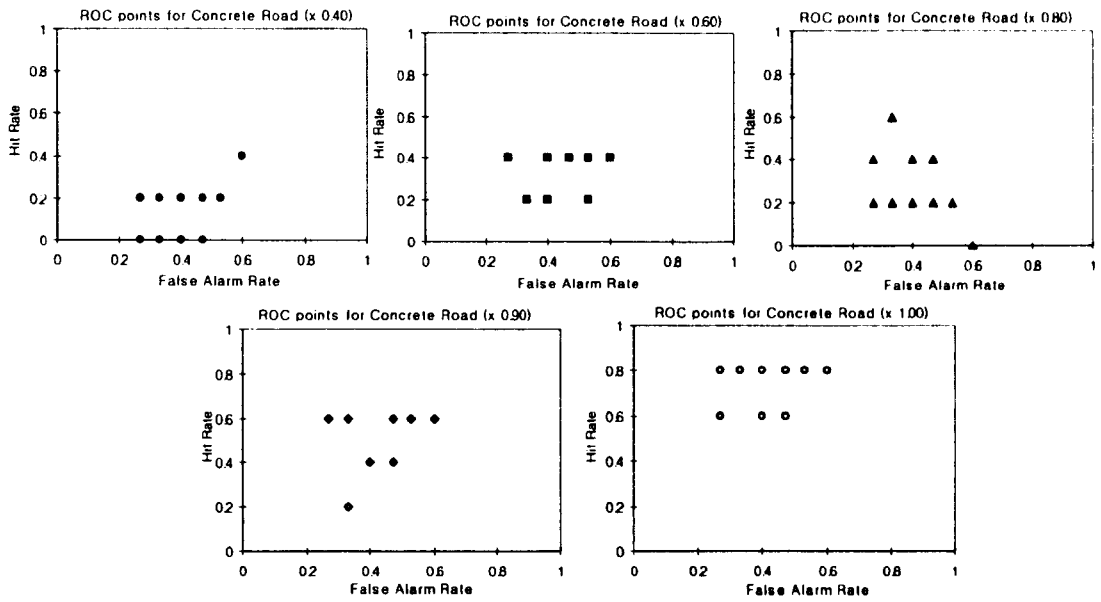


Figure D.7 ROC points of concrete surface for the laboratory experiment to measure the effect of steering wheel acceleration compression on the human detection of road surface type ($\pm 2\text{STD}$, $n=15$).

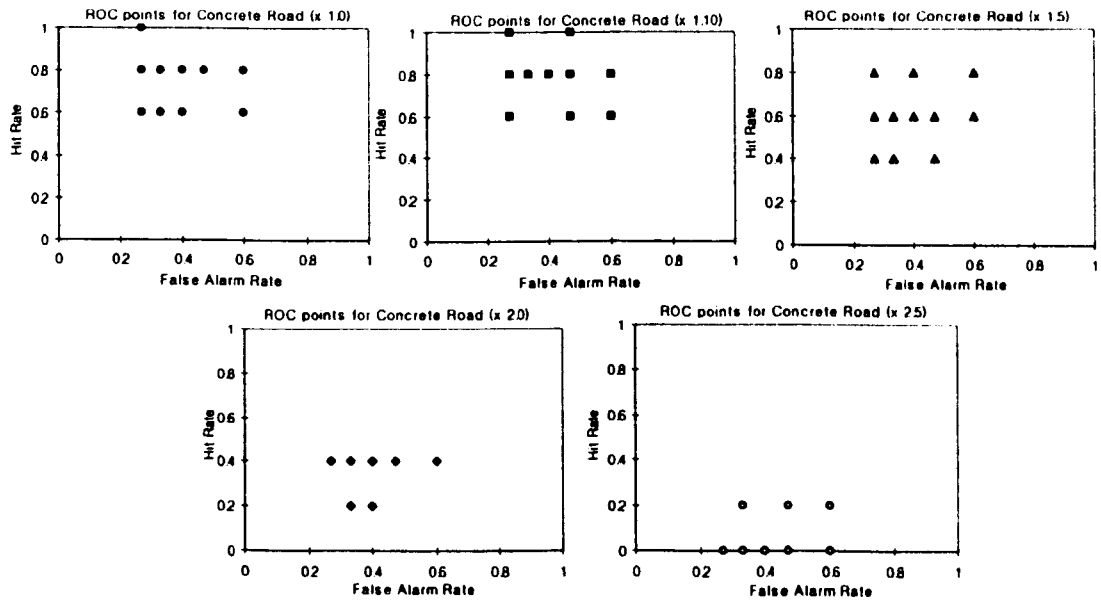


Figure D.8 ROC points of concrete surface for the laboratory experiment to measure the effect of steering wheel acceleration expansion on the human detection of road surface type ($\pm 2\text{STD}$, $n=15$).

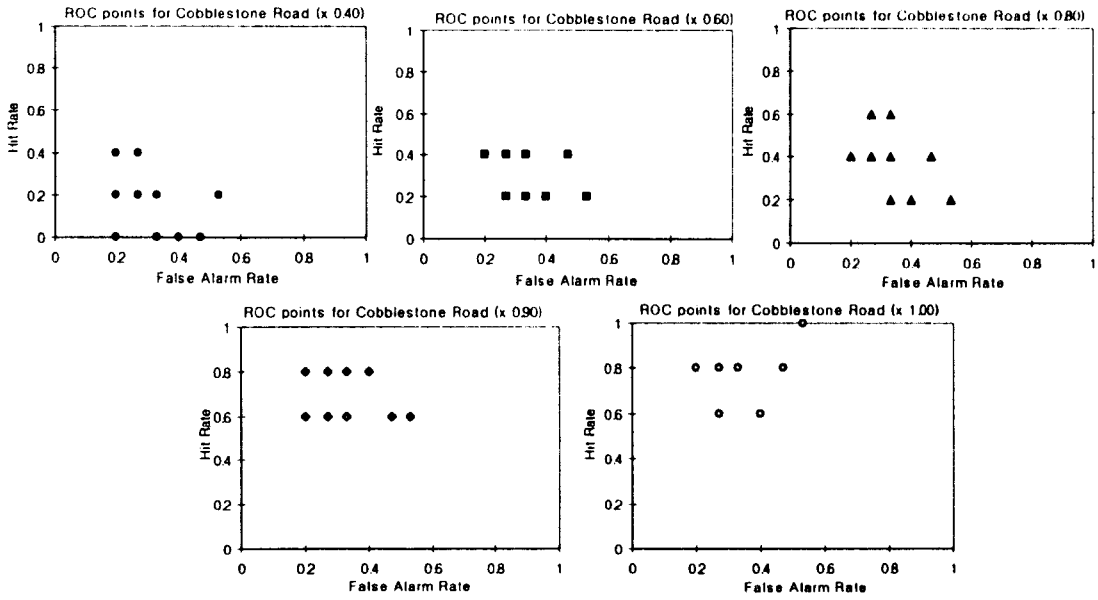


Figure D.9 ROC points of cobblestone surface for the laboratory experiment to measure the effect of steering wheel acceleration compression on the human detection of road surface type ($\pm 2\text{STD}$, $n=15$).

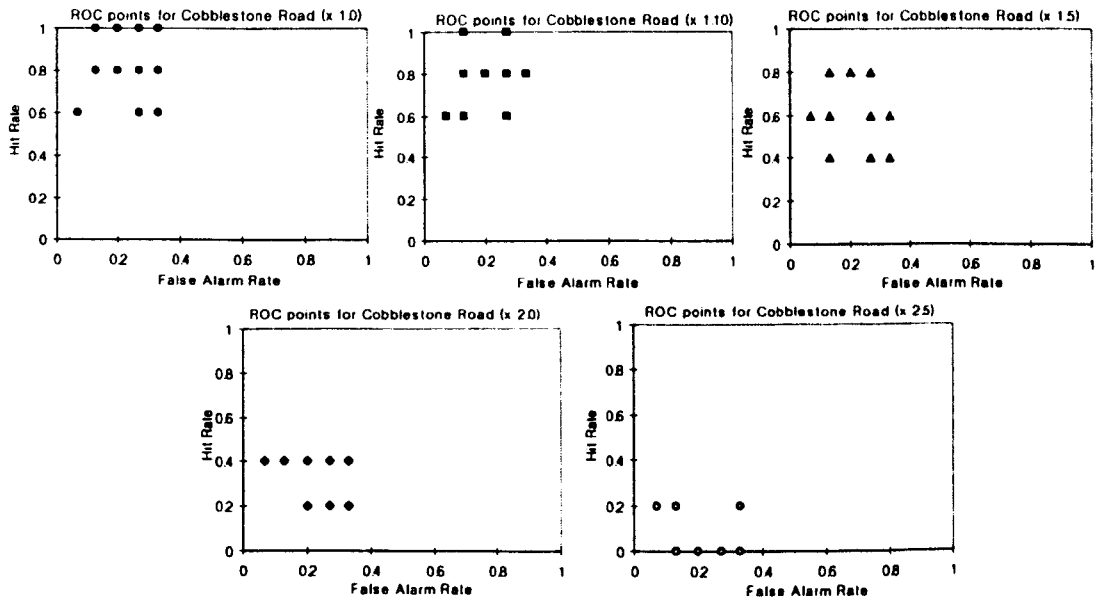


Figure D.10 ROC points of cobblestone surface for the laboratory experiment to measure the effect of steering wheel acceleration expansion on the human detection of road surface type ($\pm 2\text{STD}$, $n=15$).

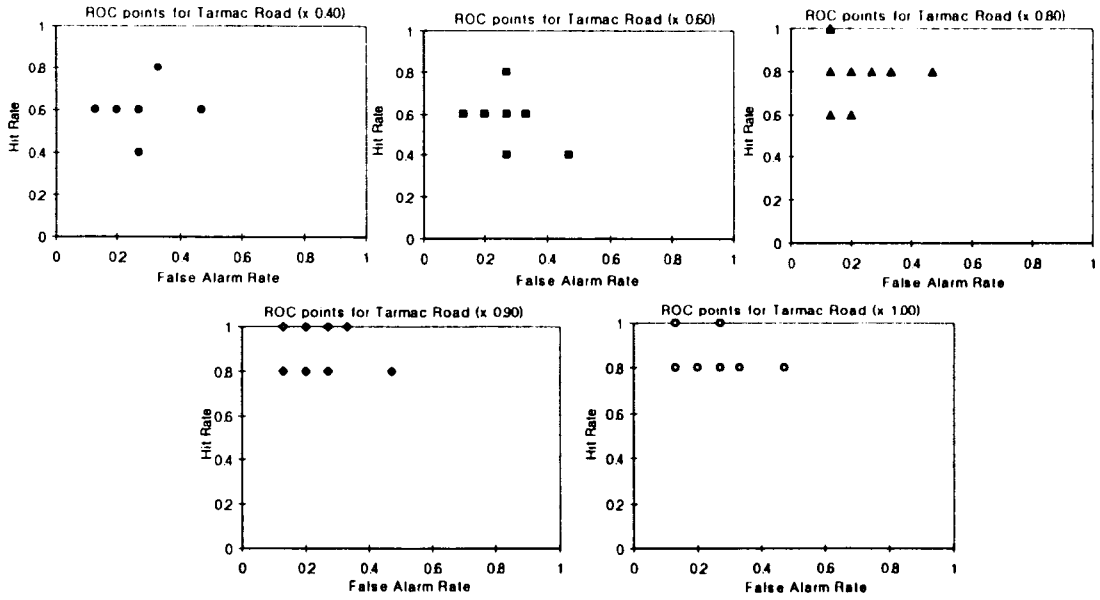


Figure D.11 ROC points of tarmac surface for the laboratory experiment to measure the effect of steering wheel acceleration compression on the human detection of road surface type ($\pm 2\text{STD}$, $n=15$).

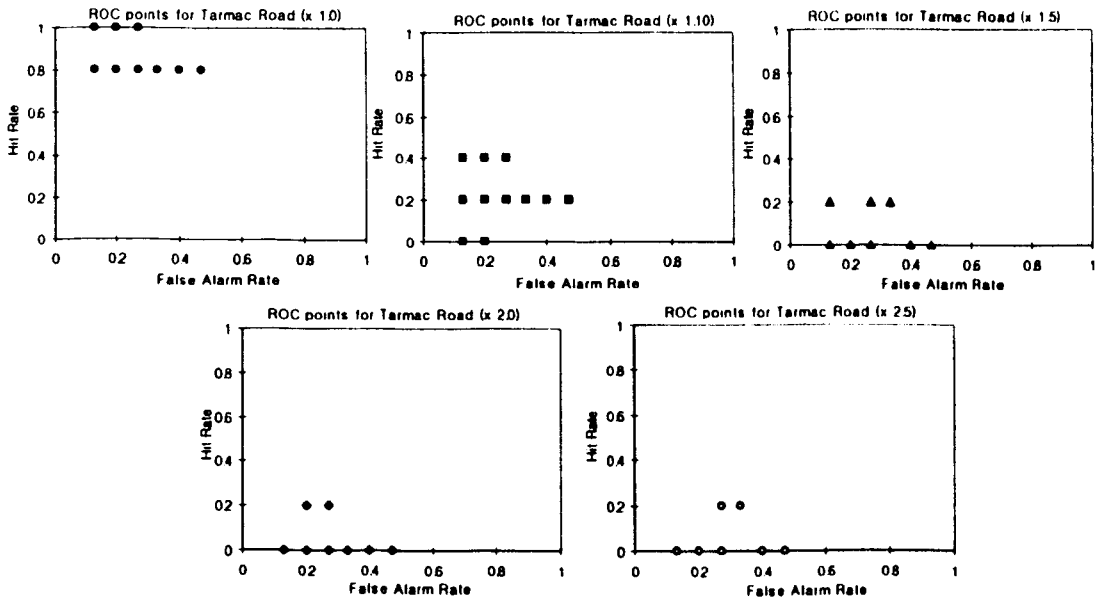


Figure D.12 ROC points of tarmac surface for the laboratory experiment to measure the effect of steering wheel acceleration expansion on the human detection of road surface type ($\pm 2\text{STD}$, $n=15$).

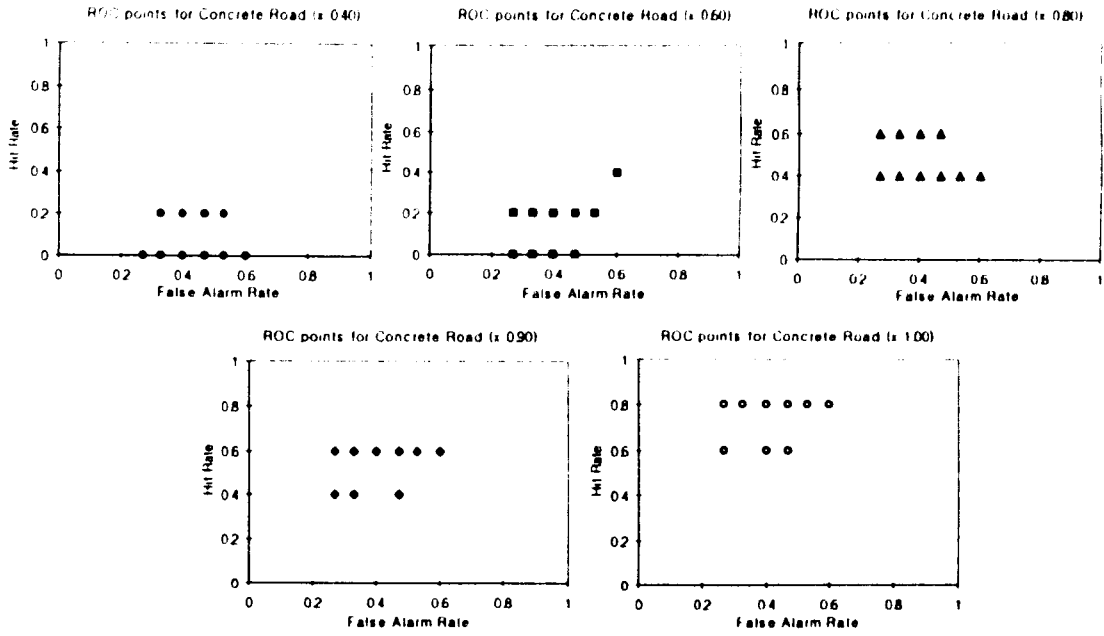


Figure D.13 ROC points of concrete surface for the laboratory experiment to measure the effect of steering wheel acceleration compression on the human detection of road surface type (± 1 STD, $n=15$).

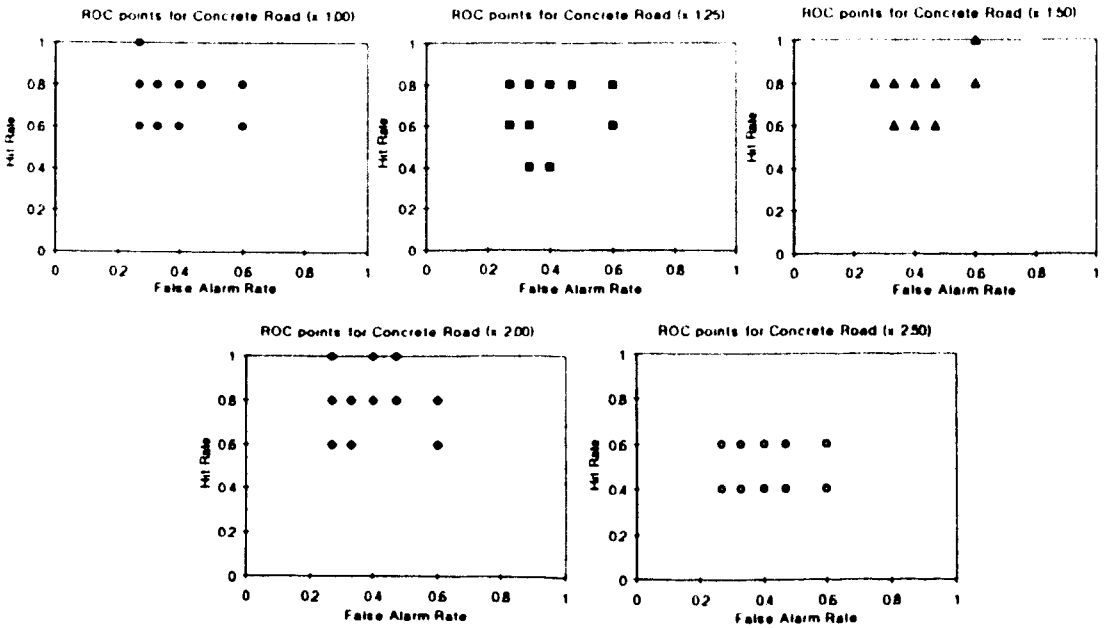


Figure D.14 ROC points of concrete surface for the laboratory experiment to measure the effect of steering wheel acceleration expansion on the human detection of road surface type (± 1 STD, $n=15$).

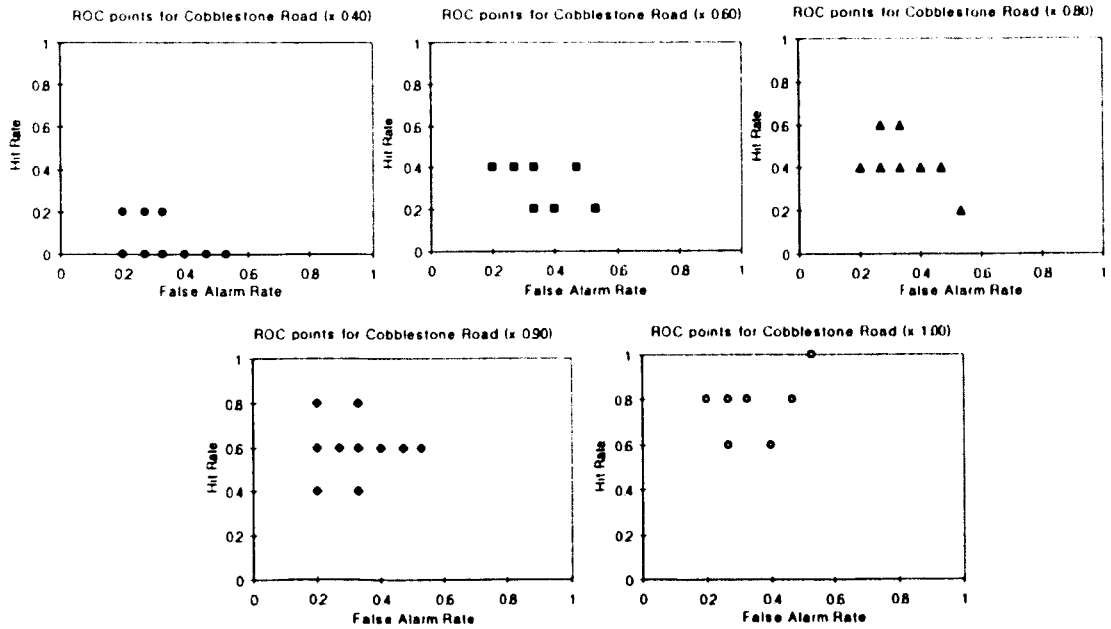


Figure D.15 ROC points of cobblestone surface for the laboratory experiment to measure the effect of steering wheel acceleration compression on the human detection of road surface type (± 1 STD, $n=15$).

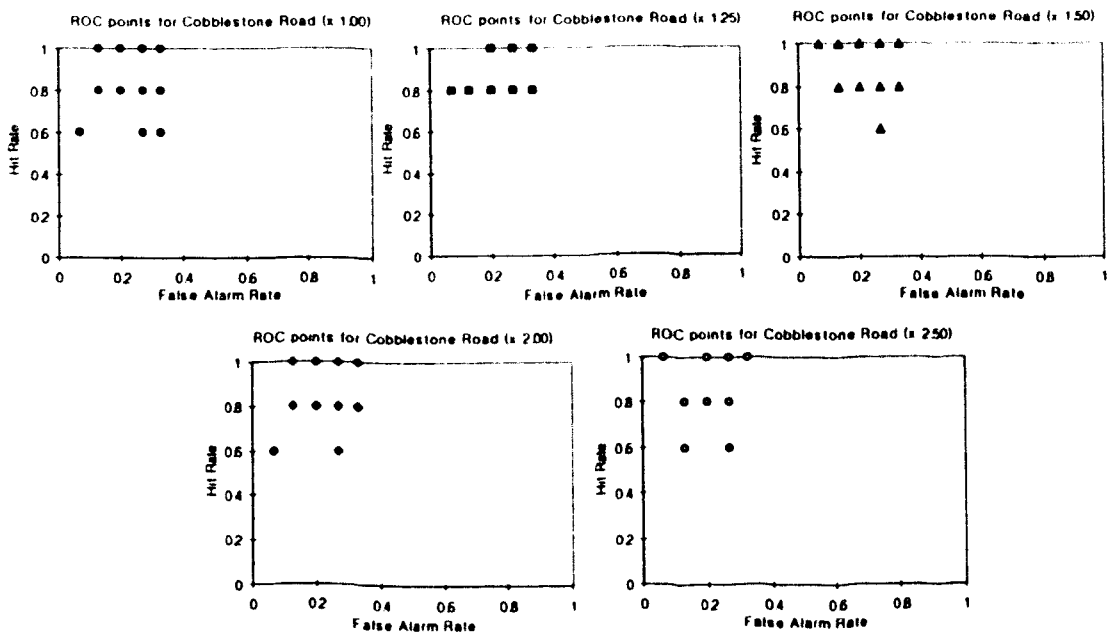


Figure D.16 ROC points of cobblestone surface for the laboratory experiment to measure the effect of steering wheel acceleration expansion on the human detection of road surface type (± 1 STD, $n=15$).

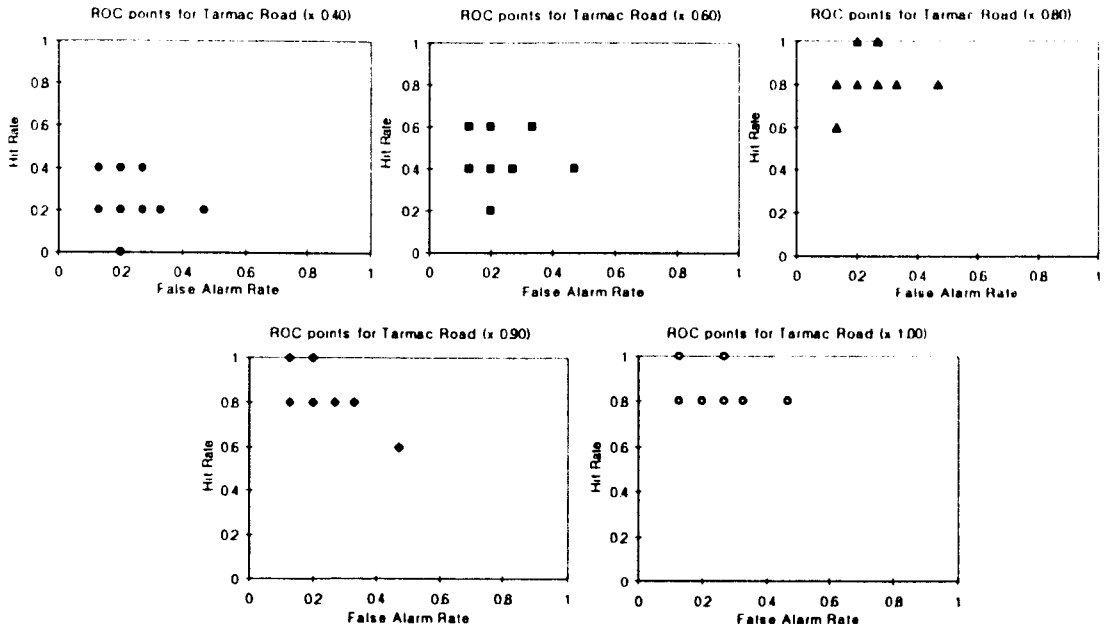


Figure D.17 ROC points of tarmac surface for the laboratory experiment to measure the effect of steering wheel acceleration compression on the human detection of road surface type (± 1 STD, $n=15$).

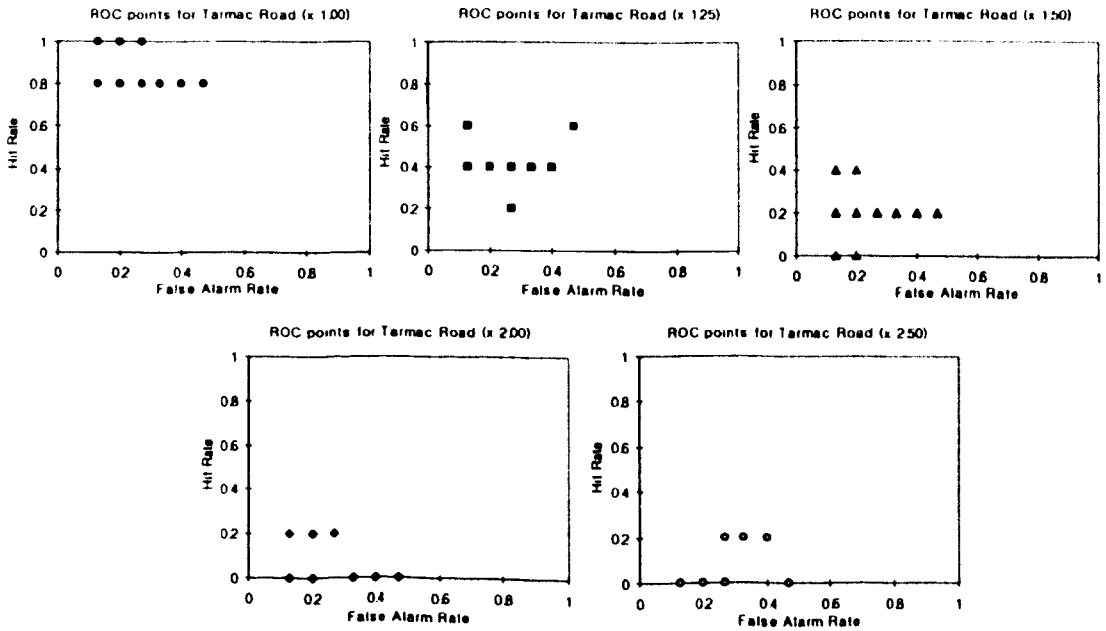


Figure D.18 ROC points of tarmac surface for the laboratory experiment to measure the effect of steering wheel acceleration expansion on the human detection of road surface type (± 1 STD, $n=15$).

D.2 ROC points for the laboratory experiment to measure the effect of steering wheel acceleration Threshold Trigger Level on the human detection of road surface type.

Figures D.19 to D.21 present the Receiver Operating Characteristic (ROC) points obtained for the 15 test participants for the broken concrete surface, the broken lane surface and the cobblestone surface. Results are presented according to the threshold trigger level (TTL) values from 2.4 to 3.4 investigated.

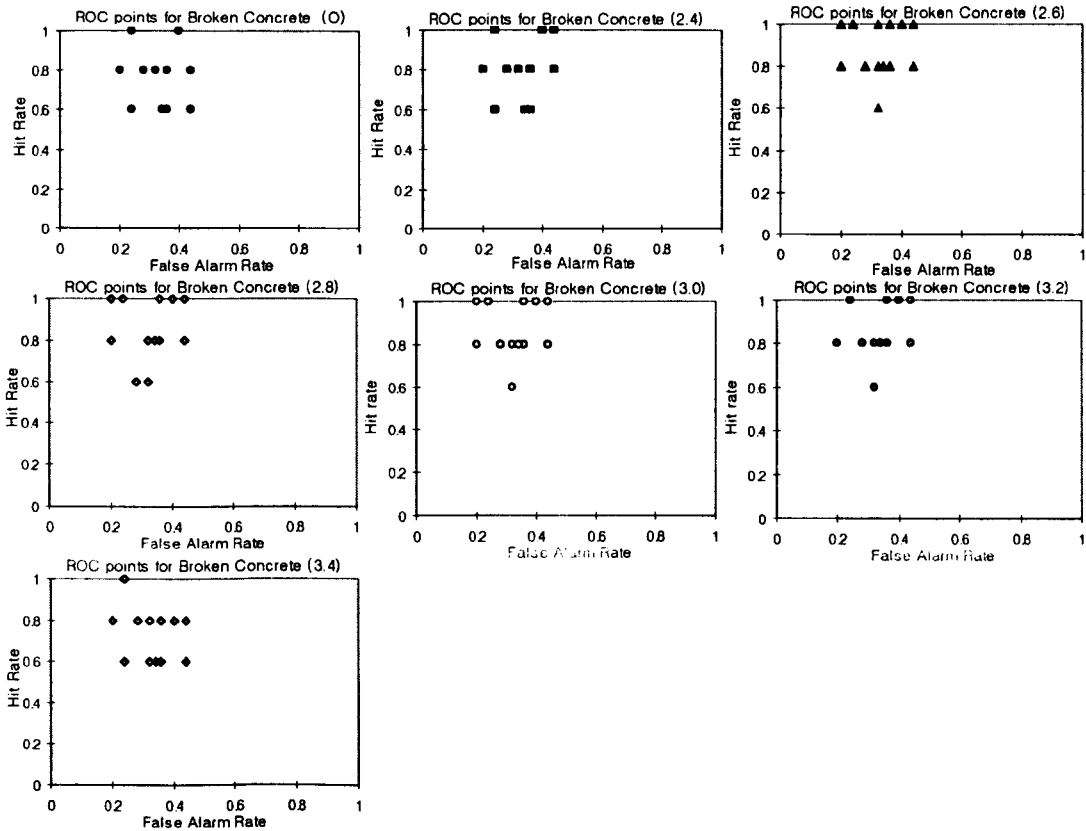


Figure D.19 ROC points for the Broken Concrete surface stimuli regarding the effect of the threshold trigger level (TTL) of the steering wheel acceleration signal (n= 15).

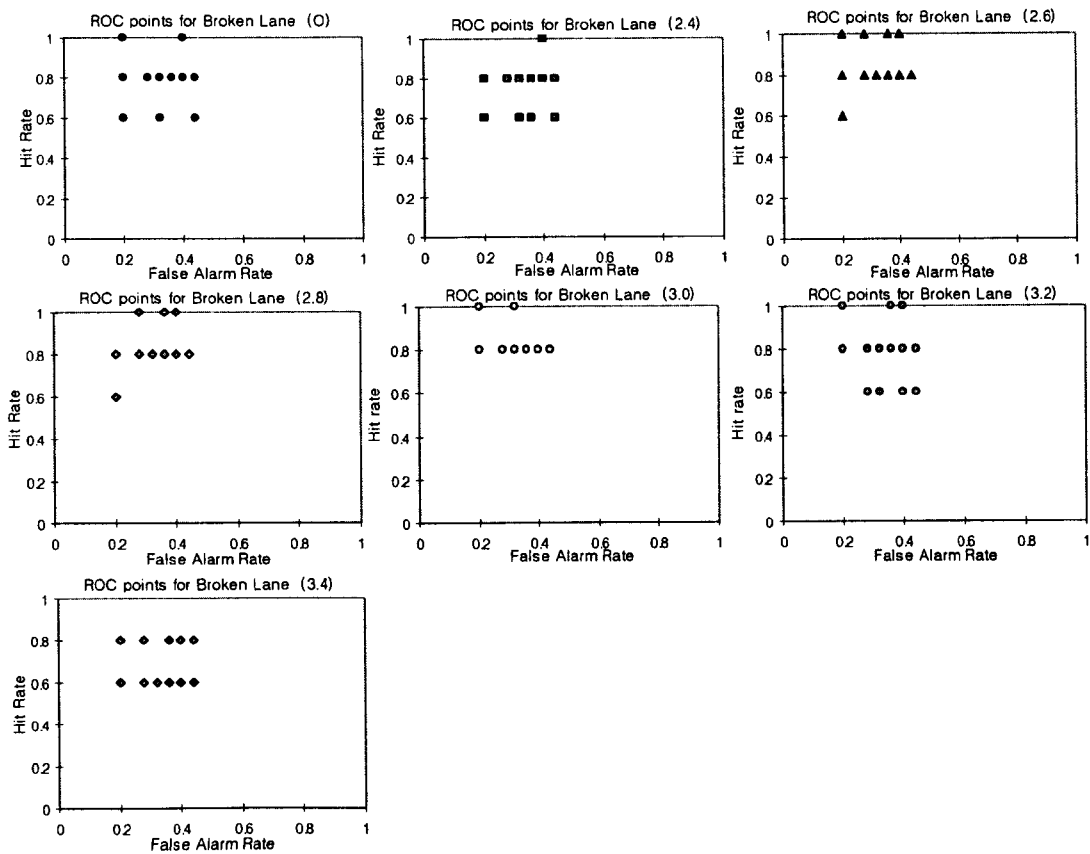


Figure D.20 ROC points for the broken lane surface stimuli regarding the effect of the threshold trigger level (TTL) of the steering wheel acceleration signal ($n= 15$).

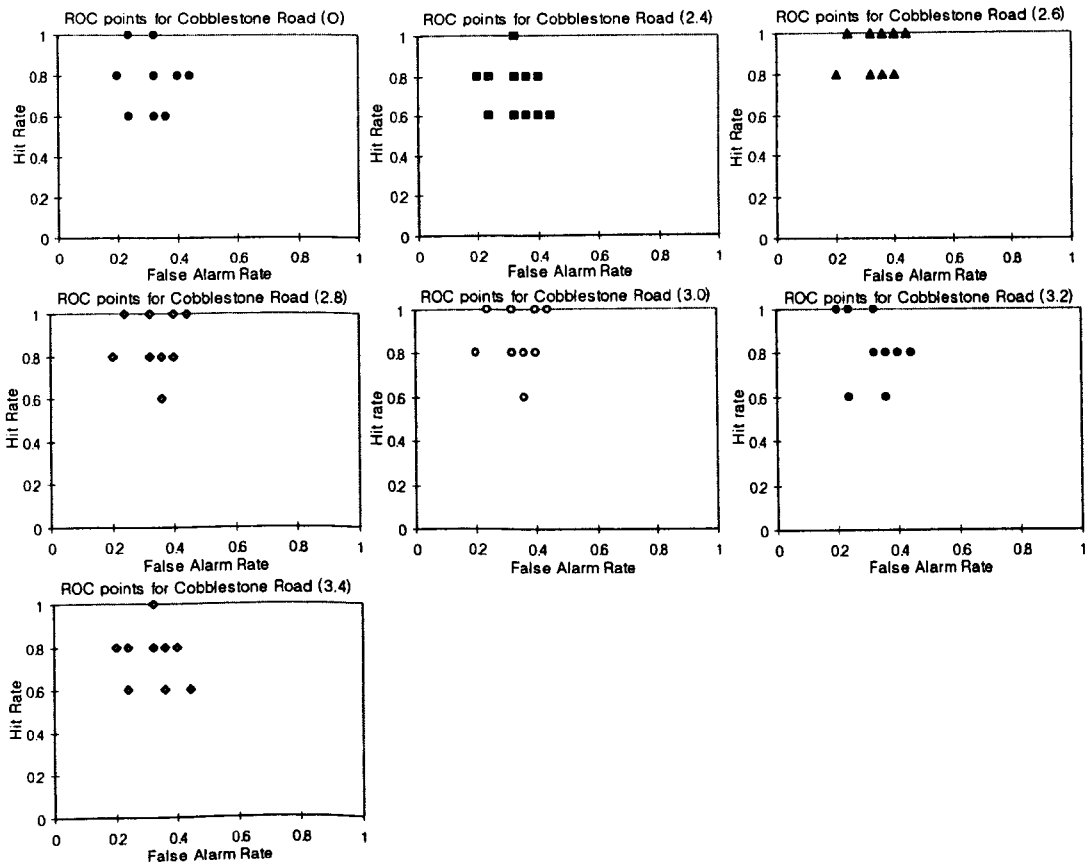


Figure D.21 ROC points for the Cobblestone surface stimuli regarding the effect of the threshold trigger level (TTL) of the steering wheel acceleration signal ($n= 15$).

D.3 ROC points for the laboratory experiment to measure the effect of the number of the transient events on the human detection of road surface type.

The Receiver Operating Characteristic (ROC) points results obtained for the 15 test participants for the cobblestone surface, the concrete surface and the tarmac surface are presented in Figures D.22 to D.24. Results are presented according to the four compression ratios investigated along with the original stimuli (O, 1+, 2+, 3+ and 4+).

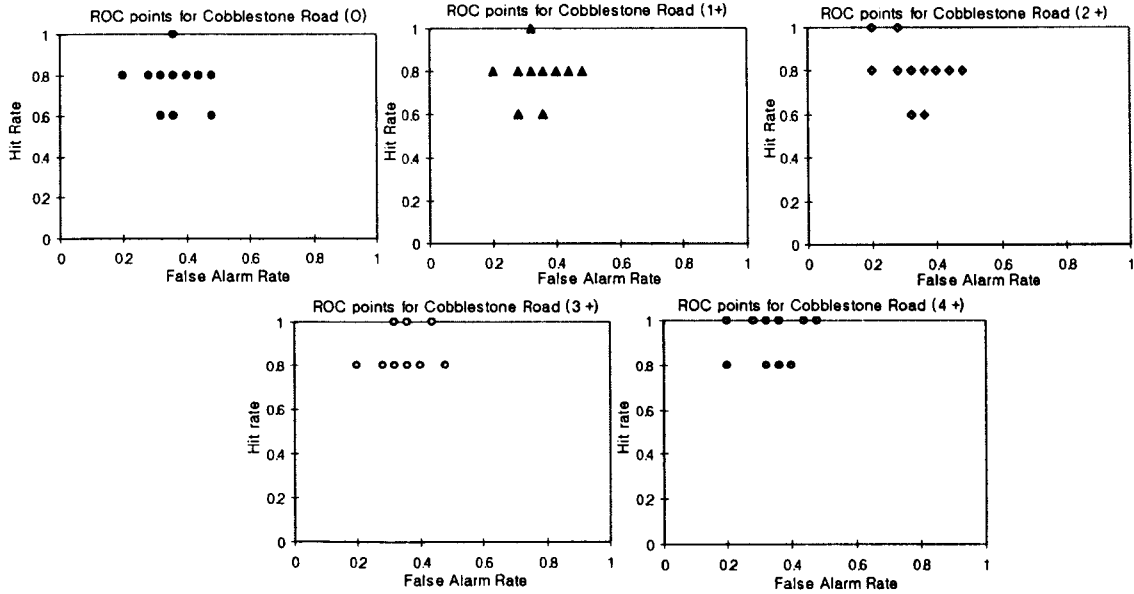


Figure D.22 ROC points for the cobblestone surface stimuli regarding the effect of the number of the transient events of the steering wheel acceleration signal (n= 15).

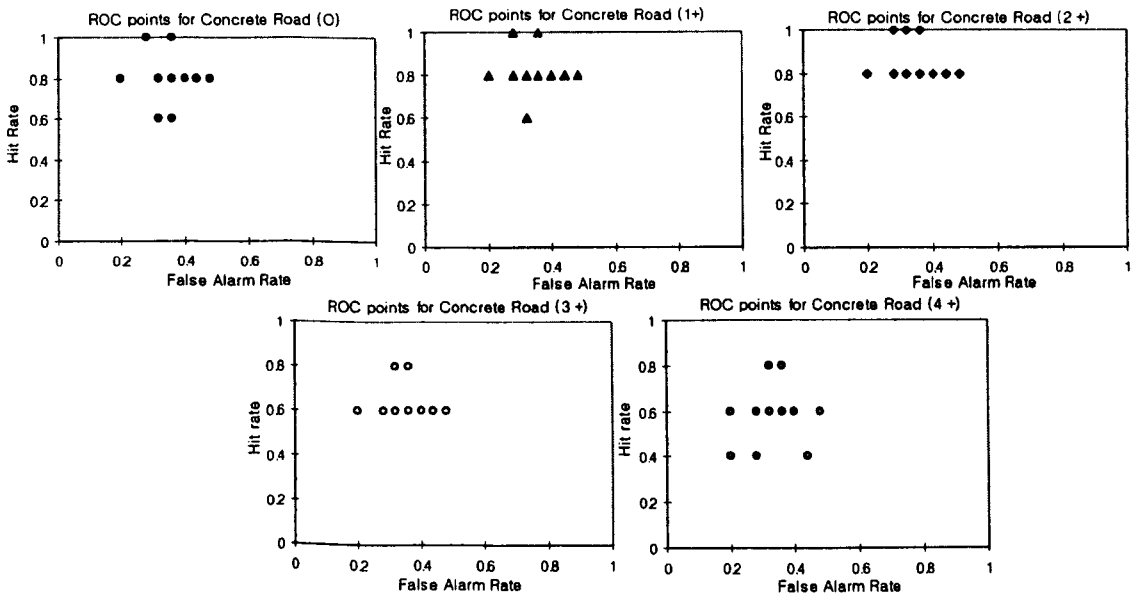


Figure D.23 ROC points for the concrete surface stimuli regarding the effect of the number of the transient events of the steering wheel acceleration signal (n= 15).

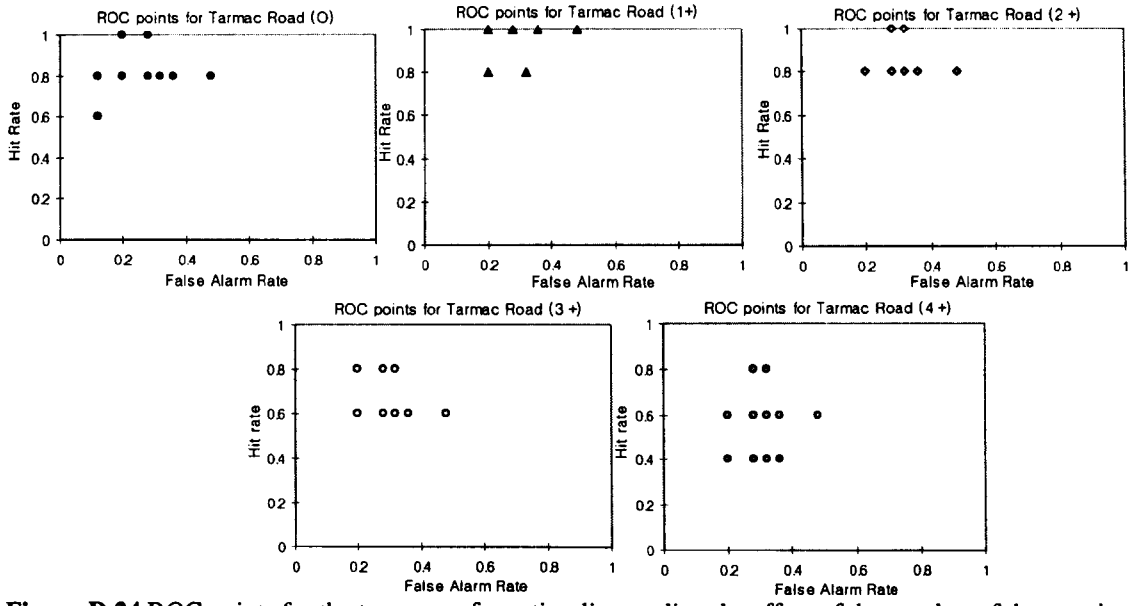


Figure D.24 ROC points for the tarmac surface stimuli regarding the effect of the number of the transient events of the steering wheel acceleration signal (n= 15).

D.4 ROC points for the laboratory experiment to measure the effect of the scale of the transient events on the human detection of road surface type.

The Receiver Operating Characteristic (ROC) points results obtained for the 15 test participants for the cobblestone surface, the concrete surface and the tarmac surface are presented in Figures D.25 to D.27. Results are presented according to the five bump scale factors investigated (x0.8, x1.0, x2.0, x3.0 and x4.0).

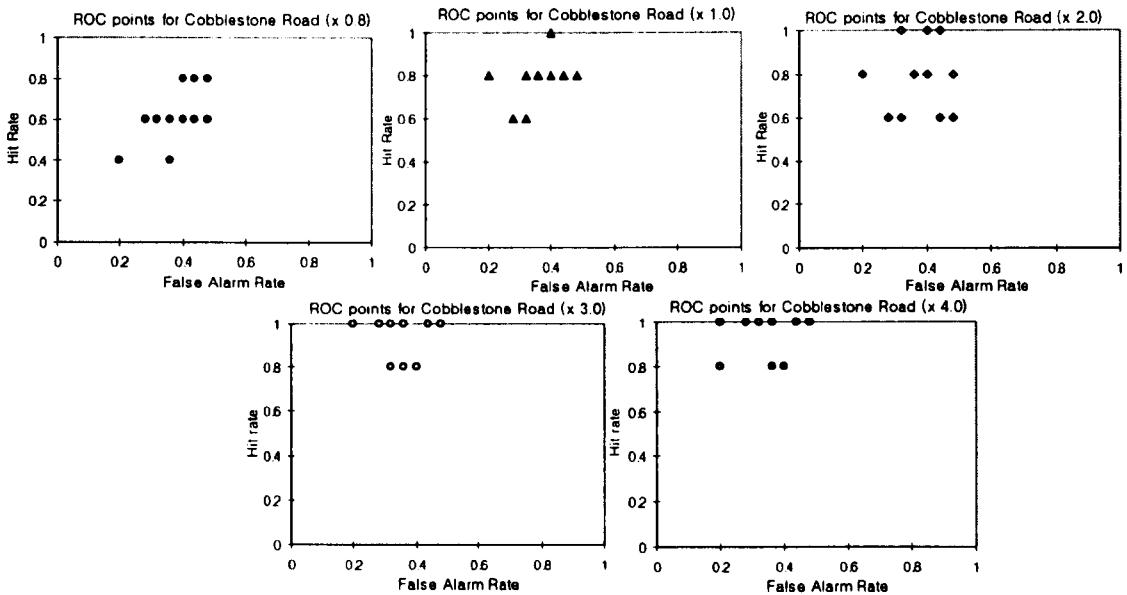


Figure D.25 ROC points for the cobblestone surface stimuli regarding the effect of the scale of the transient events of the steering wheel acceleration signal (n= 15).

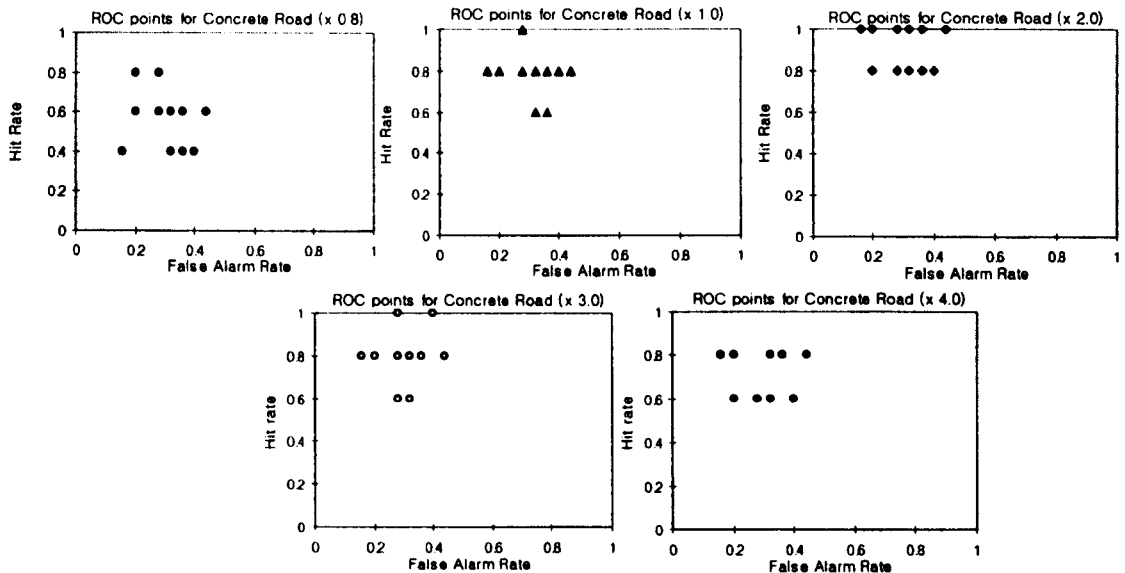


Figure D.26 ROC points for the concrete surface stimuli regarding the effect of the scale of the transient events of the steering wheel acceleration signal (n= 15).

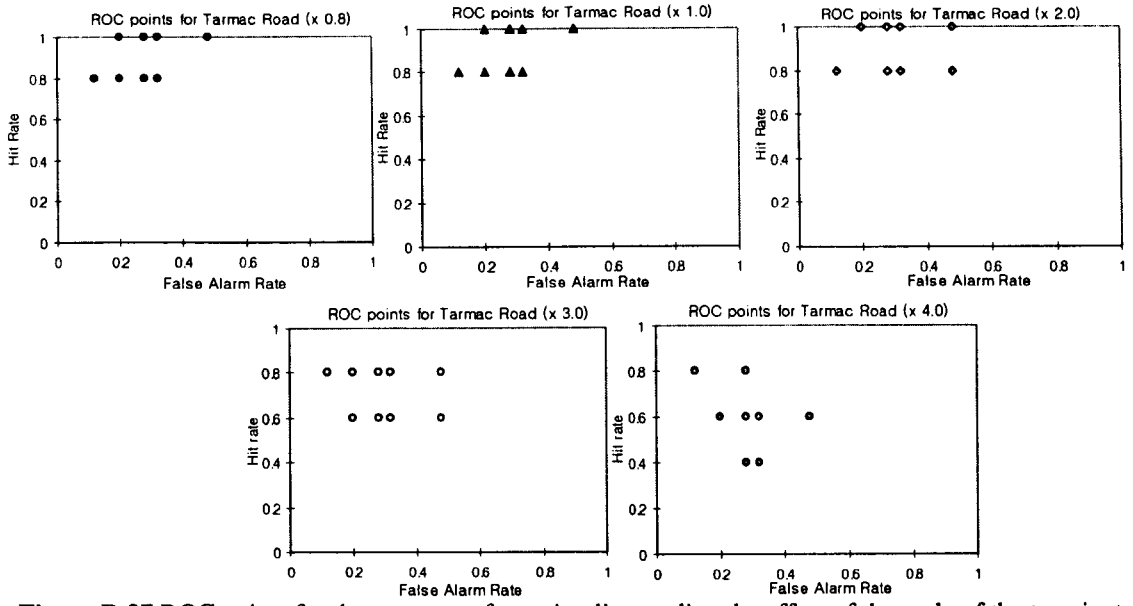


Figure D.27 ROC points for the tarmac surface stimuli regarding the effect of the scale of the transient events of the steering wheel acceleration signal (n= 15).

D.5 ROC points for the laboratory experiment to measure the effect of the first set of guidelines for an automotive steering feedback.

The Receiver Operating Characteristic (ROC) points results obtained for the 15 test participants for the ten road surface investigated in the effect of first set of guidelines for an automotive steering feedback are presented in Figures D.28 to D.37. Results are presented for both the original stimuli and the manipulated stimuli.

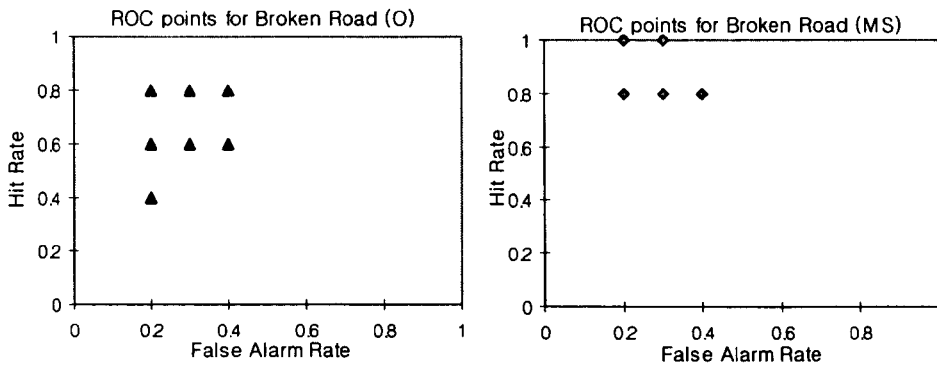


Figure D.28 ROC points for the original and the manipulated broken surface stimuli regarding the effect of first set of guidelines for an automotive steering feedback (n= 15).

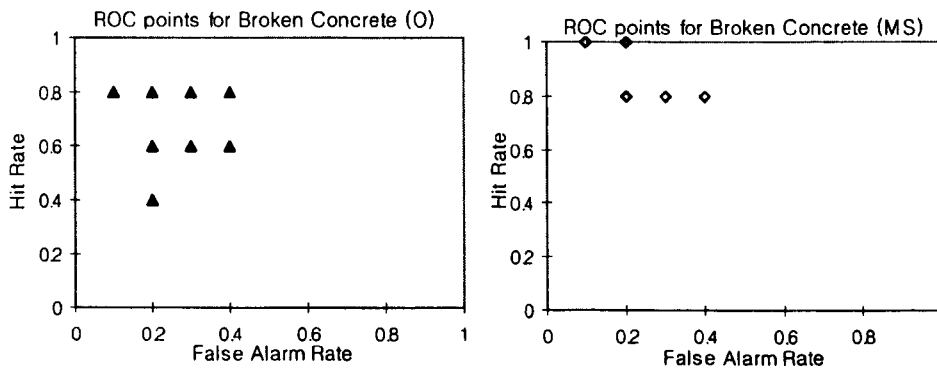


Figure D.29 ROC points for the original and the manipulated broken concrete surface stimuli regarding the effect of first set of guidelines for an automotive steering feedback (n= 15).

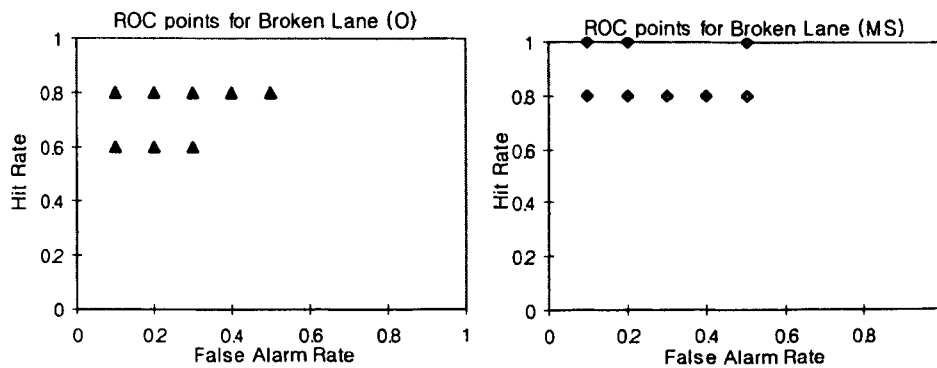


Figure D.30 ROC points for the original and the manipulated broken lane surface stimuli regarding the effect of first set of guidelines for an automotive steering feedback (n= 15).

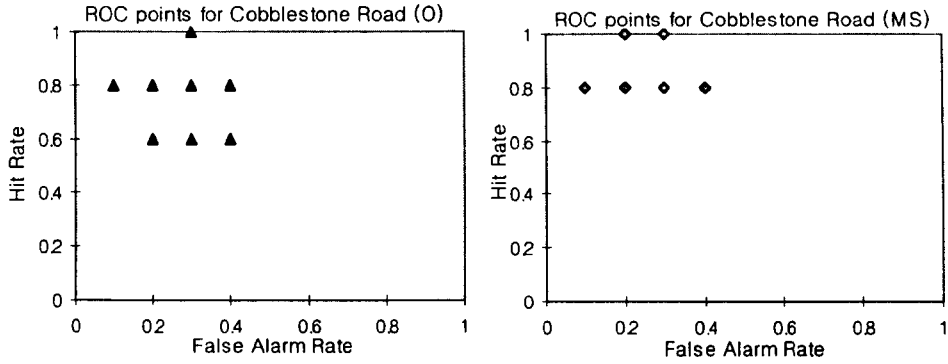


Figure D.31 ROC points for the original and the manipulated cobblestone surface stimuli regarding the effect of first set of guidelines for an automotive steering feedback (n= 15).

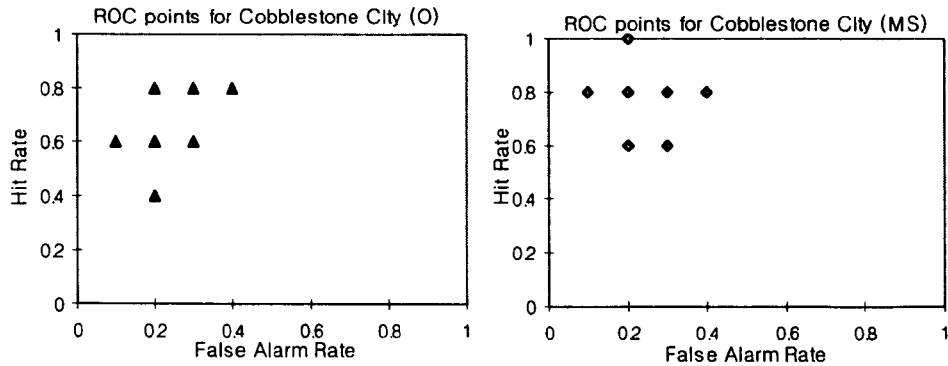


Figure D.32 ROC points for the original and the manipulated cobblestone city surface stimuli regarding the effect of first set of guidelines for an automotive steering feedback (n= 15).

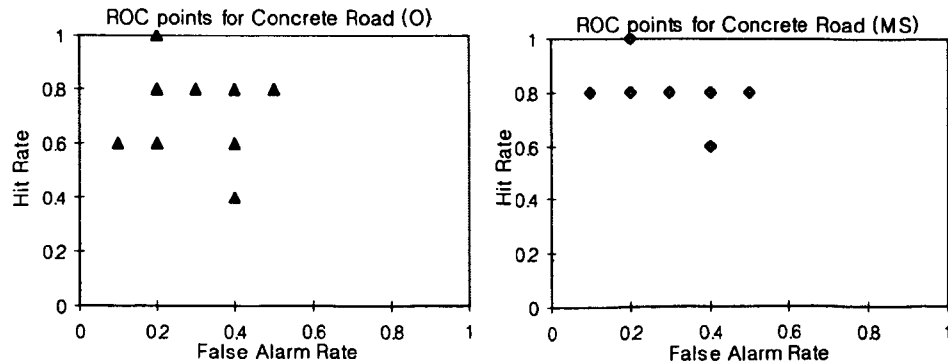


Figure D.33 ROC points for the original and the manipulated concrete surface stimuli regarding the effect of first set of guidelines for an automotive steering feedback (n= 15).

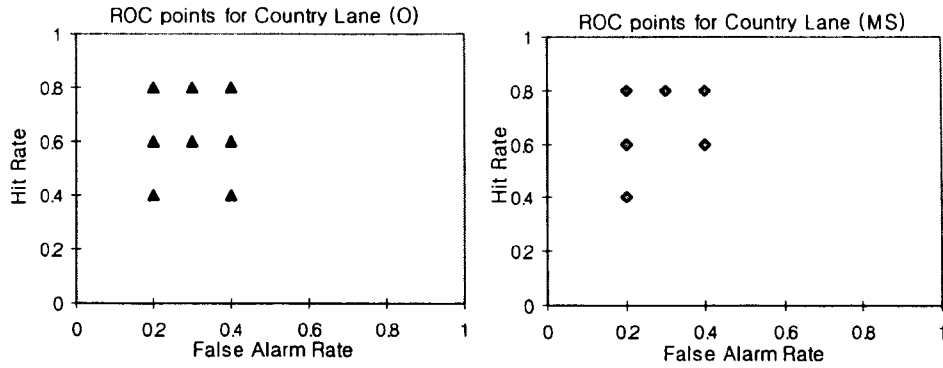


Figure D.34 ROC points for the original and the manipulated country lane surface stimuli regarding the effect of first set of guidelines for an automotive steering feedback (n= 15).

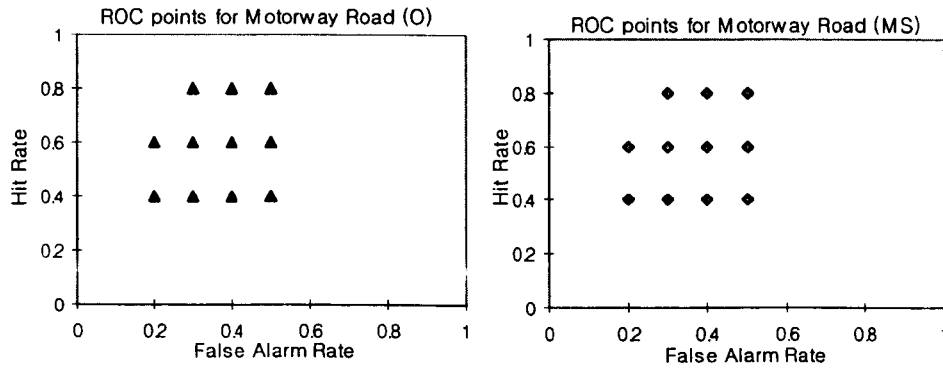


Figure D.35 ROC points for the original and the manipulated motorway surface stimuli regarding the effect of first set of guidelines for an automotive steering feedback (n= 15).

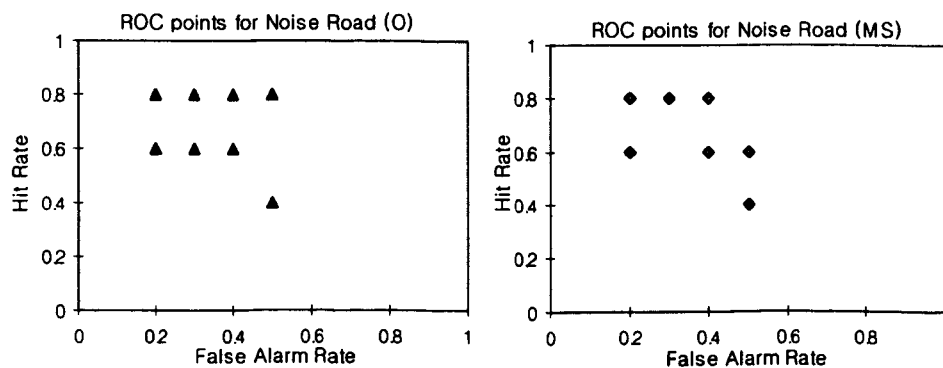


Figure D.36 ROC points for the original and the manipulated noise surface stimuli regarding the effect of first set of guidelines for an automotive steering feedback (n= 15).

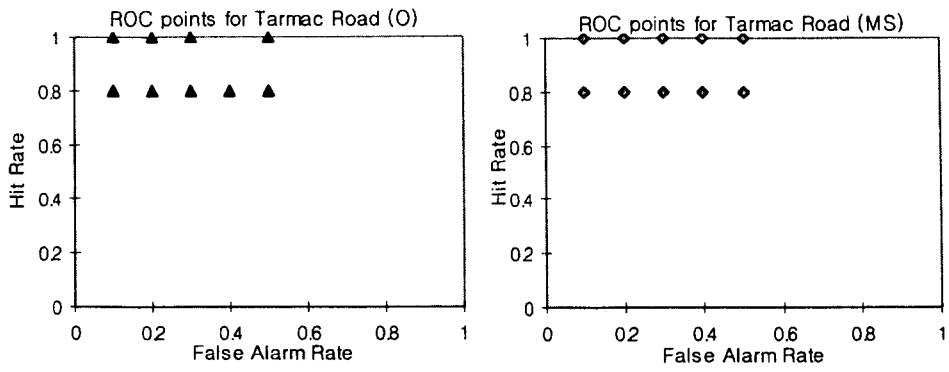


Figure D.37 ROC points for the original and the manipulated tarmac surface stimuli regarding the effect of first set of guidelines for an automotive steering feedback (n= 15).